The Characterization and Engineering of Human Antigen-Specific Cytotoxic T Cells

Chi Zhang

Thesis Submitted for the Degree of Doctor of Philosophy

Wolfson College

Trinity Term 2017

Supervisors:
Professor Tao Dong
Professor Sir Andrew J McMichael, FRS

MRC Human Immunology Unit
MRC Weatherall Institute of Molecular Medicine
Nuffield Department of Medicine
University of Oxford

Abstract: The Characterization and Engineering of Human Antigen-Specific Cytotoxic T Cells

Chi Zhang, Wolfson College, Oxford
D.Phil. Thesis, Trinity Term 2017

This D.Phil. thesis focuses on human antigen-specific cytotoxic T lymphocytes (CTLs). In the first part of the thesis, the impact of antigen stimulation strength on CTL activation was investigated by evaluating the global transcriptomes of a well-characterized CTL clone and some of its surface protein expressions, with particular focus on immune checkpoint receptors. Based on the gene differentiations, an 'EGR2-CCL1-4-1BB' pathway, which is sensitive to very low-strength antigen stimulation, was identified. We proposed to block CCL1/CCR8 for future cancer therapeutic treatment as this could be a key mechanism for attracting immune-suppressive cells to local tumour-specific CTLs. Further, an 'inverse correlation of inhibitory signal and expression level' model was developed to explain the expression patterns of five inhibitory immune checkpoint receptors (CTLA-4, PD-1, LAG-3, TIM-3 and TIGIT). These findings throw lights on the understanding of CTL functions and the future design of T cell-based cancer immunotherapy. In the second half the thesis, the potential use of CRISPR/Cas9 technology was explored in manipulating antigen-specific CTLs and the antigen-specific CTL clone gene delivery method was optimised. Successful disruption of PD-1 gene by CRISPR/Cas9 via lentivirus has been achieved on several antigen-specific CTL lines and clones. After disrupting PD-1 gene, CTLs function better when the target cells express high level of PD-1 ligand. This part of work is the first study to knock out PD-1 gene on human antigen-specific primary CD8+ T cells and has the potential for clinical applications such as the treatment of infection, autoimmunity and cancer.

Acknowledgement

I am sincerely grateful to my supervisors, Professor Tao Dong and Professor Sir Andrew McMichael. It has been an honour and a pleasure to work with them both. I would particularly like to thank Tao for the opportunity to study at Oxford, her enthusiasm, inspiring ideas and tremendous support. None of this would have been possible without her. And also for the Chinese New Year and Christmas parties at her house, countless nice group lunch and dinner, and an unforgettable high table experience at University College. It is also my privilege to thank Sir Andrew who provided valuable advice and guidance throughout each stage of my study at Oxford, and not to mention inviting me twice to his fascinating cottage for the very British summer garden parties.

1 thank profusely all the current members of TD lab and those who has already left, especially Peng, Xi, Yan, Lili, Megat, Henry, Rhys and Sophie, thank you - for the help, the friendship, the scientific debate and the great adventures in science and outside. I would also like to acknowledge and thank all my collaborators, Dr Yanchun Peng for the T cell work, Dr Philip Hublitz for the CRISPR work; Dr Dilair Baban, Dr Ben Wright and Mr Stephen Taylor for the microarray experiment and initial analysis; Mr Craig Waugh who helped me with the cell sorting; and Dr Mei-yi Sun, for the help on lentiviral work.

A special thanks to Clarendon Scholarship (Oxford University Press) and China Scholarship Council - University of Oxford Scholarship, who jointly sponsored my study and living at Oxford; and also Nuffield Department of Medicine, who welcomed me and generously topped up my stipend.

Finally, I would like to express great thankfulness to my parents for supporting me spiritually throughout my study and life these years in general. I hope I have made you proud of me. I owe a deep sense of gratitude to my friends for their support, encouragement and company throughout my four years in Oxford, particularly Mei-yi, Xi, Peng, Zhu, Yiwen, Qingji and Jiahe. It's my genuine pleasure to meet you in Oxford and become close friends with you. A big thanks to my buddy and flatmate Haoyu Liu, thank you for always being on my side and acting as my private cook for the past two years' time!

Declaration

I declare that the work presented in this D.Phil. thesis entitled "The Characterization and Engineering of Human Antigen-Specific Cytotoxic T Cells" is entirely my own work, except for where the contributions of collaborators have been clearly acknowledged.

No part of my thesis has been submitted for any other degree or other qualification in this university or elsewhere.

Chi Zhang

MRC Human Immunology Unit

MRC Weatherall Institute of Molecular Medicine

Trinity Term 2017

Presentations and Awards

2016: Poster presentation at WIMM Day in the title of "Generation of PD1 Knock-out Human Antigen-Specific T cells via the CRISPR/Cas9-mediated Genetic Engineering".

2016: Oral presentation at ESMO Immuno-Oncology Symposium in the title of "Generation of Immune Checkpoint Knock-out Human Antigen-Specific T cells via CRISPR/Cas9-mediated Genetic Engineering", awarded with ESMO travel grant, WIMM student travel grant and Wolfson College travel award.

2017: Oral presentation at HIU Student Seminar in the title of "Generation of PD1 Knock Out Human Antigen Specific CD8+ T Cells".

2017: Oral presentation at HIU Friday-Morning Talk in the title of "Analysis of Immune Checkpoint Receptors on T Cells Indicates the Design of Mono- and Combinatorial Blockade Immunotherapy".

List of Abbreviations

AA	amino acid
AF9	ARMILMTHF NS5B.2831-2849 epitope, HLA B*27 restricted
AIDS	acquired immunodeficiency syndrome
APC	antigen presenting cell
APC	allophycocyanin
ART	antiretroviral treatment
BSA	Bovine Serum albumin
β_2m	beta-microglobulin
Cas9	CRISPR associated protein 9
CCL	C-C motif ligand
CD	cluster of differentiation
CDR	complementary determining region
CRISPR	clustered regularly interspaced short palindromic repeats
CTL	cytotoxic T lymphocyte
CXCL	cysteine-cysteine linked chemokine ligand
CXCR	cysteine-cysteine linked chemokine receptor
D10	DMEM supplemented with 10% FCS, 50U/ml P/S, 2mM L-glutamine
DMEM	Dulbecco's Modified Eagle's Medium
DMSO	dimethyl sulphoxide
DNA	deoxyribonucleic acid
EBV	Epstein-Barr virus
ELISA	enzyme-linked immune absorbent assay
ELISPOT	Enzyme-Linked ImmunoSpot
FACS	fluorescence-activated cell sorting (flow cytometry)
FCS	foetal calf serum
FITC	fluorescein isothiocyanate
FL8	FLKEKGGL Nef.90-97 epitope, HLA B*08 restricted
FPLC	fast protein liquid chromatography
GFP	green fluorescent protein
GL9	GILGFVFTL M1.58-66 epitope, HLA A*02 restricted
GSEA	Gene Set Enrichment Analysis
H10	RPMI 1640 supplemented with 10% heat inactivated human AB serum, 50U/ml P/S, 2mM L-glutamine
HA	hemagglutinin
HCV	hepatitis C virus
HIV	human immunodeficiency virus
HLA	human leukocyte antigen
ICS	intracellular cytokine staining
IFN	interferon
IL	interleukin
lTAM	immunoreceptor tyrosine-based activation motif
lTlM	immunoreceptor tyrosine-based inhibition motif
LB	lysogeny broth
limma	linear models for microarray analysis
LTNP	long-term non-progressors
LTR	long terminal repeat
KV9	KASEKIFYV SSX-2.41-49 epitope, HLA A*02 restricted
M1	matrix protein

MHC	major histocompatibility complex
MIP	macrophage inflammatory protein
MOI	multiplicity of infection
mRNA	messenger ribonucleic acid
Nef	negative factor
NK	natural killer cell
NS5B	non-structural protein 5b
O/N	overnight
P/S	penicillin/streptomycin
PANTHER	protein analysis through evolutionary relationships
PBMC	peripheral blood mononuclear cells
PBS	phosphate buffered saline
PD1	programmed cell death protein 1
PDL1	programmed death-ligand 1
PCR	polymerase chain reaction
PE	phycoerythrin
PHA	phytohemagglutinin
PMA	phorbol myristate acetate
R0	RPMI-1640 with 50U/ml P/S, 2mM L-glutamine
R10	RPMI-1640 supplemented with 10% FCS, 50U/ml P/S, 2mM L-glutamine
RI11	RGIFGAIAGFI HA.345-354 epitope, HLA DRB1*0901 restricted
RANTES	regulated upon activation. normal T cell expressed and secreted
RNA	ribonucleic acid
S/N	supernatant
SFFV	spleen focus-forming virus
SD	standard deviation
sgRNA	single-guide RNA
SSX	synovial sarcoma X
TCR	T cell receptor
TNF	tumour necrosis factor
w/	with
w/o	without

Table of Contents

Figures and Tables

1 Chapter 1: Introduction

The human adaptive immune system consists of cellular and humoral immune responses. The former response is mediated by T lymphocytes (T cells) and the latter by B lymphocytes (B cells). Though both the two cell types arise from bone marrow, unlike B cells, T cells migrate to thymus for maturation. After the completion of maturation in thymus, T cells enter the bloodstream and circulate to peripheral lymphoid organs, and re-circulate to the bloodstream via lymphatics. Upon encountering their specific antigens, naïve T cells (T cells that have not yet encountered their specific antigens) proliferate and differentiate into effector T cells with the help of professional antigen presenting cells (APCs) and acquire new capacities to remove antigens. Simultaneously with the production of effector T cells, memory T cells are also generated. These long-lived cells protect the body from subsequent challenge by the same antigens. Unlike naïve T cells, memory T cells respond to antigen stimulation in a more rapid and heightened reaction. In general, T cells express either CD4 or CD8 molecules on their surface, allowing the categorization of the CD4+ T cells and the CD8+ T cells. Naïve CD8+ T cells can differentiate into cytotoxic T lymphocytes (CTLs) that can recognize and kill virus-infected or tumour cells. In contrast, naïve CD4+ T cells can differentiate into several different subtypes with distinguished immunological functions depending on the contexts, such as T-helper 1 cells (T_H1), T-helper 2 cells (T_H2), T-helper 9 cells (T_H9), T-helper 17 cells (T_H17), regulatory T cells (T_{REG}) and follicular helper T cells (T_{FH}) (Murphy et al., 2012d).

1.1 Basic Concepts of Cytotoxic T Lymphocytes (CTL).

Cytotoxic T lymphocytes (CTL) monitor almost all the cells inside the body, ever ready to destroy any 'abnormal' cells. In a successful viral clearance, CTLs kill virus-infected cells and prevent them from being the cradles of more viruses. In addition, CTLs also protect the body against tumour cells by their capacity to detect quantitative and qualitative antigenic differences on the surface of transformed cells (Castelli et al., 2000).

1.1.1 The T Cell Receptor (TCR).

After maturation in the thymus, each T cell expresses a unique cell surface antigen-binding molecule called the T cell receptor (TCR). Each T cell bears about 30,000 identical TCRs on its surface, each receptor consisting of two different polypeptide chains. The majority of T cells inside the human body express αβ TCRs, consisting of one TCR α-chain and one TCR β-chain, linked by disulphide bond (Murphy et al., 2012b). A minority of T cells bears an alternative but structurally similar γδ receptor. αβ T cells contribute primarily to the cellular immune response, while γδ T cells are distinct in that they combine conventional adaptive features with rapid, innate-like responses. In addition, unlike traditional αβ T cells, γδ T cells usually lack of CD4 or CD8 co-receptors (Vantourout and Hayday, 2013).

Total diversity of αβ TCRs could be as high as 10^{18}. (Table 1-1) This structural diversity of αβ TCRs is mainly attributed to the combinatorial diversity and the junctional diversity generated during the process of TCR gene rearrangement

(Murphy et al., 2012c). (Table 1-1) The TCR non-covalently associates with the non-polymorphic CD3 complex, which comprises the CD3εγ, CD3εδ, and CD3ζζ dimers, to form a functional TCR complex on the cell surface (Acuto et al., 1983). Different from the B cell receptors (BCRs) on B cells, which directly recognize antigen, αβ TCR recognizes a complex ligand that includes an antigenic peptide loaded in the groove on the surface of a major histocompatibility complex (MHC) molecule. (Figure 1-1)

Table 1-1 The numbers of human TCR gene segments and the sources of TCR diversity

Element	**TCRα**	**TCRβ**
Variable segments (V)	~70	52
Diversity segments (D)	0	2
Joining segments (J)	61	13
Joints with N- and P-nucleotides	1	2
Number of V gene pairs	5.8×10^6	
Junctional diversity	$\sim 2 \times 10^{11}$	
Total diversity	**$\sim 10^{18}$**	

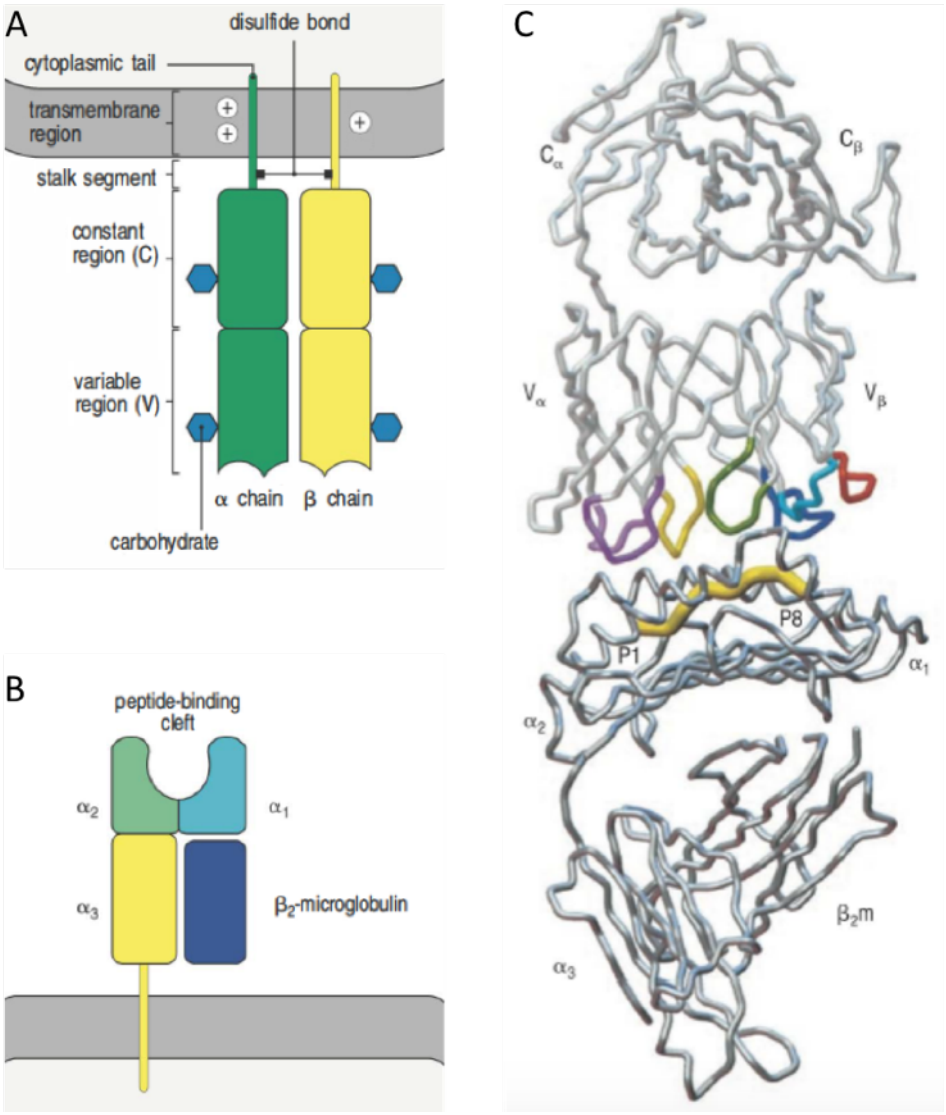

Figure 1-1 Structures of T cell receptor and MHC class I molecule.

(A)(B) Schematic representation of TCR structure and MHC class I molecule structure. (C) Crystal structure of the TCR binds to the peptide-MHC class I complex. Figure adapted from Janeway's Immunobiology 8th Edition Chapter 4.

1.1.2 Peptide-MHC Class I Molecules (p-MHC I).

The human leukocyte antigen (HLA) system is a gene complex encoding the major histocompatibility complex (MHC) proteins in humans. The MHC locus spans at least four million base pairs (bp) on the short arm of chromosome 6 at 6p21.3, and contains the most polymorphic genes of the human genome. It has been discovered that CD8 CTLs are restricted in their recognition of foreign viral antigens to targets that shared the same self-MHC class I antigen (McMichael et al., 1977; Zinkernagel and Doherty, 1974), and recognize virus infection by the proteolytic cleavage of viral proteins in the cytosol of the cell, which are bound to MHC class I molecules and displayed on the cell surface (Townsend et al., 1986).

There are three MHC gene families, MHC class -I, -II, and -III. MHC class I molecules consist of two polypeptide chains. The α-chain or heavy chain, encoded in the MHC gene loci, is non-covalently associated with a smaller chain or light chain, β_2-microglobulin (β_2m), which is not polymorphic and is encoded on chromosome 15. Human somatic cell expresses up to six different MHC class I antigens (HLA-A, -B, -C, -E, -F and -G). There have been reports of 3,913 HLA-A alleles (2,747 proteins), 4,765 HLA-B alleles (3,465 proteins), 3,519 HLA-C alleles (2,450 proteins), 25 HLA-E alleles (8 proteins), 22 HLA-F alleles (4 proteins) and 54 HLA-G alleles (18 proteins) on IMGT/HLA database (Robinson et al., 2000).

The MHC class I α-chain is co-translationally translocated into the endoplasmic reticulum (ER), where it is folded and glycosylated in association with the chaperone protein - calnexin. The α-chain then associates with β_2m and dissociates from the chaperone protein to form a loading complex with the

transporter associated with antigen processing (TAP), tapaisin, calreticulin, and protein disulphide isomerase and ERp57. (Figure 1-2A) The intracellular antigens are produced either by viruses/bacteria within a host cell or from the host's own 'abnormal' proteins. The host cell digests cytoplasmic proteins into small peptides through proteasome and the TAP complex moves these peptides into ER, allowing the antigenic peptides to be coupled to MHC I molecules. Binding of a peptide to an MHC class I molecule is stabilized at both ends of the peptide-binding cleft by contacts between atoms in the free carboxyl- (C-) and amino- (N-) termini of the peptide and invariant sites of MHC class I molecules. (Figure 1-2B) The peptide-bound MHC class I complexes are then transported to the cell surface and available for TCR to 'scan' (Murphy et al., 2012a).

In addition, extracellular antigens could also be processed and presented to CTLs via cross-presentation carried out by specific dendritic cell (DC) subsets through an adaptation of their endocytic and phagocytic pathways (Joffre et al., 2012), and macrophages and B cells have also been shown to capable of doing so (Fehres et al., 2014). This process is essential for immunity against viruses that do not readily infect APCs, or impair DC normal function.

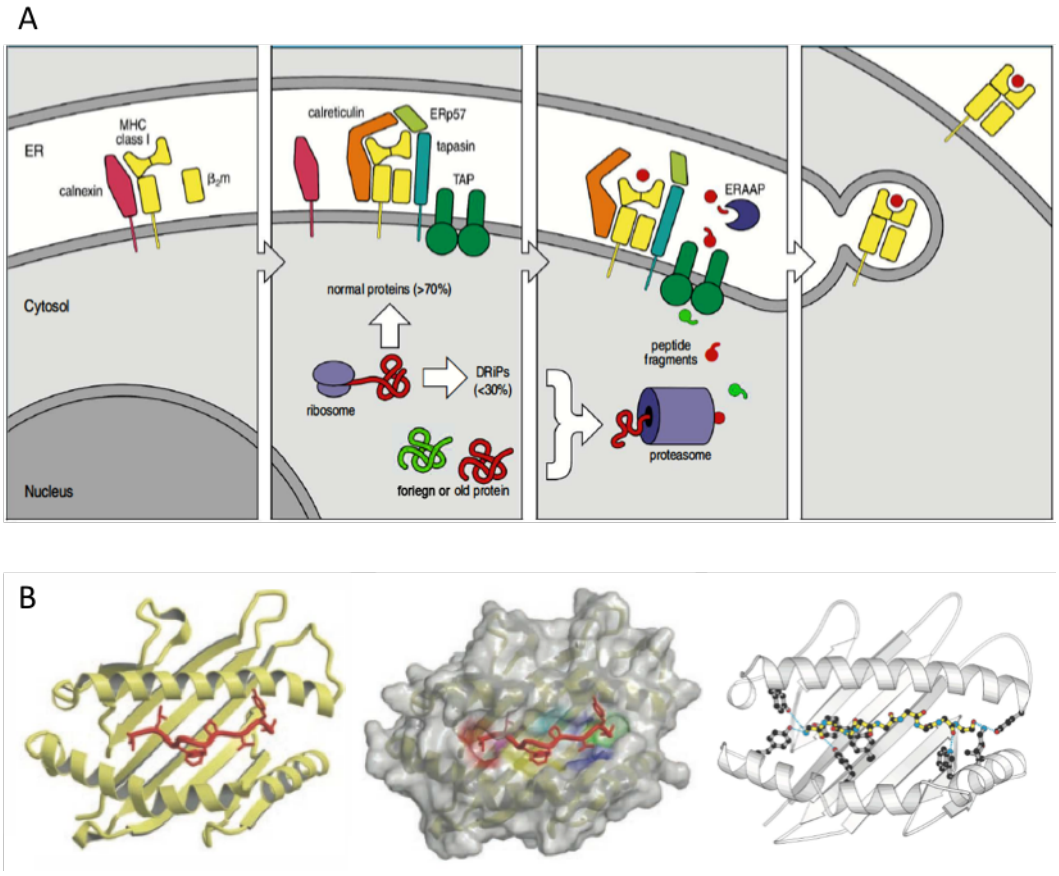

Figure 1-2 The generation of TCR ligand for CD8+ T cells.

(A) Schematic diagram of MHC class I molecule assembling and presenting peptide to the cell surface. (B) MHC class I molecules interact with the backbone of a bound peptide. Left, ribbon diagram; middle, solvent accessible surface; right, ribbon diagram with hydrogen bonds and ionic interactions. DRiP: defective ribosomal products. Figured adapted from Janeway's Immunobiology 8th Chapter 4&6.

1.1.3 Cluster of Differentiation 8 (CD8).

Apart from engaging a p-MHC I via TCR, a CTL makes additional interaction by CD8 co-receptor with the p-MHC I invariant region away from the peptide-binding site that stabilises the interaction and is required for the cell to respond effectively to the antigen. CD8 αβ heterodimeric form is found on ~90% of CTLs (Norment and Littman, 1988) and is a disulphide-linked dimer of two different chains (α and β), each containing a single Ig-like domain linked to the membrane by a segment of extended polypeptide, which is extensively glycosylated. CD8α chains can also form homodimers on the surface of some cell types within the lymphoid system, including $CD3^-$ natural killer (NK) cells, some γδ TCR T cells, certain $CD4^+CD8^+$ T cells (Moebius et al., 1991), intestinal intra-epithelial T cells (Leishman et al., 2001) and certain DC subsets (Vremec et al., 2000). The functional role of the CD8αα homodimer has not been formally identified, although a regulatory role has been proposed in the case of intestinal intra-epithelial T cells. In contrast, the CD8αβ co-receptor plays a major role in CD8+ T cell activation by increasing antigen sensitivity and by stabilizing the TCR-p-MHC I interaction at the cell surface (Cole et al., 2012).

1.1.4 TCR Engagement and Downstream Signalling Pathways.

Interactions of TCRs and p-MHC I are among the weakest protein-protein interactions that can initiate a biological response. A CTL needs to discriminate between foreign and self p-MHC molecules, even though the differences in the affinity and kinetics of binding to foreign and self p-MHC molecules are not large. Following TCR binding to agonist p-MHC I, Lck is recruited to the TCR complex and activated by the Tyr505 dephosphorylation via CD45. In the basal state, the CD3ζ-chain immunoreceptor tyrosine-based activation motifs (ITAMs) are phosphorylated (red dots in Figure 1-3A) and bound to Zeta-chain-associated protein kinase 70 (Zap70). Lck phosphorylates Tyr319 on Zap70, relieves Zap70 auto-inhibition and creates a binding site for the Lck SH2 (Src homology 2) domain, further stabilizing the activated state of Lck. Activated Zap70 induces the assembly of the signal diversification and regulation module by phosphorylating the scaffold proteins LAT (linker for activation of T cells) and SLP-76 (SH2 domain-containing leukocyte protein of 76 kDa). This module includes regulators of Ca^{2+} signalling and diacylglycerol (DAG) production (*i.e.* PLCγ1 (phospholipase Cγ1) and ITK (IL2-inducible T cell kinase)), actin polymerization (*i.e.* NCK (non-catalytic region of tyrosine kinase) and VAV1) and integrin activation (*i.e.* ADAP (adhesion and degranulation promoting adaptor protein)), all of which are activating signalling pathways that control cell adhesion, cytoskeletal rearrangements and gene expression (Figure 1-3B) (Acuto et al., 2008; Chakraborty and Weiss, 2014).

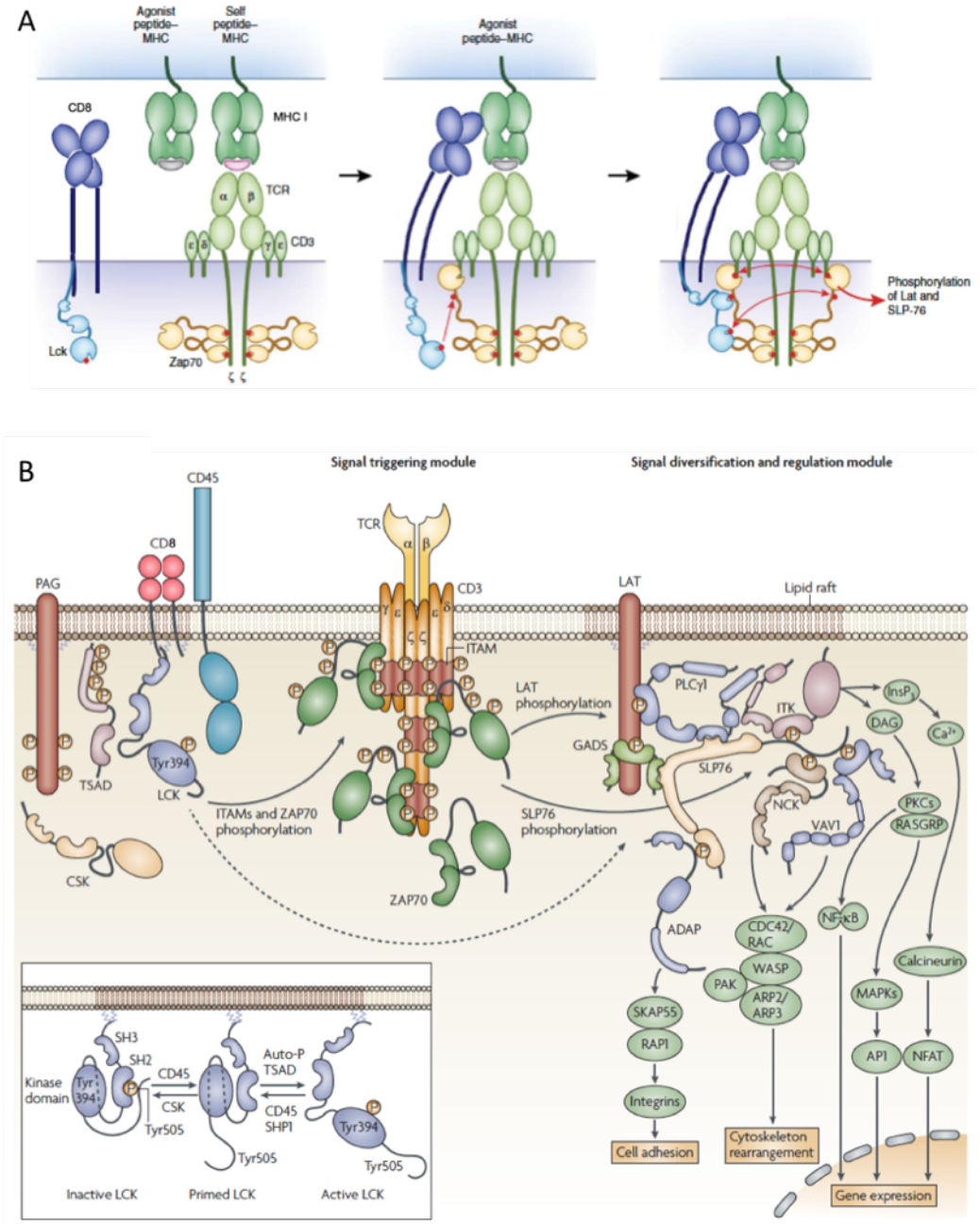

Figure 1-3 TCR signalling components and pathways.

(A) TCR activation as a consequence of the combined re-localization of CD8 co-receptor and bound Lck. Figure adapted from (Chakraborty and Weiss, 2014). (B) Detailed schematic representation of TCR signalosome modules and their connections. Figure adapted from (Acuto et al., 2008). AP1: activator protein 1; ARP: actin-related protein homologue; CDC42: cell-division cycle 42; GADS: growth-factor-receptor-bound-protein-2-related adaptor protein; InsP3: inositol-1,4,5-trisphosphate; MAPK: mitogen-activated protein kinase; NFAT: nuclear factor of activated T cells; NF-κB: nuclear factor-κB; PKC: protein kinase C.

1.2 CTL Priming and Differentiation.

1.2.1 Priming of Naïve CD8+ T cells by Antigen Presenting Cells.

T cell responses are initiated when a mature naïve CD8+ T cell encounters a properly activated APC displaying the appropriate p-MHC I ligand. The activation and differentiation of naïve T cells is often referred as 'priming'. Priming of naïve CD8+ T cells generates cytotoxic T cells capable of directly killing target cells. As a naïve CD8+ T cell migrates through the cortical region of the lymph node (LN), it binds transiently to each APC that it encounters. Mature DCs bind naïve CD8+ T cells very efficiently through interactions between LFA-1 (lymphocyte function-associated antigen 1) and CD2 on T cell, and their ligands (ICAM (intercellular adhesion molecule)-1, ICAM-2 and CD58) on the DC. The transient binding of a naïve CD8+ T cell to a DC is crucial in providing time for the T cell to 'scan' large numbers of MHC molecules on the surface of the APC for the presence of agonist peptide. In those rare cases, in which a naïve CD8+ T cell recognizes a p-MHC I ligand on the APC, signalling through the T cell receptor induces a conformational change in LFA-1 that greatly increases its affinity to ICAM-1 and ICAM-2, which stabilizes the association between the antigen (Ag)-specific naïve CD8+ T cell and the APC. This association can last a couple of days, during which the naïve cell proliferates and its descendants, which also attach to the APC, differentiate into effector and memory cells. (Murphy et al., 2012d)

1.2.2 Linear Model of T Cell Differentiation.

In the current linear or developmental model of CD8+ T cell central and effector memory generation for mouse and human T cells, T cells can be divided into five categories - T_N (naïve T cell, $CD45RA^+CD95^-IL2R\beta^-CCR7^+CD62L^+$), T_{SCM} (T memory stem cell, $CD45RA^+CD95^+IL2R\beta^+CCR7^+CD62L^+$), T_{CM} (central memory T cell, $CD45RO^+CD95^+IL2R\beta^+CCR7^+CD62L^+$), T_{EM} (effector memory T cell, $CD45RO^+CD95^+IL2R\beta^+CCR7^-CD62L^-$) and T_{EFF} (effector T cell, $CD45RA^+CD95^+IL2R\beta^+CCR7^-CD62L^-$) (Restifo, 2014). Each category represents a distinct activation/differentiation status. Activation of naïve T cells by APCs results in proliferation as well as differentiation of the cells. T_{SCM} is the newest identified category based on the observation that some cells in the $CD62L^{hi}$ CD8+ T cell populations have a stem cell-like property (Stemberger et al., 2014). T_{EFF} has high levels of perforin with strong cytolytic activity, and produces low levels of cytokines (such as IL-2 and IFN-γ), whereas T_{EM} displays medium levels of perforin and limited cytotoxic activity, but produces high levels of cytokines. In contrast, T_{CM} fails to kill target cells but can proliferate and produce cytokines in response to antigen stimulation (Kaech et al., 2002; Tomiyama et al., 2002).

1.3 CTL Effector Responses and Functions.

1.3.1 Mechanisms of modulating the strength of TCR Signalling.

T cell-mediated immunity involves the clonal selection of antigen-specific cells, their activation and proliferation in secondary lymphoid tissues, their trafficking to sites of antigen and inflammation, the execution of direct effector functions and the provision of help (through cytokines and membrane ligands) for a multitude of effector immune cells (Pardoll, 2012). The specific recognition of antigenic peptides presented by MHC molecules triggers TCR signalling, but it is the co-stimulatory and co-inhibitory (co-signalling) receptors on T cells that direct T cell function and determine T cell fate. These responses occur at the initiation of T cell responses (where the major APCs are DCs) or in peripheral tissues or tumours (where effector responses are regulated). Following recognition of p-MHC I by the TCR, co-signalling receptors co-localize with TCRs at the immunological synapse, where they synergize with TCR signalling to control the T cell activation and functions. In general, T cells do not respond to these co-signalling ligands in the absence of TCR-p-MHC I recognition. (Figure 1-4) (Chen and Flies, 2013; Saito et al., 2010)

Most co-signalling molecules are members of the immunoglobulin superfamily (IgSF) and tumour necrosis factor receptor superfamily (TNFRSF). Table 1-2 summarizes about 60 IgSF and TNFRSF co-signalling molecules, their ligands and functions (Chen and Flies, 2013).

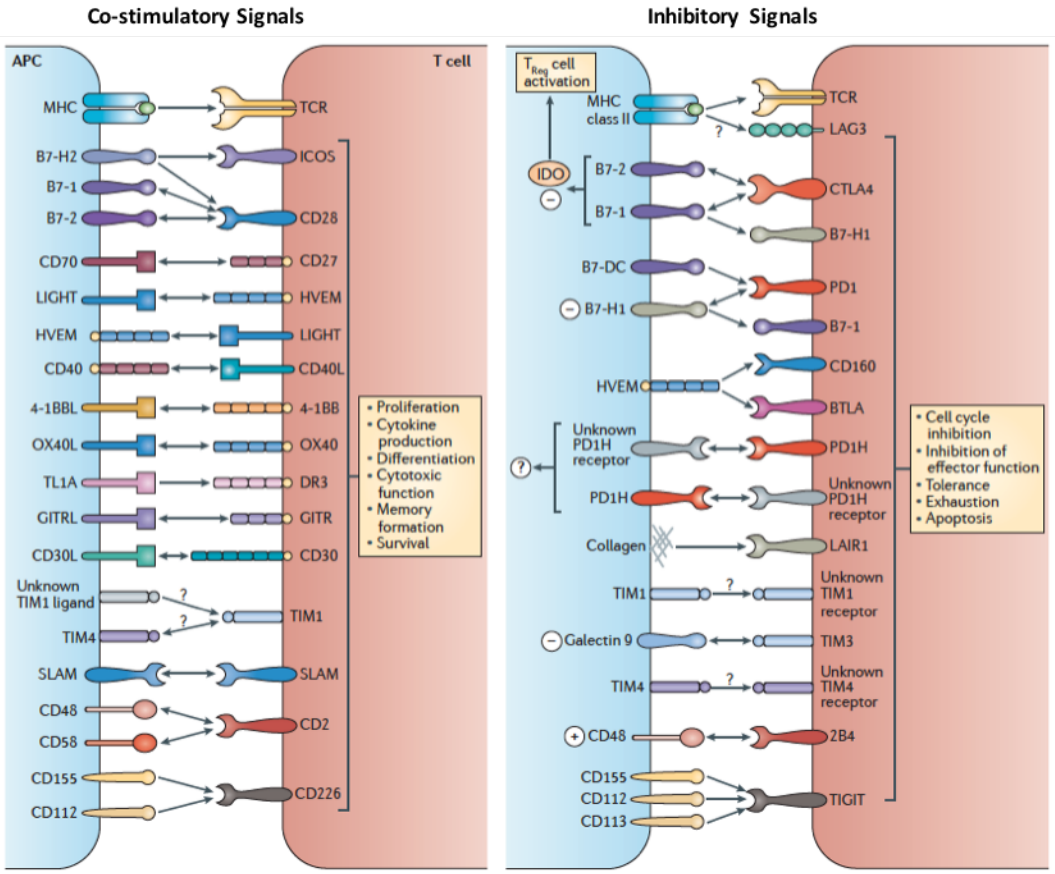

Figure 1-4 Co-stimulatory and inhibitory interactions regulate T cell responses.

Left: co-stimulatory molecules deliver positive signals to T cells following their engagement by ligands and counter-receptors on APCs, of which the interactions are usually bidirectional. Right: inhibitory molecules deliver negative signals into T cells. Figure adapted from (Chen and Flies, 2013).

Table 1-2 IgSF and TNFRSF co-signalling molecules.

IgSF T cell co-stimulatory and co-inhibitory receptors

Receptor subfamily	Molecule name	Extracellular domains	T cell co-signalling	Ligand/counter receptor
CD28	CD28		Stimulatory	B71,B72,B7H2 (human)
	ICOS (CD278)		Stimulatory	B7H2
	CTLA4 (CD152)		Inhibitory	B71,B72,B7H2 (human)
	PD1 (CD279)		Inhibitory	B7H1,B7DC
	PD1H (VISTA)		Inhibitory	Unknown
	BTLA (CD272)		Inhibitory	HVEM, UL144
B7	B71 (CD80)		Inhibitory	B7H1,CD28,CTLA4
	B7H1 (CD274,PDL1)		Inhibitory	PD1, B71
CD226	CD226 (DNAM1)		Stimulatory	CD112, CD155, LFA-1
	CRTAM (CD355)		Stimulatory	NECL2
	TIGIT (VSIG9,VSTM3)		Inhibitory	CD112,CD113,CD155
	CD96 (TACTILE)		Unclear	CD111,CD155
TIM	TIM1 (HAVCR1,KIM1)		Stimulatory	TIM4, TIM1,PS
	TIM2 (TIMD2)		Inhibitory	SEMA4A,H-ferritin
	TIM3 (HAVCR2,KIM3)		Inhibitory	Galectin9,PS,CEACAM-1,HMGB1
	TIM4 (TIMD4)		Unclear	TIM1,PS
CD2/SLAM	CD2 (LFA2,OX34)		Stimulatory	CD48
	SLAM (CD150,SLAMF1)		Stimulatory	SLAM
	2B4 (CD244,SLAMF4)		Stimulatory/inhibitory	CD48
	Ly108 (NTBA,CD352,SLAMF6)		Stimulatory/inhibitory	Ly108,NTB-A (human)
	CD84 (SLAMF5)		Stimulatory	CD84
	Ly9 (CD229,SLAMF3)		Stimulatory	Ly9
	CRACC (CD319,BLAME)		Stimulatory	CRACC
BTN	BTN1 (BTN1A1)		Unclear	Unknown
	BTN2 (BTN2A1-3)		Unclear	Unknown
	BTN3 (BTN3A1-3)		Unclear	Unknown
LAIR	LAIR1		Inhibitory	Collagens
Orphan	LAG3 (CD223)		Inhibitory	MHCII (CD4) and LSECtin(CD8)
	CD160 (BY55,NK28)		Inhibitory	HVEM

Legend: IgV IgC mucin-like ◇GPI-linked; PS= phosphatidylserine

TNFRSF co-stimulatory and co-inhibitory molecules

Receptor subfamily	Molecule name	CRD types (order from cell membrane)	T cell co-signalling	Ligand/counter receptor
Type-V (Divergent)	4-1BB (CD137)		Stimulatory	4-1BBL
	OX40 (CD134)		Stimulatory	OX40L
	CD27 (TNFRSF7)		Stimulatory	CD70
	GITR (CD357)		Stimulatory	GITRL
	CD30 (TNFRSF8)		Stimulatory	CD30L
Type-L (Conventional)	TNFR1 (CD120a)		Apoptosis/Survival	TNF-β
	TNFR2 (CD120b)		Apoptosis/Survival	TNF-α
	HVEM (CD270)		Stimulatory	LIGHT,BTLA,CD160, LTα3,HSV1gD
	LTβR (TNFRSF3)		Stimulatory	LTα1β2, LIGHT
	DR3 (TNFRSF25)		Stimulatory	TL1A
	DcR3 (TNFRSF6B)			LIGHT,TL1A,FASL
	FAS (CD95)		Apoptosis	FASL
	CD40 (TNFRSF5)			CD40L
	RANK (CD265)		Unclear	RANKL
	OPG (TNFRSF11B)		Unclear	RANKL
	TRAILR1-4 (TNFRSF10A-D)		Apoptosis	TRAIL
Type-S (EF-disulfide)	TACI (CD267)			BAFF,APRIL
	BAFFR (CD268)			BAFF
	BCMA (CD269)			BAFF,APRIL
	TWEAKR (CD266)		Unclear	TWEAK
	EDAR		Unclear	EDA-A1
	XEDAR (TNFRSF27)		Unclear	EDA-A2
Orphan	RELT (TNFRSF19L)		Unclear	Unknown
	DR6 (CD358)		Inhibitory	Unknown
	TROY (TNFRSF19)		Unclear	Unknown
	NGFR (CD271)		Unclear	Unknown

CRD types: L1 L2 L3 L4 S Undetermined

The CD28 and B7 families are the most well-described families of co-signalling molecules. CD28 associates with proximal signalling molecules through the YMNM and PYAP motifs to co-stimulate major signalling nodes, leading to activation of distal pathways involved in cell growth, activation of effector function and survival. ICOS (inducible T cell co-stimulator, CD278) lacks a PYAP motif but contains a YMFM motif that recruits the more active phosphatidylinositol-3-kinase (PI3K) subunit p50α, thus leading to enhanced AKT signalling. In contrast, CTLA-4 (cytotoxic T lymphocyte antigen 4, CD152), PD-1 (programmed cell death 1, CD279) and BTLA (B and T lymphocyte attenuator) suppress T cell activation and function through the recruitment of the phosphatases SH2 domain-containing tyrosine phosphatase (SHP) 1, SHP2 and serine/threonine protein phosphatase 2A (PP2A). These phosphatases dephosphorylate major signalling nodes that are essential for co-stimulation of T cells (Figure 1-5A) (Chen and Flies, 2013).

TNFRSF receptors, including 4-1BB (CD137, TNFRSF9), OX40 (CD134, TNFRSF4), CD27 (TNFRSF7), CD30 (TNFRSF8), DR3 (death receptor 3, TNFRSF25), GITR (glucocorticoid-induced TNFR-related protein, TNFSFR18) and HVEM (Herpesvirus entry mediator, TNFSFR14), synergize with TCR-CD3 signalling to promote cell cycle progression, cytokine production and T cell survival (Croft, 2009). TNFRSF receptors associate with TRAF (TNF receptor-associated factor) adaptor molecules to activate primary signalling nodes that in turn activate the distal pathways resulting in enhanced cell growth, effector function and survival. For example, TRAF2 is the prototypical TRAF and is involved in c-Jun N-terminal kinase (JNK) activation, NF-κB activation and anti-apoptotic signalling. TRAF5 also mediates NF-κB activation, and TRAF1 and

TRAF3 also function in T cell co-stimulation and anti-apoptotic signalling. 4-1BB can bind TRAF1, TRAF2 and TRAF3, OX40 and CD27 can bind TRAF2, TRAF3 and TRAF5, HVEM and CD30 can bind TRAF1, TRAF2, TRAF3 and TRAF5, whereas GITR recruits only TRAF2. In addition, DR3 associates with the adaptor molecule TRADD (TNFR-associated death domain), which recruits a TRAF2–receptor-interacting protein (RIP) complex that activates both NF-κB and MAPK signalling pathways. CD27 and GITR share the ability to associate with SIVA1, a molecule involved in apoptotic pathways. 4-1BB and OX40 have been shown to promote memory T cell function in the absence of TCR signalling (Figure 1-5B) (Chen and Flies, 2013).

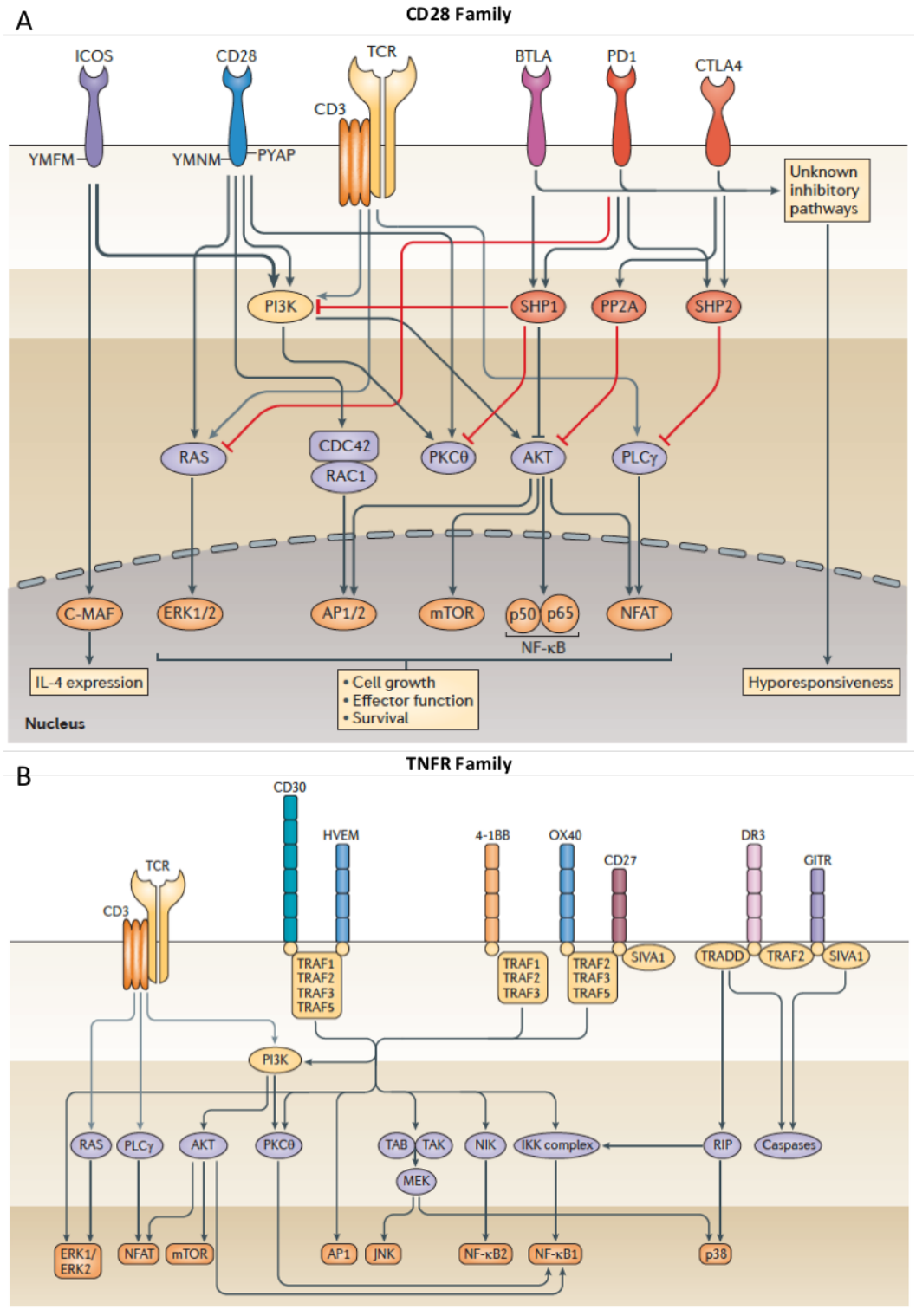

Figure 1-5 Co-signalling pathways downstream of CD28 superfamily receptors and TNFR superfamily receptors.

Apart from receptors within CD28-B7 and TNF/TNFR superfamily, other co-signalling receptors are also known to modulate TCR signalling for the maintenance of immune homeostasis. (Table 1-2) For example, LAG-3 (lymphocyte activation gene-3), TIM-3 (T cell immunoglobulin and mucin-domain containing-3) and TIGIT (T cell immunoreceptor with Ig and ITIM domains) comprise the next generation of co-inhibitory receptors to be translated to the clinic, and inhibit T cells via completely different pathways. LAG-3 structurally resembles the CD4 molecule, could bind to MHC II on APC to inhibit $CD4^+$ T cell activation and LSECtin (liver and lymph node sinusoidal endothelial cell C-type lectin) on tumour or liver cells to inhibit CD8+ T cell or NK cell activation through KIEELE motif. TIM-3 could bind to several ligands, including Galectin-9, Ceacam (carcinoembryonic antigen related cell adhesion molecule)-1, PtdSer (phosphatidylserine) and HMGB1 (High mobility group box 1), and subsequently dissociated from Bat3 suppressive binding and inhibit T cell, NK and APC activation. TIGIT binds to CD155 (higher affinity) and CD112 (lower affinity) and could compete with CD226 (co-stimulatory receptor) and CD96 (inhibitory receptor). CD226 binds to CD155 and CD112, while CD96 binds to CD155, both receptors bind to their ligands with lower affinity than TIGIT. TIGIT inhibits T cell and NK cell activation through its ITT (immunoreceptor tyrosine tail)-like and ITIM motifs (Anderson et al., 2016).

1.3.2 Immune Synapse Formation.

Naïve CD8+ T cells are small, relatively quiescent cells that circulate between lymphatic and blood vessel searching for their specific antigen. When they encounter cognate antigenic peptide presented with MHC I molecules by professional APCs (usually in the peripheral lymphoid organs), naïve CD8+ T cells slow down and stop by integrin signalling (Dustin and Springer, 1989), and form highly specialised cell-to-cell contact, referred to as an immune synapse, which induces the rapid clonal expansion and effector differentiation of the T cells. Over the next 4-5 days, 'unarmed' CD8+ T_N cells differentiate into heavily 'armed' effector CTLs that are loaded with specialized cytolytic granules. Simultaneously, these small, round CD8+ T_N cells (~5μm in diameter) increase in size to ~10μm in diameter and develop a much more sophisticated cytoskeletal apparatus, which is required to deliver cytolytic granules into the immune synapse. Once an effector CTL recognizes its target cell in the periphery, a synapse is formed again, where the cytolytic granules can be secreted within minutes. Though structurally, the synapses formed by T_N and T_{EFF} with their APCs are very similar, the purpose of these synapses is very different: naïve CD8+ T cells become primed to proliferate and differentiate into effector cells (this contact lasts for several days), whereas effector CTLs are triggered to undergo rapid degranulation towards the synapse within minutes (de la Roche et al., 2016).

1.3.3 CTL Killing via Direct or Indirect Contact.

Cytolytic degranulation by direct cell-to-cell contact can result in the destruction of the target cells. The cytolytic granules contain perforin and granzymes, which could damage the target cells' membrane as well as activate cellular death pathways. In addition, CTL could also induce the programmed cell death (apoptosis) of the target cells via death ligands (FasL), which are expressed on the surface of CTLs and could bind to the Fas receptor (CD95) on the target cells. (Barry and Bleackley, 2002) Since these molecules are highly cytotoxic, the CTLs have developed an elaborate mechanism to protect themselves as well as neighbour cells from being killed by accident. For example, CTLs do not degranulate randomly over the cell surface but only to a defined secretory domain, which is right opposite the target cell (Andersen et al., 2006).

In addition to killing via direct cell-to-cell contact, CTLs also kill target cells indirectly mediated by cytokines such as interferon (IFN) γ and TNFα. TNFα binds to its receptor on the target cell and triggers the caspase cascade, leading to the apoptosis of the target cell. IFNγ, however, induces transcriptional activation of the MHC class I antigen presentation pathway and Fas in target cells, leading to enhanced presentation of endogenous peptides by MHC class I, and increases Fas-mediated target cell lysis (Andersen et al., 2006).

1.3.4 Metabolism Reprogramming of CTLs upon Activation.

During the course of an immune response, naïve CD8+ T cells recognize antigen with proper co-signalling and become activated with subsequent rapid proliferation and production of effector molecules. The quiescent T_N and T_{CM} only require minimum energy to maintain the functions required for survival and migration; by contrast, effector CTLs have higher energy demands, because they need to proliferate rapidly and produce effector molecules (Chang and Pearce, 2016; Finlay and Cantrell, 2011). Activation of the CD8+ T cells induce the up-regulation of glucose transporters (mostly by glucose transporter 1, GLUT1), amino acid (AA) transporters and iron transporters (transferrin) at the cell surface to ensure that nutrient uptake meets the demand of metabolic and biosynthetic need of the cell (Buck et al., 2015; Fox et al., 2005). In addition, similar to cancer cells, activated T cells switch from aerobic metabolism to anaerobic metabolism for the generation of sufficient 'building blocks' for proliferation and effector functions (Wang and Green, 2012). (Figure 1-6)

Figure 1-6 Metabolic reprogramming - pathways and key regulators in activated T cells.

(A) Mitochondria-dependent catabolic pathways, including glucose oxidation through the tricarboxylic acid (TCA) cycle and β-oxidation of fatty acids, provide most of the metabolic support for basic cellular functions in naïve and memory T cells. After T cell activation, β-oxidation rapidly decreases and other metabolic pathways increase, including glycolysis and glutaminolysis. (B) Metabolic checkpoints in T cell function. F-6-P, fructose-6-phosphate; 3-P-G, glycerate-3-phosphate; Pyr, pyruvate; Lac, lactate; Glc: glucose; Gln: glutamine; Glu, glutamate; Orn, ornithine; KG: ketoglutarate; FFA, free fatty acids; OAA, oxaloacetate; PEP, phosphoenolpyruvate; P-5-C, 1- pyrroline-5-carboxylate; PHD: prolyl-4-hydroxylase; HIF: hypoxia-induced factor; STAT: signal transducer and activator of transcription AMPK: 5' AMP-activated protein kinase; PKM2: pyruvate kinase M2; TOR: target of rapamycin; PARP: poly ADP ribose polymerase; ROR: RAR-related orphan receptor; LXR: liver X receptor. Figure adapted from (Wang and Green, 2012).

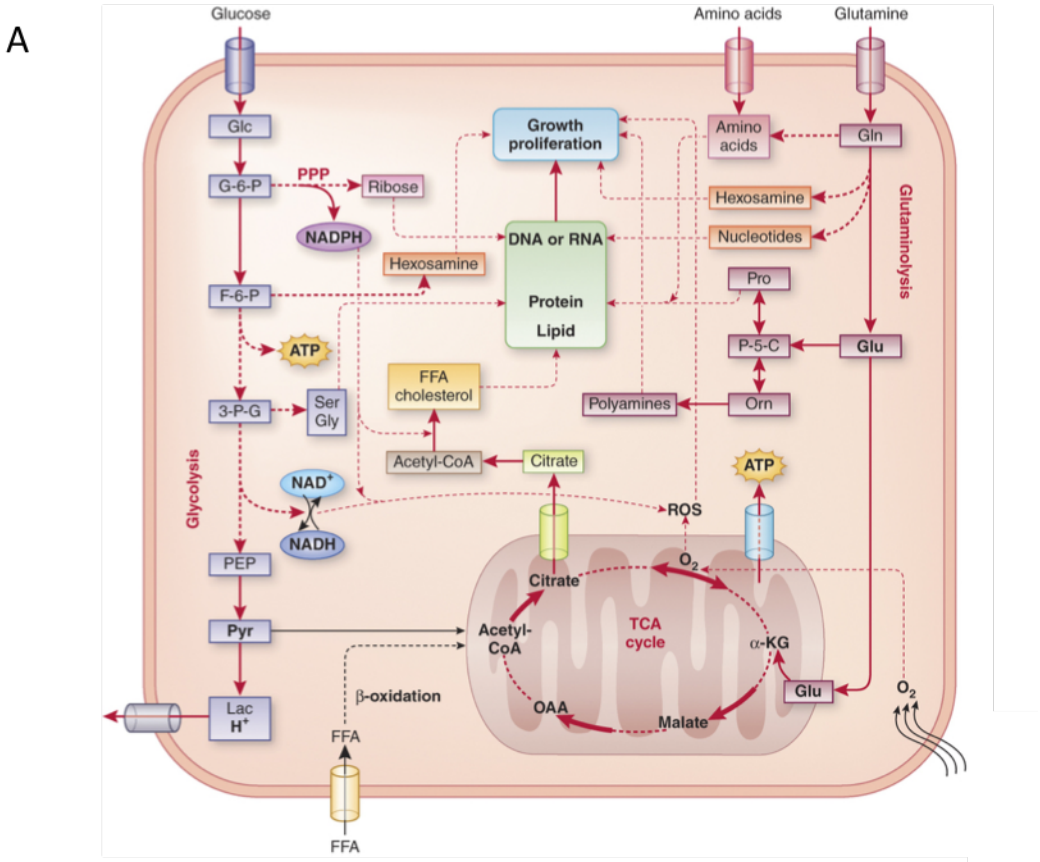
A
Glucose
Amino acids
Glutamine
Glc
G-6-P
PPP
Ribose
NADPH
Hexosamine
F-6-P
ATP
3-P-G
Ser
Gly
Glycolysis
NAD+
NADH
PEP
Pyr
Lac
H+
Growth proliferation
DNA or RNA
Protein
Lipid
FFA
cholesterol
Acetyl-CoA
Citrate
ROS
Amino acids
Gln
Hexosamine
Nucleotides
Pro
P-5-C
Glu
Glutaminolysis
Polyamines
Orn
ATP
Citrate
O2
Acetyl-CoA
TCA cycle
α-KG
Glu
OAA
Malate
β-oxidation
FFA
FFA
O2

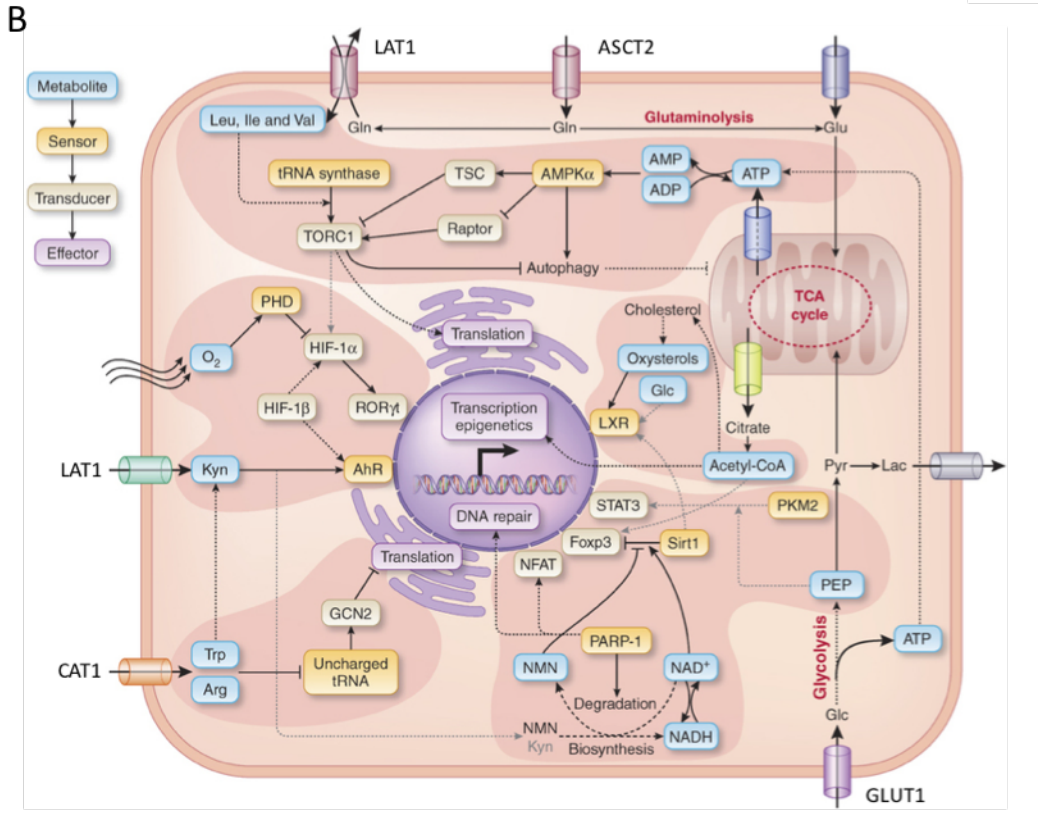
B
LAT1
ASCT2
Metabolite
Sensor
Transducer
Effector
Leu, Ile and Val
Gln
Gln
Glutaminolysis
Glu
tRNA synthase
TSC
AMPKα
AMP
ADP
ATP
TORC1
Raptor
Autophagy
PHD
O2
HIF-1α
HIF-1β
RORγt
Translation
Transcription epigenetics
DNA repair
Translation
GCN2
Cholesterol
Oxysterols
Glc
LXR
TCA cycle
Citrate
Acetyl-CoA
Pyr
Lac
LAT1
Kyn
AhR
STAT3
PKM2
Foxp3
Sirt1
NFAT
PEP
CAT1
Trp
Arg
Uncharged tRNA
PARP-1
NMN
NAD+
Degradation
NMN
Kyn
Biosynthesis
NADH
Glycolysis
ATP
Glc
GLUT1

1.4 CTL Functions in Diseases.

1.4.1 CTLs in Autoimmune Diseases.

CD8 effector T cells normally function as a protection against viruses and as eliminators of tumour cells, but could also attack self cells, when dysregulated and thus cause autoimmune diseases. In T cell-dependent autoimmune disease, there is likely to be an imbalance between T_{EFF} and T_{REG} cells, with the reduction of functional T_{REG} cells or the resistance of effector T cells to regulation increases. It could also associate with the abnormalities of the self-antigens displayed to the immune system, genetic predisposition (such as mutations in HLA genes, AIRE (autoimmune regulator) or genes regulating cytokine pathways) and environmental factors (such as infection, microbiome or traumatic insult) (Rosenblum et al., 2015).

1.4.2 CTL Responses Decide the Outcome of Viral Infections.

Viral infection occurs when pathogenic viruses invade the organism's body. CTL is one of the essential components of effective host immune responses to all viral infections (McMichael, 2003). CTL cells suppress viral replication by producing IFN-γ, lysing virus-infected target cells by the delivery of granzymes and perforin to the infected cell (which is the most rapid and usually the most important in anti-viral defence), lysing target cells via Fas–FasL interaction, and induce the apoptosis of target cells by IFNγ and TNFα.

In acute viral infections like influenza, the viruses are rapidly cleared by host immune responses and CTLs contribute to the successfully control of the viruses;

however, in chronic viral infections, like the human immunodeficiency virus (HIV) infection or the hepatitis C virus (HCV) infection, the viruses are not cleared but remain in specific cells of the infected individuals. The CTL response to control of HIV is usually unsuccessful due to the rapid emergence of escape mutations (viral escape). HIV elite controllers, many of whom have protective HLA genotypes which focus on more conserved viral epitopes, have very low plasma viral load at the beginning. In addition, their CTLs showed better suppression of HIV *in vitro* replication compared to CTLs from HIV chronic patients (Saez-Cirion et al., 2007). However, it is still under debate and the observations in our group and others (Almeida et al., 2007; Beatriz Mothe, 2012; Berger et al., 2011) have suggested that the 'quality' (*i.e.* antigen sensitivity) rather than the 'quantity' of CTLs contributes to the control of HIV viral load. Similar to HIV, HCV has a high replication rate, but lacks a proofreading mechanism; mutations are readily generated and are subject to immune selection pressure. Chronic HCV infection (up to 80% of the patients) has been associated with impaired function of HCV-specific CD8+ T cells (*e.g.* reduced secretion of IFNγ (Gruener et al., 2001)), the mechanisms of which are not completely understood but are most likely to include intrinsic regulatory pathways (such as signals mediated by the inhibitory receptor PD-1) and extrinsic regulatory pathways (such as immunoregulatory cytokines or T_{REG} cells) (Klenerman and Thimme, 2012).

1.4.3 CTL Dysfunctions in Tumour Microenvironment.

Tumour cells are those cells that grow and divide in an unregulated, rapid manner. The situation becomes malignant when the host immune system cannot control and destroy the tumour cells. Tumour antigen is an antigenic molecule produced on tumour cells, which triggers immune responses in the host. Ideally, CTLs have the capacity to eradicate tumour cells via cytolytic granules; however, in many cases in real life, these transformed tumour cells present considerable challenges that render CTLs ineffectual (Kershaw et al., 2013). The mechanistic reasons why CTLs fail to control tumour cells still remain elusive, but so far, we know tumour cells employ a variety of immunosuppressive mechanisms in the tumour microenvironment (TME), to make themselves 'invisible'. These include defects in TCR proximal signals, tumour-induced impairment of the antigen presentation machinery, the activation of negative co-stimulatory signals in TME, the elaboration of immunosuppressive factors (IL-10, TGF (transforming growth factor) -β, galectin-1, gangliosides, PGE2 (prostaglandin E2)), the activation of pro-apoptotic pathways (FasL, TRAIL (TNF-related apoptosis inducing ligand), IDO (indoleamine 2,3-dioxygenase), RCAS1 (Receptor-binding cancer antigen expressed on SiSo cells 1)), and the inhibition of DC differentiation and maturation (STAT3, VEGF (vascular endothelial growth factor), IL10, SOCS1 (suppressor of cytokine signalling 1), arginase, etc.) (Figure 1-7A) (Becker et al., 2013; Lakshmi Narendra et al., 2013; Rabinovich et al., 2007).

In both chronic viral infections and tumours, CTLs are not efficient enough to eradicate diseased cells due to the fact that CTLs are functionally impaired (*i.e.* exhaustion) (Ahmadzadeh et al., 2009; Baitsch et al., 2011; Day et al., 2006; Trautmann et al., 2006) or even erased from the circulation. The amplitude and

the quality of CTL responses are exquisitely regulated by a balance between the stimulatory signals and the inhibitory signals on a cellular level in CTLs. T cell 'exhaustion' is a T cell status defined by poor effector function, sustained expression of inhibitory receptors and a transcriptional state distinct from that of functional effector or memory T cells, which prevents optimal control of viral infections and tumours (Wherry, 2011). The current understanding of T cell exhaustion is that both extrinsic negative regulatory pathways (such as immune regulatory cytokines) and cell intrinsic negative regulatory pathways have key roles in the T cell exhaustion (Bengsch et al., 2014; Fourcade et al., 2010; Woo et al., 2012). In particular, immune checkpoint receptors (such as CTLA-4, PD-1, TIM-3, LAG-3, 2B4, BTLA and TIGIT) expressed on T cells have been identified to deliver negative signals to the cells, thus leading to T cell exhaustion and , eventually, cell death (Figure 1-7B) (Wherry and Kurachi, 2015).

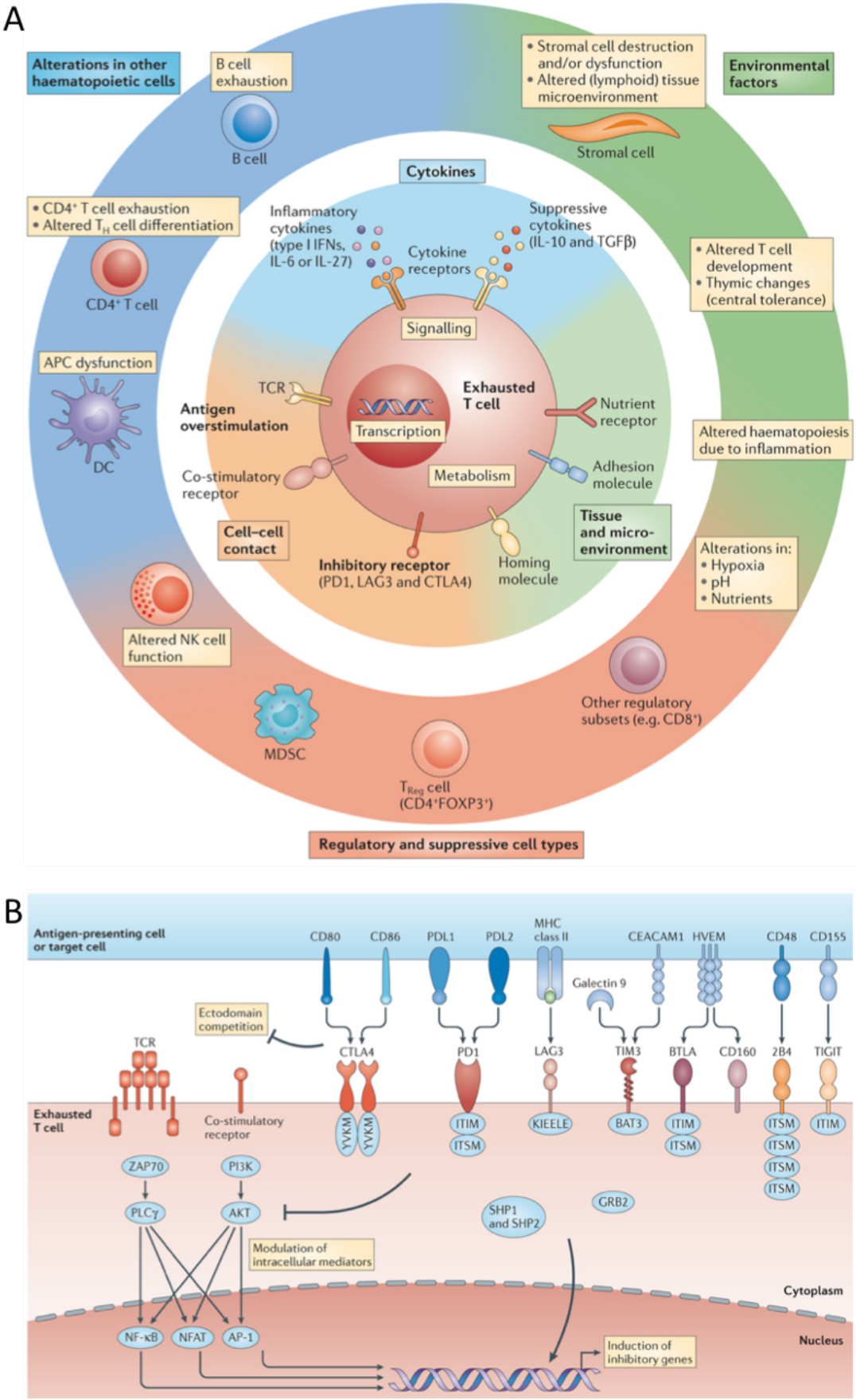

(Figure adapted from (Wherry and Kurachi, 2015)

Figure 1-7 Overview of the mechanisms of T cell exhaustion and associated inhibitory pathways.

1.5 Current Cancer Immunotherapies.

Cancer immunotherapy, which is an important part of current cancer therapy, is the use of the immune system to treat cancer. There are three main groups of cancer immunotherapy: antibody-based therapies, cell-based therapies, and cytokine-based therapies.

1.5.1 Antibody-based Immune Checkpoint Blockade/Activation.

Manipulation of the immune responses with monoclonal antibodies (mAb) has become the most successful applications in the field of the treatment of autoimmune diseases and certain types of cancer. The framework comes from the concepts of T cell co-stimulation signalling (press the gas pedal using receptor agonists) and T cell co-inhibition signalling (release the brakes via receptor antagonists) (Zhu et al., 2011).

1.5.1.1 Approved Immune Checkpoint Blockade Therapies.

The majority of the T cell co-stimulatory or co-inhibitory receptors belong to either the Ig superfamily or the TNFR superfamily. A total of around 60 Ig superfamily and TNFR superfamily co-stimulatory or co-inhibitory receptors have been identified that are expressed on T cells, providing ‘fertile ground’ for the development of therapeutic anti-cancer agonistic or antagonistic mAb or small molecules (Giuroiu and Weber, 2017). Among them, the CTLA-4 and PD-1 immune checkpoints are the pioneers. Inhibition of these targets, resulting in increased activation of the immune system, has led to new immunotherapies for melanoma, non–small cell lung cancer and other cancers. Ipilimumab, the antibody that acts against CTLA4 was approved by the FDA (US Food and Drug

Administration) for treatment of advanced melanoma, based on an observed response rate of 11% and prolonged survival in 22% of patients (Hodi et al., 2010). Since 2014, with anti-PD1 or PD-L1 therapy, more durable objective responses and extended mortality were observed (relative to conventional therapies) in approximately 31-44% of patients with advanced melanoma (Hamid et al., 2013; Robert et al., 2015a; Robert et al., 2015b; Topalian et al., 2014; Valsecchi, 2015; Wang et al., 2017), a fifth of patients with non-small-cell lung cancer (Borghaei et al., 2015; Brahmer et al., 2015; Garon et al., 2015), 22-25% of renal cell carcinoma cases (Motzer et al., 2015; Motzer et al., 2014), 26% of urothelial carcinoma cases (Rosenberg et al., 2016), 13.3% of head and neck cancer cases (13.3%) (Ferris et al., 2016) and finally, in 69% of patients who suffer from lymphoma (Armand et al., 2016). In addition, further FDA approvals are anticipated for the use of PD-1/L1 blockade in treating other cancer types (Lipson et al., 2015; Topalian et al., 2016). Furthermore, a formula that combines the use of Ipilimumab (anti-CTLA4) and Nivolumab (anti-PD1) was approved by the FDA in 2015 (Larkin et al., 2015), altogether highlighting the significant milestones achieved in implementing immune checkpoint-based immunotherapy.

The roles of CTLA-4 and PD-1 in inhibiting immune responses are distinct (Table 1-3) (Buchbinder and Desai, 2016). CTLA-4 is homologous to the T cell co-stimulatory receptor CD28. CTLA-4 and CD28 both bind to CD80 and CD86 on professional APCs like DCs; however, the inhibitory signalling molecule CTLA-4 binds with higher affinity enabling it to outcompete CD28 for its ligands and consequently ‘overwrite’ co-stimulatory immune signals with co-inhibitory signals. The CTLA-4 pathway predominantly functions during early T cell events such as priming and also plays a role in enhancing the immunosuppressive

activity of T_{REG} cells (Topalian et al., 2016). PD-1 (which is also a CD28 family receptor) binds to PD-L1 or PD-L2 to negatively regulate TCR signalling by dephosphorylating and inactivating Zap70 via SHP2 (Okazaki et al., 2001; Yokosuka et al., 2012) and down-regulating TCR expression via E3-ubiquitin ligases CBL-b and c-CBL (Karwacz et al., 2011). It is now well accepted that PD1-PDL1 is a dominant immune check point pathway within the TME, where cancer cells upregulate PD-L1 (usually induced by IFNγ) to evade immune surveillance (Table 1-3, Figure 1-8) (Topalian et al., 2016).

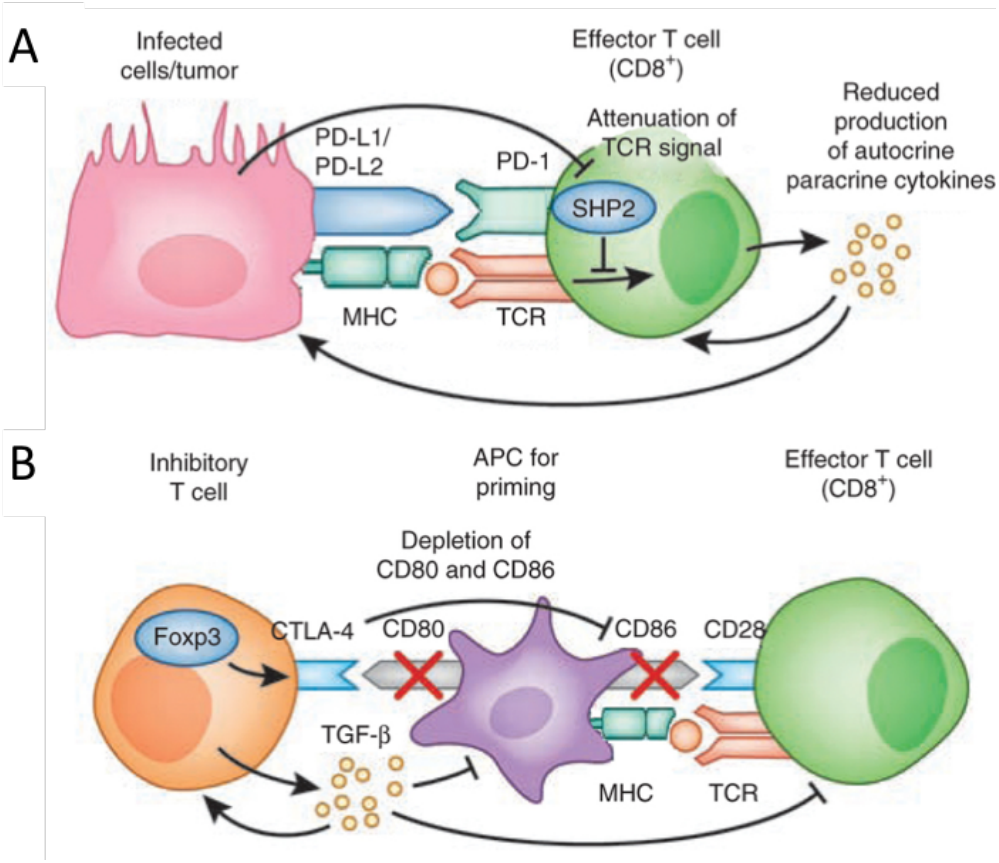

Figure 1-8 Distinct mechanisms of PD-1 and CTLA4 in immunosuppression.

(A) PD-1 controls the effector T cell functions by inducing unresponsiveness through attenuating TCR signals via SHP-2. Autocrine and/or paracrine regulation by PD-1 is also possible by inhibiting cytokine expression. (B) CTLA-4 controls, in particular, the function of activated CD4+ T cells that express Foxp3. CTLA-4 also dominantly captures CD80 and CD86 on APC and down-modulates the costimulatory activity of CD28 on CD8 effector T cells. Figure from (Okazaki et al., 2013).

Table 1-3 Distinct mechanisms of PD-1 and CTLA-4 in immunosuppression.

SIMILARITIES		
1. B7 receptor family members 2. Expressed by activated T cells 3. Level of expression affected by the strength and/or duration of TCR signalling 4. Regulate an overlapping set of intracellular T cell signalling proteins 5. Reduce T cell proliferation, glucose metabolism, cytokine production, and survival		
DIFFERENCES		
	CTLA-4	**PD-1**
Limits T cell responses	early in an immune response	later in an immune response
Location	primarily in lymphoid tissues	primarily in peripheral tissues
Expressed by	only T cells	T cells and other immune cells, such as some NK and B cells
Ligand expressed by	APCs	APCs and other immune cells, and can be inducible expressed on non-immune cells, including tumour cells
Affects T_{REG} function	yes	unclear

1.5.1.2 Future Generations of Immune Checkpoint Based Therapies

The CTLA-4 and PD-1 are only two of many checkpoints and agonistic regulatory receptors expressed on T cells. The manipulation of other co-signalling molecules in cancer patients may also be clinically beneficial. Preclinical data suggest that the greatest utility of many of these reagents will be in combination either with established checkpoint inhibitors such as PD-1/PD-L1 antibodies or CTLA-4 antibodies (Table 1-4) (Giuroiu and Weber, 2017). Promising 4-1BB-mediated therapies and combinations are designed based on augmenting NK cell and T cell functions in the TME, including combination of agonistic anti-4-1BB with tumour-targeting mAb to enhance 4-1BB expression on NK cells and their ADCC (antibody-dependent cell-mediated cytotoxicity) activity, and with immune checkpoint blockade for T cell-based killing of tumour cells by enhancing T cell tumour localization, cytotoxicity and protecting cells from

activation-induced cell death (AICD) (Makkouk et al., 2016). In addition to the substantial efforts of developing mAb to stimulate 4-1BB receptor, the successful applications of inhibitory immune checkpoint receptors have prompted intense investigations into the targeting of other co-inhibitory receptors in order to broaden the therapeutic repertoire. In particular, blocking LAG-3, TIM-3, and TIGIT alone or in combination with PD-1 blockade could rescue dysfunctional NK cell and CD8+ T cells by improving their effector functions and inhibiting T_{REG} functions (Anderson et al., 2016).

Table 1-4 Active clinical trials for immune checkpoint receptors.

Target	ClinicalTrials.gov Identifier	Description	Phase
LAG-3	NCT01968109, NCT02460224, NCT02676869, NCT02750514, NCT02658981, NCT02061761	In combination with anti-PD1 for advanced solid tumours or relapsed/refractory (r/r) B-cell malignancies	I/II
TIM-3	NCT02817633, NCT02608268	In combination with anti-PD1 for advanced solid tumours	I/II
TIGIT	NCT03119428	Alone for locally advanced or metastatic solid tumours	I
VISTA	NCT02812875, NCT02671955	In combination with anti-PD-L1/2 or alone for advanced solid tumours or lymphomas	I
A2aR	NCT02403193, NCT02655822	In combination with anti-PD-L1 or -PD1 for advanced solid tumours	I/Ib
4-1BB	NCT01471210, NCT01307267, NCT01775631, NCT02110082, NCT02252263, NCT02253992, NCT02179918,	Alone or in combination with tumour-targeting mAb or anti-PD-1 or -CCR4 for advanced solid tumours or lymphomas	I/II
OX-40	NCT02318394, NCT02274155, NCT01862900, NCT02705482, NCT02315066, NCT02410512, NCT02528357	Alone or in combination with anti-PD1 or –PD-L1 or CTLA-4 or –4-1BB in advanced solid tumours or r/r B cell lymphomas	I/II
CD27	NCT02335918, NCT02302339, NCT02543645, NCT02386111	In combination with anti-PD1 or -PD-L1 or tumour-targeting mAb in advanced solid tumours	I/II
ICOS	NCT02520791, NCT02723955, NCT02904226	Alone or in combination with anti-PD-1 in r/r peripheral T cell lymphoma follicular variant and angioimmunoblastic T cell lymphoma or advanced solid tumours	I/II

Data adapted from (Giuroiu and Weber, 2017; Makkouk et al., 2016)

1.5.2 Adoptive Cell Therapy.

Adoptive cell therapy (ACT) is a highly personalized cancer therapy that involves administration of immune cells with direct anti-tumour activity to the cancer-bearing host. Allogeneic adoptive transfer is usually referred to as donor lymphocyte infusion and autologous lymphocyte adoptive transfer is known as adoptive transfer therapy. Both of them have been used for years, while the interest in genetically modifying autologous lymphocytes has increased dramatically in recent years (Barrett et al., 2014; Dotti et al., 2014; June et al., 2009).

1.5.2.1 Overview of the Field.

Although derived from self-tissue, tumour cells can express certain tumour antigens (including tumour specific antigens (TSA) and tumour associated antigens (TAA)), which can be used to discriminate tumour cells from most normal cells. Tumour antigens can be intact on the cell surface or, in the case of cellular proteins, peptide-bound to MHC I molecule. The transfer of autologous patient T cells in the treatment of cancer has a long history that began in 1988 (Rosenberg et al., 1988), but has until recently achieved only limited success. The most successful clinical trials on ACT targeting TAA so far is the one using tumour- recognizing chimeric antigen receptors (CARs) transduced T cells (CAR-T) against haematological malignancies (Brentjens et al., 2011; Jensen et al., 2010; Kalos et al., 2011; Kochenderfer et al., 2012). The extracellular antigen-recognition domain of a CAR is typically a single-chain variable fragment (scFv) of an antibody but can also be a ligand for a receptor that is expressed on tumour cells, that is linked, via a hinge and a trans-membrane domain, to an intracellular

signalling domain. CARs can recognize TAAs without the MHC restriction, which is a distinct advantage over TCRs. The molecular hinge can lift the antigen-binding domain away from the membrane and provide flexibility for a CAR to re-orientate if necessary to bind the antigen. The intracellular domains of CARs evolve from CD3ζ or FcεRIγ (high-affinity receptor for immunoglobulin E) to include co-stimulatory signals (such as CD28 and 4-1BB) for enhancing the survival and proliferation of CAR T (Kershaw et al., 2013). Despite the observed lack of long-term persistence of CARs in most patients, impressive clinical outcomes have been observed with CARs that target CD19, with complete response rates of 70–90% reported across a range of different trials (Jackson et al., 2016). In addition, the simultaneous use of immune check point blocking antibodies with CAR-T was found to be effective in treating certain types of lymphomas (Grupp et al., 2013; Porter et al., 2011). The first reported clinical study that employed TCR transgenic T cells (TCR-T) in the treatment of cancer involved the insertion of an anti‑MART1 TCR transgene into human T cells that were isolated from patients with melanoma, where 4 of the 31 patients demonstrated sustained objective responses (Duval et al., 2006). In a similar fashion, NY-ESO-1-specific transgenic T cells have generated objective clinical responses in patients with advanced multiple myeloma (16 out of 20 patients) (Rapoport et al., 2015a), synovial cell sarcoma (4 out of 6 patients) and melanoma (5 out of 11 patients) (Robbins et al., 2011). (Figure 1-9, Table 1-5)

An exciting recent development is the use of CRISPR/Cas9 as an RNA-guided endonuclease system that provides a more affordable and direct method to edit the mammalian cell genome (Gaj et al., 2013; Kim and Kim, 2014; Sander and Joung, 2014), and has contributed to the treatment of human diseases. In 2016, the first

human trials to utilize CRISPR was initiated by a Chinese group, which injected genome-edited (PD-1 mutated) immune cells into a patient with advanced NSCLC. This ongoing trial is mainly focused on safety and will enrol 10 subjects. Moreover, combining CRISPR therapy to disrupt checkpoints to current CAR-T therapy is being studied by CAR-T developers, which may yield a better clinical outcome than receiving CAR-T therapy alone. In a recent study, CRISPR has also been utilized to facilitate CAR gene insertion into a very specific location in the genome of the T cell, which resulted in longer tumour killing action and safer profile (Eyquem et al., 2017). Currently, the performance of engineered T cell adoptive cell therapy is not optimal for all cancer types and further refinement is expected in the future. Nevertheless, significant progress has been made in the field. New technologies, including CAR-T, TCR-T and CRISPR/Cas9, are undoubtedly represent significant progress and are going to revolutionise the field of current cancer therapies in the foreseeable future.

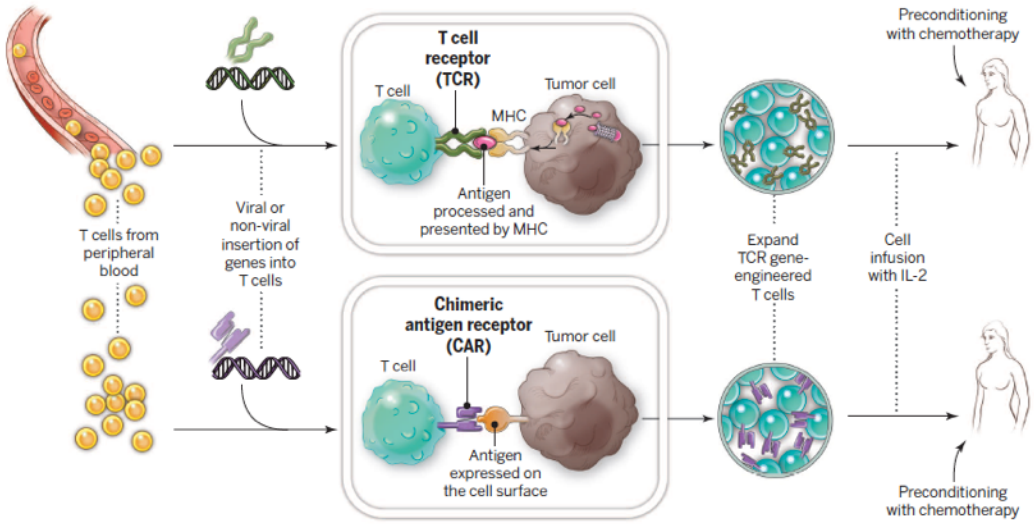

(Figure from (Rosenberg and Restifo, 2015).)

Figure 1-9 Scheme of generating gene-engineered T cells for cancer therapy.

Table 1-5 Clinical trials of ACT for cancer treatment.

Cells for ACT	Target	Cancer Type	Description
Tumour infiltrating lymphocytes	-	Melanoma, cervical cancer	▪ since 1998 ▪ 9-93 patients ▪ 33-56% OR rate
In vitro sensitization	NY-ESO-1, WT-1	Melanoma, leukaemia	▪ 9-11 patients ▪ 33% OR rate
CAR T	CD19, GD2, BCMA	Lymphoma, ALL, CLL, neuroblastoma	**Blood cancer** ▪ 1-30 patients ▪ 67-100% OR rate **Solid tumour** ▪ 11 patients ▪ 27% OR rate
TCR-T	NY-ESO-1, MART-1	Synovial sarcoma, melanoma	▪ 6-11 patients ▪ 45-67% OR rate

OR: objective response*, Modified from (Rosenberg and Restifo, 2015)*

1.5.2.2 Gene Delivery Techniques Used for Adoptive Cell Transfer.

Various technologies, viral or non-viral, have been developed to introduce foreign nucleotides into human T cells (Figure 1-20), a major challenge of which is the difficulty with which genetic manipulation can be achieved with high efficiency and preservation of T cell proliferation and viability. Canonical transient transfection methods, including lipofection, polyethylene glycol and calcium phosphate, work poorly on human T cells and could cause lymphocyte apoptosis (Ebert et al., 1997). Electroporation-based transfection has been widely used on many types of human T cells with an efficient transfection, but was usually accompanied by significant cell death. Transducing human T cells with retroviruses, on the other hand, provides a more rapid and efficient approach, although it carries the risk of unfavourable mutagenesis. So far, electroporation and retroviral transduction produce the highest efficiency of nucleotide delivery into human T cells (Agosto et al., 2009; Bilal et al., 2015; Chicaybam et al., 2013).

Electroporation is a technique in which an electrical field is applied to cells to transiently increase the permeability of the cell membrane, allowing small or large molecules to be pulsed into the cell. It was first utilized to deliver foreign nucleotides into eukaryotic cells in 1982 (Neumann et al., 1982), and has been continuously optimized. The Lonza Nucleofection system, one of the most commonly used methods for the delivery of siRNAs or plasmids into primary T cells, consists of a proprietary device, cell type-specific solutions and optimised electroporation programs for the delivery of siRNAs or plasmids into cells. The system can transfect primary human cells in mesenchymal stem cells (Hamm et al., 2002) and also many other primary cells (Gresch et al., 2004). Loss of cell viability is the common issue with electroporation method and results from the high voltages that transiently permeate the cell membrane. Therefore, the transfection programs have been optimized by developers and other scientists (Freeley and Long, 2013; Liu et al., 2011). According to the manufacturer, the recommended nucleofection programs of Nucleofector for the delivery of siRNAs/plasmids into primary human T cells are T20 and T23, with a transfection efficiency of 40% and 55% respectively, excluding dead cells.

As a matter of fact, gene transfer to T lymphocytes has historically relied on viral-based gene transfer. For example, CD4+ T cells targeted therapy has focused on disrupting CCR5 or CXCR4 via lentivirus to confer on the cells resistance to HIV (Agosto et al., 2009; Yi et al., 2014). Manipulations of CD8+ T cells with transgenic CARs or TCRs delivered by retrovirus or lentivirus has provided new strategies to treat different malignancies (Grupp et al., 2013; Porter et al., 2011; Rapoport et al., 2015b; Robbins et al., 2015).

Retroviruses are single-stranded positive-sense RNA viruses that possess the ability to reverse-transcribe their sequences into DNA, which are ultimately incorporated into the host genome. Because of their capacity to efficiently integrate into the human genome, leading to persistent gene expression with relatively low toxicity, some laboratory-modified replication-deficient retroviral vectors have been utilized in clinical trials for the gene therapy to treat some human diseases such as inherited genetic disorders (Brenner and Malech, 2003; Charrier et al., 2007). One significant drawback of γ-retroviral vectors is their inability to transduce non-proliferating cells, as the transportation of viral pre-integration complex into the nucleus requires the breakdown of the nuclear membranes during mitosis (Miller et al., 1990; Roe et al., 1993). To overcome this shortcoming, vectors based on lentiviruses, a subtype of retroviruses derived from HIV-1, were developed (Naldini et al., 1996). These vectors are capable of transducing non-dividing and quiescent cells, although progression through cell cycle is necessary for some cell types like human T cells (Korin and Zack, 1998). A primary concern over the use of viral vectors is biosafety. Five cases of leukaemia have been reported from two X-linked severe combined immunodeficiency (SCID-X1) trials via retrovirus-mediated gene transfer into autologous CD34 bone marrow cells (Hacein-Bey-Abina et al., 2003; Howe et al., 2008), while two cases of myelodysplasia occurred in a clinical trial for X-linked chronic granulomatous disease (X-CGD) (Stein et al., 2010). In contrast, clinical trial based on lentiviral vector appears to be safe, none of the five patients in an X-CGD clinical trial developed leukaemia in the following five years (De Ravin et al., 2016). Compared to γ-retroviral vectors, lentiviral vectors showed reduced genotoxicity (Montini et al., 2006). Firstly, the lentiviral vectors deleted viral LTR

enhancer elements to form self-inactivating (SIN) vectors; this modification results in lower viral titre for γ-retroviral vectors, but not for lentiviral vectors. Secondly, lentiviral vectors integrate somewhat randomly throughout the entire genome, while the γ-retroviral vectors preferentially interact with active host cell promoters and enhancers—regions that are enriched for transcription factor binding sites and cancer-related genes (Felice et al., 2009). Furthermore, viral accessory genes, which are associated with virulence, have been eliminated from the vector genome and genes on the packaging plasmid have been further separated on to two plasmids to improve safety (Costello et al., 2000). VSV-G (Vesicular stomatitis virus - G glycoprotein) has been used for pseudo-typing lentiviral vectors due to its broad tropism, allowing entry of viral particles into most of the cell types. However, unstimulated primary T cells are significantly less receptive to VSV-G pseudotyped lentivirus. Several factors like low levels of nucleotide in the resting T cells or lack of ATP-dependent nuclear import (Agosto et al., 2009; Bukrinsky et al., 1993b; Frecha et al., 2008; Korin and Zack, 1999) may contribute to this phenomenon. Thus, current T cell transduction protocols usually activate G_0 T lymphocytes prior to lentiviral transduction to transit cells from G_0 to G_{1b} thus relieving those blocks. Nevertheless, activating cells through TCR and CD28 alters the natural physiology of the target cells, skews the cell population to a memory phenotype and may affect their immune competence. Otherwise, exposing T cells to cytokines, such as IL7, that do not trigger cell division could increase the permissiveness of the cells for the transduction with HIV-1-vectors (Unutmaz et al., 1999). On top of that, modifications are constantly being made to improve human T cell transduction method, including incubation of viruses and target cells in the presence of polycations, co-centrifugation of viruses

and target cells, and co-localisation of viruses and target cells on the extracellular matrix molecule fibronectin or similar protein (Lamers et al., 2002).

1.5.3 Cytokine-based Immunotherapy.

Cytokines are a large and very heterogeneous family of small and generally soluble glycoproteins that regulate nearly all biological functions via autocrine, paracrine or endocrine circuitries. It is noteworthy that three cytokines are currently licensed by the FDA and equivalent regulatory agencies worldwide for use as immune-stimulatory interventions in cancer patients, the recombinant IFN-α 2A, the recombinant IFN-α 2B and the recombinant IL-2. Recombinant IFN-α 2A is employed for the treatment of HCV infections, hairy cell leukaemia and Philadelphia chromosome positive chronic myelogenous leukaemia (CML); recombinant IFN-α 2B is approved for use in patients with follicular non-Hodgkin's lymphoma, malignant melanoma, hairy cell leukaemia, AIDS-related Kaposi's sarcoma, genital warts and HCV infections; and recombinant IL-2 is employed for the therapy of metastatic forms of melanoma and renal carcinoma. In addition, the recombinant granulocyte colony-stimulating factor (G-CSF), the recombinant granulocyte monocyte colony-stimulating factor (GM-CSF) and the recombinant TNF are approved by various regulatory agencies worldwide for use in cancer patients. These molecules are not employed to boost tumour-targeting immune responses, but rather as immune-reconstituting (G-CSF, GM-CSF) or onco-toxic (TNF) factors (Vacchelli et al., 2016).

2 Chapter 2: Materials and Methods.

2.1 Regents.

2.1.1 Peptides.

The following peptides were purchased from Sigma Aldrich or synthesized by WIMM (Oxford, UK) using FMOC protection on an automated synthesizer (Zinsser. California. USA).

AF9: B*2705/HCV.NS5B.2831-2849 ARMILMTHF

FL8: B*0801/HIV.Nef.90-97 FLKEKGGL

GL9: A*0201/Flu-M1.58-66 GILGFVFTL

GL9 (EBV): A*0201/EBV-BMLF1.280-288 GLCTLVAML

KV9: A*0201/SSX-2.41-49 KASEKIFYV

NV9: A*0201/CMV-pp65.495-503 NLVPMVATV

RI11: DRB1*0901/Flu-H3HA.345-354 RGIFGAIAGFI

2.1.2 Monoclonal Antibodies.

PD-1 (APC), PD-L1 (APC) IFN-γ (PE-Cy7), TNF-α (APC), CD107a (PE), CD3 (APC-H7), CD25 (FITC), SLC3A2 (FITC), 4-1BB (PE), 4-1BB (PE/Cy7), CD4 (PerCP), CD4(FITC), CD8 (PerCP) and CD8 (BV650) antibodies were purchased from BD Biosciences; IL-2 (BV421), TIM-3(BV421), CRTAM (APC), PD-1 (Purified), Mouse IgG1 Isotype (Purified) were purchased from BioLegend; PD-L1(Purified), Mouse IgG K Isotype Control (Purified) were purchased from eBiosciences; LIVE/DEAD® Fixable Dead Cell Stain Kits was obtained from Life Technologies; a series of TCR Vβ-PE antibodies was obtained from Beckman Coulter; anti-GAPDH, anti-actin were obtained from Millipore UK;

Goat anti-Mouse IgG and Goat anti-Rat IgG were obtained from Li-Cor Biosciences.

2.1.3 p-MHC I tetramers.

The HLA-A*0201-GILGFVFTL, HLA-A*0201-GLCTLVAML and HLA-A*0201-NLVPMVATV monomers used were synthesized and biotinylated by Dr. Yanchun Peng. ln brief, the HLA molecule heavy chain cDNAs were obtained from EBV-transformed B-cell-lines from healthy donors. Specific primers were used to amplify the extracellular region of the HLA heavy chain and incorporate a biotinylation signal sequence for enzymatic addition of biotin to the C-terminus of the heavy chain. The PCR product was cloned and expressed using heavy chain transformed E. coli. The heavy chain protein was purified and refolded with β_2m and the CTL epitope to form a monomer complex. The refolded product was concentrated, enzymatically biotinylated, and purified by gel filtration using a FPLC machine (Pharmacia) and Superdex-75 column. The monomer complex was concentrated and protease inhibitors added. Tetrameric complexes were formed by the slow addition of 1 molar PE coupled extravidin (Sigma) to four molars of monomer complex using a simplified working ratio of 0.312mg of extravidin PE for 1 mg biotinylated monomer.

2.1.4 Plasmids.

pX330: pX330-U6-Chimeric_BB-CBh-hSpCas9 was a gift from Feng Zhang (Addgene plasmid # 42230) (Cong et al., 2013) and pL-CRISPR.SFFV.GFP was a gift from Benjamin Ebert (Addgene plasmid # 57827) (Heckl et al., 2014). pMD2.G (Addgene plasmid # 12259) and psPAX2(Addgene plasmid # 12260)

were gifts from Didier Trono. EX-U0767-Lv105 for overexpressing PD-L1 was purchased from GeneCopoeia.; Sigma CRISPR Lenti non-targeting control vector, Sigma CRISPR lentivector for genes of interests were purchased from Sigma.

2.2 Molecular Experiment.

2.2.1 CRISPR/Cas9 plasmid/lentivector construction.

- sgRNA design off-target settings: PAM type NRG; core length: 2; max core mismatches: 2; max total mismatches: 3 or 4
- HLA-A*02 sgRNA

  CCTTGCCGTCGTAGGCGTACTGG (designed by CBRG CRISPRscreen, Oxford)
- PD-1 sgRNA #1

  CACC GGCGCCCTGGCCAGTCGTCT (SIGMA designed and verified sgRNA targeting exon 1, no extra bases since guide already starts with double G). reverse – AAAC AGACGACTGGCCAGGGCGCC
- PD-1 sgRNA #2

  CACCGGACGAAGCTCTCCGATGTGT (SIGMA designed and verified sgRNA. However, different to SIGMA, it is designed to let it start with a double G, and reconstituting full length to 21 bb, leaving out the initial C that has also been omitted by SIGMA, and adding the 0 position extra G as suggested by Feng Zhang.

  reverse – AAAC ACACATCGGAGAGCTTCGTCC

- DNA oligos were synthesized from Sigma Aldrich (smallest amount, no special purification) with respective overhangs (underlined) as in the following example. The sgRNA must start with a 'G' that serves as the transcriptional initiation for the U6 Promoter. If the target site does not naturally start with a 'G', add a 5'G. Some very efficient sgRNAs have been generated that way strongly indicating that the additional 5'G does not disturb the targeting. Avoid poly-T stretches (four or more) since 5xT serves as RNA-Pol-III termination signal.

Primer Phosphorylation

Sense Primer (100µM)	1µl
Antisense Primer (100µM)	1µl
T4 DNA Ligase buffer	1µl
T4 PNK	0.5µl
H_20	6.5µl
Total	10µl

PCR Programme

37°C	45min
95°C	2:30min
cool down at 0.1°C/s to 22°C	pause

Vector Digest

2µg vector	x µl
2µl FastDigest buffer	2 µl
1µl FastDigest Esp3I	1 µl
2µl DTT (10mM)	2 µl
H_20	x µl
Total	20µl

- Incubate at 37°C for 45min. Then add 1ul of FastAP and incubate for an additional 15min. Gel purify the vector.
- Ligation, dilute annealed and phosphorylated Oligo 1:500 in H20.

Ligation Reaction

~30-50ng vector	x µl
Annealed & phosphorylated Oligo duplex (1:500)	1 µl
T4 DNA Ligase buffer	0.5µl
T4 DNA Ligase	0.5µl
H20	x µl
Total	5µl

- Set up one additional ligation without inserting oligo as control. Incubate according to manufacturer's instructions. In general, 1-2 hrs at RT yields good results.
- Transformation into competent E. coli (Top10, DH5α)
- Plasmids were purified by miniprep and confirmed by sequencing.

2.2.2 Genomic DNA Preparation.

A total of 2×10^5 cells re-suspended in 100 µl of Quick Extraction solution (Epicenter, Illumina, UK) were added to lyse the cells and extract the genomic DNA. The cell lysate was incubated as below and stored at −20°C. The concentration of genomic DNA was determined by NanoDrop (Thermo Scientific).

genomic DNA Extraction Programme

65 °C	20min
95 °C	20min

2.2.3 PCR, TA TOPO Cloning and Sanger Sequencing.

PCR were carried out using Taq PCR Master Mix Kit (Qiagen, UK) or Kapa HiFi HotStart ReadyMix Kit (Roche, UK) according to manufacturer's instruction. In brief, genomic regions containing the PD-1 target sites (5′- GGC GCC CTG GCC AGT CGT CTG GG -3′) were PCR-amplified using forward primer 5′- CCG ACC CCA CCT ACC TAA GA -3′ and reverse primer 5′- GGG CGG GAT ATG GAA AGA GG -3′ (amplicon size is 452bp). The PCR products were then purified using QIAquick PCR Purification Kit (Qiagen). 4µl of purified PCR products were cloned into TOPO TA vector according to manufacturer's instruction (Invitrogen, UK). Competent cells were transformed with the ligation product and were cultured on LB/ampicillin agar plate O/N at 37°C. Colonies were validated by colony PCR, selected colonies were inoculated from the plate to LB medium with ampicillin and were shake at 200rpm/37°C O/N. Plasmids were purified usingmini Prep Kit from Qiagen for sequencing (Source Biosciences, Oxford, UK).

PCR reaction component

Template (gDNA)	200ng
Sense Primer (10µM)	2.5µl
Antisense Primer (10µM)	2.5µl
Mater or Ready Mix (2X)	25µl
H_20	Xµl
Total	50µl

PCR programme (Qiagen Tag MaterMix):

94 °C	3min

94 °C	45s
55 °C	45s
72 °C	1min
Go to step 2	X34
72 °C	10min
4 °C	∞

PCR programme (KAPA HiFi HotStart):

95 °C	10min
98 °C	20s
68 °C	15s
72 °C	1min
Go to step 2	X34
72 °C	10min
4 °C	∞

2.2.4 T7E1 Cleavage Assay.

Genomic regions containing the PD-1 target sites (5′- GGC GCC CTG GCC AGT CGT CTG GG -3′) were PCR-amplified with KAPA HiFi HotStart ReadyMix PCR Kit (Roche) according to manufacturer's instruction.

Forward Primer: CCGACCCCACCTACCTAAGA;

Reverse Primer: GGGCGGGATATGGAAAGAGG.

The PCR products (452bp) were then purified using QIAquick PCR Purification Kit (Qiagen). Purified PCR products were then used for T7 endonuclease I (NEB), in brief, buffer 2 and 5 units of T7 endonuclease I (NEB) were added to digest the reannealed DNA. After 1 h of incubation at 37 °C, the reaction was quenched with gel loading dye (Thermo Scientific) at 70 °C for 10min. The product was resolved on 2% agarose gel containing SYBR gold (Life Technologies). Expected

digestion bands are 375bp and 77bp. The DNA band intensity was quantitated using Fiji ImageJ. The percentage of editing was calculated using the following equation

$$\text{editing } \% = \left[1 - \sqrt{(1 - \frac{b + c}{a + b + c})}\right] \times 100\ \%$$

where a is the band intensity of DNA substrate and b and c are the cleavage products.

2.2.5 HLA Typing.

HLA Class I and II molecular typing was performed by the amplification refractory mutation systems PCR (ARMS-PCR) by Tim Rostron (WIMM, Oxford, UK), using sequence-specific primers (Bunce et al., 1995). 144 allele specific primer pairs simultaneously detect all known HLA-A, B, C, DRBI, DRB3, DRB4, DRB5 and DQB1 specificities. PCR products from each individual reaction including the internal positive control, a 796bp fragment from the third intron of HLA*DRBl are visualized following electrophoresis on a 2% agarose gel, in a process known as "phototyping". This gives absolute HLA typing to 2 digits and a high probability resolution to 4 digits.

2.3 Gene Expression Arrays.

2.3.1 Magnetic Separation, RNA Extraction and Quality Control.

CD4+ T cell line (C8166) pulsed for one hour at 37°C with 0μM, 0.001μM, 0.01μM, 0.1μM, 1μM or 10uM epitope (FL8) was used as targets. CD8+ CTL clones (5 x 10^6) from three separate batches of re-stimulation (biological replicates) were mixed with targets at 10:1 ET ratio in 24-well plates and separated after 6h of co-culture at 37°C /5% CO_2. The supernatant was harvested and frozen immediately at -80°C for cytokine analysis. The cells were washed with R10 at 1500rpm 5min, the supernatant aspirated and the cells re-suspended in 1ml PBS. The cells were spun (up to 10M total cells) down again and re-suspended in 80μl of MACS buffer (PBS, pH7.2, 0.5% BSA and 2mM EDTA) with 20μl CD8 Microbeads (Milteny Biotec, UK) added, mixed well and incubated for 15min on ice. The cells were washed again by adding 1-2 ml of MACS buffer at 1500rpm 10min and then re-suspended in 500μl buffer. Place Columns were placed in the magnetic field of octoMACS separator, the columns prepared by rinsing with 500μl buffer and cell suspension applied onto the column. Unlabelled cells were discarded and the columns washed thrice with 500μl buffer. The columns were removed from the separator and placed on a suitable collection tube. 1.5ml buffer was pipetted onto the column, the magnetically labelled cells flushed out immediately by firmly pushing the plunger into the column and the cells were collected. (Figure 2-1A) Isolated CD8 cells were counted and RNA extracted from equal cell numbers using RNeasymini Kit (Qiagen, Crawley, UK). And RNA quality and quantity was measured using Agilent Bioanalyzer TapeStation (Agilent Santa Clara, USA) (Figure 2-1 B,C).

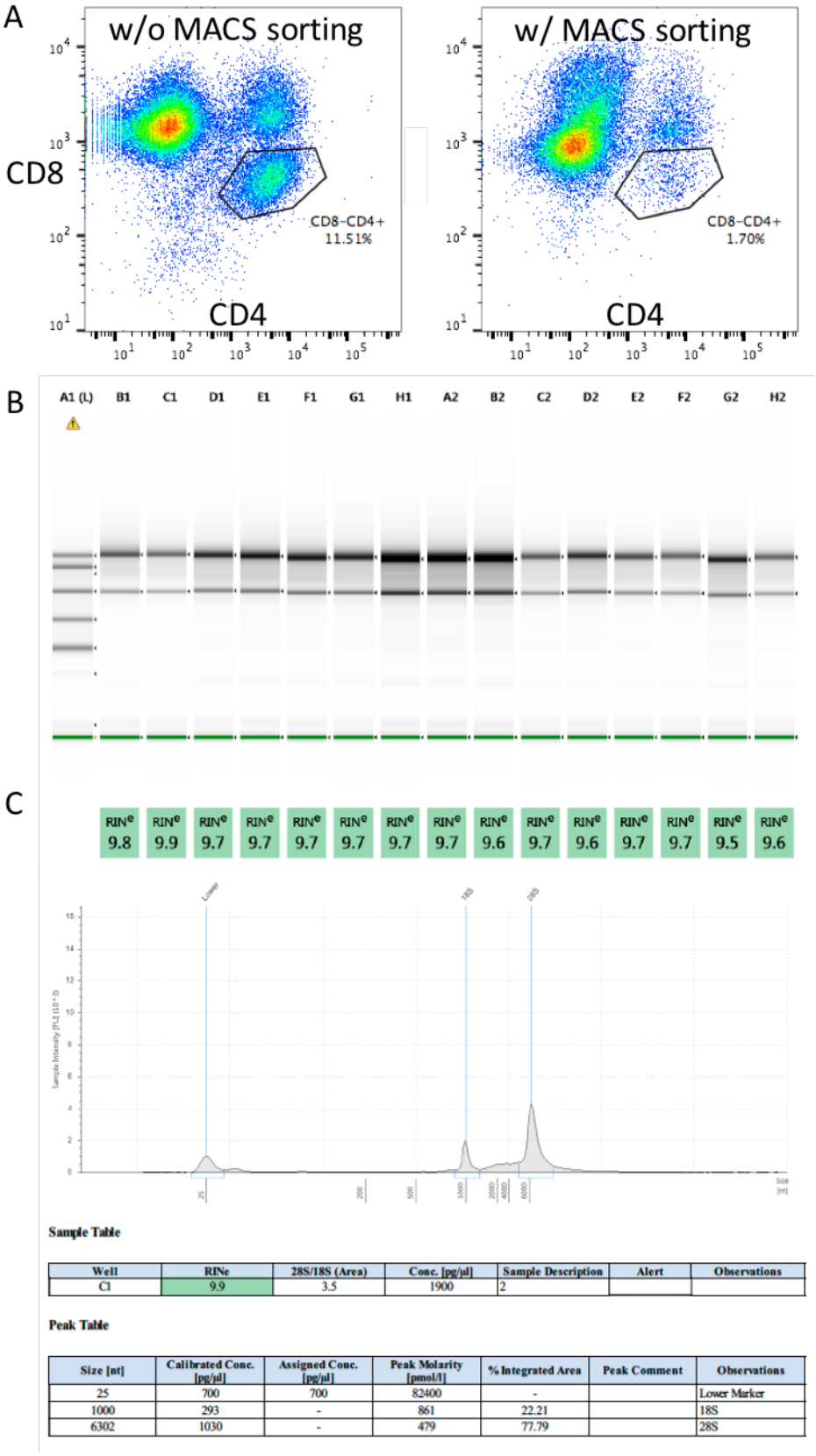

Figure 2-1 MACS separation, RNA extraction and quality control.

(A) Representative FACS plot of cells before and after MACS separation. (B) Representative RNA quality checked by BioAnalyzer Tape Station. (C) Detailed RNA electrophoresis of sample C1. RIN, RNA integrity number.

2.3.2 Gene Expression Profiling.

Samples were analysed for gene expression using Human Bead Chip HT12 chips (Illumina) by Dr Dilair Baban. Samples were amplified using the Illumina "total Prep-96 RNA Amplification Kit" (Applied Biosystems) prior to hybridization onto Chips. Chips were scanned with Illumina BeadArray Reader and GenomeStudioV2010.l (Illumina Inc) was used for data extraction.

2.3.3 Data Analysis.

Data was analysed by Dr. Dilair Baban. Data was imported to GeneSpring OX 1 1.0.2 (Agilent Technologies), normalized with Shift to 75 percentile and baseline transformed to median of all samples to identify significantly differentially expressed genes, which were then interrogated using PANTHER (Mi et al., 2013). Data was also analysed by Mr. Steve Taylor, Computational Biology Research Group (CBRG), WIMM, University of Oxford. Normalization was achieved using the LUMI package in R (Du et al., 2008). Genes with altered expression were detected using an empirical Bayes analysis approach, as implemented in the LIMMA package of the R programming language (Ritchie et al., 2015). PCA (principal component analysis) plot was compiled by Dr. Ben Wright in the Wellcome Trust Centre for Human Genetics (WTCHG). Hierarchical clustering and ANOVA (Analysis of variance) was performed in MeV 4.8.1. (Saeed et al., 2003) Venn diagrams were drawn using InteractiVenn. (Heberle et al., 2015) Gene ontology (GO) classifications were analysed by using pantherdb.org. (Mi et al., 2017)

2.4 Cellular Experiment.

2.4.1 Preparation of Peripheral Blood Mononuclear Cells.

Blood was taken from median cubital vein of healthy donor to vacutainer (BD-Plymouth, UK) by trained phlebotomist. Whole blood was carefully layered on Ficoll-Hypaque (Sigma-Aldrich, UK) and centrifuged without braking for 23min at 2000rpm. Peripheral blood mononuclear cells (PBMCs) were carefully collected and washed twice with RPMI-1640 medium (Sigma-Aldrich, UK) by centrifuging for 10min at 1500rpm. PBMCs were then re-suspended in R10 (RPMI-1640 medium, with 10% foetal calf serum (FCS) (Sigma-Aldrich, UK), 2mM L-glutamine (Sigma-Aldrich, UK), 50 U Penicillin/Streptomycin (Sigma-Aldrich, UK) per ml).

2.4.2 EBV-transformed B Lymphoblastoid Cell Lines (B-LCL).

One million PBMCs were washed with R0 and spun down at 1500 rpm for 5min and re-suspended in 100µl of EBV supernatant. After 3h incubation at 37°C/5% CO2, 100µ1 of R15 (RPMI-1640 medium, with 15% FCS, 2mM L-glutamine, 50 U penicillin/streptomycin per ml) containing 2µg/ml cyclosporine A (CsA, Sandimmun) was added and the cells were transferred into 5 wells of a round bottom 96-well plate. At Day2, supernatant was replaced with 100 µl fresh media (CsA in R15). Two weeks later, CsA was omitted and the cells were cultured with R10.

2.4.3 Maintenance of CD4+ Cell Line, B-LCL and 293 TLA Cell Line.

The C8166 human T-lymphoblastoid cell line stably expresses HLA B*08 and was obtained at no charge from the National Institute for Biological Standards and Control (NIBSC), Jurkat E6 T cell line and TLA-HEK293T cell line (293TLA) were kindly given by Dr. Mei-Yi Sun (WIMM, Oxford, UK). Suspended cells were cultured in R10 in T75 flask at 37°C/5% CO_2. 293TLA cells were cultured in D10 medium (DMEM medium, with 15% FCS, 2mM L-glutamine, 50 U penicillin/ streptomycin per ml) at 37°C/5% CO_2, and were split about every 3 days using Trypsin-EDTA solution (Sigma Aldrich, UK) according to manufacturer's instructions. All cell lines were routinely screened for mycoplasma (negative).

2.4.4 Establishment of CTL Lines and Clones.

Cytotoxic T lymphocyte (CTL) lines were generated as previously described (Dong et al., 1996). Briefly, PBMCs were stimulated with specific peptides at 2μM. Cells were cultured in H10, and on day 3, cells were fed with H10 with 100U/ml recombinant human interleukin-2 (IL-2) (Peprotech, UK). CTL clones were generated as previously described (Dong et al., 2004) by limited dilution from sorted cells (such as tetramer positive and CD8 positive CTL lines, HLA-A*0201 negative and CD8 positive CTL cells) and co-cultured with 0.1 million feeders (a cell mix of PBMCs from at least three healthy donors) in H10 with 50 μg/ml PHA (Oxoid, UK) in a round-bottom 96-well plate. On day 3, cells were fed with H10 with 100U/ml IL-2. On day 14, cells were expanded using feeders again.

2.4.5 T Cell Transfection.

T cell transfection was carried out using Human T Cell Nucleofector Kit (Lonza, UK) with a Nucleofector I according to manufacturer's instructions. In brief, 1 million cells were washed and re-suspended in 100µl nucleofection medium containing 1µg plasmid, before being pulsed and immediately transferred and cultured in H10 with IL-2 in a 96-well U-bottom plate.

2.4.6 Beads-based T Cell Activation.

The Dynabeads Human T-Activator CD3/CD28 (Thermo Scientific, UK) was re-suspended in the vial by vortexing for 30s and the desired volume of Dynabeads was transferred into a 1.5 ml tube, with the addition of 1 ml R0 and vortexed for 5 s. The tube was placed on a magnet for 1min and the supernatant discarded. The tube was removed from the magnet and the washed Dynabeads re-suspended in the same volume of culture medium as the initial volume of Dynabeads taken from the vial. Dynabeads Human T-Activator CD3/CD28 was added at a bead-to-cell ratio of 1:1, supplemented with 100 U/ml rIL-2 and incubated for 24h, before checking T cell surface activation marker.

2.4.7 Pseudotype-viral Particle Construction and T Cell Transduction.

A replication incompetent recombinant lentivirus was generated using the three plasmids system by co-transfection of 293TLA cells. A DNA mix composed of 150ng CRISPR/Cas9 inserted lentiviral vector, 100ng packaging plasmid (psPAX2) and 40ng envelop plasmid (pMD2.G) per cm^2 was used. After 48hrs, supernatant was collected and filtered by 0.45µm syringe filter, and concentrated by Lenti-X™ Concentrator (Clontech) according to manufacturer's instruction. To

determine the viral titres, 1×10^5 Jurkat cells were spin-transduced with serially diluted lentivirus preparations in R10 medium in the presence of 6 μg/ml polybrene (Sigma-Aldrich) at 1,000g at 32°C for 2h, and then incubated at 37 °C for 48h. The cells were then fixed with 1% formaldehyde. The transduction efficiency was quantified by evaluating the infected cells for GFP expression by flow cytometry.

$$Viral\ Titre = \frac{(Number\ of\ Cells) \times [Frequency\ of\ GFP{+}ve\ Cells]}{Volume\ of\ Supernatant\ in\ (ml)} \times (Dilution\ Fold)$$

1×10^5 cells per well of T cell clones or lines were added to U-bottom 96 well plate and centrifuged at 1,000g at 32°C for 2h with viral particles at desired MOI in R10 medium with 6μg/mL polybrene. The cells were then cultured in H10 medium with 100U/ml rIL2 for 3 days prior to be checked by FACS.

2.4.8 *ex vivo* IFN-γ Enzyme-Linked ImmunoSpot (ELISpot).

MultiScreen filter plate (MAIP S45, Millipore, MA) was coated with 15 μg/ml anti-IFN-γ capture antibody (Mabtech, Sweden) and incubated at 37°C for 1 hour or 4°C O/N. The plate was washed six times with 200μl/well RPMI 1640 and blocked at 37°C for 1 hour in 200μl/well R10. For CTL lines or CTL clones, 400 CTLs and 20,000 peptide-pulsed target cells were put into each well. The plate was then incubated at 37°C and 5% CO_2 O/N before being washed with 200μl/well PBS. 50μl of 1μg/ml biotinylated anti-IFN-γ mAb was added to each well and the plate was incubated at RT for 2h before being washed with 200μl/well PBS. 50μl streptavidin-conjugated alkaline phosphatase antibody (Mabtech, Sweden) was added to each well and the plate was incubated at RT for 45min before being washed with 200μl/well PBS. The plate was developed using

an alkaline phosphate conjugate substrate kit (Bio-Rad laboratories, USA) and the spots were read using an AID ELISpot reader (Autoimmune Diagnostika GmbH, DE).

2.4.9 Setting up T Cell Intracellular Staining.

Antigen-specific T cells were stimulated with peptide-pulsed HLA-matched target cells in an effector to target (E: T) ratio of 1:1 with the presence of anti-CD107a, 0.7 μg/ml Monensin (BD Biosciences), 10 μg/ml Brefeldin A (BD Biosciences) in R10 medium for 4 h at 37°C. Negative controls included un-stimulated cells.

2.4.10 FACS Analysis of T cells.

For each staining, cells were stained with LIVE/DEAD® Fixable Dead Cell Stain Kit (Thermo Scientific) for 20min first. If tetramer staining was required, cells were then stained with homemade tetramer for 30min at 37°C as previously described (Dong et al., 2007). The surface staining was performed with conjugated antibodies for 20min. If intracellular staining was required, cells were then fixed in Cytofix/Cytoperm^{TM} (BD Biosciences) for 20min before being stained with conjugated antibodies in 1X Perm/Wash buffer (BD Biosciences) for 20min. Cells were kept on ice throughout the staining procedure, except tetramer staining to minimize antibody-mediated internalization and degradation of the antibody. Cells were then fixed with Cell Fix solution (BD Biosciences) and acquired on Cyan^{TM} (Beckman Coulter) or Fortessa^{TM} (BD Biosciences) flow cytometer. Cell sorting followed the same procedure with surface staining, but cells were not be fixed. Stained cells were kept in culture medium on ice and

sorted on FACS Aria III (BD Biosciences) with help from Craig Waugh (WIMM, Oxford, UK). FCS files were then transferred and analyzed using FlowJo™ 10.

Panel 1 Immune Check Points Phenotyping

Marker	**Fluorophore**	**Manufacturer**
CD3	BV785	BD
CD4	APC-Cy7	BD
CD8	PerCP-Cy5.5	BD
CD14	BV510 (Dumping)	BD
CD19	BV510 (Dumping)	BD
CD56	BV510 (Dumping)	BD
Aqua L/D staining	BV510 (Dumping)	Life Technologies
Tetramer	PE	Home-made
TIM-3	BV421	BioLegend
CTLA-4	PE-Cy7	BioLegend
PD-1	BV650	BD
TIGIT	FITC	BD

Panel 2 Cytokine Intracellular Staining

Marker	**Fluorophore**	**Manufacturer**
CD8/CD4	APC	BD
CD107a	PE	BD
IL2	BV421	BD
TNFα	BV650	BD
IFNγ	PE-Cy7	BD
GFP	FITC	-
Aqua L/D staining	BV510	Life Technologies

2.4.11 Western Blotting.

Cells were counted and lysed in RIPA buffer (Sigma Aldrich, UK) with protease inhibitor cocktail (Roche, DE). Protein concentrations were measured by BCA Protein Assay Kit (Novagen, UK) according to manufacturer's instructions and NuPAGE Sample Buffer (4X) and NuPAGE Reducing Agent (10X) were added to each sample before electrophoresis. NuPAGE Running Buffer (20X), NAGE Gel, NuPAGE Transfer Buffer (20X) were bought from Life Technologies. Proteins were transferred onto Immobilon membrane, before 1 hour RT blocking in TBST with 5% milk, 4°C O/N incubation in the first antibody and 1 hour RT incubation in the second antibody. The bands of protein were acquired by Odyssey machine (Li-COR, USA) and the quantification was done using Fiji software.

2.4.12 Cytokine Bead Array (Luminex Multi-plex System).

Supernatant from the co-culture of CTL clones and peptide-pulsed target cells were harvested after O/N incubation, and cytokines were measured by Luminex cytokine bead array analysis according to the manufacturer's instructions (Bio-Rad Laboratories, USA). Luminex is a flow cytometry-based assay, which combines a capture sandwich immunoassay for each molecule with a unique fluorescently dyed bead allowing simultaneous detection of up to 100 molecules. In brief, the antibody against the molecule of interest is coupled to an internally dyed bead. Coupled beads were incubated with the supernatant sample, standards (Range 0 to 32 000 pg/ml) and blanks in a 96-well filtration plate (Millipore, USA) for 30min at room temperature on a plate shaker at 300rpm. The beads were

washed to remove unbound protein using a vacuum manifold and incubated with biotinylated anti-cytokine-detection antibodies. A streptavidin-PE reporter complex was added for 10min to bind the detection antibody on the bead surface. Beads were washed and collected on a Luminex 100 IS System (Bio-Rad Laboratories).

2.4.13 Data Analysis.

SPICE (Simplified Presentation of Incredibly Complex Evaluations) (Roederer et al., 2011) was used to subdivide cells into subsets by differential combinations of protein expression, to plot the complex multi-dimensional data.

viSNE algorithm was applied to *ex vivo* antigen-specific T cell data, which is a program that reduces high dimensional flow cytometric data into 2-dimensional scatter plot while maintaining the structure of cells. Its core algorithms were to visualize high-parameters data in multiple fields, known as t -Distributed Stochastic Neighbour Embedding (t-SNE), as described in the paper. (Amir el et al., 2013)

FACS data analysis was performed with Flowjo^{TM} 10 and Prism 7 (Graphpad, San Diego, USA) was used for data presentation.

2.5 Statistical Analysis.

Statistical analysis of the data was performed using Prism 7 (Graphpad, San Diego, USA), MeV 4.8, R or Excel. Statistical differences between groups were determined using the two-tailed unpaired student's t test. *p*-values below 0.05 were considered as significant. Significantly altered expression of genes was analysed using the LIMMA package for R and corrected for multiple comparisons. *p*-values below 0.05 were considered significant. Statistically significant differential gene expression was also analysed using the one-way Analysis of variance (ANOVA) and corrected for multiple comparisons. *p*-values below 0.05 were considered significant.

3 Chapter 3: Correlation of Antigen Sensitivity to T Cell Function – Genetic and Functional Evaluation of Cytotoxic T Cell in Response to Different Strengths of Antigen Stimulation

3.1 Introduction.

Antigen-experienced CTLs are important in controlling viral infections and cancers (Tscharke et al., 2015). CTL cells suppress viral replication by secreting IFN-γ, lysing virus-infected or tumour cells (target cells) directly by degranulation or Fas–FasL interaction (IFN-γ also up-regulates Fas expression on target cells), and inducing the apoptotic pathways in target cells by IFNγ and TNFα (Andersen et al., 2006). Maintaining key functions of CTLs in the body (such as proliferation, killing, cytokine production) requires different strengths of the stimulation (Au-Yeung et al., 2014; Gett et al., 2003).

Antigen processing and presentation is a complicated process, but is the key determinant of T cell priming, immunodominance and T cell functionalities (such as killing, exhaustion and proliferation). However, it is not clear from the molecular mechanisms as to how the strength of the stimulation determines the functionality of the T cells. The amount of epitopes presented to T cells depends upon the individual protein levels in the cells, proteasome cleavage, peptidase digestion, transporter, HLA type, affinity of MHC binding and peptide/MHC complex binding to T cell receptor and many more factors. The antigen sensitivity to each individual epitope peptide varies, which is one of the key determinants affecting the quality of the T cells in our body (Almeida et al., 2009; Appay et al.,

2008). In chronic viral infections and cancers, the antigen stimulation to T cells is persistent, but the strength of the stimulation could differ significantly at different stages of the disease (McMichael et al., 2010). This is largely due to the complicated micro-environment at T cell acting site, amount of antigen available and the amount of epitope peptide presented to the T cells: all of which in combination determine the T cell proliferation and killing. Therefore, understanding the optimal dose of antigens required for individual T cell function (*i.e.* amount of antigen required for up-regulation of individual functional regulators, cytokines release and immune checkpoint receptors) are important and could provide valuable insights into clinical applications on the treatment of viral infections or cancers and the vaccine design.

As more than 65% of the genome is active in one or more immune cell types, with only about 1-2% of the genes expressed exclusively in a given type of cell (Hyatt et al., 2006), studying the heterogeneous immune cell population could miss many items of information that can only be identified by investigating at clonal or single-cell level. In addition, fixation of the framework on classic immune-related genes attracts the risks of missing out other less-known genes that also contribute to relative functions, which could lead to simplified paradigms. Thanks to the development of genome-wide approaches allowed by gene-expression microarrays and related techniques, the transcriptome can be reliably tackled in its entirety (Heng and Painter, 2008). Although the techniques are 'blind' to some aspects of cellular regulation, such as epigenetic change, signalling transduction and intracellular compartmentalisation, the evaluation of steady-state amounts of coding mRNA provides a direct representation of all

transcripts and splice variants, demonstrating the genome's global activity (Hyatt et al., 2006).

The characteristics of an effector CTL in response to a given antigen are influenced by many factors such as the nature and abundance of antigen, the cells that present the antigen, the regulatory environment and the CTL itself. These controversial factors make *in vivo* study technically difficult. For example, it is obvious that the abundance of antigen available to a given CTL population will influence the final magnitude of its response. However, due to the complexity of the context and technical difficulty of the analysis (at the level of the APC and T cells), there are very few clear demonstrations of such types of study (Tscharke et al., 2015). The availability of a population of human CD8 cytotoxic T lymphocytes deriving from the same progenitor with a unique phenotype and function (clone) and a homogenous population of APCs may therefore be very helpful. Functional study of *in vitro* cultured T cell clones limits the variable factors, including the source of APCs, the nature of the T cells and the amount of antigen load, effector cell to target cell ratio as well as the time of stimulation. CTLs can recognize the peptide-MHC I displayed on all the somatic cells. It has been reported that as few as 1 agonist peptide-MHC molecules, in a sea of thousands of self-peptide-MHC molecules, can trigger T cell activation and cytokine productions (Huang et al., 2013). Interestingly, MHC I molecule downregulation occurs frequently in many cancers, which limits the amount of antigen that can be presented to tumour-specific CTLs and has been found to be associated with poor prognosis (Hicklin et al., 1999). Not to come singly but in pairs, *Nef* protein in HIV-1 can down-regulate the MHC I expression on the

infected CD4+ T cells (Akari et al., 2000). Thus, it seems that the abundance of antigen presented to CTL, to some extent, plays a key role in the outcome of CTL killing. Comparing of T cell responses between low dose and high dose antigen stimulation therefore provides clues to understanding the CTL key regulator genes and pathways.

3.1.1 The Aim of This Chapter.

In this Chapter, we aimed to study the functional impact on cytotoxic T cells with different strengths of antigen stimulation.

Specific aims:

1. To study the global gene expressions and to identify changes at transcript level on the homogenous CTL clones that receive different amount of antigen stimulation, which could mimic the activation of CTLs when encountering the cognate antigen.
2. To focus on the genes that can be up-regulated or down-regulated at low antigen dose and how they might relate to the function of the T cells. As in tumour micro-environment (TME), due to down-regulation of MHC- I, it is likely the amount of tumour antigen presented on cancer cells is low, leading to suboptimal antigen presentation. In this situation, the triggered CTL effector functions may not be enough to eliminate the cancer cells but enough for T cell to survive and proliferate;
3. To focus on the genes that could only be induced or suppressed at high dose antigen stimulation. CTL receives potent stimulation, triggers fully activation and becomes highly cytotoxic.

By studying these gene expression changes, we could understand more about the gene regulations of CTL activation, thus providing insights for future T cell based therapy and vaccine design.

3.2 Results.

3.2.1 Cytotoxic T Cell Clones Used for This Study.

Antigen sensitivity of cytotoxic T cells varies with each individual epitope peptide, and is depends largely on the epitope sequencing, binding affinities of peptide to MHC and TCR to p-MHC complex. In order to avoid these key confounding factors which would affecting the later data analysis of T cell functional profiling in T cells upon stimulation, we used T cell clones where identical TCRs expressed and with same epitope peptide presented by same HLA.

Two well-characterized representative clones were chosen for this study. The CTL clone A3 was generated by Prof Tao Dong from the PBMC sample of an HIV-1 long term non-progressor (LTNP005) (Dong et al., 2004), is specific to FL8 (HIV.Nef.90-97 FLKEKGGL) and restricted by HLA-B8. It has an intermediate antigen sensitivity (avidity) among the sister clones generated from the same patient. The other one is a HCV epitope-specific CTL clone C23, which was generated by Dr Yanchun Peng from the PBMC sample of SM197, an HIV-HCV co-infection patient. This clone is restricted by the epitope AF9 (B*2705/HCV.NS5B.2831-2849 ARMILMTHF). The antigen-sensitivities of these two clones are quite different; A3 exerts half maximum lysis potency or of producing IFNγ at about 0.025μM peptide stimulation (Figure 3-1A), while C23 exerts half maximum IFNγ at about 1μM. (Figure 3-2A) (10μM was set as the epitope concentration to trigger the maximum events) The functionalities of cytokine productions and degranulation were further explored for each clone. (Figure 3-1B and Figure 3-2B)

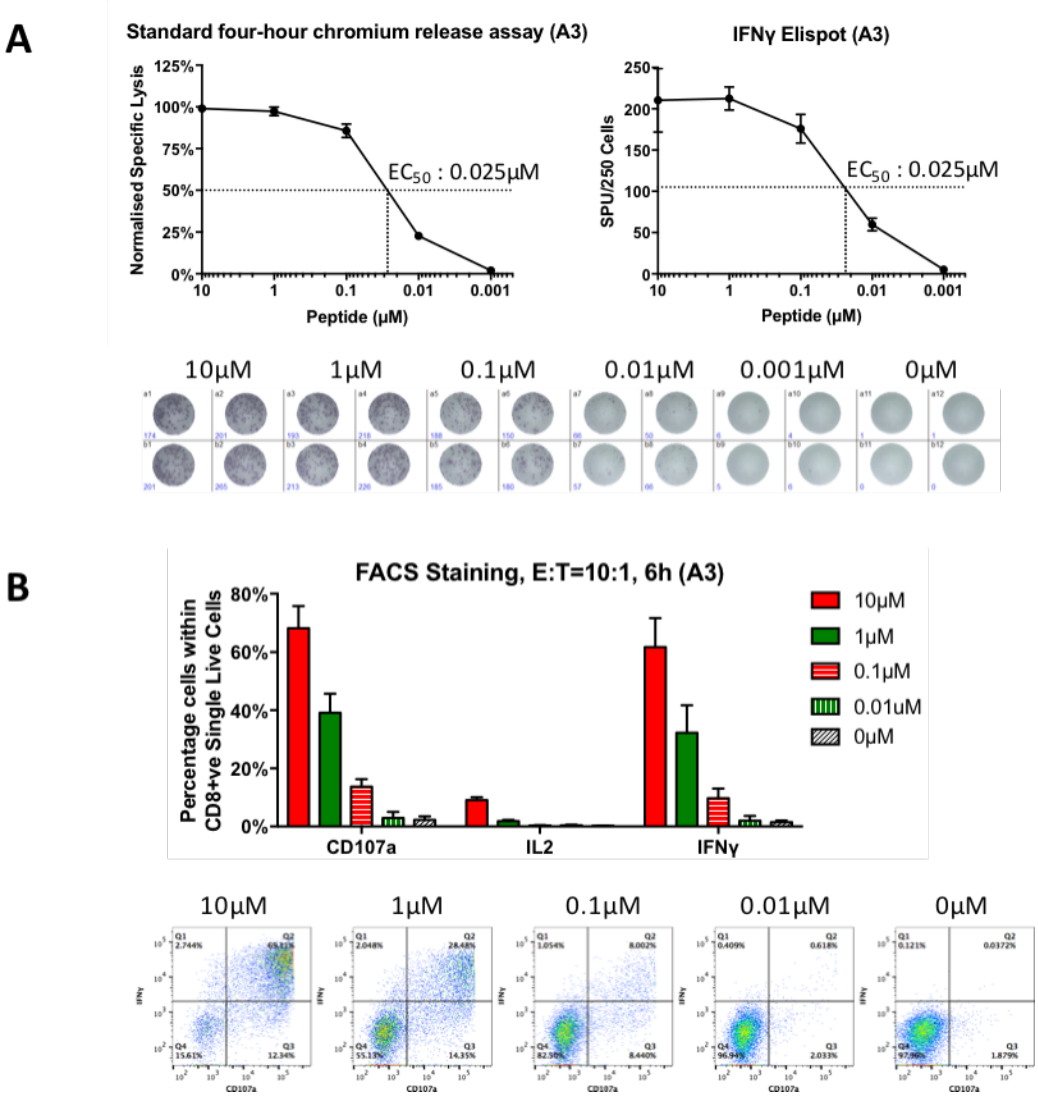

Figure 3-1 Functional studies of CTL clone A3.

(A) Standard four-hour chromium release assay (left, data generated by Prof Tao Dong) and IFNγ Elispot (right) were used to determine the sensitivity (EC_{50}= peptide concentration (μM) for 50% maximal lysis or SPU) for A3 CD8 CTL clone. Effector-to-target (E:T) ratio 3:1. SPU: spot forming units. (B) ICS was performed following 4h incubation (10:1 ratio) with peptide pulsed HLA-B*08+ CD4+ T cell line C8166 cells (10μM, 1μM, 0.1μM, 0μM) in the presence of Golgi Stop/Plug. Cells were stained for surface CD107a and intracellular IL2 and IFNγ, and gated on live, single CD8+ cells. (n=3) The representative FACS plots (x-axis CD107a, y-axis IFNγ) are shown below the bar chart.

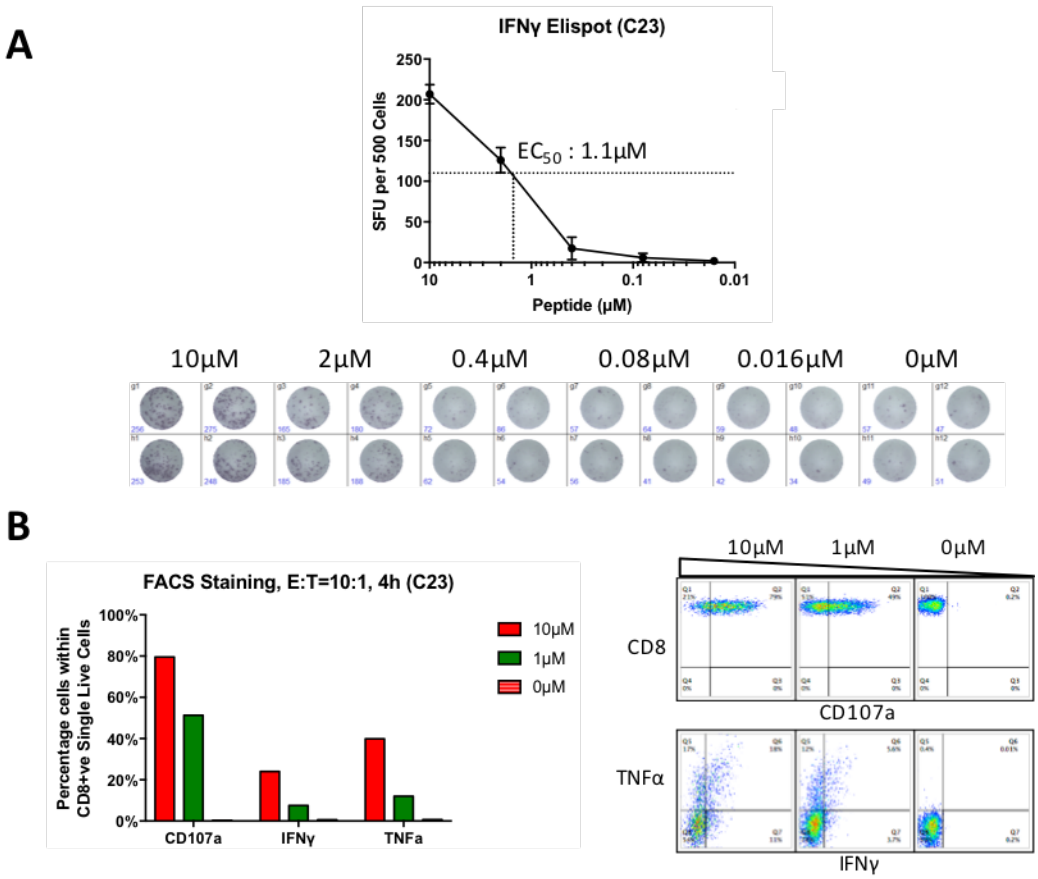

Figure 3-2 Functional studies of CTL clone C23.

(A) IFNγ Elispot assay was used to determine the antigen sensitivity of clone C23. SPU: spot forming units. (B) Left: ICS was performed following 4h incubation (10:1 ratio) with peptide pulsed autologous EBV transformed B cells (10μM, 1μM, 0μM) in the presence of Golgi Stop/Plug. Cells were stained for surface CD107a and intracellular IFNγ and TNFα, and gated on live, single CD8+ cells. The FACS plots are shown next to the bar chart.

Table 3-1 Sequence analysis of the CDR3 regions of the TCR α- and β-chains of the CTL clones.

Clone	Vα	CDR3	Jα	Vβ	CDR3	Jβ
A3	26-1	CIVRAPGRADMR	44	6-2	CASSYLPGQGDHYSNQPQH	1-5
C23	4	LVGEGQQAGTALI	15	4-1	ASSFTTPGTRYEQY	2-7

Ex vivo activation, with the simultaneous analysis of multiple parameters of HIV-1 specific CD8+ T cells with 2uM peptide for 5.5h has been reported to correlate with viral load (Betts et al., 2006). Similar evaluation assays have been used to monitor vaccine efficacy, as one of the best available approaches (McElrath et al., 2008). Although the signalling transductions from the TCR happen in a very short time (within a few minutes) on a CTL, cellular functions such as metabolic changes, proliferation or apoptosis take hours to take place. One possible way to increase the likelihood of 'capturing' critical genes related to CTL functions, is to collect RNA samples at 2h, 4h and 6h and pool them together in equal parts for transcriptome profiling (Safford et al., 2005). However, both RNA-seq and microarray data indicate that gene differential expressions at 6h after T cell activation are greater than those at 2h and 4h, although similar to 24h and fewer than 72h (Zhao et al., 2014). As we were trying to characterize the different gene expressions (correlated to functions) for a CTL receiving different dose of antigen stimulation, later transcriptomes would be complicated owing to the influences from the secreted cytokines and nutrient depletions in the medium. Thus, the total RNAs were extracted for microarray at 6h post CTL-antigen encounter to allow the cells to transcribe new mRNAs in response to antigen stimulation. CTL co-cultured with target cells only (no antigen added, mock stimulation) were also harvested as the control group to represent the baseline global transcriptome.

3.2.2 Quality Control of Microarray Expression Data.

The Microarray project comprised 36 samples hybridized to Illumina Human HT-12 Expression BeadChip, which provides genome-wide transcriptional coverage of well-characterized genes, gene candidates, and splice variants; each array on the Human HT-12 Expression BeadChip targets more than 25,000 annotated genes with more than 48,000 probes. For clone A3, three batches (biological replicates) of A3 cells (5 million T cells for each group) were stimulated with 10μM, 1μM, 0.1μM, 0.01μM, 0.001μM (10-fold dilution) or no peptide (FL8) pulsed HLA-matched CD4+ C8166 T cell line. For clone C23, cells were stimulated with 2μM, 0.4μM, 0.08μM, 0.016μM, 0.0032μM (5-fold dilution) or no peptide pulsed autologous BCLs. The differences in peptide concentration and dilution fold were due to previous experiment design, nevertheless, the A3 and C23 were from two individuals and the antigen specificity, sensitivity, TCR subtype of the clones and the APCs used for experiment were also completely different. Thus, it is not possible to make a direct comparison between the two clones. However, common candidate genes identified on both clones could be more meaningful than comparing two CTL clones from the same individual. Figure 3-3 shows the technical and sample metrics of the 36 samples. All the samples gave good overall signal, and the housekeeping gene signal was very high, as expected. No individual sample gave any cause for concern based on these metrics.

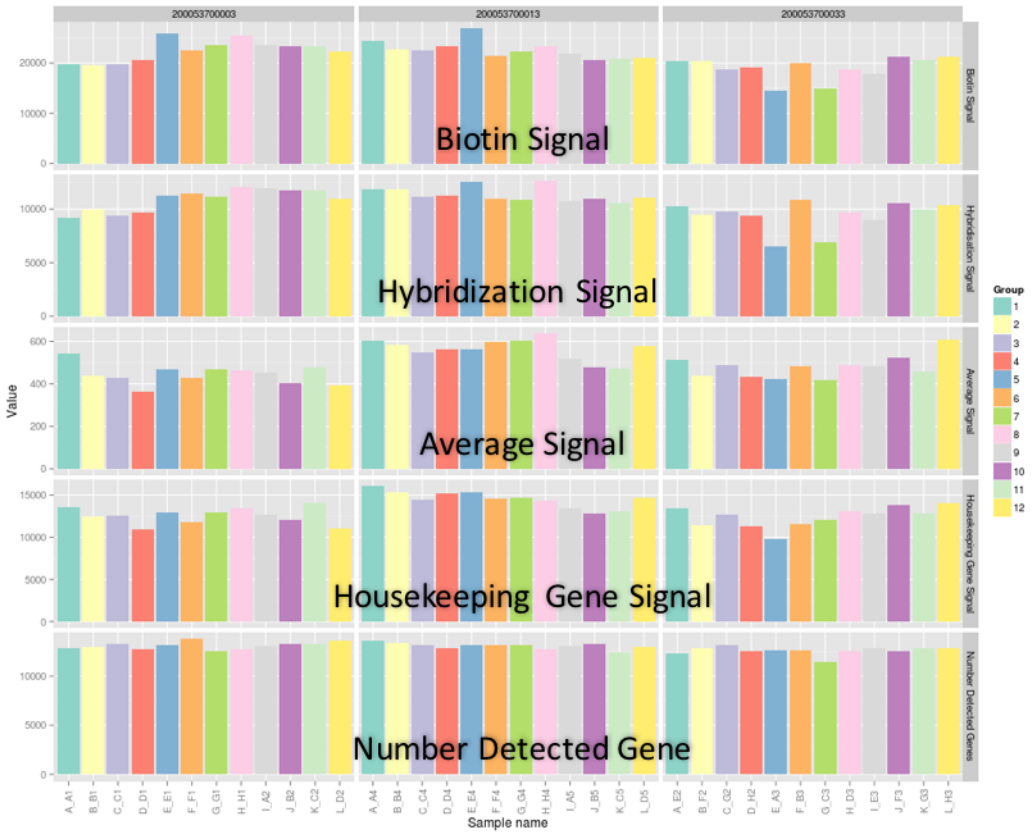

Figure 3-3 Technical and sample QC metrics.

The QC metrics show the samples ordered by chip and position (A-L) and coloured by the groups listed in the sample sheet. The control probes for biotin and hybridization (rows 1&2) are sample-independent and gave consistently high signal, indicating that the experimental steps were successful. The sample-dependent plots of average signal intensity and signal from housekeeping genes are shown in rows 3&4. Any variability here can be attributed to several different factors (sample quality, labelling efficiency, amount of material loaded, etc.) and should largely be corrected by normalization. The number of detected genes (row 5) is also consistently high. Group 1-6: clone C23, dose high to low: 2μM, 0.4μM, 0.08μM, 0.016μM, 0.032μM, 0μM; Group 7-12: clone A3, dose high to low: 10μM, 1μM, 0.1μM, 0.01μM, 0.001μM, 0μM.

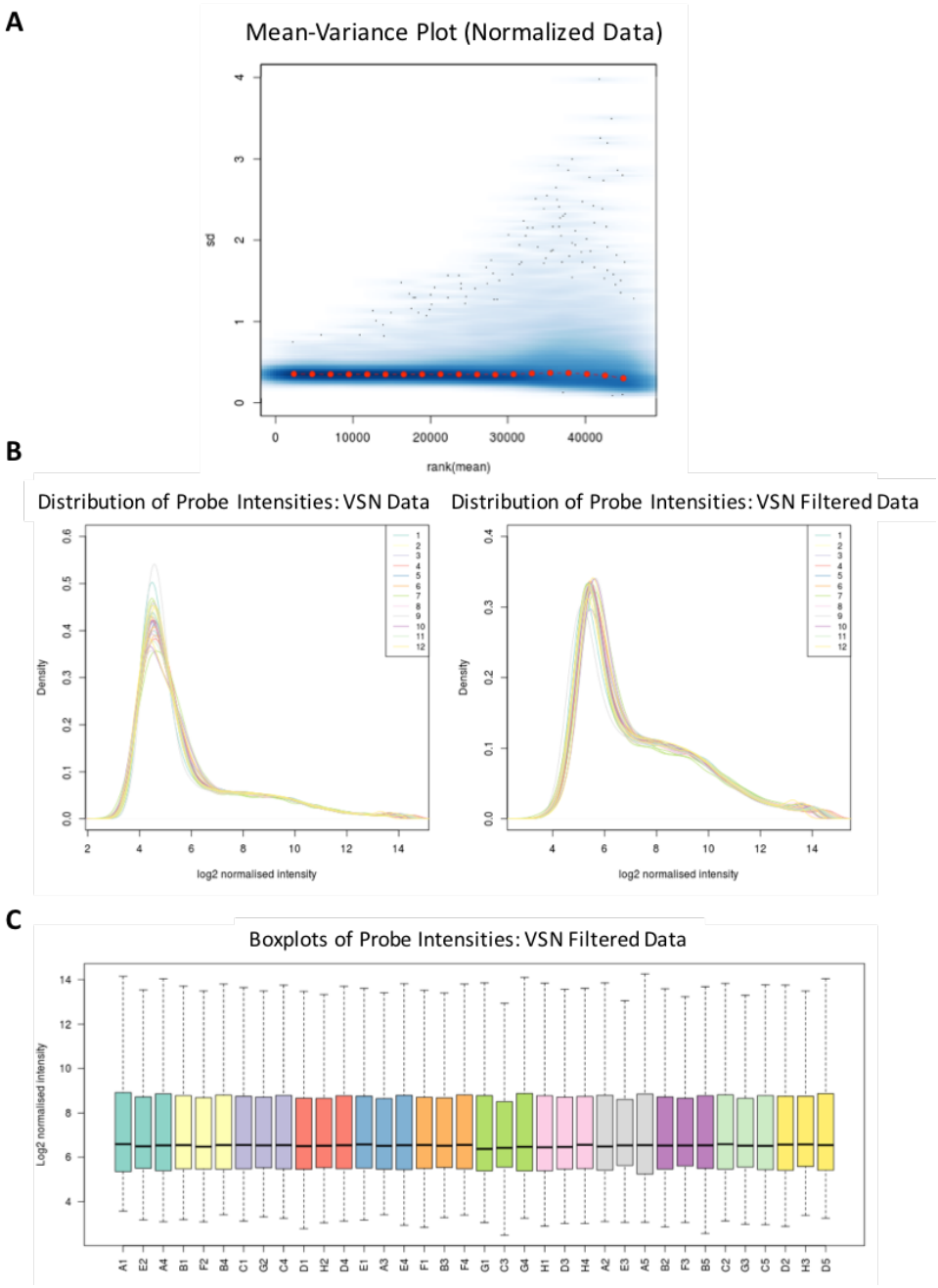

Figure 3-4 Data pre-processing and exploratory QC plots.

(A) VSN (variance-stabilisation and normalisation) algorithm was used to process raw data from Illumina gene expression arrays, which performs two main steps to make the data suitable for further analysis: (i) stabilises the variance to better meet the assumptions of the statistical test for differential expression and (ii) normalises signal intensities from different samples so that they are comparable. After this step, the intensities are on the log2 scale. (B) The distribution of probe intensities (VSN normalized data) can be visualized for each sample as density plots (left shows data for all the 47,231 probes; right shows data for 20,657 probes after filtering to remove probes detected in fewer than 3 samples). (C) The filtered data is also shown as boxplots.

The raw data from Illumina gene expression arrays was first processed using the VSN (variance-stabilisation and normalisation) algorithm. The mean-variance plot was expected to show approximately constant variance across the entire intensity range; in the other words, the red dots should be roughly in a straight line. The assessment we obtained here was with very good results (Figure 3-4 A). We then generated further Quality Control (QC) plots to explore various features of the data, looking at overall data quality, potential outlier samples and the main sources of variation. The profile for the probe intensity distribution is characteristic of high quality data and the samples are highly consistent with each other (Figure 3-4 B and C).

Hierarchical clustering (Figure 3-5) and PCA (principal components analysis) (Figure 3-6) were used to identify outlier samples and assess the main factors influencing the expression profile (e.g. experimental condition or technical factors such as batch or chip). The samples formed two very distinct lines, separated primarily by PC1 (x-axis), dividing the groups into 1-6 (C23) and 7-12 (A3), similar to the clustering plots previously. Within each of these arms, there was a gradient along PC2 (y-axis), which was more pronounced at the beginnings of each arm (Group 1: C23-2μM, Group 2: C23-0.4μM and Group 7: A3-10μM, Group 8: A3-1μM, Group 9: A3-0.1μM). As the sequential numbering of the groups represents a continuous experimental variable, there is strong evidence that the variable (antigen stimulation strength) affects gene expression.

To summarise, all technical aspects of the experiment worked well and no outlier samples were identified. High quality data was obtained and the clustering patterns were strongly linked to the antigen stimulation strength. The groups were

separated into two distinct branches of the experiment (two CTL clones, C23 and A3), and there was strong evidence of a gene expression gradient along each of these arms.

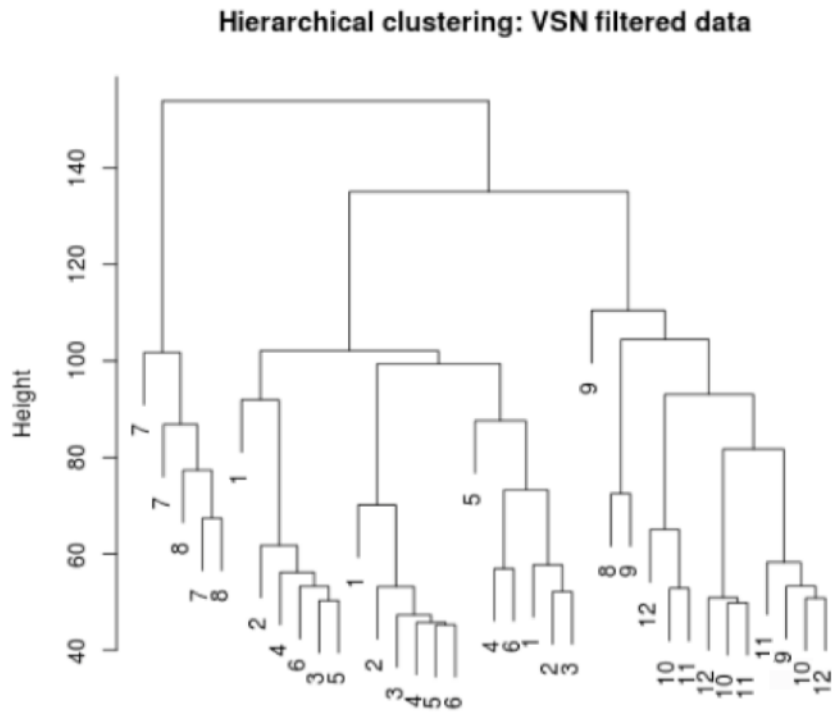

Figure 3-5 Hierarchical clustering analysis.

Clustering of the filtered data shows that the samples generally cluster into 3 super-groups; groups 1-6, groups 7-8 and groups 9-12. Group 1-6: clone C23, dose high to low: 2μM, 0.4μM, 0.08μM, 0.016μM, 0.032μM, 0μM; Group 7-12: clone A3, dose high to low: 10μM, 1μM, 0.1μM, 0.01μM, 0.001μM, 0μM.

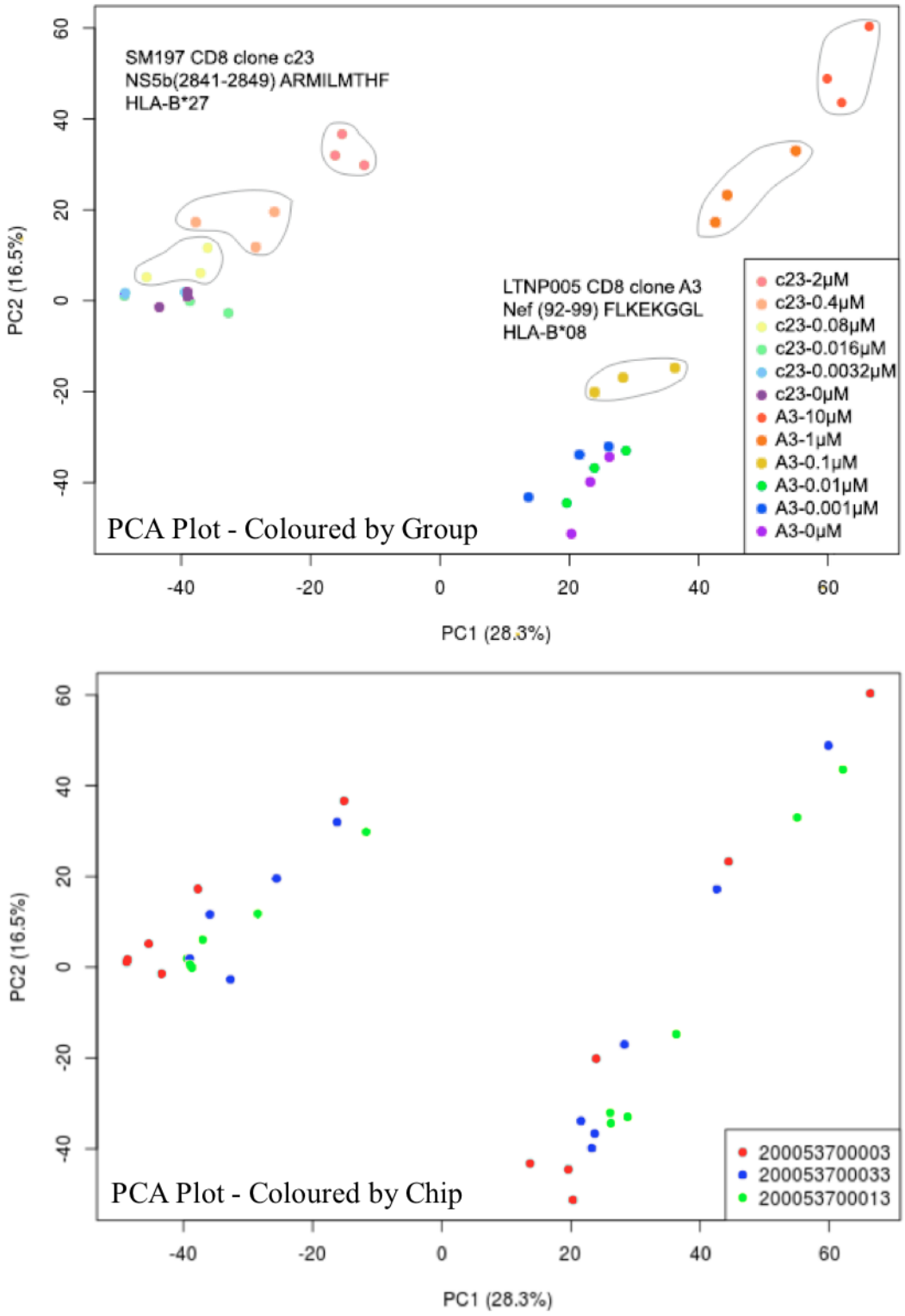

Figure 3-6 PCA plots coloured by experimental group and microarray chip.

In the PCA plots coloured by the experimental group (upper) and coloured by microarray chip (lower), samples close together have similar overall expression profiles and the primary source of variation will separate samples on the x-axis (PC1) and secondary source on the y-axis (PC2).

3.2.3 Gene Differential Expressions of CTLs Receiving Five Different Strengths of Antigen Stimulation.

From the PCA plot (Figure 3-6), 18 arrays of A3 clone clearly separated into 4 sub-groups, 10μM group, 1μM group, 0.1μM group and 0.01μM&0.001μM&0μM combined group. For the C23 arm, only 2μM group separated clearly from the 5 other groups. Both A3 and C23 showed a significant gradient of gene differential expressions along the antigen strength (same direction between the two completely different clones). As the gene differential expressions within A3 group were much more prominent than in the C23 group, the 18 arrays of A3 clone were continued for more detailed analysis. Volcano plot, often used when analysing microarray data sets to give an overview of interesting genes, was exploited to depict the overview of the gene differential expressions at high-to-low strength of antigen stimulation. The log2 value of fold change between each antigen strength group and control group (mock stimulation) was plotted on the x-axis and the negative log10 *p*-value was plotted on the y-axis (Figure 3-7). It was very clear that more and more genes were differentially expressed by increasing the antigen stimulation strength.

Figure 3-7 Volcano plots of differential gene expressions between antigen dose group and no antigen group (A3).

Volcano plots of all pairwise comparisons for A3. Comparisons of all mRNAs assessed in microarray analysis of RNA isolated from CTLs (clone A3) with different strength of antigen stimulation (n = 3) and without antigen as control (n =3). The volcano plot displays the relationship between fold-change and significance between each of the two groups, using a scatter plot view. The y-axis is the negative log10 of *p*-values (a higher value indicates greater significance) and the x-axis is the difference in expression between two experimental groups as measured in log2 scale. The most significantly differentially expressed genes were labelled on each volcano plot.

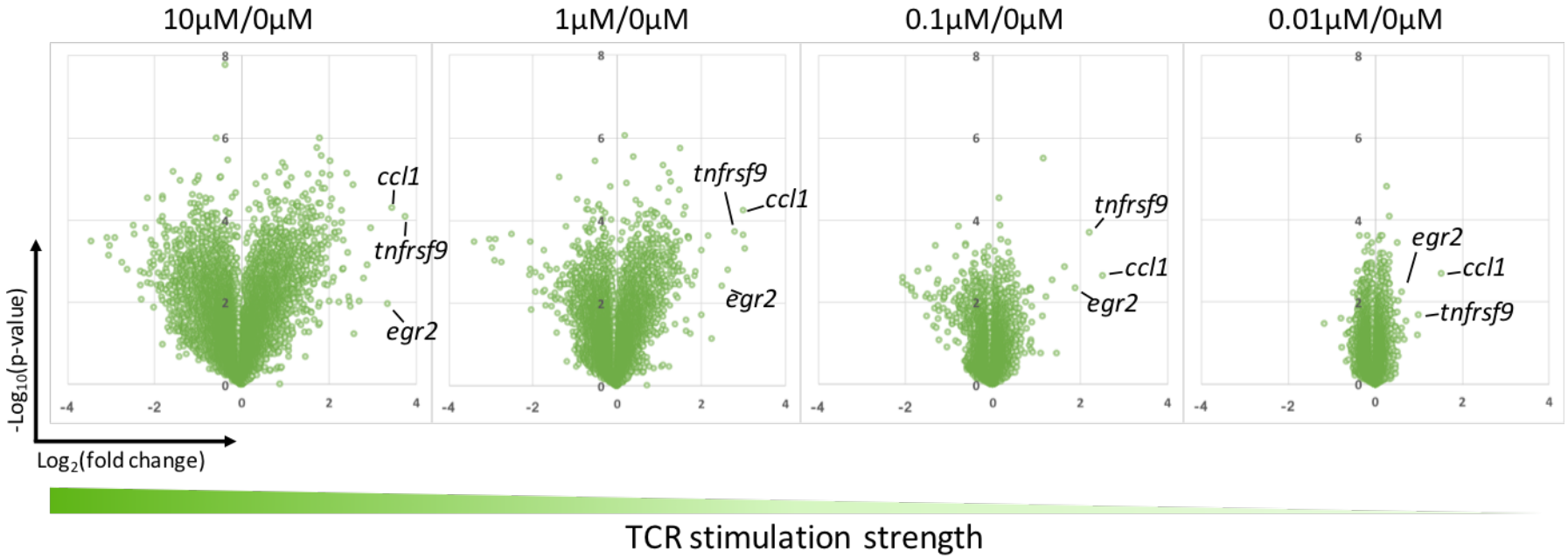

	10μM vs 0μM		1μM vs 0μM		0.1μM vs 0μM		0.01μM vs 0μM		0.001μM vs 0μM	
	1.5-fold	2-fold	1.5-fold	2-fold	1.5-fold	2-fold	1.5-fold	2-fold	1.5-fold	2-fold
Number of Up-regulated Genes	1042	383	474	121	20	8	5	1	0	0
Number of Down-regulated Genes	938	339	354	66	67	27	1	0	0	0

There were 383 candidate genes (447 probes) up-regulated and 339 candidate genes (380 probes) down-regulated comparing 10μM group to the 0μM group; 121 candidate genes (140 probes) up-regulated and 66 candidate genes (73 probes) down-regulated comparing 1μM group to the 0μM group; there were 8 candidate genes (*TNFRSF9, EGR2, ZBED2, TIMD4, C12ORF48, HAVCR2, CCL1, HBA2*, 8 probes) up-regulated and 27 candidate genes (29 probes) down-regulated comparing 0.1μM group to the 0μM group and only 1 candidate gene (*CCL1*, 1 probe) up-regulated comparing 0.01μM group to the 0μM group. The cut-off threshold was fold change greater than 2 and *p*-value less than 0.05 (Figure 3-8). Within these candidate genes, very interestingly, CCL1 identified in 0.01μM comparison was also identified in 10μM, 1μM and 0.1μM. 7 out of the 8 up-regulated genes identified in 0.1μM were also identified with 10μM and 1μM (5.9%). 119 out of the 121 up-regulated genes identified in 1μM were also identified with 10μM (31.1%). On the down-regulation side, 26 out of the 27 down-regulated gene identified in 0.1μM overlapped with 10μM and 1μM (40.6%). 64 out of the 66 down-regulated genes identified in 1μM overlapped with 10μM (18.9%). Similar phenomena were also prominent, if the threshold applied was changed to 1.5-fold change.

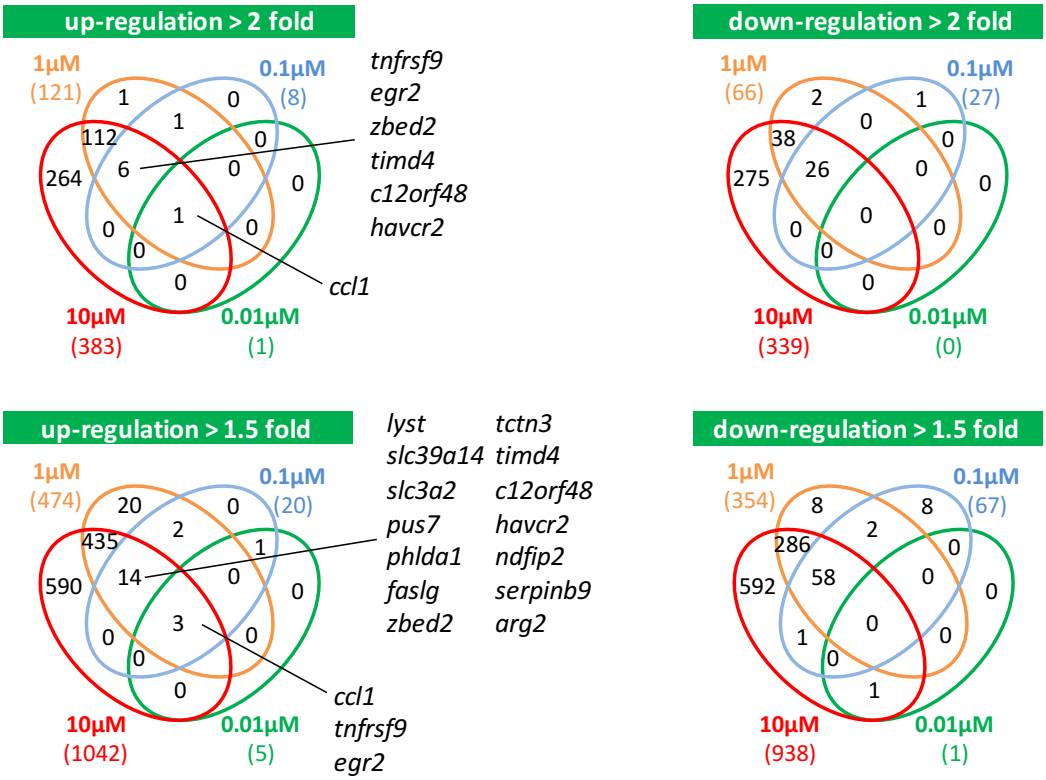

Gene Symbol	Probe ID	Protein Name and Function	log_2 (fold change to 0μM group)				
			10 μM	1 μM	0.1 μM	0.01 μM	0.00 1μM
CCL1	ILMN_1727043	CCL1, chemokine, binds to CCR8	2.81	3.04	2.53	1.52	0.53
TNFRSF9	ILMN_1743199	4-1BB or CD137, co-stimulatory receptor	3.46	3.00	2.21	0.99	0.31
EGR2	ILMN_1663131	EGR2, regulatory transcription factor	2.96	2.81	1.89	0.72	0.22
ZBED2	ILMN_1767658	Zinc Finger BED-Type Containing 2	3.35	2.50	1.15	0.18	0.00
HAVCR2	ILMN_2414399	TIM3, inhibitory receptor	2.88	2.64	1.65	0.62	0.29
TIMD4	ILMN_1748883	TIM4, ligand for TIM1	2.25	2.19	1.38	0.39	0.13
C12ORF48	ILMN_1813379	PARP-1 binding protein, enhances PARP-1 activity and protects cells from DNA damage.	3.75	3.01	1.22	0.15	0.23
SLC3A2	ILMN_1668822	LAT1 heavy chain, amino acid transporter	1.91	1.45	0.86	0.48	0.27
SLC39A14	ILMN_2383306	ZIP14, divalent metal transporters	2.14	1.67	0.89	0.16	0.01
LYST	ILMN_1708605	LYST, regulates intracellular protein trafficking in endosomes	1.06	0.86	0.71	0.43	0.19
PUS7	ILMN_1682857	Relates to tRNA processing	2.30	1.72	0.61	-0.05	-0.18
C10ORF61	ILMN_1773865 ILMN_3287266 ILMN_3300663	TCTN3, Hedgehog signal transduction	1.06/ 1.04/ 1.14	1.20/ 1.17/ 1.20	0.78/ 0.90/ 0.71	0.20/ 0.33/ 0.09	0.02/ 0.00/ 0.06
PHLDA1	ILMN_1665483	in regulation of apoptosis	2.16	1.57	0.77	0.08	-0.04
FASLG	ILMN_1682792	Direct CTL killing	1.68	1.27	0.65	0.34	0.28
NDFIP2	ILMN_2045729	Limits the cytokine signaling, promotes degradation of JAK1	2.12	1.88	0.90	0.32	0.13
SERPINB9	ILMN_1751425	Inhibits the activity of the granzyme B	1.05	0.91	0.75	0.14	0.24
ARG2	ILMN_1799028	Arginase 2, hydrolysis of arginine to ornithine and urea	1.09	1.18	0.60	0.15	0.04

Figure 3-8 Differentially expressed genes in different antigen dose group vs no antigen group, with detailed expression value on selected genes (A3).

Venn diagram showing the number of significantly differentially expressed genes.

The differentially expressed genes were then categorized based on the minimum antigen stimulation strength required for differential expression and their molecular and cellular function (Figure 3-9).

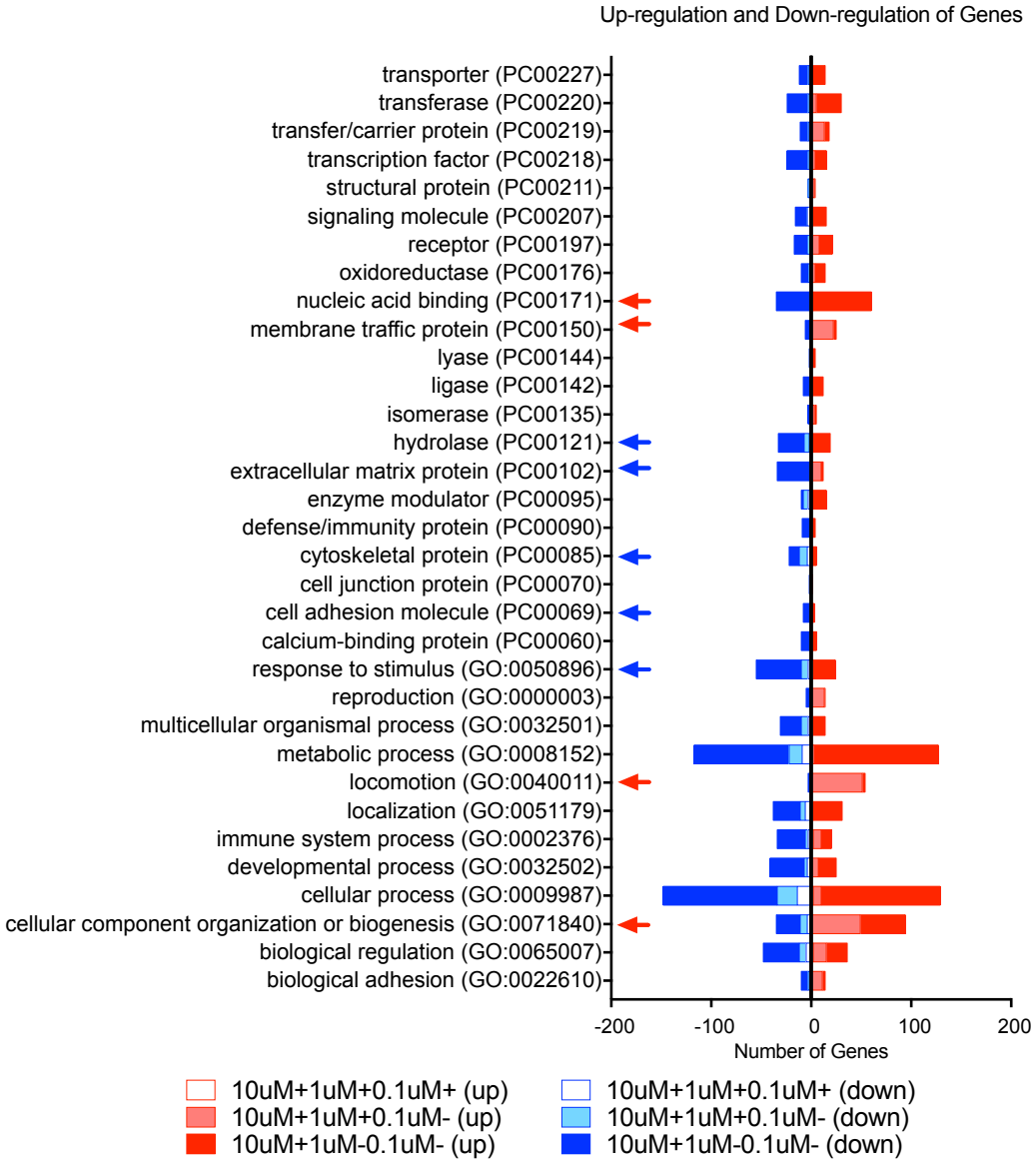

Figure 3-9 Number of differentially expressed genes with each functional category and antigen stimulation strength (A3).

Staggered bar chart of gene categorized by the biological process and protein class with increased expression in a dose-dependent manner by functional classification in PANTHER (Mi et al., 2017; Mi et al., 2013). The up-regulated (2-fold) genes were coloured in red and down-regulated (2-fold) genes were coloured in blue (with different gradients to indicate the minimum antigen stimulation strength required for differential expression). Coloured arrows indicate the trend of overall differentiation.

The functions of the genes were further analysed by statistic enrichment test (SET) (Figure 3-10), which is a binomial statistics tool to compare classifications of multiple clusters of lists with a reference list, to statistically determine over- or under-representation of PANTHER classification categories.

Based the absolute number of changed genes, genes that related to nucleic acid binding, biogenesis and metabolic process were most differentially expressed. Certain genes related to locomotion, membrane traffic, reproduction and biogenesis were over-represented at 1μM antigen stimulation, while more genes related to response to stimulus down-regulated at 10μM antigen stimulation (Figure 3-9). Similarly, in SET result, the most significant change upon TCR engagement on this CTL clone was that cells started to undergo active metabolism and decreased cell communication and signal transductions, which reflects the situation that after receiving antigen stimulation, T cell down-modulates its receptors (Liu et al., 2000) and starts to prepare for biogenesis and proliferation. The RNA and nucleic acid binding protein was the most sensitively up-regulated protein category, indicating that proteins bound to RNA or nucleic acid and involved in processing or metabolism were first up-regulated with sub-optimal antigen stimulation. On the other hand, the G-protein modulator and cytoskeletal protein down-regulated, although the powers were only intermediate (Figure 3-10).

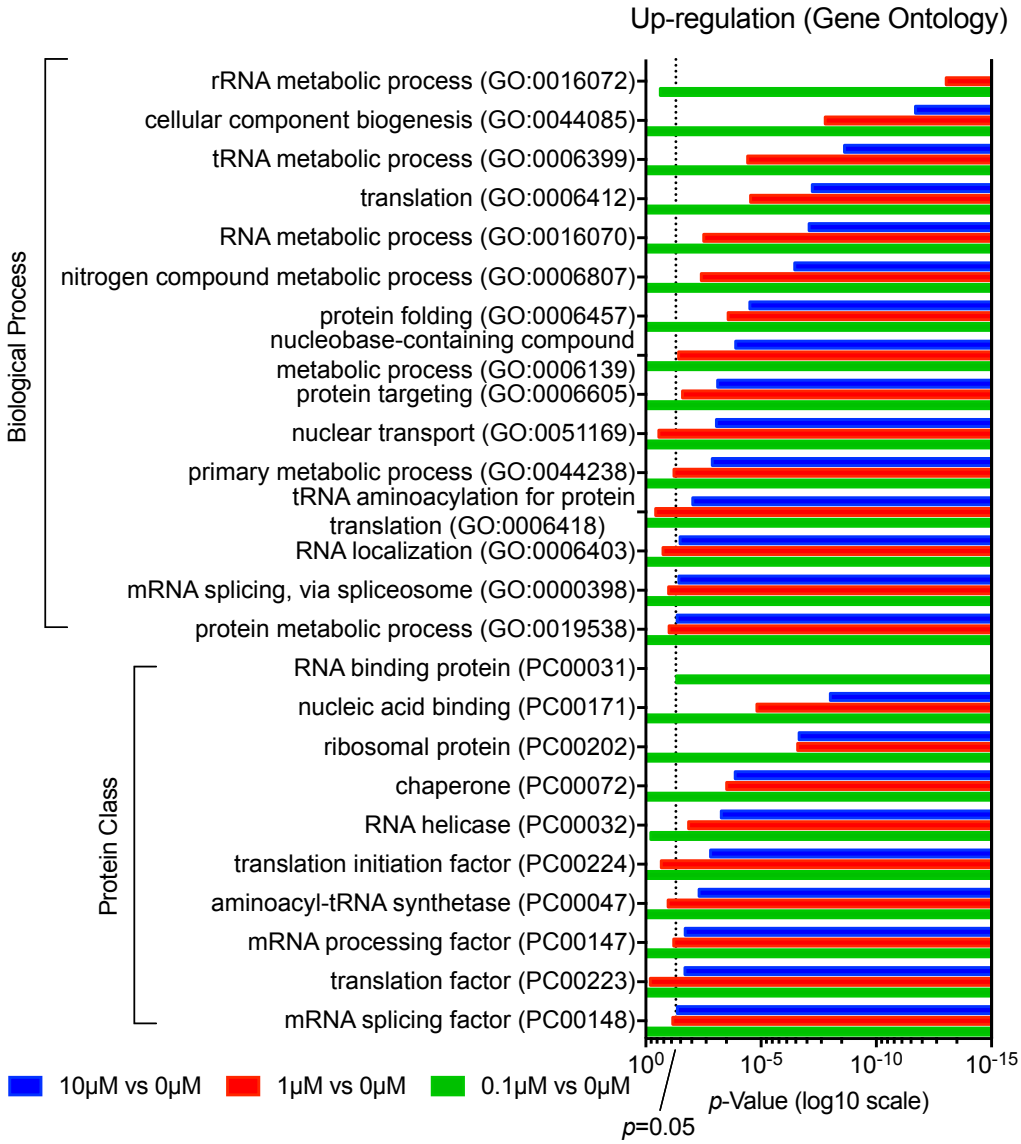
Up-regulation (Gene Ontology)
Biological Process
rRNA metabolic process (GO:0016072)
cellular component biogenesis (GO:0044085)
tRNA metabolic process (GO:0006399)
translation (GO:0006412)
RNA metabolic process (GO:0016070)
nitrogen compound metabolic process (GO:0006807)
protein folding (GO:0006457)
nucleobase-containing compound metabolic process (GO:0006139)
protein targeting (GO:0006605)
nuclear transport (GO:0051169)
primary metabolic process (GO:0044238)
tRNA aminoacylation for protein translation (GO:0006418)
RNA localization (GO:0006403)
mRNA splicing, via spliceosome (GO:0000398)
protein metabolic process (GO:0019538)
Protein Class
RNA binding protein (PC00031)
nucleic acid binding (PC00171)
ribosomal protein (PC00202)
chaperone (PC00072)
RNA helicase (PC00032)
translation initiation factor (PC00224)
aminoacyl-tRNA synthetase (PC00047)
mRNA processing factor (PC00147)
translation factor (PC00223)
mRNA splicing factor (PC00148)
10μM vs 0μM
1μM vs 0μM
0.1μM vs 0μM
10^0
10^-5
10^-10
10^-15
p-Value (log10 scale)
p=0.05

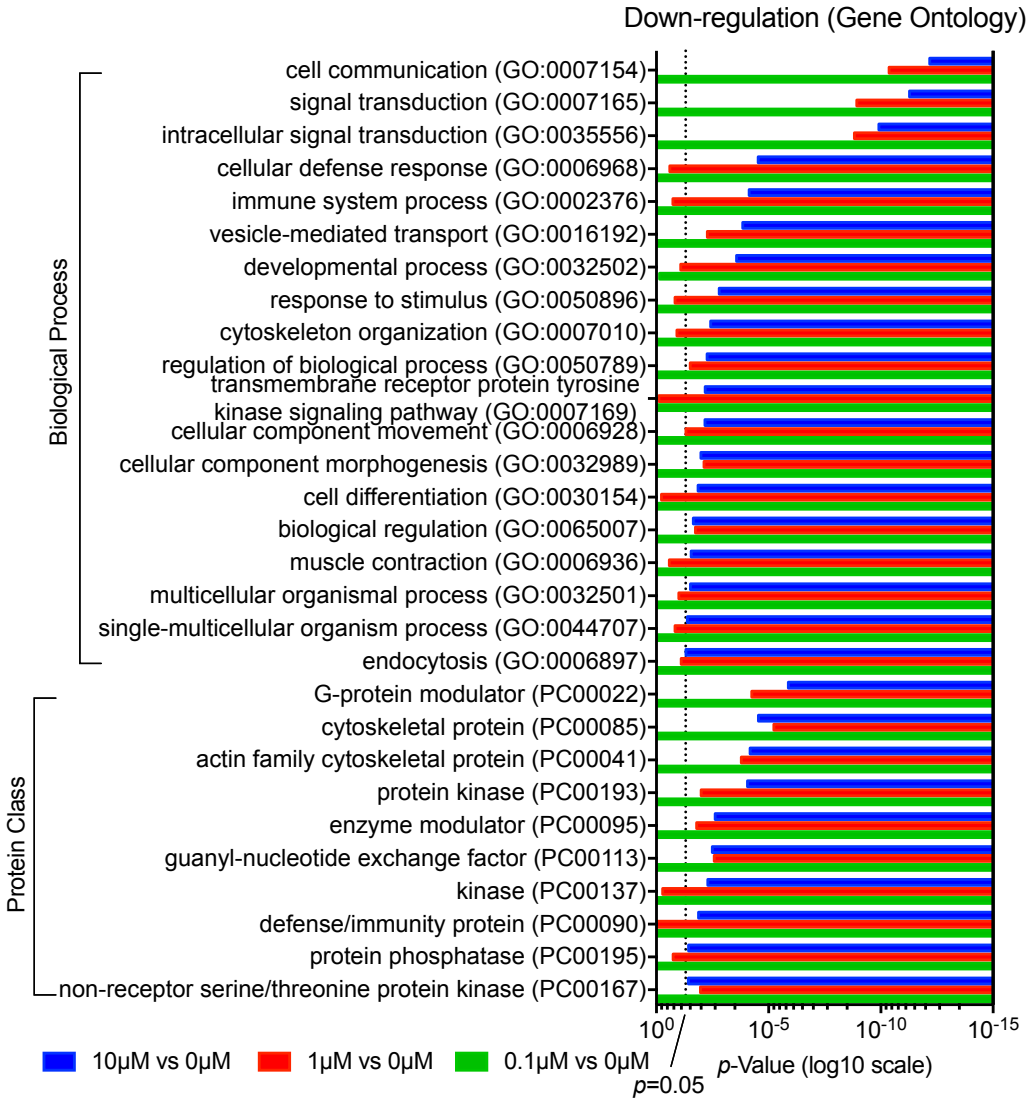

Figure 3-10 Classification of genes with significant differential expression by biological process (A3).

Bar chart of the biological process and protein class within the genes with altered expression compared to no antigen group (p-value<0.05) by gene set enrichment analysis in PANTHER. Longer bar means the p-value is less significant. The enrichment test is to evaluate the likelihood of the numerical values of genes associated with a particular ontology term being drawn randomly from the overall distribution of values. The Mann-Whitney U Test (Wilcoxon Rank-Sum Test) is used here. p-value (y-axis) indicates the probability that the biological pathway is indicated by chance alone, while a small, significant p-value indicates that the distribution for this category is non-random and different from the overall distribution. A dashed line was shown on each graph to indicate p-value =0.05.

3.2.4 Dose-Dependent CTL Gene Differential Expressions.

All the normalized and filtered probes (20,657 probes) were also analysed using one-way ANOVA (analysis of variance) to determine the dose-dependent differentially expressed genes within the global genome. 342 genes (347 probes) were significantly changed (adjusted *p*-value<0.05). These significant genes were clustered according to Pearson correlation. The One-way ANOVA turned out to be more stringent than t-test as fewer genes were considered significantly differentially expressed. There were two major branches (up-regulated and down-regulated) on the heat map. Within the down-regulated branch, there were clear separation of two sub-branches (significant down-regulation at 0.1μM group and significant down-regulation at 1μM group). In contrast, the majority of the up-regulated genes changed at 1μM, while only a few genes changed at 0.1μM. (Figure 3-11A) Among these ANOVA significant genes, 212 genes (62%) overlapped with genes that up-regulated greater than 1.5-fold at 10μM/0μM comparison group, 81 genes (24%) overlapped with genes than down-regulated greater than 1.5-fold at 10μM/0μM comparison group. This was quite interesting, as based on the t-test, the up-regulation and down-regulation were comparable on A3; however, one-ANOVA filtered many down-regulated genes that were not changed in a pattern that responded to antigen stimulation dose (Figure 3-11B). The gene functions were further categorized by gene ontology, in terms of biological process and protein class. Similar to what we found in the previous student's t-test based analysis, genes that were involved in the metabolism and biogenesis process were most significantly up-regulated, while from the

perspective of the protein class, nucleic acid binding, hydrolase and transporter were the most up-regulated. (Figure 3-11C)

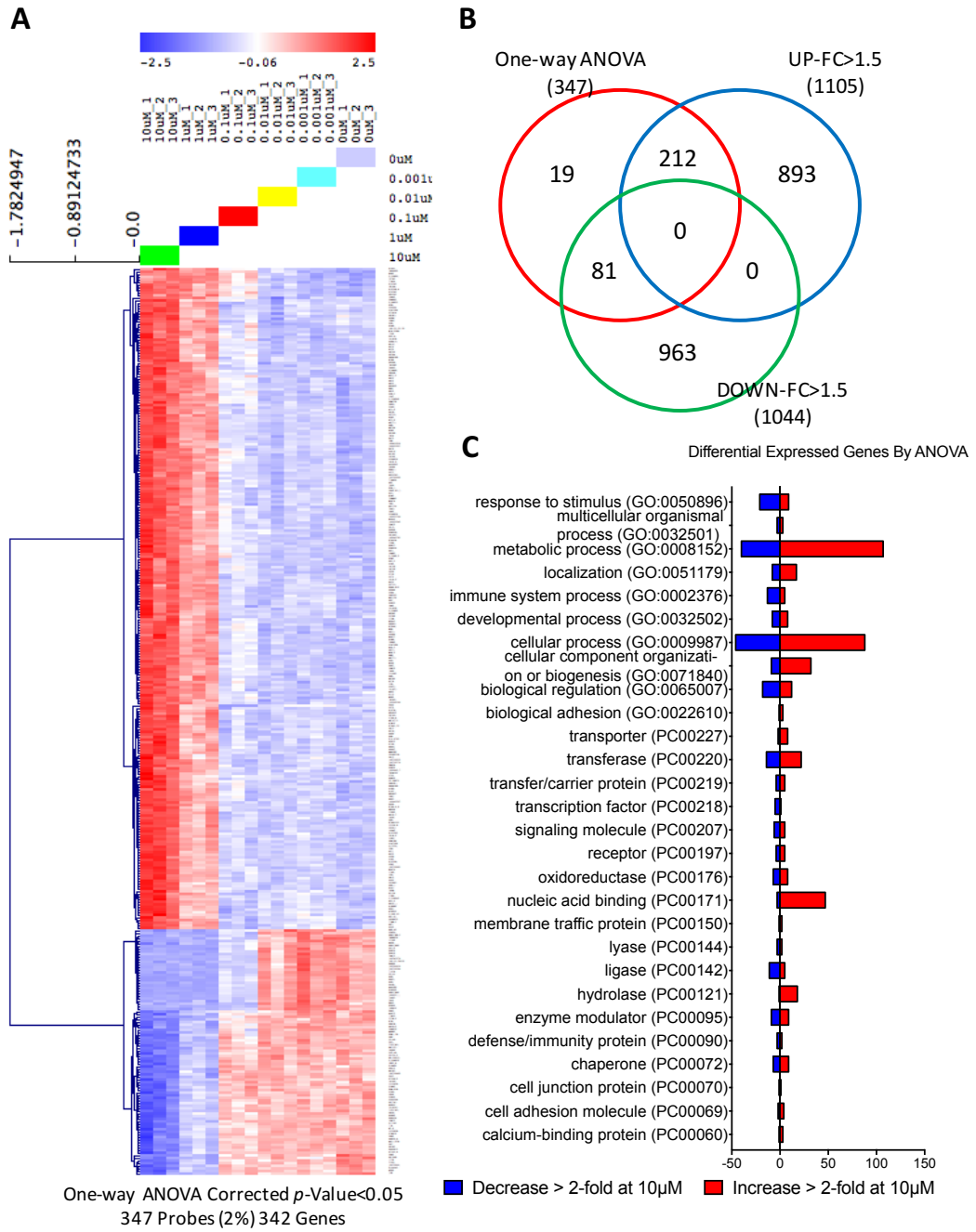

Figure 3-11 Differential gene expressions identified by one-way ANOVA (A3).

(A) Heatmap of ANOVA significantly differentially expressed genes. (B) Venn diagram shows within the 342 genes; 212 genes up-regulate more than 2-fold at highest strength (10μM) compared to control group (0μM), while 81 genes down-regulate more than 2-fold. (C) Up-regulated and down-regulated significant genes are further categorized by functional classification using PANTHER.

3.2.5 CTL Cytokine/Chemokine Productions with Antigen Stimulation.

Although CTLs kill the targets mainly through the secretion of perforin and granzymes with the expression of FasL playing a less significant role (Barry and Bleackley, 2002), the CTLs also release different cytokines and chemokines to contribute a more effective killing as well as attracting other immune cells to the inflammatory site. The most well-known CTL cytokines are IFNγ and TNFα, while the relative importance of other cytokines and the mechanisms are yet to be determined.

The cytokines, chemokines and some of their receptors were checked and mapped at 10μM and 1μM on clone A3 (too few changes at 0.1μM and below). (Figure 3-12) IFNG, CSF2 (GM-CSF), CCL1, CCL3, FASLG and IL5 up-regulated at high strength of stimulation while CCL22, IL6, IL23A and TNFSF12 (TWEAK, TNF-related weak inducer of apoptosis) down-regulated. From the receptor aspect, TNFRSF9 (4-1BB), TNFRSF1B (TNFR2), IL2RA and CCR4 up-regulated, in contrast to IL10RA and CCR3. It is noteworthy that CCL1 and 4-1BB highly were significantly up-regulated even at 0.01μM antigen stimulation. Further, from the FACS data (Figure 3-1 and 3-2), after re-encountering the antigen, the antigen-specific T cells (memory cells) start releasing TNFα within 2 hours, quicker than IFNγ, which usually peaks at 4-6h post TCR engagement. This phenomenon provides the explanation that in this microarray data (6h post antigen stimulation), TNFα mRNAs didn't show large fold-change, as they were already translated into protein and secreted out, in contrast to IFNγ, which was still detectable. In addition, there was a clear trend that clone A3 (at 1μM and above) preferentially up-regulated CCR4 and down-regulated CCR3, both of

which are receptors that bind and respond to a variety of chemokines. CCR3 binds to CCL5, CCL7, CCL11, CCL13 and CCL26, while CCR4 binds to CCL2, CCL4, CCL5, CCL17 and CCL22. Similarly, clone A3 also up-regulated IL2RA, and down-regulated IL10RA, and switched other cytokine and chemokines in response to different strengths of antigen stimulation. The detailed differential expressions of these genes on A3 could be found in Figure 3-12.

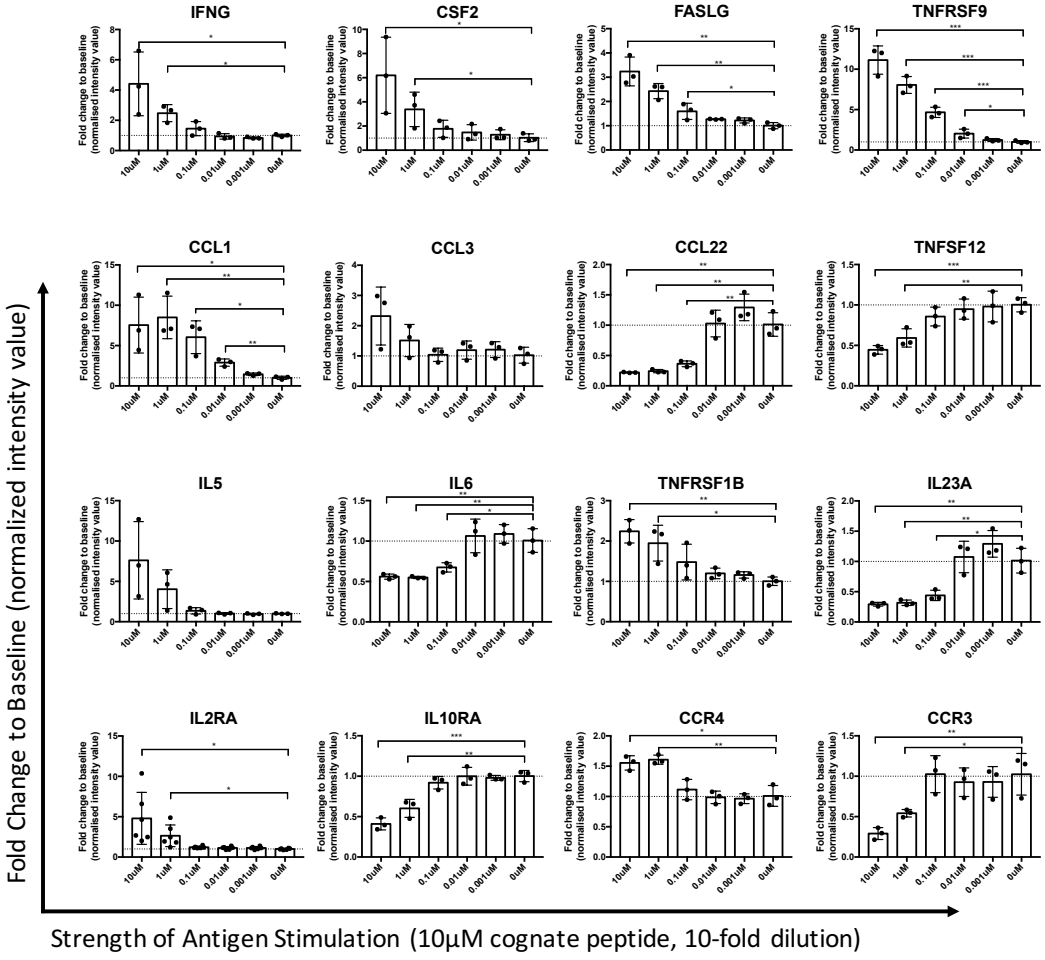

Figure 3-12 Detailed gene expression levels of some of the most differentially expressed cytokine, chemokines and cytokine/chemokine receptors genes (A3).

Gene expression levels were plotted to depict fold change at each antigen dose compared to the no antigen group. The error bar represents SD, * indicates $p<0.05$, ** indicates $p<0.01$, *** indicates $p<0.001$, p-values were calculated using 2-tail non-paired student's t-test. Error bar represents the standard deviation.

3.2.6 Identification of the Most Sensitive Transporter Genes in Response to Antigen Stimulation on Clone A3.

Quiescent naïve and memory CD8 CTLs only require a small amount of energy to prevent cell atrophy and maintain essential cellular functions and migration. By contrast, activated CTLs demand much higher energy as they need to proliferate, produce effector cytokines and cytotoxic granules. Thus, it is essential for $CD8^+$ CTLs to increase cellular metabolism and nutrient uptake to satisfy the increased biogenesis when it occurs (Cham et al., 2008). One important metabolic change is that activated T cells switch the metabolism from oxidative phosphorylation to glycolysis (Vander Heiden et al., 2009). To satisfy the high demand on a variety of substrates for glycolysis, activated T cells up-regulate glucose transporters (Cham et al., 2008) and amino acid transporters (Hayashi and Anzai, 2017; Timosenko et al., 2016) at the cell surface in response to antigen and cytokine stimulation, which ensures satisfaction of the metabolic and biosynthetic needs of the cells.

Solute carrier (SLC) transporters - a family of more than 300 membrane-bound proteins that facilitate the transport of a wide array of substrates across biological membranes - have important roles in physiological processes ranging from the cellular uptake of nutrients to the absorption of drugs and other xenobiotics. (Lin et al., 2015) To check the expression levels of the SLC transporters, 191 SLC probes were selected for study (some other SLC probes were filtered for low intensity value). Significantly changed SLC genes (10μM vs 0μM, 52 SLC genes) were clustered and formed two distinguished arms – up-regulated arm and down-regulated arm (Figure 3-13A).

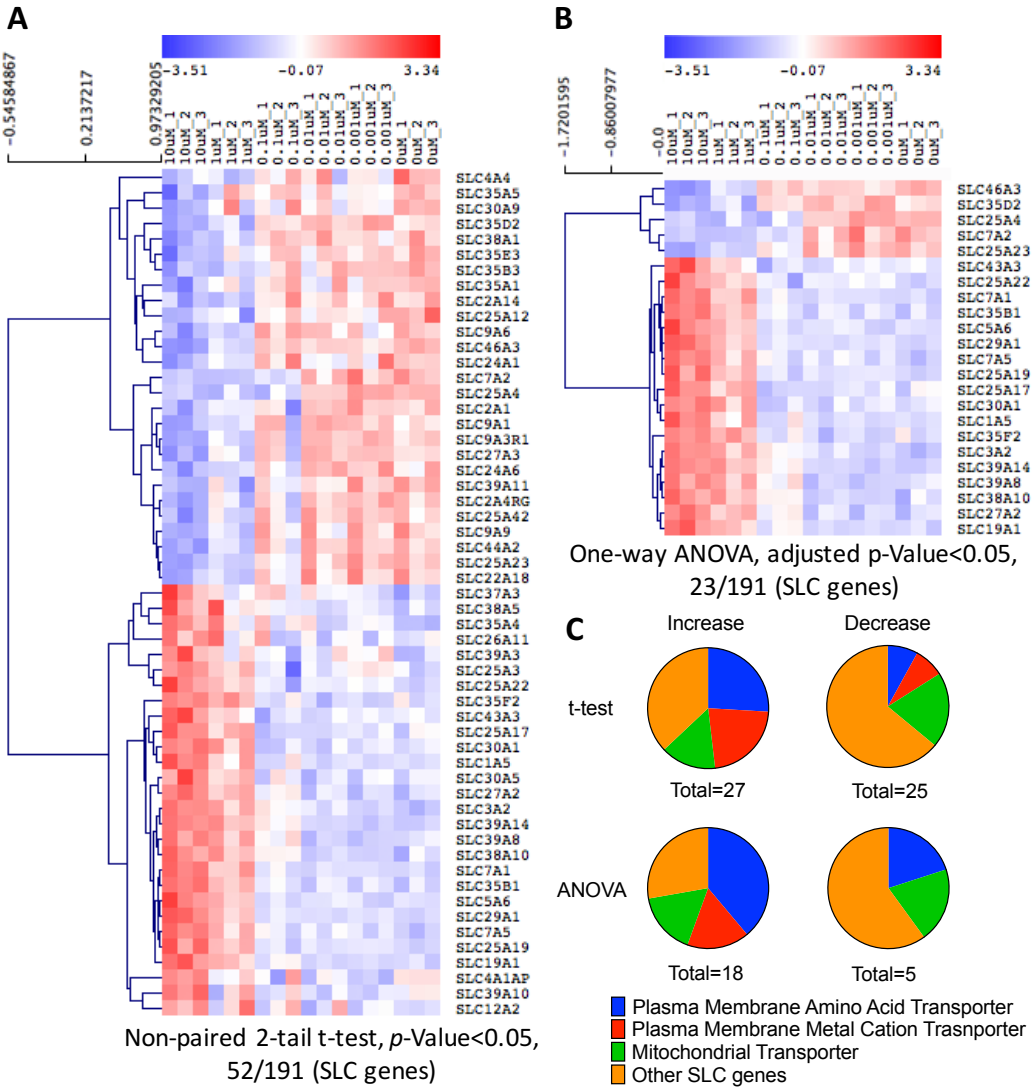

Figure 3-13 Gene differential expressions on SLC (solute carriers) genes (A3).

(A) Hierarchy clusters (HCL) of significantly changed SLC genes at 10μM antigen stimulation based on non-paired 2-tailed student's t-test. (B) HCL of SLC genes based on one-way ANOVA among different antigen dose groups. Two clusters were formed based on mRNA levels. (C) Pie chart of significant genes categorized by protein functions.

If the 191 probes were analysed using one-way ANOVA to compare all the six dose groups, 23 genes were identified as significantly changed in response to antigen dose (Figure 3-13B). The 23 ANOVA identified SLC genes overlapped with the 52 t-test identified genes (10μM versus 0μM). The significantly changed genes were mostly amino acid transporters (14/52 by t-test, 8/23 by ANOVA), Zinc transporters (8/52 by t-test, 3/23 by ANOVA) and mitochondrial transporters (9/52 by t-test, 4/23 by ANOVA). Other transporters include ion transporters, vitamin transporter and fatty acid transporters. Detailed information is shown in Table 3-4.

Table 3-2 Significantly changed SLCs with fold change at 10μM stimulation with detailed information (A3).

Gene ID	Gene Name	log_2(10μM/0μM)	log_2(1μM/0μM)	log_2(0.1μM/0μM)	log_2(0.01μM/0μM)	Prot. ID	Substrate	Location
SLC7A5	large neutral amino acids transporter small subunit 1	2.18	1.42	0.47	0.53	LAT1	L-type amino acid	PM
SLC39A14	Zn2+ transporter ZIP14	2.14	1.67	0.89	0.16	ZIP14	Zn2+, Fe2+	PM
SLC3A2	4F2 cell-surface antigen heavy chain	1.91	1.45	0.86	0.48	4F2	Ca2+, L-type amino acid	PM, NM
SLC1A5	neutral amino acid transporter B (0)	1.61	0.81	0.17	-0.04	ASCT2	neutral amino acid	PM
SLC7A1	high affinity cationic amino acid transporter 1	1.52	0.97	0.21	0.09	CAT1	cationic amino acid	PM
SLC27A2	very long-chain acyl-CoA synthetase	1.45	0.98	0.47	0.08	FATP2	long-chain fatty acid	ER, PM, P
SLC25A19	mitochondrial thiamine pyrophosphate carrier	1.43	0.92	0.08	0.16	TPC	thiamine pyrophosphate	M
SLC25A22	mitochondrial glutamate carrier 1	1.19	0.68	-0.01	0.21	GC1	glutamate	M
SLC39A8	Zn2+ transporter ZIP8	1.16	0.87	0.34	-0.25	ZIP8	Zn2+, Fe2+	PM
SLC35B1	solute carrier family 35 member B1	1.07	0.67	0.18	0.09	UGTREL1	UDP-galactose	G, ER
SLC29A1	equilibrative nucleoside transporter 1	1.00	0.56	0.11	0.05	ENT1	equilibrative nucleoside	PM
SLC5A6	Na+-dependent multivitamin transporter	1.00	0.56	-0.03	0.05	SMVT	multivitamin	PM
SLC35F2	solute carrier family 35 member F2	0.98	0.75	0.00	-0.26	HSNOV1	no data	ND
SLC19A1	folate transporter 1	0.91	0.54	0.20	0.00	FOLT	folate	PM
SLC30A5	Zn2+ transporter 5	0.87	0.47	0.06	-0.12	ZNT5	Zn2+	G, PM
SLC39A3	Zn2+ transporter ZIP3	0.81	0.37	0.10	0.27	ZIP3	Zn2+	PM
SLC43A3	solute carrier family 43 member 3	0.78	0.24	-0.19	-0.07	EEG1	equilibrative nucleobase	ND
SLC38A5	Na+-coupled neutral amino acid transporter 5	0.66	0.47	0.17	0.02	SNAT5	Na+-coupled amino acid	PM
SLC35A4	probable UDP-sugar transporter protein SLC35A4	0.59	0.39	0.31	0.18	SLC35A4	sugar/proton	G
SLC38A10	putative Na+-coupled neutral amino acid transporter 10	0.50	0.38	0.19	-0.01	PP1744	amino acid	G

SLC25A3	phosphate carrier protein, mitochondrial	0.44	0.29	-0.10	0.06	PTP	phosphate ion	M
SLC25A17	peroxisomal membrane protein PMP34	0.44	0.26	-0.13	-0.07	PMP34	ATP, ADP, AMP, CoA	P, M
SLC12A2	solute carrier family 12 member 2	0.40	0.26	0.16	0.08	BSC2	Na+, K+, Cl-	PM
SLC37A3	sugar phosphate exchanger 3	0.35	0.13	0.19	0.15	SLC37A3	carbohydrate	ER
SLC30A1	Zn2+ transporter 1;SLC30A1	0.33	0.24	-0.05	-0.02	ZNT1	Zn2+	ER, G, PM, NM
SLC26A11	Na+-independent sulphate anion transporter	0.27	0.14	0.01	-0.01	SLC26A11	anion	G, ER, PM, L
SLC39A10	Zn2+ transporter ZIP10	0.21	0.01	-0.04	-0.09	LZT-Hs2	Zn2+	PM
SLC4A4	electrogenic Na bicarbonate cotransporter 1	-0.17	-0.18	-0.07	-0.09	NBC2	sodium bicarbonate	PM
SLC2A14	solute carrier family 2, facilitated glucose transporter member 14	-0.19	-0.18	0.00	-0.03	GLUT14	D-glucose	PM
SLC24A1	Na+/K+/Ca2+ exchanger 1	-0.23	-0.12	0.03	-0.10	NCKX	Na+, K+, Ca2+	PM
SLC25A12	Ca2+-binding mitochondrial carrier protein Aralar1	-0.26	-0.23	-0.11	-0.13	AGC1	L-aspartate, L-glutamate	M
SLC2A1	solute carrier family 2, facilitated glucose transporter member 1	-0.40	-0.20	-0.24	0.04	GLUT1	D-glucose	PM
SLC9A6	Na+/H+ exchanger 6	-0.41	-0.28	0.02	-0.04	NHE6	Na+, H+	endosome
SLC35B3	Adenosine 3'-phospho 5'-phosphosulfate transporter 2	-0.41	-0.35	-0.13	-0.13	PAPST2	3-prime phosphoadenosine 5-prime phosphosulfate	NM, G
SLC35A1	CMP-sialic acid transporter	-0.42	-0.18	-0.03	-0.13	CST	nucleotide sugars	G
SLC35D2	UDP-N-acetylglucosamine/UDP-glucose/GDP-mannose transporter	-0.45	-0.28	0.03	0.12	HFRC1	nucleoside sugars	G
SLC39A11	Zn2+ transporter ZIP11	-0.46	-0.36	-0.22	-0.16	ZIP11	Zn2+	PM, G
SLC30A9	Zn2+ transporter 9	-0.52	-0.18	-0.13	-0.22	ZNT9	Zn2+	NM
SLC9A1	Na+/H+ exchanger 1	-0.55	-0.26	-0.02	0.26	NHE1	Na+, H+	PM
SLC25A4	ADP/ATP translocase 1	-0.57	-0.56	-0.52	-0.10	ANT1	ADP, ATP	M
SLC22A18	solute carrier family 22 member 18	-0.63	-0.48	-0.21	-0.04	HET	organic cations	PM

SLC7A2	cationic amino acid transporter 2	-0.67	-0.70	-0.54	-0.10	CAT2	cationic amino acid	PM
SLC24A6	Na+/K+/Ca2+ exchanger 6, mitochondrial	-0.69	-0.41	-0.16	0.24	NCLX	Na+, K+, Ca2+	PM, M
SLC35A5	probable UDP-sugar transporter protein SLC35A5	-0.70	-0.15	-0.09	-0.20	SLC35A5	nucleoside sugars	G
SLC27A3	long-chain fatty acid transport protein 3	-0.78	-0.28	-0.11	0.20	FATP3	long-chain fatty acid	ER, M
SLC46A3	solute carrier family 46 member 3	-0.81	-0.46	-0.09	-0.13	FKSG16	catabolites	L
SLC9A9	Na+/H+ exchanger 9	-0.83	-0.57	-0.15	-0.17	NHE9	Na+, H+	endosome
SLC38A1	Na+-coupled neutral amino acid transporter 1	-0.94	-0.64	-0.05	-0.01	PP1744	neutral amino acid	G
SLC25A42	mitochondrial coenzyme A transporter SLC25A42	-1.00	-0.51	-0.21	0.13	SLC25A42	CoA, adenosine 3',5'-diphosphate	M
SLC25A23	Ca2+-binding mitochondrial carrier protein SCaMC-3	-1.34	-0.93	-0.48	-0.05	APC2	Ca2+	M
SLC44A2	choline transporter-like protein 2	-1.41	-0.85	-0.29	0.06	CTL2	Cl-	PM, L

FC: fold change; PM: plasma membrane; NM: nucleus membrane; ER: endoplasmic reticulum; P: peroxisome; M: mitochondria; G; Golgi apparatus; L: lysosome; ND: no data.

Glucose transport is important for CTLs, and published studies have focused on the glucose transporter GLUT1 in T cells. GLUT1, also known as SLC2A1, is rapidly up-regulated following T cell stimulation for transporting extracellular glucose into the cell (Cretenet et al., 2016). In the microarray data, we were surprised to observe a decreased trend of GLUT1 transcripts along with the increased antigen dose. A similar phenomenon was also observed on GLUT3 (SLC2A3), another glucose transporter expressed in amounts equivalent to those of GLUT1 in CTLs, but with higher glucose transporter capacity (Hukelmann et al., 2016). To validate this at the protein level, the cell surface expression of GLUT1 was checked by flow cytometer. Interestingly, the surface expression of GLUT1 was, in fact, up-regulated with the increased antigen dose, and the GLUT1 were expressed on all the 'resting' A3 T cells. Thus, the inconsistent expression patterns between protein and transcripts may have resulted from the fact that GLUT1 regulation is controlled at the level of transcription, translation and translocation from intracellular vesicles to the cell surface (Buck et al., 2015; Cretenet et al., 2016) (Figure 3-14).

In addition to increased glucose uptake, another significant metabolic reprogramming that a T cell undertakes after being stimulated is increasing the level of amino acid transporters on the surface. SLC7 is one of the most representative amino acid transporter families and is composed of two groups: cationic amino acid transporters (CATs; SLC7A1-4 and SLC7A14) and light or catalytic chains of heteromeric amino acid transporters (HATs; SLC7A5-13 and SLC7A15) (Verrey et al., 2004). Both SLC7A5 and SLC7A8 associate with SLC3A2 (4F2 cell-surface antigen heavy chain) via disulphide bridge.

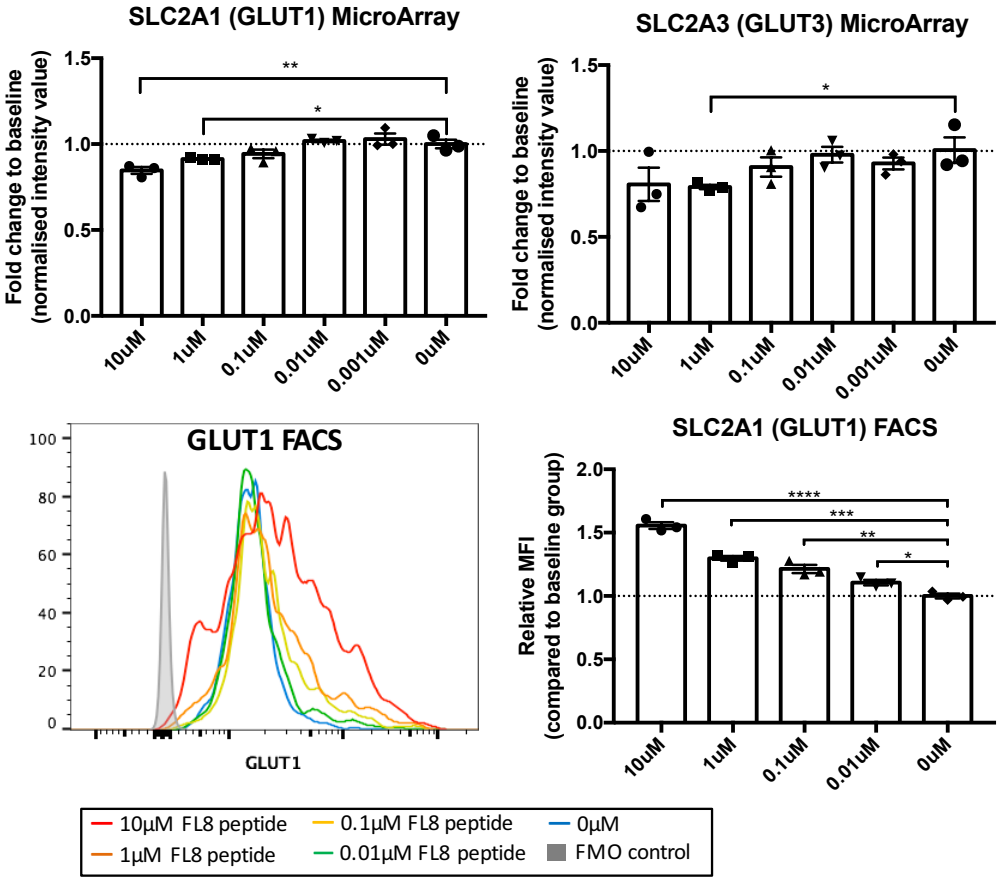

Figure 3-14 Detailed expression levels of glucose transporters (A3).

Gene expression levels were plotted to depict fold change at each antigen dose compared to the no antigen group. For GLUT1, protein level was also checked by FACS and plotted below microarray data. The error bar represents SD, * indicates $p<0.05$, ** indicates $p<0.01$, *** indicates $p<0.001$, p-values were calculated using 2-tail non-paired student's t-test. Error bar represents the standard deviation.

Metabolically active cells preferentially use LAT1 (large neutral amino acid transporter 1, SLC7A5-SLC3A2 dimer) despite the existence of LAT2 (SLC7A8-SLC3A2 dimer) as the affinity of LAT2 for leucine is much lower than that of LAT1. LAT1 is thus suitable for the rapid uptake of a large amount of amino acids in metabolically active cells (Hayashi and Anzai, 2014). Proteomic data revealed that the predominant CTL nutrient transporters are amino acid transporter SLC7A5 and SLC3A2 (Hukelmann et al., 2016). From our microarray data, both SLC3A2 and SLC7A5 transcripts were up-regulated more than 4-fold in high antigen dose groups (10μM and 1μM). FACS of LAT1 revealed a dramatic increase of LAT1 surface expression at 1-10μM antigen stimulation (10μM MFI: 23777 ± 2942; 1μM 11916 ± 825; vs 0μM MFI: 5856 ± 228.5) and a noticeably increased shift at 0.01-0.1μM antigen stimulation (0.1μM MFI: 7590 ± 104.3 and 0.01μM MFI: 6914 ± 63.79). This concerted with the observation of SLC3A2 and SLC7A5's transcription levels, as their transcriptions dramatically up-regulated at 1-10μM antigen stimulation, while the marginal up-regulation of their mRNAs could contribute to the increased shift at 0.01-0.1μM antigen stimulation. (Figure 3-15A) ASCT2 (SLC1A5), a sodium-dependent glutamine transporter that forms a complex with LAT1 at the plasma membrane and imports glutamine (Xu and Hemler, 2005), was also up-regulated in the array data (10μM and 1μM). (Figure 3-15B) On the other hand, CAT proteins mediate Na^+-independent transport of cationic L-amino acids. CAT-1 (SLC7A1) has the most pronounced *trans* stimulation among the CATs (Hatzoglou et al., 2004), and was also up-regulated in response to antigen stimulation. (10μM and 1μM) By contrast, the other CAT protein (CAT2, SLC7A2) down-regulated (10μM, 1μM and 0.1μM) (Figure 3-15B).

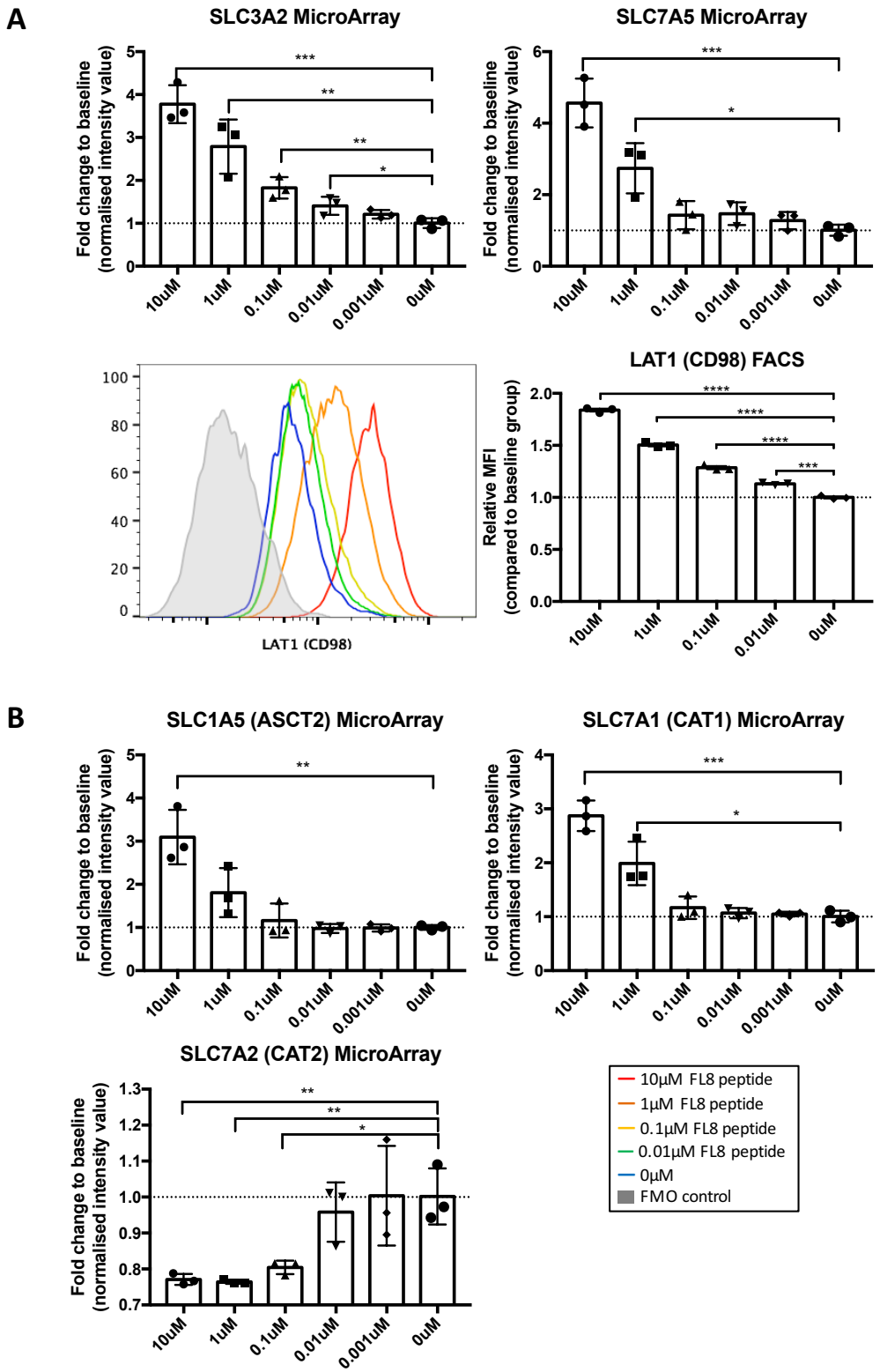

Figure 3-15 Detailed expression levels of amino acid transporters (A3).

Gene expression levels were plotted to depict fold change at each antigen dose compared to the no antigen group. For LAT1, protein level was also checked by FACS and plotted below microarray data. The error bar represents SD, * indicates $p<0.05$, ** indicates $p<0.01$, *** indicates $p<0.001$, p-values were calculated using 2-tail non-paired student's t-test. Error bar represents the standard deviation.

Metals are also key components of cellular functions. Iron, an essential growth trace element, is required for proliferation of all living cells, including T lymphocytes (Kuvibidila et al., 2003). Transferrin1 (TRFC), the major iron transporter, transcribed more mRNA at 1-10μM, its protein up-regulated at surface as low as 0.1μM. (Figure 3-16A) Furthermore, increased Zinc influx reduced the recruitment of SHP-1 to the TCR activation complex, augmented ZAP70 phosphorylation and sustained calcium influx (Yu et al., 2011). ZIP proteins of the SLC39A family are zinc importers mediating the influx from extracellular or intracellular sources into the cytoplasm (Eide, 2004). ZIP14 (SLC39A14) is a broad-scope metal ion transporter with a preference for zinc uptake, which also mediates cellular uptake of non-transferrin-bound iron (Pinilla-Tenas et al., 2011). ZIP8 (SLC39A8) is most closely related to ZIP14, which can transport iron, zinc, manganese, and cadmium. (Wang et al., 2012) Both the transporters were up-regulated (0.1-10μM) (Figure 3-16B). Several other essential transporters involved in biosynthesis, including SMVT (SLC5A6), RFC (SLC19A1) and ENT1 (SLC29A1), were also up-regulated in the microarray data. (Figure 3-16C) Cells respond to proliferation with increased accumulation of biotin and the abundance of the SMVT was similar at all phases of the cell cycle, suggesting that proliferation enhances biotin demand (Stanley et al., 2002). RFC is the principal mechanism by which folates are delivered to mammalian cells (Matherly et al., 2007). ENT1 is a transmembrane glycoprotein that localizes to the plasma and mitochondrial membranes and mediates the cellular uptake of nucleosides from the surrounding medium.

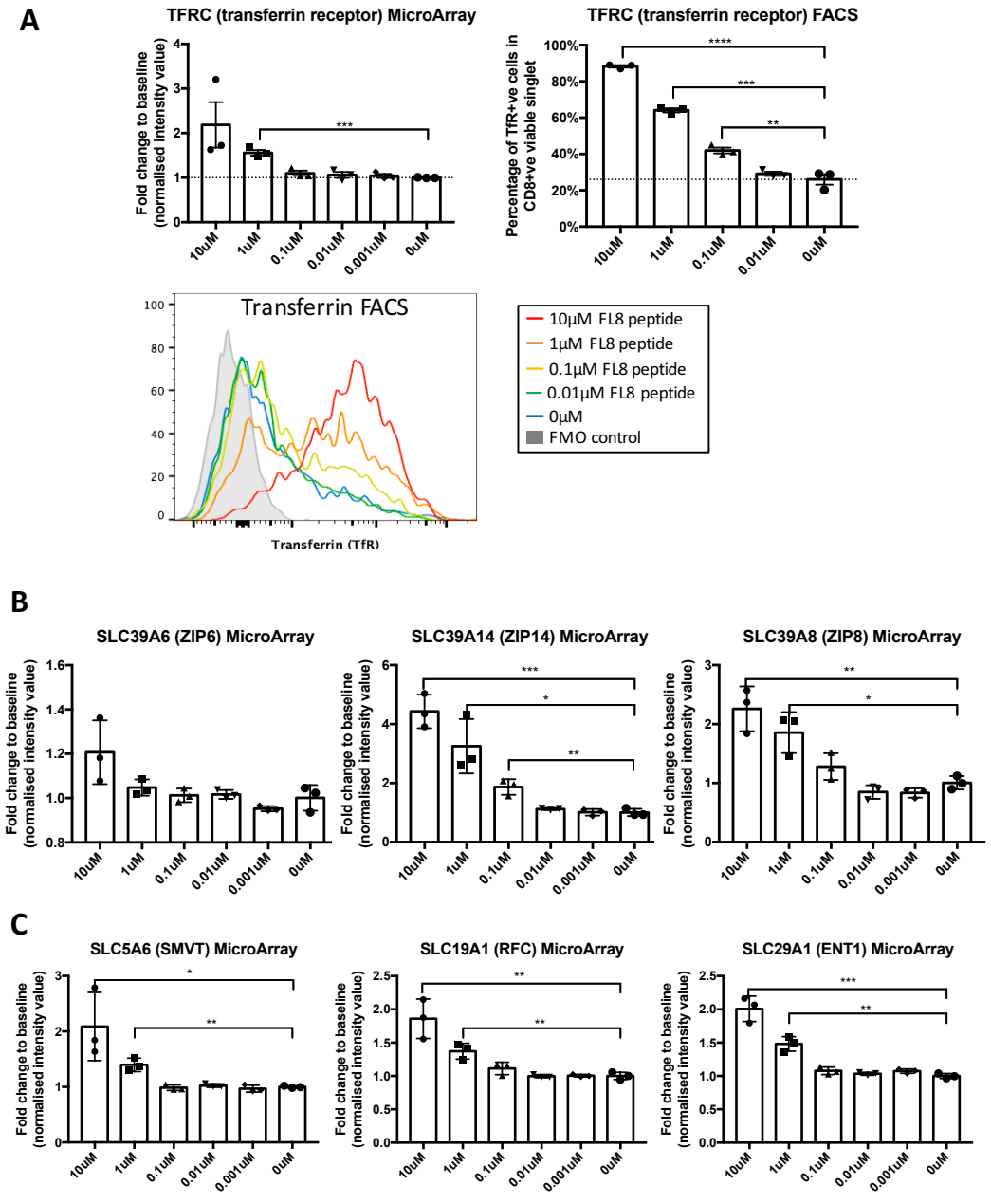

Figure 3-16 Detailed gene expression levels of metal and some most differentially expressed transporter genes (A3).

Gene expression levels were plotted to depict fold change at each antigen dose compared to the no antigen group. For Transferrin, protein level was also checked by FACS and plotted next to microarray data. The error bar represents SD, * indicates $p<0.05$, ** indicates $p<0.01$, *** indicates $p<0.001$, p-values were calculated using 2-tail non-paired student's t-test. Error bar represents the standard deviation.

3.2.7 Identification of the Most Sensitive Genes in Response to Antigen Stimulation Shared by Two CTL Clones Reveals a Pathway Involving EGR2, 4-1BB and CCL1.

From the microarray data, the clone C23 differentially expressed much fewer genes compared to the other clone A3 (Figure 3-15A). There are at least three explanations here. First, these two clones were generated from two individuals and were specific to very different antigens; second, the antigen sensitivity of clone C23 (1.1μM) is lower than that of clone A3 (0.025μM) and third, the target cells were different. In the microarray dataset, the clone C23 down-regulated much fewer genes than its up-regulated genes. For example, the number of down-regulated genes (FC>1.5, p<0.05) at 0.4μM antigen stimulation was only 8, in contrast to up-regulated genes (76 genes) in this clone. Similar to clone A3, the clone gene differential expressions on C23 were also strictly correlated to the antigen dose (Figure 3-17A). Although there were quite large differences of gene expression between A3 and C23, certain common candidate genes were still identified to be significantly up-regulated (155 genes) and down-regulated (47 genes) (Figure 3-17B). Among the common candidate genes, some key cellular regulators were identified, including genes that regulate glycolysis (PKM2), transporters (SLC3A2, SLC7A1, SLC7A5, SLC39A14, SLC27A2, SLC35F2, TRFC), mitosis check points (CDK4, CDK6), T cell transcription factors (BATF, BATF3), immune check points (CTLA4, HAVCR2) and CTL functions (IFNG, FASLG). (Appendix 1) Similar to what we discovered in A3 only, the majority of the common genes were involved in metabolism and nucleic acid binding. (Figure 3-18)

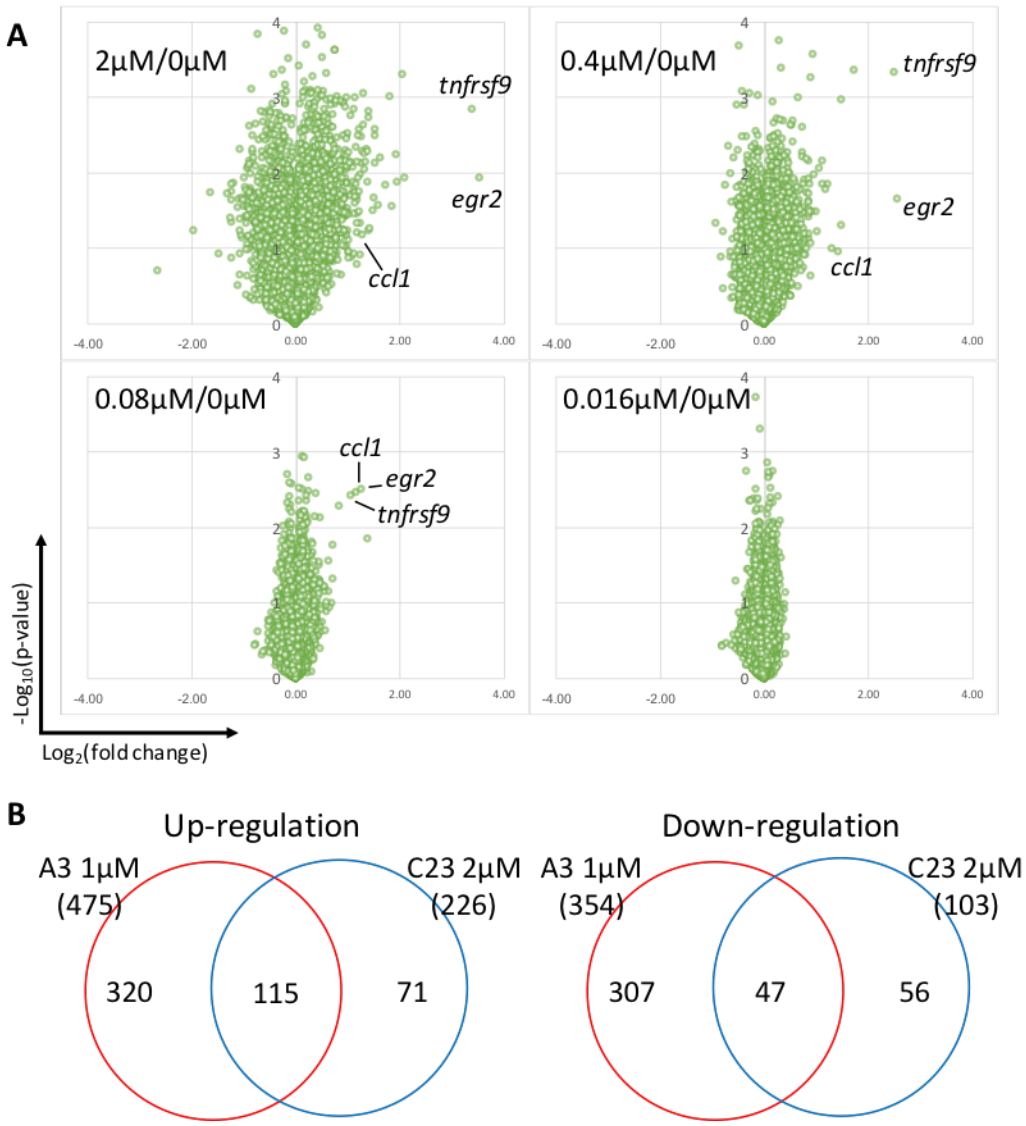

Figure 3-17 Gene differential expressions on CTL clone C23 vs A3.

(A) Volcano plots of pairwise comparisons for C23. The y-axis is the negative log10 of *p*-values (a higher value indicates greater significance) and the x-axis is the difference in expression between two experimental groups as measured in log2 scale. The most significantly differential expressed genes were labelled on each volcano plot. (B) Venn diagram showing the overlapped genes between C23-2μM and A3-1μM (left, up-regulate FC>1.5; right, down-regulate FC>1.5).

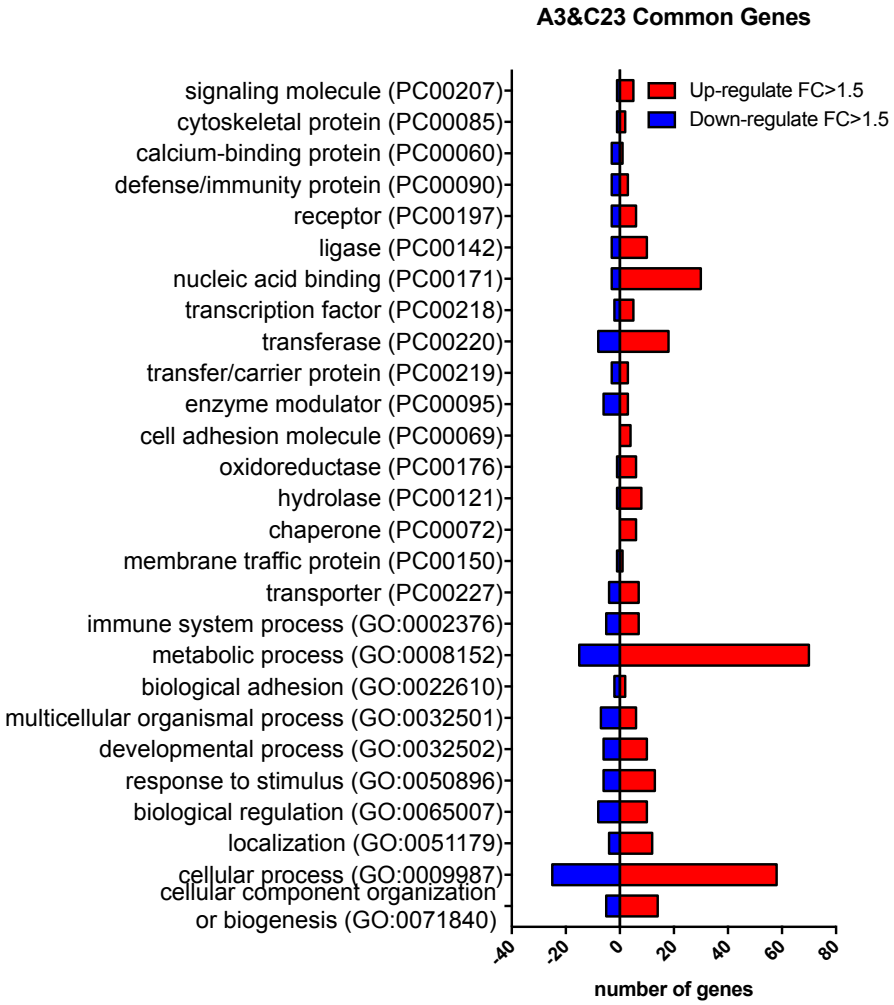

Figure 3-18 Classification of shared genes between A3 and C23.

Staggered bar chart of gene categorized to the biological process and protein class by functional classification in PANTHER. The up-regulated genes were coloured red and down-regulated genes in blue.

By overlapping the A3 differentially expressed genes (A3 [10μM&1μM&0.1μM], |FC|>1.5, p<0.05) and C23 differentially expressed genes (C23 [2μM&0.4μM&8μM], |FC|>1.5, p<0.05), the two CTL clones shared the common genes EGR2, TNFRSF9 and CCL1. All these three genes were up-regulated at very low strength of antigen stimulation as the most sensitive genes in response to antigen stimulations. The detailed gene expressions were depicted for both CTL clones (Figure 3-19). The EGR2 (also termed Krox20) is a transcription regulatory factor, containing two zinc finger DNA-binding sites. EGR2 and/or EGR3 directly induce the expression of SOCS1 and SOCS3 (inhibitors of STAT1 and STAT3) and also block the function of BATF, an AP-1 inhibitor, in B and T cells. Thus, EGR2 and EGR3 regulate B and T cell function in adaptive immune responses and homeostasis by promoting antigen receptor signalling and controlling inflammation (Li et al., 2012). EGR3, the transcription of which peaks at 3h post TCR stimulation, is different from EGR2, transcription of which peaks at 6h (Safford et al., 2005). The difference of peak-time provided the explanation that EGR3 expressions were filtered from the microarray data, while EGR2 stood out as the most highly expressed gene. EGR2 has also been shown to drive cell surface proteins LAG-3 and 4-1BB on T cells, which can identify dysfunctional antigen-specific CD8+ tumour infiltrating lymphocytes (TILs), as the co-expression of 4-1BB and LAG-3 was seen on a majority of $CD8^+$ TILs (Williams et al., 2017). In addition, EGR2 also directly bind to the promoter of CCL1 and drives gene expression, while blockade of CCL1 significantly reduced CD4+ T cell migrations in a mast cell study (Wu et al., 2013).

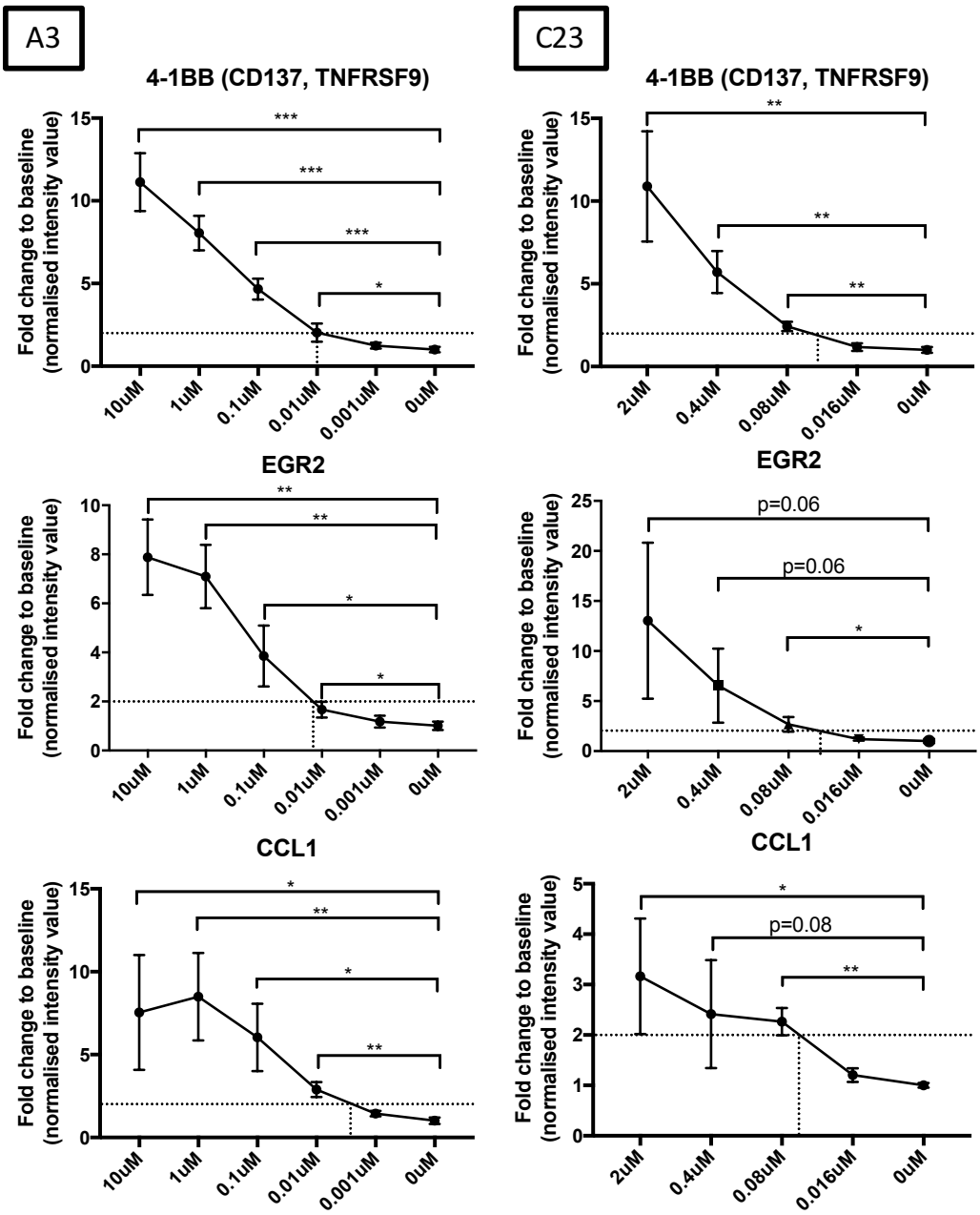

Figure 3-19 The RNA expressions of 4-1BB, EGR2 and CCL1 in response to antigen stimulation by microarray.

Line graphs of mRNA expressions of 4-1BB, EGR2 and CCL1 in two CTL clones (A3: left, C23: right) at 6 hours' post antigen stimulation with different strength of antigen stimulation. Fold change was calculated by dividing each normalised intensity value to the average value of control group (n=3). The error bar represents SD, * indicates $p<0.05$, ** indicates $p<0.01$, *** indicates $p<0.001$, p-values were calculated using 2-tail non-paired student's t-test. Dashed lines were shown on each graph to demonstrate the minimum antigen strength for up-regulating the corresponding mRNA to 2-fold change. Error bar represents the standard deviation.

4-1BB is expressed by activated T cells rather than resting T cells. Its ligand (CD137L) is predominantly expressed by activated APCs, including DCs, macrophages and B cells (Makkouk et al., 2016). In T cells, 4-1BB cross-linking induces proliferation, production of IFN-γ and IL-2, and enhances survival through up-regulation of anti-apoptotic pathways (Snell et al., 2011). The detailed 4-1BB expressions overtime with 5 doses of antigen stimulation on A3 clone were shown in Figure 3-20.

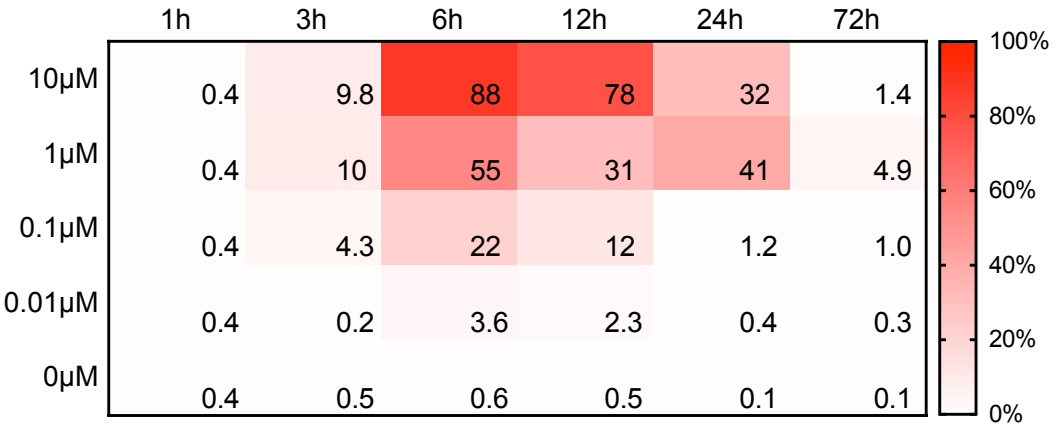

Figure 3-20 4-1BB expression pattern on clone A3 (time & dose).

FACS was performed following 1h, 3h, 6h, 12h, 24h, 72h incubation (10:1 ratio) with peptide pulsed HLA-B*08+ CD4+ T cell line C8166 cells (10μM, 1μM, 0.1μM, 0.1μM, 0μM). Cells were gated on single live CD8+ cells. Data from 3 batch experiments, mean values of the percentage of all cells positive for 4-1BB were presented in the heatmap.

As previously described, 4-1BB only expressed only on the stimulated CTLs and was in a dose-dependent manner. In addition, from the microarray data, some molecules from the 4-1BB pathway were also up-regulated, including TRAF1 (1μM and above) and anti-apoptotic mitochondrial proteins such as Bim (1μM and above), Bcl-2 (10μM) and Bcl-xL (10μM). (Figure 3-21)

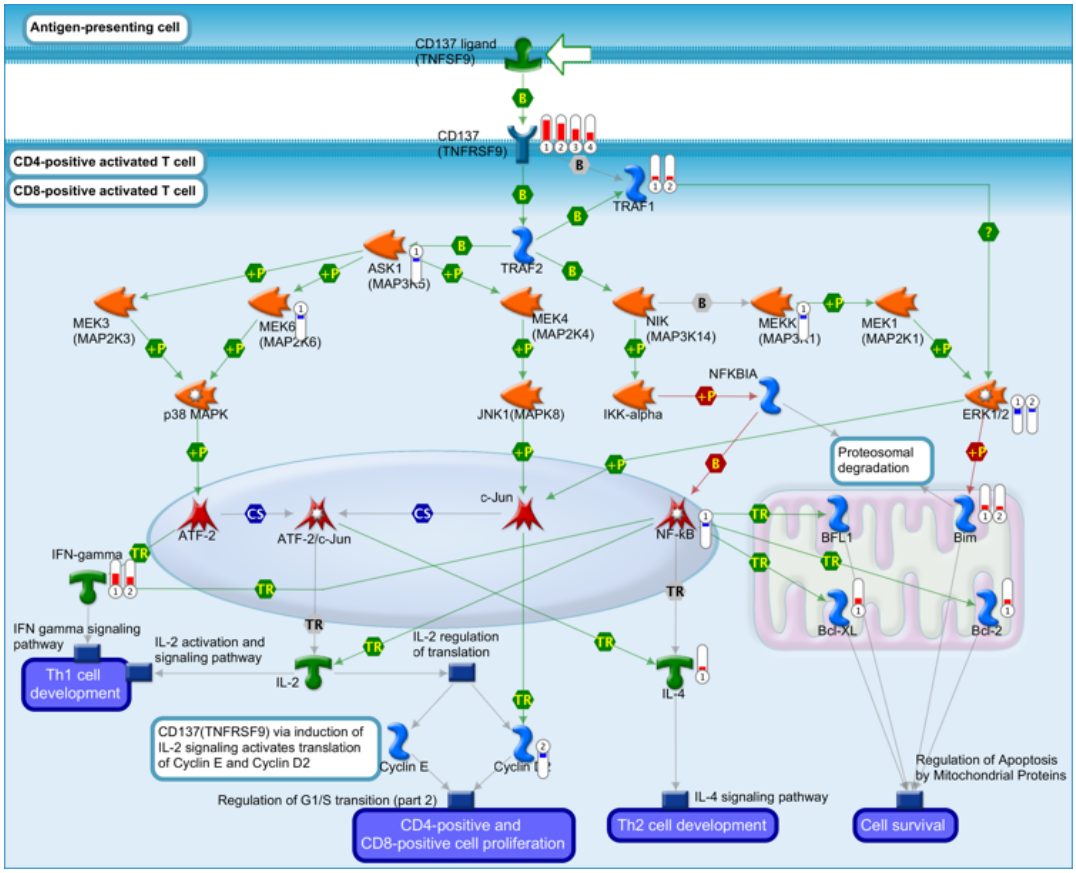

Figure 3-21 Immune response 4-1BB signalling in immune cell.

Pathway analysis of 4-1BB (CD137) signalling using MetaCore (Thomson Reuters). Gene differential expression value are shown in log2 scale next to each significantly differentially expressed gene. ① : 10μMvs0μM, 8/29, *p*-value=9.164E-03, FDR=3.845E-02; ② : 1μMvs0μM, 6/29, *p*-value=8.936E-03, FDR=6.618E-02.

Collectively, these observations provide further evidence of the important roles of 4-1BB in regulating CTL functions. The proposed pathway of these three most responsive CTL genes in response to antigen stimulation was depicted in Figure 3-22 - TCR signal activates EGR2 expression about 3-6 hours post TCR engagement. Thereafter, EGR2 directly or indirectly binds to the promoters of CCL1 and 4-1BB to promote their transcriptions.

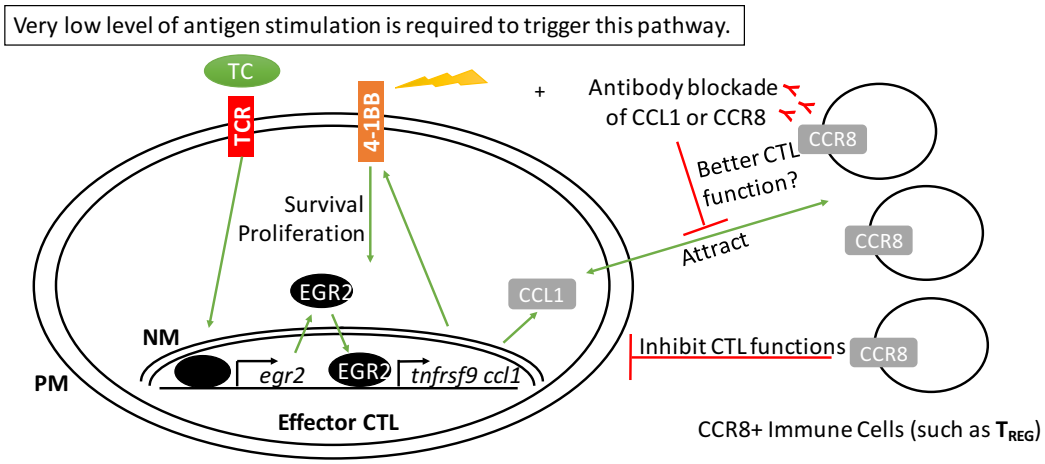

Figure 3-22 Proposed EGR2, 4-1BB, CCL1 pathway.

CTL express EGR2 molecules as a consequence of TCR engagement and subsequent TCR downstream signalling pathway activation. (peaks at 6h post) EGR2 then act as the transcription factor for CCL1 and probably TNFRSF9. The latter two proteins attract CCR8+ expressing immune cells and promote cell survival/proliferation, respectively. Ag: antigen; NM: nuclear membrane; PM: plasma membrane.

3.3 Discussion.

Several studies have used high-dimension genomic analysis to examine the differential expression of genes and transcriptome profiles upon T cell activation experiments (Hukelmann et al., 2016; Mattson et al., 2014; Safford et al., 2005; Zhao et al., 2014). However, few studies have been conducted to stimulate the T cells using proper peptide-loaded APCs and on the experimental settings of human primary T cell samples, which provides more meaningful data than activating T cells simply through anti-CD3 antibodies. In this study, we were trying to understand the influences of antigen abundance loaded on APCs towards the CTL's functions. And we have characterized the CTL transcriptomes on two disparate antigen-specific CTL clones (HIV-specific CTL clone A3: B*0801/HIV.Nef.90-97 FLKEKGGL, patient ID: LTNP005 and HCV epitope-specific CTL clone C23: B*2705/HCV.NS5B.2831-2849 ARMILMTHF, patient ID: SM197) that received a range of antigen stimulations (signal 1), mapping the expression of transcripts and splice variants of highly expressed genes by more than 20000 Illumina microarray probes.

There were certain technical difficulties during the preparation of RNA samples. For example, the minimal amount of RNA required for a successful library preparation of microarray was at least 0.5μg/sample for the Illumina HT12 beads chip platform. In this experiment, the same CTL clones were treated with six doses of antigen stimulation; thus, all the six RNA samples in the same batch were expected to pass QC and get enough RNA yield before proceeding to the next step. In fact, T cells are small suspended cells with a big nuclear/plasma ratio, compared to immortalized cell lines, the RNA yield is much lower per cell.

Further, during the cell preparation, cell loss was inevitable during steps such as washing and passing over a magnetic column (for depletion of target cells). All these factors made the RNA extraction quite challenging. We tried to start with 2 million CTLs but didn't get enough quantity or quality of RNA; and subsequently we increased this number to 5 million cells. This required the CTL clones for the study to be good at proliferation. However, *in vitro* cultured CTL clones were started from a single well-differentiated mother memory CTL, where there would be inevitably certain limitations for proliferation. All these factors made the RNA preparation work the most challenging part of this study.

RNA-Seq and Microarray are both widely used and reliable for RNA study. In general, RNA-Seq is superior in detecting low abundance transcripts, differentiating biologically critical isoforms, allowing the identification of genetic variants and high fold-change differentially expressed genes (Zhao et al., 2014). However, microarray is significantly cheaper and data are relatively easier to be analysed. As the sample source in this study was very homogenous (CTL clones), microarray was recommended to be good enough for our purpose. All technical aspects of this microarray experiment worked well, no outlier samples were identified, and high-quality data were obtained. A3 showed much bigger differences between each group than C22, which was attributable to the difference in many factors, including individual genetic characteristics, TCR affinity, source of target cells and peptide gradient. Nevertheless, there was a clear trend on the PCA plot with the same direction of gene expressions on both clones, indicating that the gene differential expressions were caused by the increased antigen dose loaded on APCs.

3.3.1 Hierarchy of CTL Gene Differential Expressions in Response to Different Strengths of Antigen Stimulation.

As we previously indicated, this study did not compare the differences between A3 and C23. Thus, these two clones were analysed independently. From the PCA plot, it was very clear that the HIV epitope-specific clone A3 shows substantially greater gene differential expressions than the HCV epitope-specific clone C23. We first analysed the clone A3 in detail. Each of the multiple comparison analysis (MCA) tests has its own particular strengths and limitations. Therefore, the choice of an MCA statistic should be based on the specific research questions. In the gene list analysis, the normalized microarray intensity values were first subjected for t-test between each dose group and the control group. Bonferroni correction and False Discovery Rate (FDR) approach were not applied as we have experienced that they are too conservative for T cell clone data generated from Illumina platform in our previous attempts (Glanville et al, unpublished), in the sense that while they reduce the number of false positives, they also 'kill' true discoveries. This is particularly true in this experiment as the suboptimal TCR signalling (such as 0.01μM of cognate peptide) only triggers a small number of genes for differential expression. However, genes changed consistently in different dose responses and experimental repeats could be considered as validate candidate for further investigation.

Volcano plots nicely depicted that differential gene expressions on clone A3 were in dose-dependent manner. From an elegant mice study, it was found that low levels of AKT activity (about 10-20% of that in wild-type T cells) can be

sufficient for T cell proliferation but insufficient to initiate the migratory programme (Waugh et al., 2009). In addition, supra-optimal antigenic stimulation could render CTLs susceptible to apoptosis, which usually occurs after CTLs exert their cytotoxicity functions (Alexander-Miller et al., 1996). In this study, there were too few differentially expressed genes for gene ontology study at lower strength of antigen stimulation (0.1μM and below), in which TCR downstream signalling molecules are sub-maximally activated. In higher strength groups (1μM and above), genes relating to metabolism and biogenesis were up-regulated and signalling transductions were down-regulated. Genes that relate to cytoskeleton down-regulated as well. As this microarray data only provide a snapshot of transcriptome reprogramming, it's difficult to draw a firm conclusion on the functional hierarchy in response to different strength of antigen stimulation.

	10^{-2}µM-10 µM		10^{-1}µM-10µM		1µM-10µM	
Function	up-regulated (FC > 1.5)	down-regulated (FC < 0.67)	up-regulated (FC > 1.5)	down-regulated (FC < 0.67)	up-regulated (FC > 1.5)	down-regulated (FC < 0.67)
Metabolism	PKM2 (1.8)					
Mitosis			CDK6 (2.7) CDK4 (2.7)			
Nutrient Transporter	4F2 (3.8) ZIP14 (4.4)	CAT2 (0.6)	LAT1 lc (4.5) ASCT2 (3.1) CAT1 (2.9) FATP2 (2.7) ZIP8 (2.2) TRF1 (2.0)		y+LAT2 (1.5)	GLUT3 (0.6)
Cytotoxicity	FAS ligand (3.2)				Perforin (1.6)	
Cytokine/Chemokine	CCL1 (7.0) GM-CSF (5.6)	IL23 (0.3) CCL22 (0.2)	IL5 (6.5) IFNg (4.1) M-CSF (2.0)	TWEAK (0.4)	IL13 (2.2) CCL3 (2.2) IL8 (1.7)	IL10 (0.7) IL15 (0.6) IL16 (0.5)
Cytokine/Chemokine Ligand			IL2RA (5.7) CCR4 (1.6) TNFR2 (2.2)	CCR3 (0.3) IL10RA (0.4) IL7R (0.4) CXCR4 (0.5) CX3CR1 (0.4)		TNFR1 (0.8) IL10RB (0.5) CXCR3 (0.6) CCR2 (0.5)
Transcription Factor	EGR2 (7.8)	EGR1 (0.5)	BATF3 (4.7) BATF (3.4)	KLF2 (0.3) STAT4 (0.4) STAT1 (0.5)	STAT5A (2.0)	STAT2 (0.6)

Table 3-3 Summary of differential expressed immune regulator genes with function and maximum fold change.

However, these data demonstrated very clear hierarchies of antigen sensitivity and magnitude of fold change among gene regulations within CTLs (Table 3-3). For example, PKM2, a limiting glycolytic enzyme in metabolism and cell growth (catalyses the final step in glycolysis) (Wang and Green, 2012), up-regulated 1.8-fold when the CTLs received 0.1μM antigen stimulation and its expression remained flat by increasing the stimulation strength to 10μM. Up-regulation of PKM2 leads to aerobic glycolysis, biogenesis and cell proliferation (Dayton et al., 2016). In addition, CDK4 and CDK6 up-regulated when the CTLs received 1μM antigen stimulation and above. These two cyclin-dependent kinases help to drive the progression of cells into the DNA synthetic (S) phase of the cell-division cycle from G1 phase. Therefore, from our data, metabolic re-programming (represented by PKM2) requires a lower strength of antigen stimulation than proliferation (represented by CDK4/6). In the section of cytokine/chemokines/receptors on clone A3, it's very interesting to observe multiple pairs of functionally related genes up-regulated and down-regulated in response to antigen stimulation. For example, with the increment of antigen stimulation, chemokine CCL1 up-regulated while CCL22 down-regulated; chemokine receptor CCR4 up-regulated while CCR3 downregulated; IL2RA (proliferative cytokine receptor) up-regulated while IL10RA (immune suppressive cytokine receptor) down-regulated.

In a recent mice study, comparison of the CTL transcriptome and proteome reveals moderate, positive correlation between mRNA abundance and protein abundance, with a coefficient of determination of 0.43 (Hukelmann et al., 2016). Hence, the transcripts level may not reflect the 'real' situation in some cases. For instance, from the microarray data, the transcripts of glucose transporters slightly

dropped with increased antigen stimulation. However, surface expression of GLUT1, evaluated by FACS, showed an increased expression of this glucose transporter with stimulation and a high expression at basal level, indicating that post-transcriptional regulatory mechanisms could affect the GLUT1 expression on CTLs. Although glucose is a critical substrate for T cells, glutamine is also essential during T cell activation (Buck et al., 2015). The glutamine was co-transported with Na^+ by ASCT2 and subsequently exchanged for L-leucine, an important activator of mTORC1 signalling, by LAT1 (Ren et al., 2017). While the deficiency of SLC7A5 (LAT light chain) prevents the metabolic reprogramming, clonal expansion, and/or effector function of both CD4+ and CD8+ T cells (Sinclair et al., 2013). Among the nutrient transporters, the SLC3A2 and SLC7A5 stood out as the most sensitive transporter genes to antigen stimulation, of which the mRNA up-regulations could be more than 1.5-fold as low as 0.01μM, in contrast to the glutamine transporter ASCT2 (up-regulated at 1μM and above). Compared to GLUT1, the up-regulation of LAT1 (SLC3A2-SLC7A5 heterodimer) was much more dramatic and a substantial increase was observed by FACS upon TCR engagement. Apart from glucose and amino acid transporter, TCR engagement exercised much wider influences on CTL nutrient uptake and metabolic reprogramming, such as increasing the expression of metal, vitamin and nucleoside transporters on cell surface; and modulating the SLC25 family transporters on mitochondria. In particular, metal transporters ZIP8 and ZIP14, which can transport iron, zinc, manganese, and cadmium, were significantly up-regulated at 0.1μM, even more sensitive than classical T cell zinc and iron transporters – ZIP6 and transferrin 1 (up-regulated at 10μM and 1-10μM respectively). The orchestra of these gene expression changes provides directions

for our future study for understanding the role of TCR signalling strength on CTL functions (Figure 3-23).

Figure 3-23 Summary of glucose, amino acid, zinc and iron transporters on A3 in response to different strengths of antigen stimulation.

Schematic representation of the transporter genes studied here. The mRNA levels of genes quantified by microarray were coloured in blue and the protein levels of some transporter genes quantified by FACS were coloured in red. The up-regulation magnitude was represented by the number of plus symbol '+'. Unchanged gene expression was indicated by a hyphen symbol '-'.

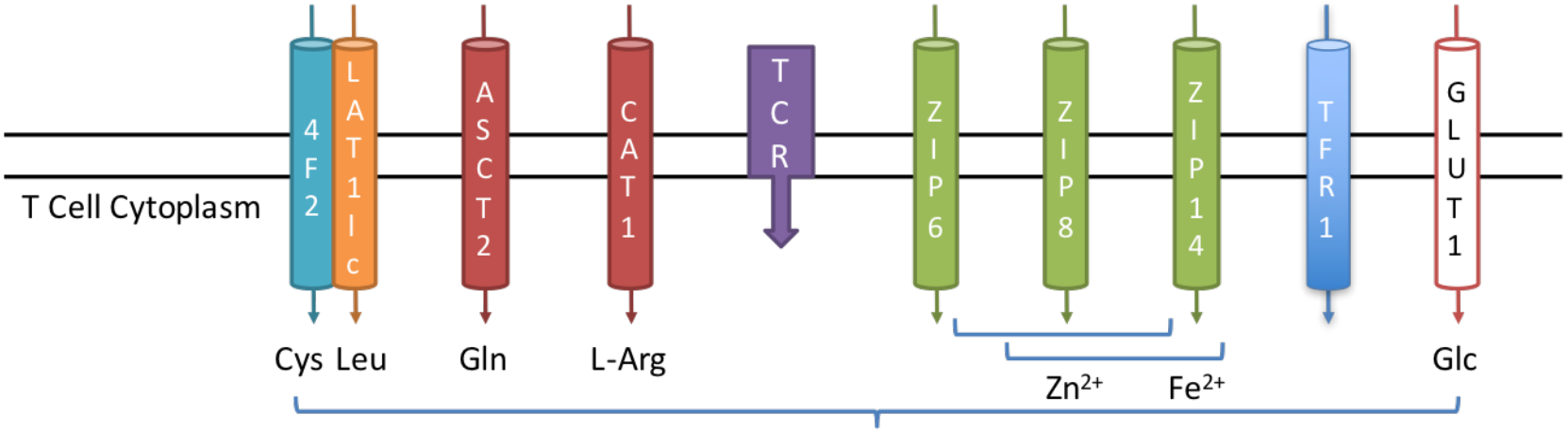

Stimulation Strength	LAT1			SLC1A5 (ASCT2)	SLC7A1 (CAT)	ZIP6	ZIP8	ZIP14	TRFC		SLC2A1 (GLUT1)	
	4F2	SLC7A5										
0-10^{-3}µM	+	+	+	-	-	-	-	-	-	-	-	-
10^{-3}-10^{-2}µM	+	+		-	-	-	-	-	-		-	
10^{-2}-10^{-1}µM	+	+	+	-	-	-	+	+	-	+	-	+
10^{-1}-1µM	++	++	++	+	+	-	++	+++	+	++	-	+
1-10µM	+++	++++	+++	+++	++	+	++	++++	++	+++	-	++

Microarray: unchanged or slightly decrease (-), intensity value fold change 1-2 (+), 2-3 (++), 3-4 (+++), 4-5 (++++)
FACS: unchanged (-), MFI fold change 1.1-1.4 (+), 1.4-1.7 (++), 1.7-2.0 (+++)

3.3.2 Seeking the 'Common Ground' Between Disparate Clones.

The A3 and C23 are two very disparate CTL clones. Thus, when we looked at the shared differentially expressed genes between these two CTL clones, it would be more likely to reflect the 'real' situation than looking at one CTL clone alone. 155 out of the 475 A3 up-regulated genes (33%) and 47 out of the 354 A3 down-regulated genes (13%) could also be detected in the same manner on clone C23. This result clearly highlighted the large differences between these two CTL clones and the complexity and heterogeneity of CTL functions and regulations. However, I hypothesize that the identified common candidate genes are those that are most likely to be expressed by other CTL clones in response to antigen stimulation. Among these shared genes, an interesting pathway containing EGR2, CCL1 and TNFRSF9 emerged as the most sensitive to antigen stimulation. This pathway could be invoked at a stimulation strength of as low as 0.01μM peptide, requires about 100-fold less antigen stimulation than most of the other antigen-triggered genes (differentially expressed at 1μM and above). Recently, it has been reported that EGR2 overexpression drives the expression of Tnfrsf9, Lag3, Ngn, Sema7a, Crtam, Ccl1 and Nrn1 on mice (Williams et al., 2017). Interestingly, in our microarray data, only TNFRSF9 and CCL1 have shown comparable expression pattern with EGR2. We could detect CRTAM and LAG3 up-regulation at 1μM and above. However, NGN, SEMA7A and NRN1 were either filtered or remained unchanged. This could be explained by a secondary or a late-stage effect of EGR2 overexpression or the differences between human and mice. In addition, SLC7A5, SLC3A2, SLC39A14, TRFC, SLC27A2, SLC35F2, CDK6, CDK4, PKM2, FASLG, IFNG, GM-CSF, CTLA4, TIM3, IL2RA, TNFR2 and BATF3 were also

identified to be up-regulated in clone C23, highlighting the importance of these T cell regulators, as they were shared by different clones.

To conclude, we have, in this chapter, conducted a high-dimension genomic analysis of CTL transcriptomic changes on antigen stimulation and observed interesting incremental gene differential expressions on clonal CTLs by stimulating the cells with a gradient dose of antigen. Notably, this dataset provides an overlook of genes' sensitivities to antigen stimulation and their expression levels at different strengths of antigen stimulation. We identified promising candidate genes that can be invoked at very low strength of antigen stimulation, particularly EGR2, CCL1 and 4-1BB. CCL1 have the potential to attract T_{REG} cells to induce the suppression of the effector cells, blocking this CCL1/CCR8 interaction might improve local T cell functions, with antagonizing 4-1BB as an additional improvement. We also observed interesting gene expression switches, such as IL2RA (up) and IL7RA, IL10RA (down), CCR4 (up) and CCR3 (down), CAT1 (up) and CAT2 (down), in response to antigen stimulation.

In this chapter, we presented a gene expression study of effector CTL that receive different strengths of antigen stimulation. Although firm conclusions may not be drawn so far, our studies provide understandings on the mechanisms employed by CTLs to undergo activation and have relevance for the identification of novel targets for candidate genes for manipulating CTL functions. In particular, chemokine CCL1, driven by EGR2, has been detected to response to very low dose of antigen stimulation. As in cases such as tumour cells, which down-regulate MHC I molecule on their surface, effector CTLs have high chance to

only receive suboptimal antigen stimulation (due to the low concentration of tumour epitope-MHC-I complexes) but still be able to secrete CCL1. Blockade of CCL1 therefore may be therapeutical beneficial as it could attract immunosuppressive T_{REG} cells.

4 Chapter 4: Investigation of Immune Checkpoint Expressions on Antigen-Specific Cytotoxic T Cells.

4.1 Introduction.

Upon full activation, CTLs upregulate several hundred genes required for proper proliferation and functions of cytotoxicity (Chapter 3). Among these up-regulated genes, immune checkpoint receptors (known as co-signalling receptors, including co-stimulatory and co-inhibitory receptors) are particularly interesting as they have been showing tremendous potentials for therapeutic applications. These receptors mediate T cell responsiveness to antigens and fine-tune the T cell activation, and play a central role in the development of immune pathology, autoimmunity, and also the destruction of cancer cells (Baitsch et al., 2012; Nirschl and Drake, 2013). For example, in some chronic infections and cancers, viruses and tumour cells could induce the expression of inhibitory immune checkpoint receptors on effector T cells and up-regulate their ligands on target cells, thus functionally silencing the effect of T cells, which leads to T cell exhaustion and immune escape (Catakovic et al., 2017).

As described in the introductory chapter, most co-signalling molecules are members of the immunoglobulin superfamily (IgSF) and tumour necrosis factor receptor superfamily (TNFRSF). Among them, CTLA-4 and PD-1are the two most well-characterized immune checkpoint receptors, both of which down-regulate TCR signalling, thus dampening the CTL functions. Therapeutic applications of several antibodies targeting CTLA-4, PD-1 and PD-L1 (ligand of PD-1) have been approved by FDA since 2011, and have revolutionized the entire

cancer treatment regimen (Armand et al., 2016; Borghaei et al., 2015; Brahmer et al., 2015; Ferris et al., 2016; Garon et al., 2015; Hamid et al., 2013; Hodi et al., 2010; Lipson et al., 2015; Motzer et al., 2015; Motzer et al., 2014; Robert et al., 2015a; Robert et al., 2015b; Rosenberg et al., 2016; Topalian et al., 2014; Topalian et al., 2016; Valsecchi, 2015; Wang et al., 2017). CD28, ICOS, CTLA-4 and PD-1 all belong to the CD28 family. Unlike CTLA-4 and PD-1, CD28 and ICOS are important co-stimulatory receptors. BTLA shares structural similarities with PD-1 and CTLA-4, however, it is transiently up-regulated upon TCR engagement and down-regulated on fully activated T cells, which is different from PD-1 and CTLA-4. VISTA is a B7 family molecule that may act as both receptor and ligand, such as the inhibitory receptor BTLA. CD96, CD226 and TIGIT bind to same ligands (CD112, CD155) with different affinities, while CD226 delivers positive co-stimulatory signal to T cells in contrast to the inhibitory signals delivered by CD96 and TIGIT. CRTAM is a T cell activation marker and has been shown to correlate with T cell polarization via Scrib and PKCζ. TIM-3 and TIM-4 belong to the TIM (T cell immunoglobulin and mucin-domain containing) family. TIM-3 is a well-studied inhibitory receptor, while TIM-4 is less studied. 2B4 (*Cd244*) and Ly108, together with SLAM, Ly9, CD84 and CRCC belongs to the co-stimulatory SLAM (signalling lymphocyte activation molecule) family, can also exert inhibitory functions, depending on the contexts. LAG-3 structurally resembles CD4 and can inhibit CD4+ T cell or CD8+ T cell activation via binding to MHC II or LSECtin, respectively. Similar to BTLA, CD160 also binds to HVEM (herpesvirus entry mediator) and mediates inhibitory activity. 4-1BB (*Tnfrsf9*), CD27(*Tnfrsf7*), OX40 (*Tnfrsf4*), GITR (*Tnfrsf18*) and CD30 (*Tnfrsf8*) are members of type-V TNFRSF receptors and could deliver co-stimulatory

signals. TNFR1(*Tnfrsf1a*), TNFR2 (*Tnfrsf1b*), Fas (*Tnfrsf6*) and TRAILRs (*Tnfrsf10a-c*) are members of type-L TNFRSF receptors and regulate T cell survival and apoptosis, HVEM (*Tnfrsf14*), DR3 (*Tnfrsf25*), CD40 (*Tnfrsf5*), RANK (*Tnfrsf11a*) are also members of type-L TNFRSF receptors but are stimulatory receptors. While, the functions of TACI (*Tnfrsf13ba*), BAFFR (*Tnfrsf13c*), BCMA (*Tnfrsf17*), TWEAKR (*Tnfrsf12a*), RELT (*Tnfrsf19l*), DR6 (*Tnfrsf21*), TROY (*Tnfrsf19*) are less studied and mostly remain unclear (Anderson et al., 2016; Catakovic et al., 2017; Chen and Flies, 2013; Pardoll, 2012). In addition to the successful development of blocking antibodies against CTLA-4, PD-1 and PDL1, other inhibitory and co-stimulatory immune checkpoint receptors (such as TIM-3, LAG-3, TIGIT and 4-1BB, OX40) are also under investigation in clinical trials as the sole cancer treatment or in combination with anti-PD-1 treatment (Giuroiu and Weber, 2017).

Although the antibody-based immunotherapy has become a new way of overcoming cancer, many patients receiving these drugs develop autoimmune manifestations - they occur in up to 90% of the patients treated with an anti-CTLA-4 antibody and 70% of patients treated with an PD-1/PD-L1 antibody (Michot et al., 2016). With more and more cancer treatment clinical trials in progress or preparing to be launched based on activating the immune system (by antagonizing or agonizing immune checkpoint receptors), the immune checkpoint blockades are expected to become routine oncological practice in the near future. This highlights the importance of investigating in greater detail the molecular properties of immune checkpoint receptors and the functions of their pathways.

4.1.1 The Aim of This Chapter.

In this chapter, we intend to characterize the immune checkpoint expression patterns on antigen-specific cytotoxic T cells by studying *in vitro* cultured CTL clones and *ex vivo* PBMC samples.

Specific Aims:

1. To characterize the immune checkpoint expression patterns on antigen-specific cytotoxic T cells, in response to different strengths of antigen stimulation.
2. To investigate the co-expression patterns of different immune checkpoint genes on antigen-specific cytotoxic T cells.
3. To examine our *in vitro* finding by exploring the correlation between different immune checkpoints on antigen-specific CTLs in *ex vivo* PBMC samples.

By studying these immune checkpoint expression changes, we would be able to understand better on the fine-balancing of CTL activation and the status of T cell exhaustion, thus providing insights for future immunotherapy development.

4.2 Results.

4.2.1 Differential Expressions of Immune Checkpoint Receptor Genes in Response to Different Strengths of Antigen Stimulation.

To characterize the expression patterns of the most well-known immune checkpoints in response to different dose of antigen stimulation, a panel of 45 co-signalling molecules - including IgSF receptors: *CD28, ICOS, CTLA4, PD1, VISTA, BTLA, CD80, CD226, CRTAM, TIGIT, CD96, TIM3, TIM4, CD2, SLAM, 2B4, LY108, CD84, LY9, CRACC, LAIR1, LAG3, CD160* and TNFRSF receptors: *4-1BB, OX40, CD27, GITR, CD30, TNFR1, TNFR2, HVEM, DR3, FAS, CD40, RANK, TRALR1-3, TACI, BAFFR, BCMA, TWEAKR, RELT, DR6, TROY* (the remaining 13 molecules were filtered for the low expression.) - were selected for clustering based on previous described microarray experiment. The heatmap of hierarchy cluster of these 45 co-signalling molecules (61 probes) has been shown in Figure 4-1, segregated into three branches.

The upper branch prises genes down-regulated in response to increased antigen stimulation. It is to be noted that these genes included Ly9, CD96, TNFR1, Ly108, BTLA, TIGIT and 2B4 (down-regulated genes). The middle branch were genes that remained unchanged, while the lower branch were genes that increased upon antigen stimulation on this CD8 antigen-specific T cell clones, which included CRTAM, CD28, CRACC, LAG3, CD160, TIM4, 4-1BB, TIM3, CTLA4, PD1, TNFR2, TWEAKR, RAFFR, BELT, VISTA and CD226 (up-regulated genes). In addition to the up-regulated pattern and down-regulated pattern, the transcription of CD84, CRTAM, CD28, CRACC was up-regulated at lower antigen dose (1μM and 0.1μM) and down-regulated to baseline level at the highest dose (10μM),

while GITR showed a trend to up-regulate (30-50%) at 0.001μM and 0.01μM but down-regulated to baseline at higher doses. Interestingly, the probes specific to TIGIT, CD40 and CD84 showed different trends for the same gene. In the case of CD40, the probes were designed to target two transcript variants. CD40 transcript variant 2 up-regulated in high antigen dose, while variant 1 remained flat. However, the probes for TIGIT and CD84 were not designed to target different transcript variants (Figure 4-1). Detailed values of each differentially expressing genes were listed in Table 4-1. *p*-values were calculated by two-tailed non-paired student's t-test. Fold change >1.5 or <1.5 and *p*-values<0.05 were highlighted in red.

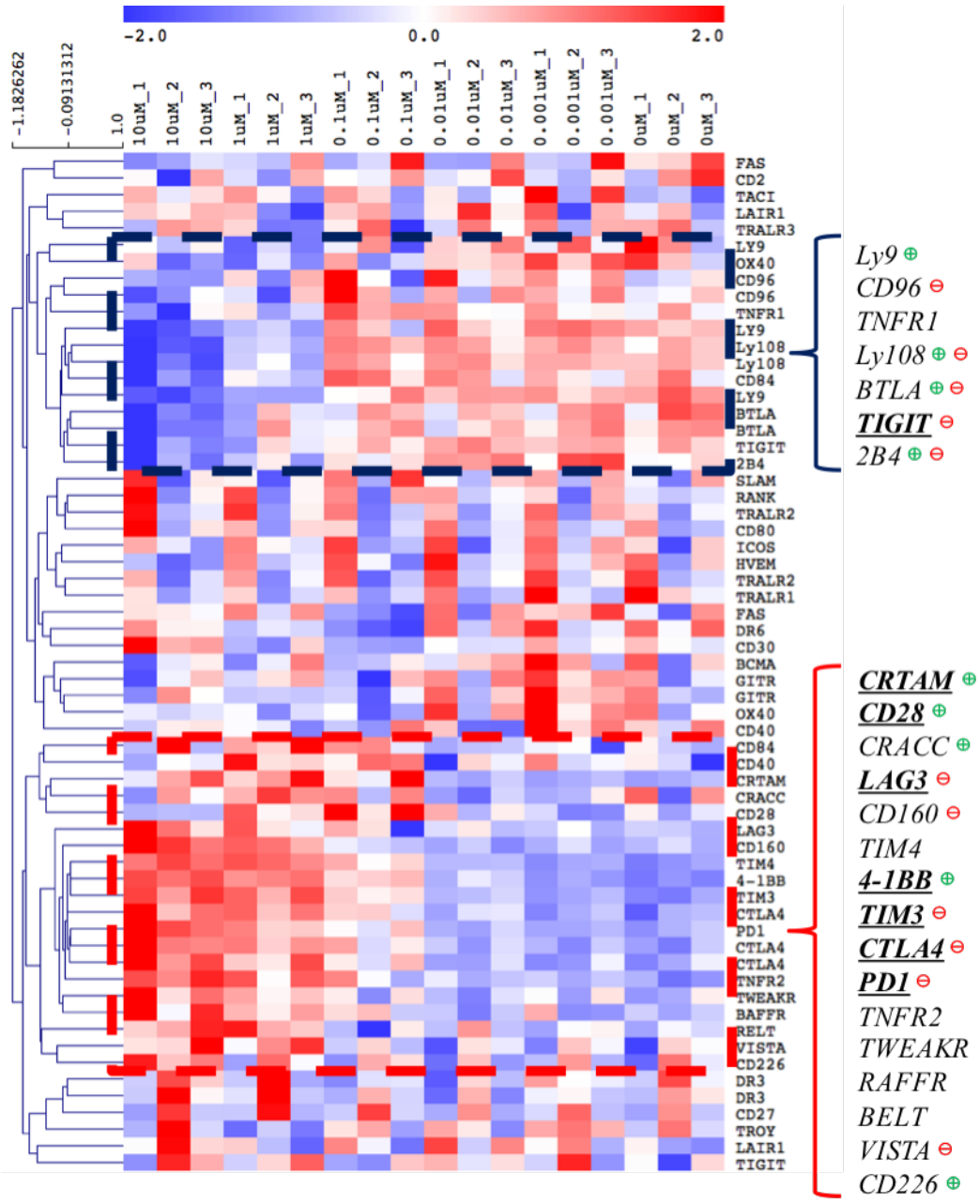

Figure 4-1 Differential expressions of most well-known immune check points in different antigen stimulations. (A3)

Hierarchy clusters (HCL) of immune check point genes (both stimulatory and inhibitory) among different antigen dose groups. Each column represents a separate mRNA sample for each clone from three replicated experiments. Each row represents a probe from the bead array that maps to a gene in the Ensembl database. The colour represents the relative quantity of complementary RNA directly hybridised to each probe for each sample and is scaled within each row, to range from -2 (blue) to +2 (red). Some genes were represented by multiple probes. The inhibitory signal was marked as ⊖ and co-stimulatory signal as ⊕.

Table 4-1 Statistics for the immune checkpoint receptor panel (A3 microarray).

Gene ID	Probe ID	log_2(fold change compared to baseline)					*p*-value (t-test)				
		10μM	1μM	0.1μM	0.01μM	0.001μM	10μM	1μM	0.1μM	0.01μM	0.001μM
CD28	ILMN_1749362	-0.03	0.07	0.14	0.03	-0.04	0.40	0.14	0.08	0.49	0.26
ICOS	ILMN_1669927	0.03	0.14	0.08	0.06	0.19	0.87	0.52	0.78	0.84	0.40
CTLA4	ILMN_2261627	1.13	0.95	0.57	0.26	0.07	0.03	0.01	0.04	0.24	0.72
	ILMN_1763487	1.22	0.86	0.56	0.15	0.05	0.02	0.01	0.05	0.42	0.74
	ILMN_2348905	0.82	0.53	0.32	0.01	-0.01	0.01	0.04	0.10	0.96	0.95
PD1	ILMN_1806725	0.85	0.48	0.30	0.03	-0.01	0.01	0.01	0.05	0.72	0.91
VISTA	ILMN_2205963	0.49	0.48	0.09	-0.01	0.08	0.21	0.20	0.78	0.97	0.81
BTLA	ILMN_2099528	-1.03	-0.31	-0.08	-0.22	-0.01	0.01	0.28	0.67	0.26	0.97
	ILMN_1778536	-0.78	-0.32	-0.15	-0.18	-0.09	0.02	0.19	0.49	0.39	0.68
CD80	ILMN_1716736	0.29	0.06	-0.05	0.09	0.08	0.49	0.80	0.83	0.74	0.73
CD226	ILMN_1687825	0.44	0.09	0.05	-0.15	0.00	0.22	0.80	0.89	0.66	1.00
CRTAM	ILMN_1796247	0.84	1.08	0.89	0.06	0.01	0.09	0.05	0.16	0.54	0.92
TIGIT	ILMN_2125017	-0.70	-0.24	-0.03	0.12	0.07	0.08	0.22	0.75	0.25	0.46
	ILMN_3236289	0.10	0.09	0.00	0.08	0.06	0.43	0.35	0.99	0.40	0.61
CD96	ILMN_2415786	-0.14	0.02	0.07	0.18	0.16	0.08	0.86	0.76	0.27	0.12
	ILMN_1711573	-0.17	-0.10	0.10	0.03	0.07	0.17	0.46	0.57	0.76	0.35
TIM3	ILMN_1693826	2.88	2.64	1.65	0.62	0.29	0.00	0.00	0.00	0.05	0.27
TIM4	ILMN_1750678	2.25	2.19	1.38	0.39	0.13	0.00	0.00	0.00	0.08	0.46
CD2	ILMN_1695025	-0.27	-0.20	-0.09	-0.05	-0.20	0.37	0.35	0.63	0.80	0.32
SLAM	ILMN_1770768	0.07	-0.06	0.19	0.02	0.10	0.80	0.76	0.43	0.89	0.60
2B4	ILMN_1702534	-0.67	-0.24	0.01	0.33	0.36	0.07	0.23	0.93	0.01	0.21
LY108	ILMN_1760109	-1.11	-0.47	0.20	0.10	0.15	0.00	0.02	0.21	0.56	0.28
	ILMN_2196078	-1.50	-0.63	0.01	0.08	0.05	0.01	0.05	0.97	0.62	0.56
CD84	ILMN_2049293	0.08	0.19	0.12	-0.03	-0.03	0.57	0.08	0.12	0.45	0.73
	ILMN_1698367	-0.82	-0.30	0.15	0.00	-0.11	0.02	0.17	0.50	0.99	0.57
LY9	ILMN_1731928	-0.57	-0.42	-0.13	-0.06	-0.09	0.00	0.01	0.22	0.31	0.24
	ILMN_1812278	-0.91	-0.53	-0.13	0.02	0.22	0.01	0.01	0.59	0.91	0.02
	ILMN_1756275	-0.06	-0.12	-0.07	-0.01	-0.03	0.37	0.14	0.39	0.84	0.69

CRACC	ILMN_1710923	-0.09	0.25	0.07	-0.35	-0.20	0.78	0.45	0.84	0.32	0.54
LAIR1	ILMN_1768598	0.03	-0.03	0.02	0.05	0.01	0.32	0.51	0.71	0.27	0.83
	ILMN_2389211	0.11	0.01	0.04	0.10	0.06	0.13	0.91	0.57	0.15	0.31
LAG3	ILMN_1813338	0.91	0.51	0.09	0.15	0.06	0.10	0.14	0.84	0.34	0.65
CD160	ILMN_1742001	1.54	1.12	0.16	-0.18	-0.04	0.01	0.00	0.30	0.37	0.83
4-1BB	ILMN_1813379	3.46	3.00	2.21	0.99	0.31	0.00	0.00	0.00	0.03	0.15
OX40	ILMN_2112256	-0.18	-0.29	-0.44	0.24	0.50	0.61	0.45	0.31	0.62	0.30
	ILMN_1710204	-0.10	-0.12	-0.07	-0.01	0.04	0.20	0.11	0.37	0.79	0.51
CD27	ILMN_1688959	0.12	0.21	0.21	-0.04	0.14	0.83	0.72	0.67	0.94	0.75
GITR	ILMN_2349633	-0.01	-0.10	-0.14	0.08	0.27	0.97	0.48	0.41	0.67	0.23
	ILMN_1743100	-0.03	0.06	-0.06	0.08	0.15	0.83	0.58	0.68	0.51	0.21
CD30	ILMN_1659257	0.48	-0.20	-0.33	-0.10	0.02	0.22	0.34	0.04	0.33	0.87
TNFR1	ILMN_1685005	-0.32	-0.12	0.16	0.01	0.02	0.23	0.29	0.12	0.89	0.80
TNFR2	ILMN_1764788	1.16	0.93	0.52	0.26	0.21	0.00	0.03	0.16	0.11	0.12
HVEM	ILMN_1697409	-0.39	-0.05	-0.06	0.05	0.08	0.17	0.85	0.85	0.88	0.75
DR3	ILMN_1765109	0.02	0.01	-0.09	-0.09	-0.01	0.83	0.96	0.30	0.33	0.93
	ILMN_2299661	0.03	0.03	-0.02	-0.06	-0.02	0.66	0.73	0.63	0.37	0.53
FAS	ILMN_2319077	-0.42	-0.22	-0.14	-0.28	-0.12	0.05	0.29	0.63	0.28	0.69
	ILMN_1808132	0.06	0.12	-0.15	0.07	0.17	0.63	0.40	0.29	0.67	0.26
CD40	ILMN_2367818	0.03	0.12	0.12	0.01	0.07	0.62	0.13	0.13	0.91	0.31
	ILMN_1779257	-0.01	-0.03	-0.02	-0.04	0.04	0.49	0.22	0.56	0.22	0.28
RANK	ILMN_1698952	0.18	0.11	0.11	0.10	0.04	0.53	0.61	0.61	0.37	0.82
TRALR1	ILMN_1721316	-0.14	-0.15	-0.14	-0.12	-0.04	0.22	0.23	0.26	0.37	0.82
TRALR2	ILMN_1699265	-0.26	-0.16	-0.20	0.07	0.11	0.60	0.75	0.73	0.88	0.82
	ILMN_2331010	0.09	0.07	0.00	0.01	0.08	0.54	0.58	0.97	0.87	0.55
TRALR3	ILMN_1672114	-0.01	-0.10	-0.06	-0.01	-0.01	0.83	0.19	0.59	0.81	0.85
TACI	ILMN_1759075	0.05	0.04	0.05	0.03	0.09	0.04	0.30	0.22	0.16	0.17
BCMA	ILMN_1768016	-0.04	-0.01	-0.03	0.01	0.04	0.52	0.82	0.60	0.87	0.60
TWEAKR	ILMN_1689004	0.44	0.22	0.07	-0.04	0.07	0.11	0.09	0.60	0.73	0.57
RELT	ILMN_1748614	0.07	0.07	-0.02	0.02	0.01	0.06	0.06	0.57	0.59	0.70
DR6	ILMN_1699695	-0.06	-0.16	-0.31	-0.04	-0.06	0.46	0.10	0.02	0.65	0.63
TROY	ILMN_1704154	0.02	-0.07	0.00	-0.01	0.05	0.79	0.15	0.93	0.85	0.29

4.2.2 Human CD8 CTL Clone (with Same TCRs) Can Have Very Variable Patterns of Immune Checkpoint Receptor Expressions.

To correlate the findings from the RNA level (microarray data) to protein level, five inhibitory immune checkpoint genes, including CTLA-4, PD-1, TIM-3, LAG-3 and TIGIT, were further characterized at the protein level by multi-colour flow cytometry. The cells were co-cultured with peptide-pulsed HLA-matched C8166 cells (with five antigen doses) for 6h same as in the microarray experiment, the 0.001μM was left out, as there was no sign of gene differential expressions compared to the control group from the microarray data. (Figure 4-2)

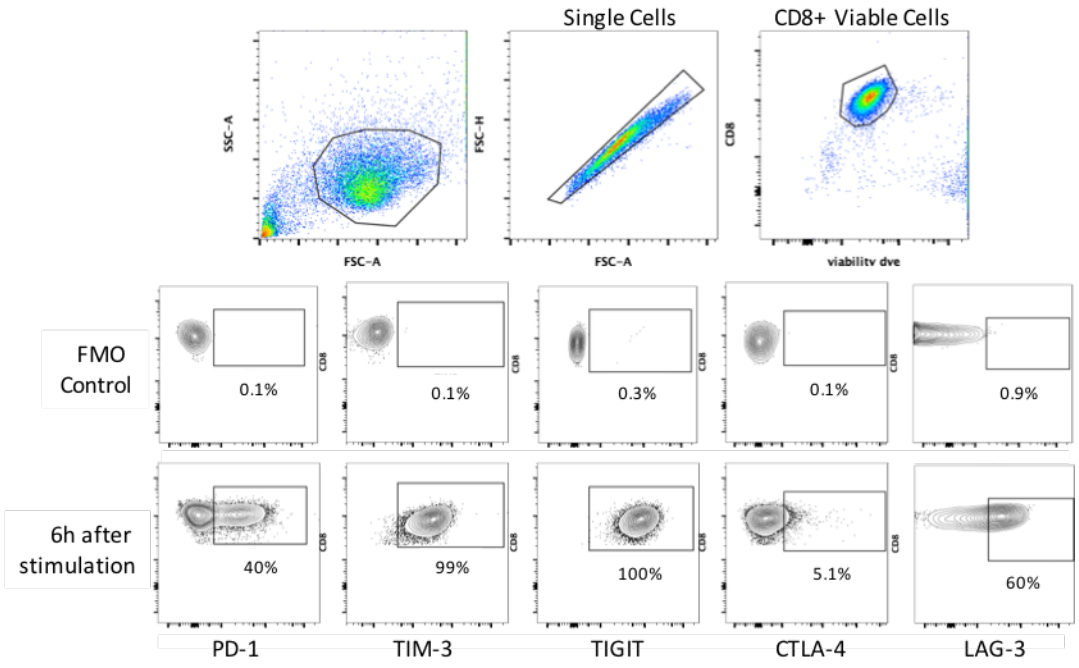

Figure 4-2 Gating strategy example from clone A3 and target cells co-culture.

Top row: flow cytometry plots were gated on live, single $CD8^+$ cells. Middle row: FMO control was applied to localise the gating position of inhibitory receptor on CD8+T cells. Bottom row: positive staining from the samples.

The surface expression levels of these five inhibitory receptors were very heterogeneous. On this HIV epitope-specific CTL clone A3, TIM-3 and TIGIT were highly expressed. PD-1 expression pattern was more similar to a bimodal distribution, while the majority of the cells were CTLA-4 negative. (Figure 4-3) From the microarray data, the mRNA level of PD-1 started to up-regulate with the antigen stimulations (0.1μM and above) in a dose-dependent manner. Identical to the microarray, FACS data revealed an increased proportion of PD-1 positive cells. (from 0μM: 37.5±0.7% to 10μM: 49.8±0.5%) (Figure 4-3A) In the case of CTLA-4, the microarray data included three different probes for this gene and all the three probes pointed to a dose-dependent up-regulation of CTLA-4 mRNA level (0.1μM and above). The CTLA-4 probe_1 also showed an up-regulated trend at 0.01μM. However, unlike PD-1, the CTLA-4 surface expression on clone A3 was rather low. The proportion of CTLA-4 positive cells increased from 0μM: 2.8±0.5% to 10μM: 5.6±0.4%. (Figure 4-3B) Although it's statistically significant, other post-transcriptional regulations could contribute to the low abundance of CTLA-4 surface expression. For example, it has been reported that the majority of CTLA-4 molecules on a T cell are actually located in intracellular compartments, from where they could be transported to the cell surface and rapidly internalised; thus only small amounts of CTLA-4 molecules can be detected on the cell surface at any given time (Schneider and Rudd, 2014). And by blocking Golgi transportation and intracellularly staining CTLA-4, much higher CTLA-4 could be detected. (Figure 4-3B) The phenomenon is very interesting, as CTLA-4 is a central inhibitory receptor of T cell proliferation and functions and minor changes in the surface expression of the receptor are expected to have significant effects.

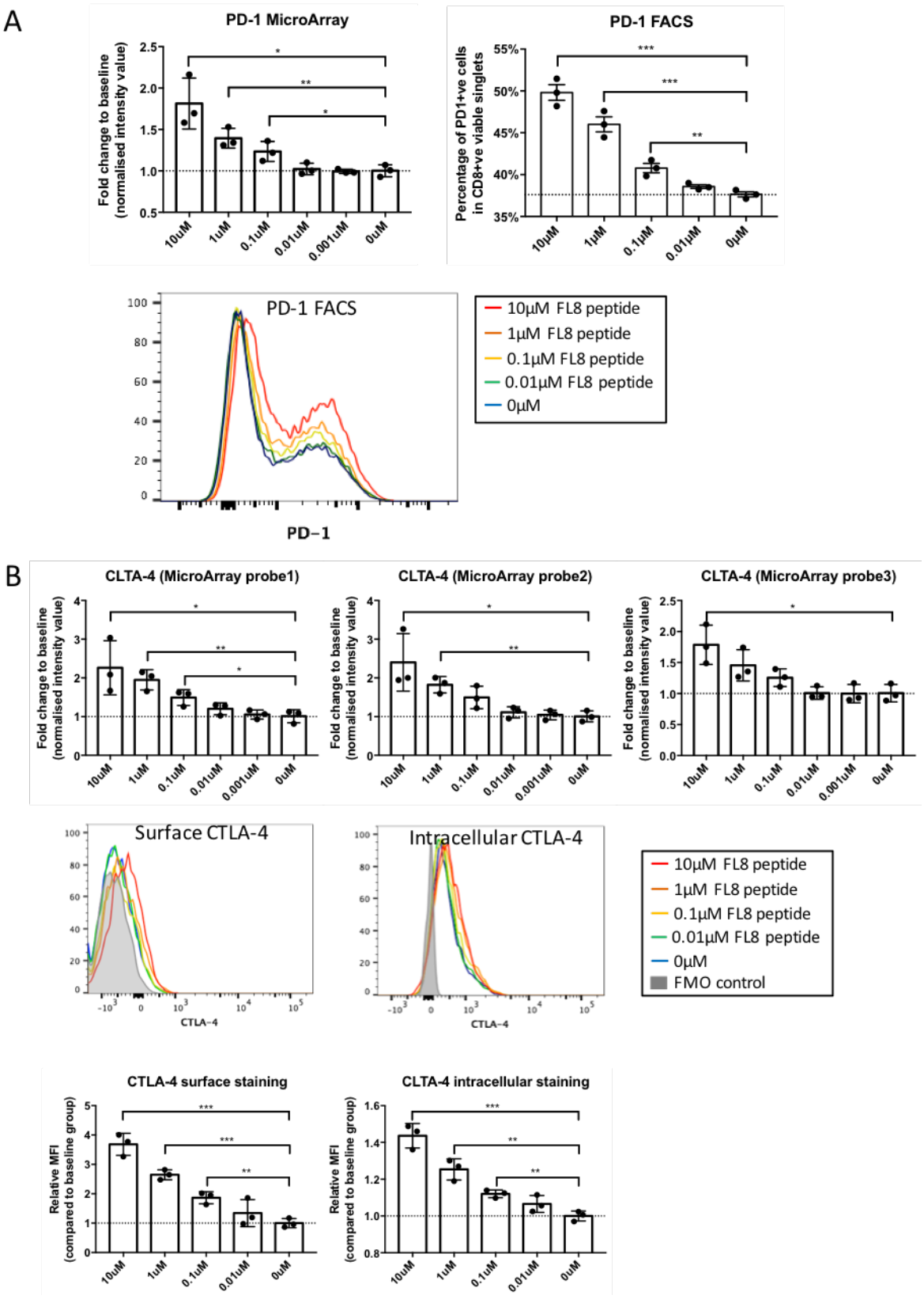
A
PD-1 MicroArray
Fold change to baseline (normalised intensity value)
10uM
1uM
0.1uM
0.01uM
0.001uM
0uM
PD-1 FACS
Percentage of PD1+ve cells in CD8+ve viable singlets
10μM
1μM
0.1μM
0.01μM
0μM
PD-1 FACS
10μM FL8 peptide
1μM FL8 peptide
0.1μM FL8 peptide
0.01μM FL8 peptide
0μM
PD-1
B
CLTA-4 (MicroArray probe1)
CLTA-4 (MicroArray probe2)
CLTA-4 (MicroArray probe3)
Surface CTLA-4
Intracellular CTLA-4
CTLA-4
10μM FL8 peptide
1μM FL8 peptide
0.1μM FL8 peptide
0.01μM FL8 peptide
0μM
FMO control
CTLA-4 surface staining
CTLA-4 intracellular staining
Relative MFI (compared to baseline group)

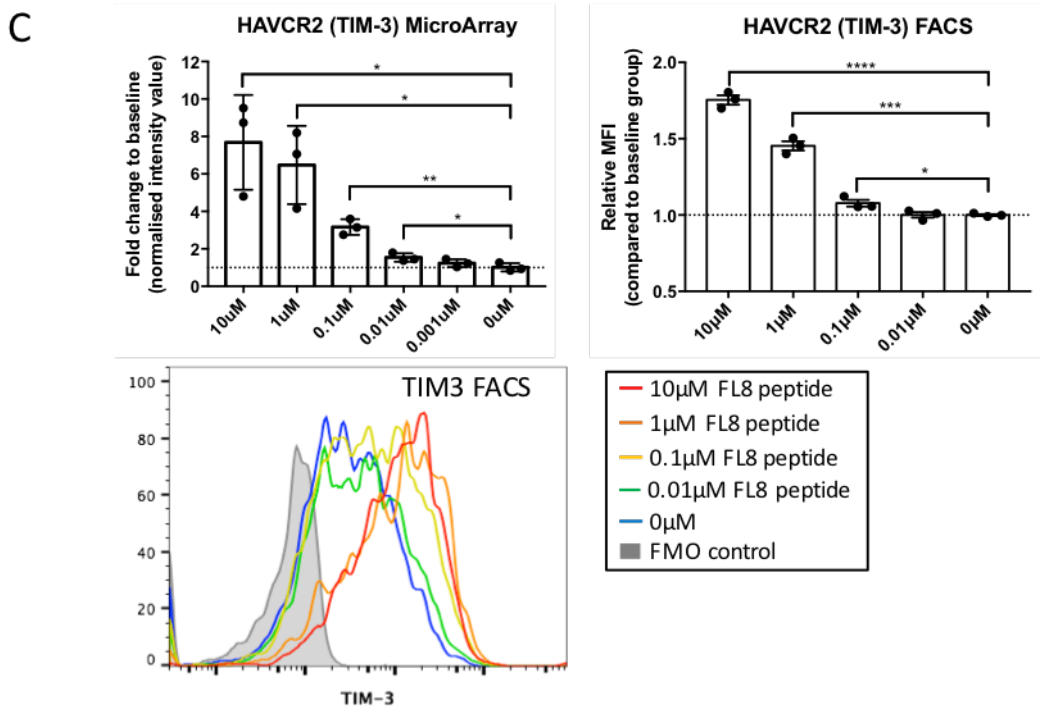
C
HAVCR2 (TIM-3) MicroArray
Fold change to baseline (normalised intensity value)
10uM
1uM
0.1uM
0.01uM
0.001uM
0uM
HAVCR2 (TIM-3) FACS
Relative MFI (compared to baseline group)
10μM
1μM
0.1μM
0.01μM
0μM
TIM3 FACS
TIM-3
10μM FL8 peptide
1μM FL8 peptide
0.1μM FL8 peptide
0.01μM FL8 peptide
0μM
FMO control

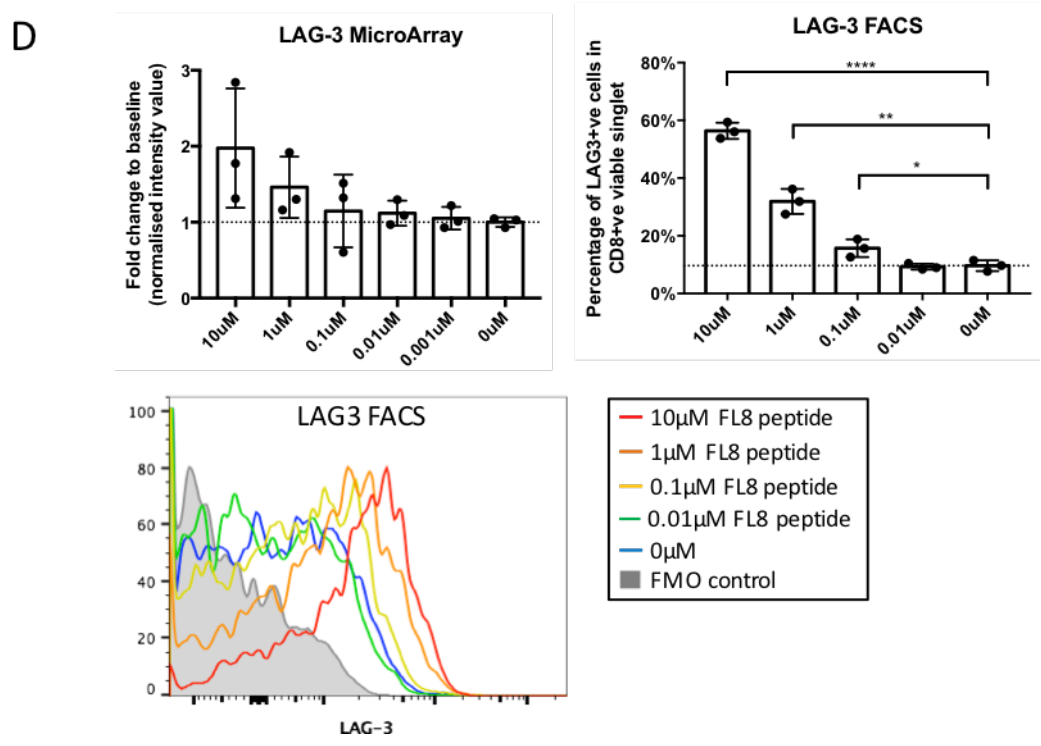
D
LAG-3 MicroArray
Fold change to baseline (normalised intensity value)
10uM
1uM
0.1uM
0.01uM
0.001uM
0uM
LAG-3 FACS
Percentage of LAG3+ve cells in CD8+ve viable singlet
10uM
1uM
0.1uM
0.01uM
0uM
LAG3 FACS
LAG-3
10μM FL8 peptide
1μM FL8 peptide
0.1μM FL8 peptide
0.01μM FL8 peptide
0μM
FMO control

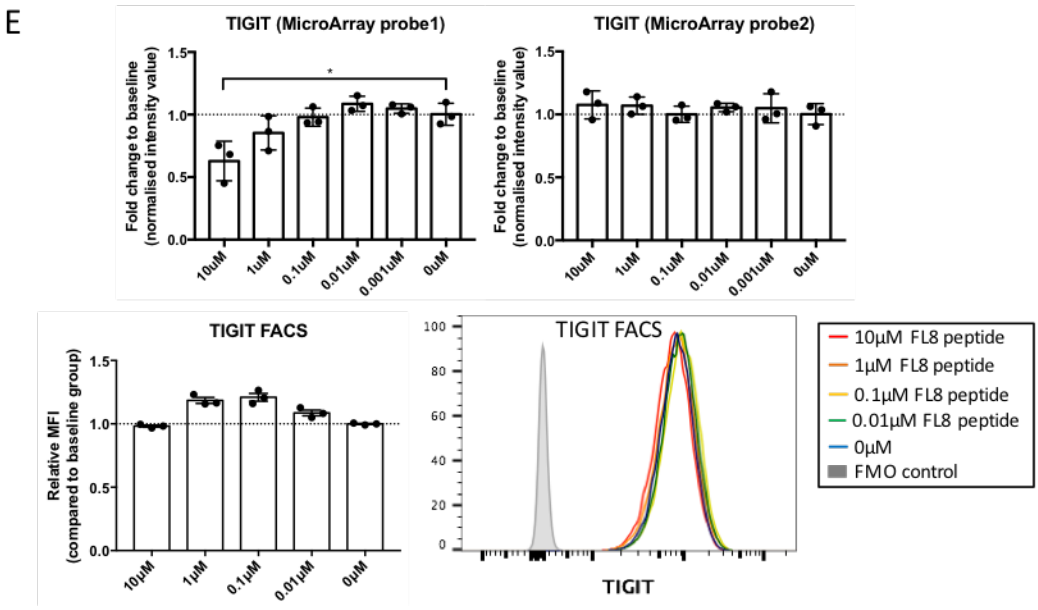

Figure 4-3 Co-inhibitory receptor expression patterns on clone A3.

The mRNA level of each immune checkpoints was quantified by microarray, PD-1, TIM-3 and LAG-3 were represented by single probe, CTLA-4 was represented by three probes and TIGIT was represented by two probes. The surface expressions of each immune checkpoint receptors were quantified by flow cytometry and overlapped in histogram to show the differences between each group. CTLA-4 expression was also checked by intracellular staining. MFI here is median fluorescence intensity; relative MFI: MFI value of experiment group/value of control group (mock stimulation group) FMO control are shown in grey (tinted) for CTLA-4, TIM-3, LAG-3 and TIGIT. (n=3)

The expression of TIM-3, and TIGIT on clone A3 were more like normal or unimodal distribution (Figure 4-3 C, E). Thus, relative median fluorescent values were used to quantify the surface expression level of these two genes. There was a significant TIM-3 up-regulation along with the increase of antigen dose from both microarray and FACS data. The TIM-3 mRNA up-regulation could be detected at 0.01μM and above, while surface expression up-regulation could be detected at 0.1μM and above (Figure 4-3C). LAG-3 were expressed at about 9% of the

resting A3 cells and could be up-regulated on about 60% of the cells when stimulated at 10μM peptide. In contrast to TIM-3, although the surface expression level of TIGIT was also very high, the expressions in response to the incremental antigen dose were of a different pattern. The two probes specific to TIGIT showed different trends. TIGIT mRNA expression levels identified by probe_1(ILMN_2125017) showed a slight increase at lower antigen dose and decrease at high antigen dose (especially at 10μM, there was 2-fold downregulation), while the TIGIT mRNA expression levels identified by probe_2 (ILMN_3236289) remained basically flat. The difference was not from the failure of the probe_2 as these two probes correlated very well on the other CTL clone C23 (Figure 4-12, expression value shown in Appendix). Thus, the differences might come from different transcription variants. The surface expression levels of TIGIT molecules were also unclear, the protein levels gradually up-regulated in low antigen dose groups, peaking at 0.1μM and down-regulated to baseline level in higher antigen dose groups (Figure 4-3D). A similar pattern was also observed on clone C23 (peaks at 2μM) (Figure 4-13). Thus, unlike the previous three immune checkpoint receptors in which the expression levels increase along with stronger antigen stimulation, TIGIT seems to slightly up-regulate with low antigen stimulation and drop back to baseline after a certain stimulation level.

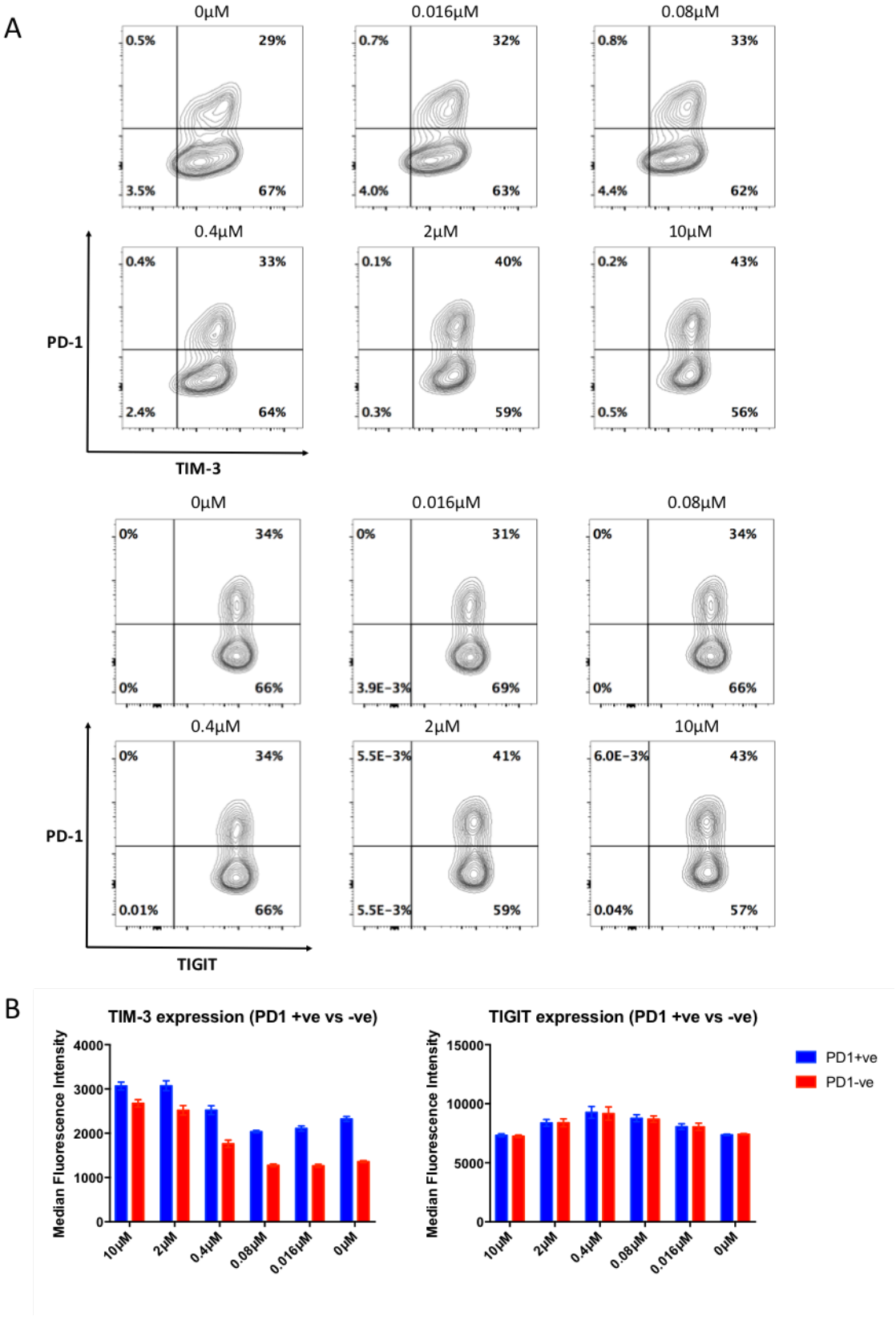

Figure 4-4 Correlation of PD-1 expression and TIM-3 or TIGIT expression on clone A3.

(A) Contour plots of PD1-TIM3, PD1-TIGIT co-expression on clone A3 and C23; (B) MFI value of TIM3 and TIGIT on PD1+ve and PD1-ve populations on clone A3. (n=3)

We next looked at the co-expression patterns between these immune checkpoint receptors CTL clone A3. The CTLA-4 expression levels were quite low and were hence left out. The co-expression contour plots of PD-1-TIM-3 and PD-1-TIGIT are shown in Figure 4-4A. Interestingly, although both TIM-3 and TIGIT have been reported to co-express on exhausted T cells inside tumours and co-blockades of PD-1 with TIM-3 or with TIGIT exerted better efficacy in controlling tumour size (Chauvin et al., 2015; Fourcade et al., 2010), only TIM-3 showed positive correlation with PD-1 expression here (Figure 4-4B). It is interesting to see that TIM-3 expression but not TIGIT expression was influenced by PD-1 expression, or *vice versa*, on the cell surface, which pointed to the different underlying regulations of TIM-3 and TIGIT on CD8+ T cells.

In addition to these inhibitory immune checkpoint receptors, 4-1BB, CD28, CD25 (IL2 receptor alpha chain), CRTAM were also characterized in similar experimental settings. In the previous chapter, 4-1BB was shown to be among the most sensitive up-regulated genes in response to antigen stimulation (0.01μM and above) on both clone A3 and C23. The surface expression pattern of 4-1BB was very bimodal and the resting T cells did not express any 4-1BB, while fully-activated T cells expressed a high level of 4-1BB molecules. The surface expression of 4-1BB highly correlated with the antigen dose and almost all the A3 cells (about 90%) expressed 4-1BB in the 10μM group (Figure 4-5A). CD28, on the other hand, is the most important co-stimulatory receptor for the T cell priming and development. However, on clone A3, CD28 disappeared (Figure 4-5B). This phenomenon could be explained as antigen-experienced and terminally differentiated T cells (usually CD8 memory T cells) lose CD28, but can be reactivated without CD28 engagement (Mou et al., 2014).

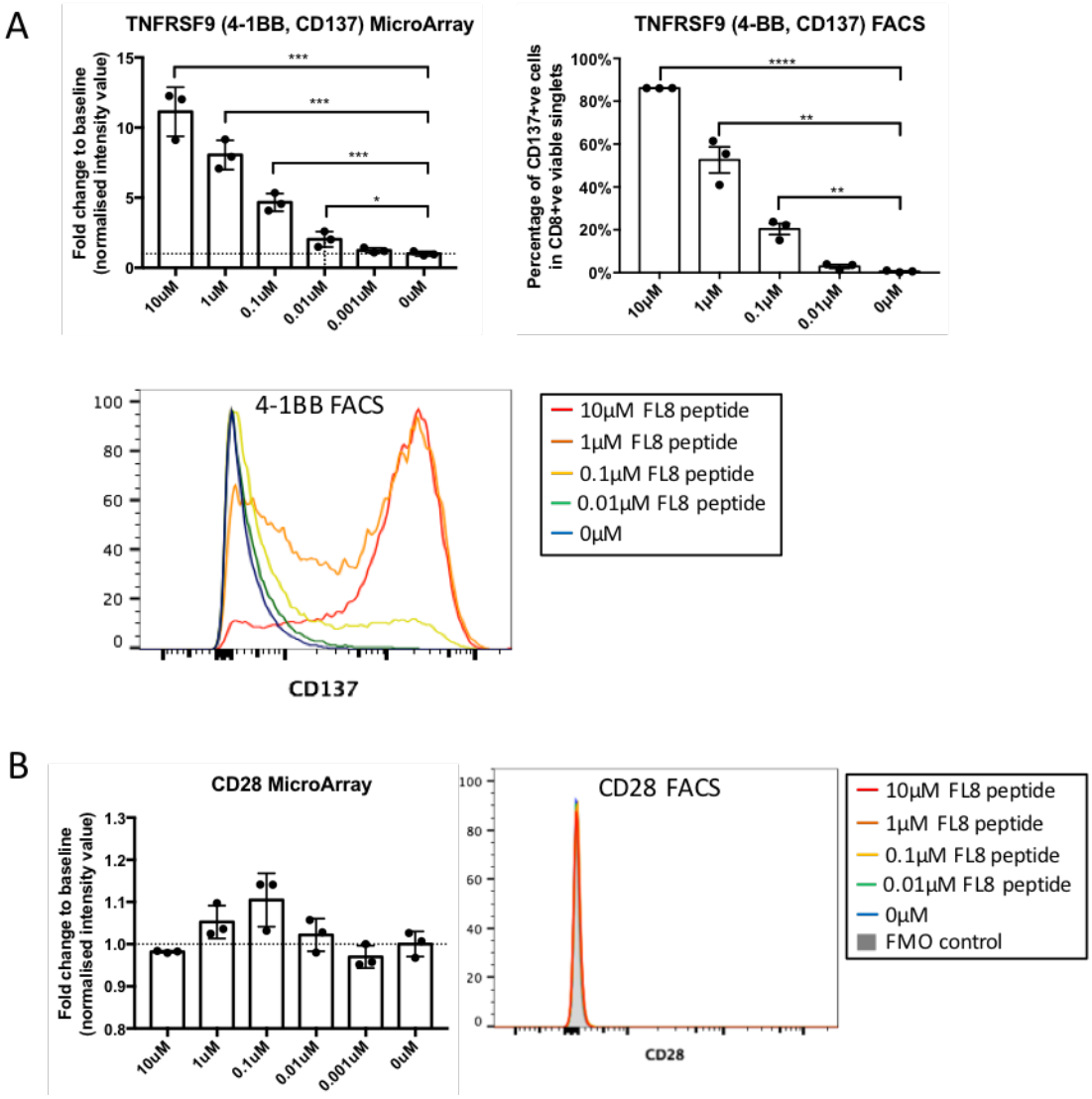

Figure 4-5 Co-stimulatory receptor expression patterns on clone A3.

The mRNA levels of 4-1BB, CD28, CD25 (IL2Ra) and CRTAM were quantified by microarray, represented by single probe. The surface expressions of the co-stimulatory receptors were quantified by flow cytometry and overlapped in histogram to show the differences between each group. MFI here is median fluorescence intensity; relative MFI: MFI value of experiment group/value of control group (mock stimulation group). (n=3) Figure continues in the next page.

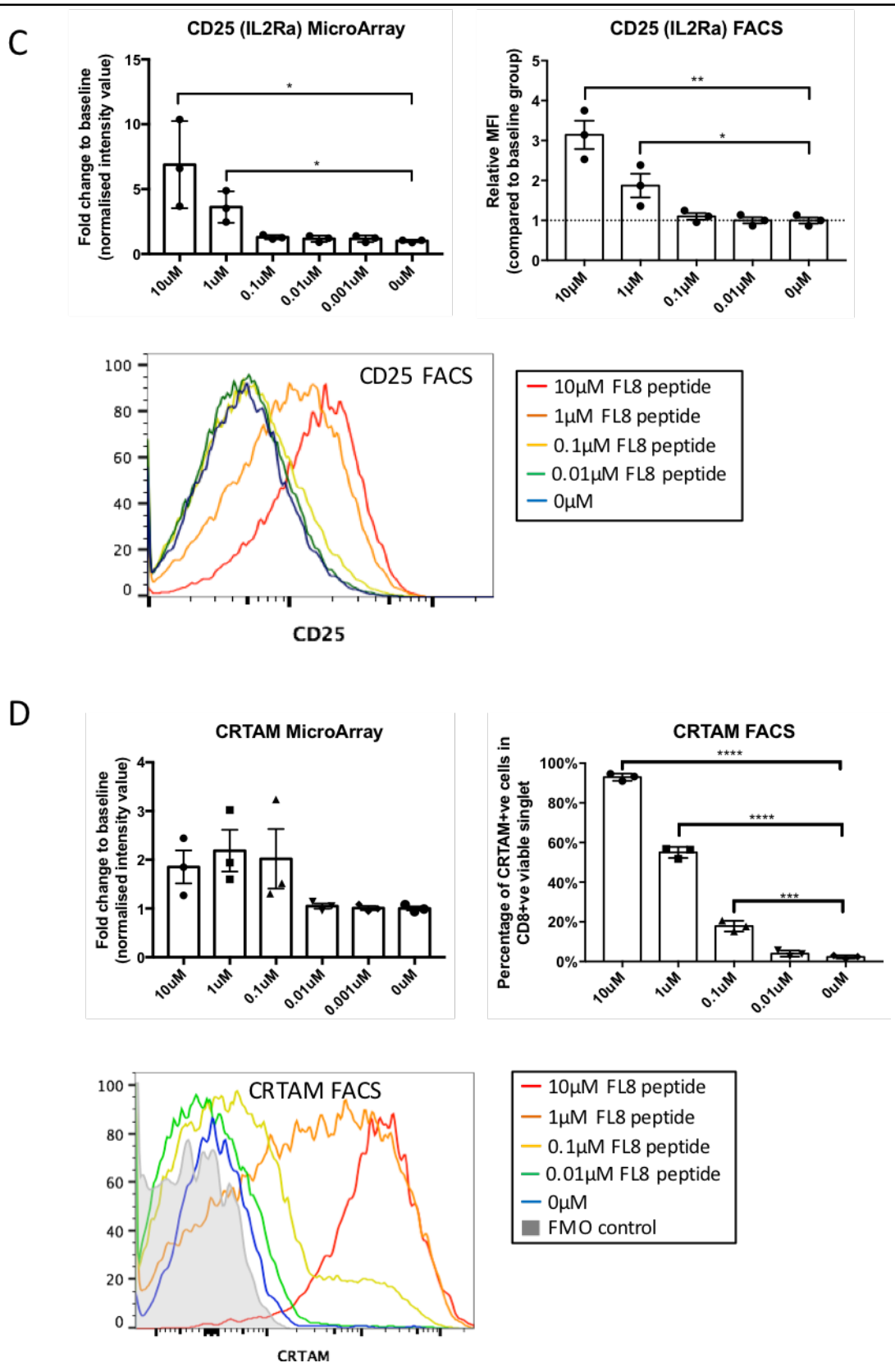

CD25 is the alpha chain of IL2 receptor, and together with the common beta and gamma chain, constitutes the high-affinity IL2 receptor. CD25 is also a T cell

activation marker. The mRNA expression level of CD25 significantly increased at 1μM and higher groups (less sensitive than 4-1BB, TIM-3, PD-1 and CTLA-4). Similar to mRNA level, the CD25 surface expression up-regulated at 1μM and 10μM. (Figure 4-5C) CRTAM is another interesting co-stimulatory receptor identified to be up-regulated in the microarray data and the up-regulation was quite sensitive (0.1μM and above) and sharp (Figure 4-5D). The surface expression pattern of CRTAM was very similar to 4-1BB. Interestingly, similar to LAG-3 and 4-1BB, overexpression of EGR2 in mice T cells also up-regulate CRTAM mRNA level (Williams et al., 2017). This gene has been also reported to confer late-stage activation of CD8+ T cells in lymph node (Takeuchi et al., 2009) and regulate late-stage T cell polarity (Yeh et al., 2008).

To summarise, the expression patterns of these 9 key immune regulator genes on *in vitro* cultured, antigen-specific CTL clones, are very heterogeneous. 4-1BB and CRTAM shared the most similar pattern – absent without stimulation and rapidly up-regulated on almost all the cells, when fully-activated. CD25 required a higher dose of antigen stimulation to be up-regulated than CRTAM. PD-1, TIM-3 and LAG-3 were expressed on about 1/4-1/2 of the total cell population without stimulation (may indicate a status of exhaustion) and up-regulated to a greater proportion when fully activated. Increased CTLA-4 expression was detected at both surface and intracellular vesicles in response to antigen stimulation, but its surface expression was tightly regulated. TIGIT were expressed on all the resting cells, with TIGIT expression basically unchanged along with antigen stimulation (Figure 4-6).

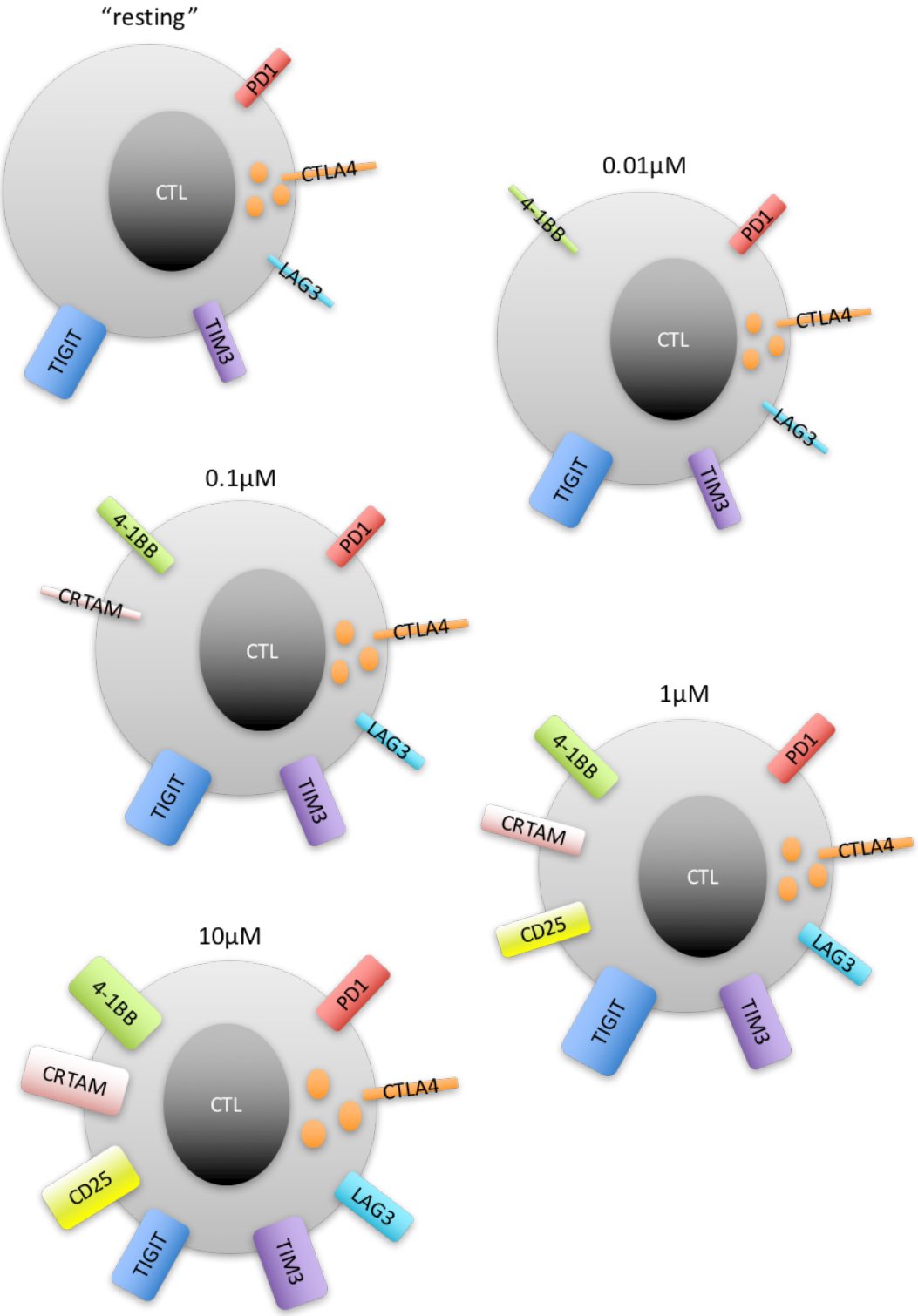

Figure 4-6 Summary of expression patterns of 7 different immune checkpoint receptors and IL2 receptor α-chain in response to different strength of antigen stimulation.

4.2.3 Co-Expressions of Immune Checkpoint Receptors on Cell Surface.

To further understand the connections between individual co-signalling receptors, the co-expression pattern was visualized by SPICE (simplified presentation of incredibly complex evaluations). In our panel, we co-stained 4-1BB, CD28, PD-1, TIGIT, LAG-3, TIM-3 and CTLA-4. TIGIT expression was all positive while CD28 expression was all negative on A3 cells; so these two receptors were left out from down-stream analysis. The expression of the other five co-signalling receptors was depicted in pie chart format, with different strengths of antigen stimulation (Figure 4-6A). There was no obvious inclusion relationship among these immune checkpoint receptors, which indicated the complexity of the immune balance of these co-stimulatory and co-inhibitory signals. The dominant up-regulation in response to antigen stimulation was clearly 4-1BB. Among the 4-1BB^{+} cells, 4-1BB^{+}PD1^{-}TIM3^{+}CLTA4^{-}LAG3^{+} and 4-1BB^{+}PD1^{-}TIM3^{+}CLTA4^{-}LAG3^{-} were the two most significantly increased subsets in response to increased antigen stimulation (Figure 4-6 B). Together with the sole expression patterns of each individual immune checkpoint receptors, co-expression pie charts demonstrated that upon T cell activation, a complicated regulatory mechanism (rather than simple hierarchy) of inhibitory receptors expression was adapted by CTLs to balance the TCR signal and effector functions. On the other hand, 4-1BB rather than CD28 serves as the dominant co-stimulatory receptor for antigen-experienced and terminally differentiated CTLs.

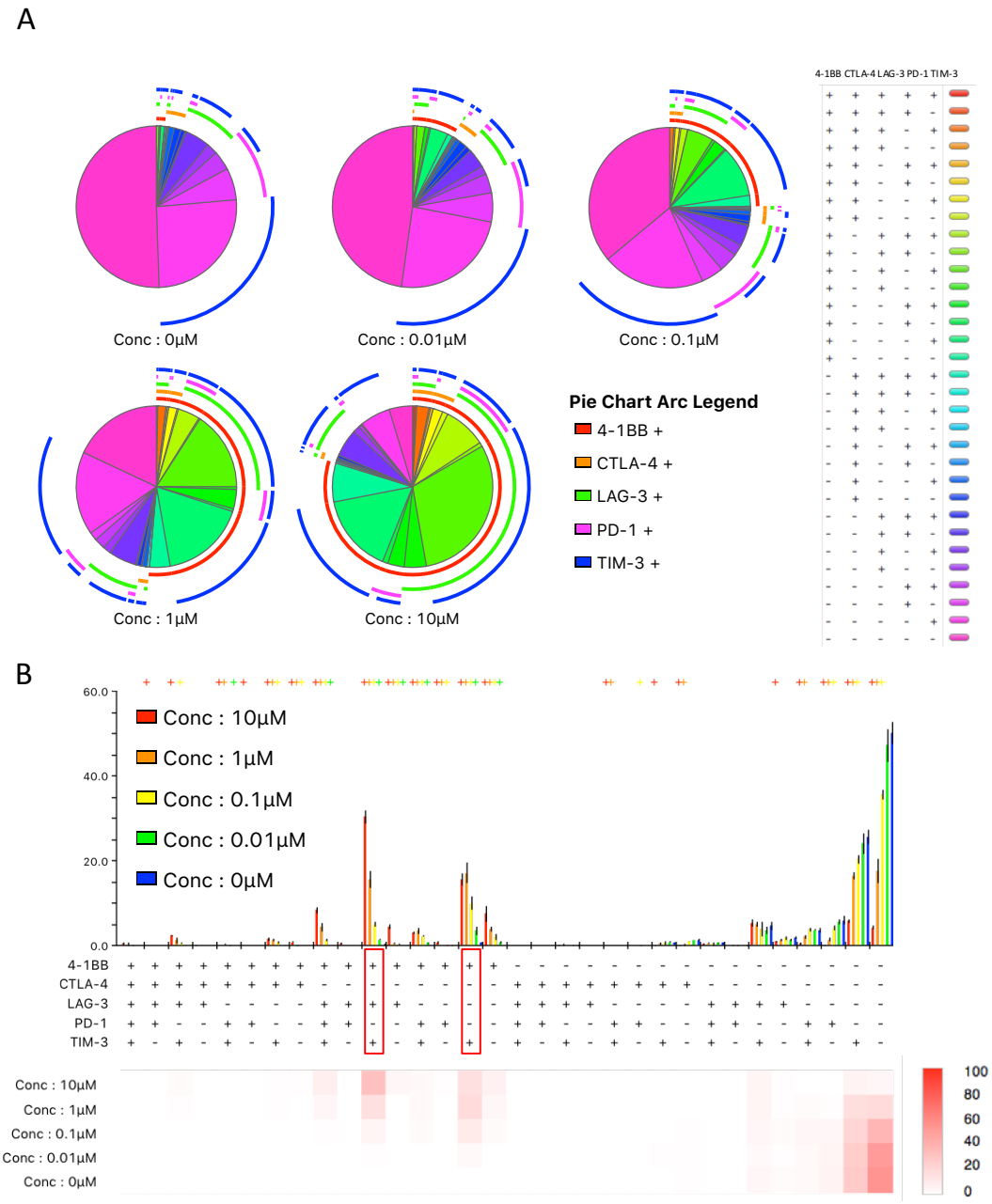

Figure 4-7 Co-expression of 4-1BB, PD-1, TIM-3, LAG-3 and CTLA-4.

(A) Pie chart depicts the average percentage of different subsets in CTL clone A3 characterized by 5 co-signalling receptors (4-1BB, TIM-3, PD-1, LAG-3 and CTLA-4) stimulated with different doses of antigenic peptide. The outer arcs illustrate the sole receptor expression in different subsets. (B) Boolean gating was applied to depict the dot plot that demonstrated the frequency of 32 subsets. t-test was applied for each stimulating group compared to 0μM group. p-value<0.05 was considered significant and was indicated above each bar. Heat map was drawn to identify the dominated and sub-dominated subsets in clone A3 in response to antigen stimulation. (n=3)

4.2.4 The Dynamic Expressions of PD-1, TIM-3, 4-1BB and CD25.

We next explored the dynamic changes after TCR engagement of PD-1, TIM-3, 4-1BB and CD25 on activated CTLs (clone A3) stimulated with five different antigen doses (10μM, 1μM, 0.1μM, 0.01μM and 0μM). PD-1 baseline expressions (0μM) were basically flat over the 72h (0h (d14): 39%, 72h (d17): 35%) The PD-1 expressions at 10μM and 1μM became disparate after 6 hours. Cells with 10μM stimulation maintained a high level of PD-1 expression, while PD-1 expression on cells with 1μM stimulation dropped after 12h. Although 0.1μM triggered a significant up-regulation of PD-1 expression, the magnitude was marginal. (Figure 4-8A) Though the expression trend of TIM-3 was very much similar to PD-1, however the baseline expression pattern was very different. Baseline expressions of TIM-3 declined over time. (MFI value 0h (d14): 2833, MFI value 72h (d17): 286) Cells maintained high TIM-3 expression after 10μM antigen stimulation. Cells with 1μM stimulation expressed significantly higher TIM-3 than the other lower dose groups over the 3 days, but with a declining trend, similar to these groups. The expression pattern of 4-1BB was unlike PD-1 or TIM-3, 4-1BB up-regulated about 3h after TCR engagement, peaked at 6-12h, and down-regulated afterwards (Figure 4-8B). The expression of 4-1BB seems to be correlated highly with the activation status of the T cells; more interestingly, the peak time of 4-1BB (6-12h) was earlier that the other three T cell activation markers (12h or 24h). In addition, 0.1μM of antigen stimulation could trigger a significant up-regulation of 4-1BB, which was not that noticeable for the other three T cell activation markers (Figure 4-8C). CD25 expression dynamic was similar to PD-1, although the PD-1 were quantified by the percentage of positive cells in contrast to the CD25, quantified by MFI (Figure 4-8D).

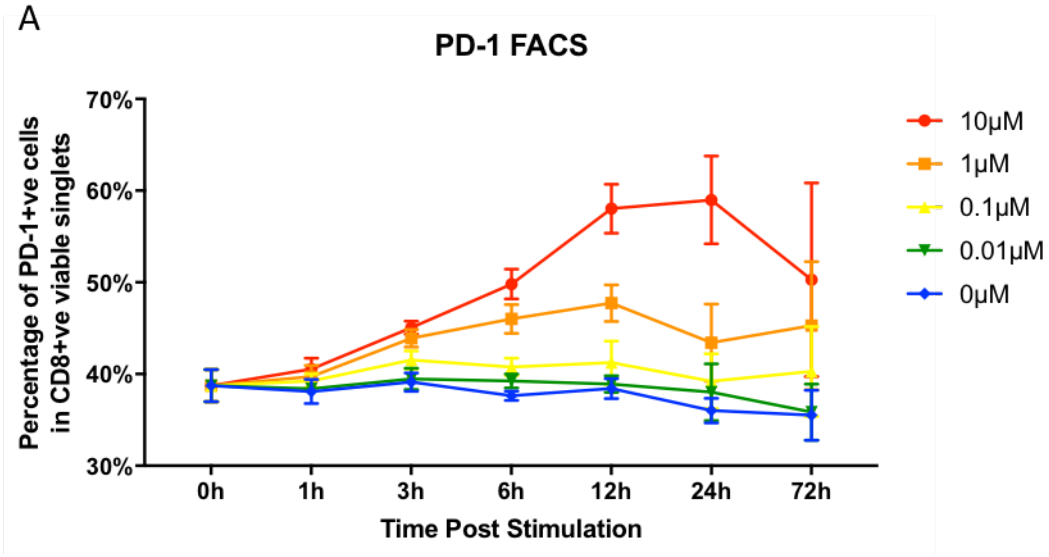
A
PD-1 FACS
Percentage of PD-1+ve cells in CD8+ve viable singlets
70%
60%
50%
40%
30%
0h
1h
3h
6h
12h
24h
72h
Time Post Stimulation
10μM
1μM
0.1μM
0.01μM
0μM

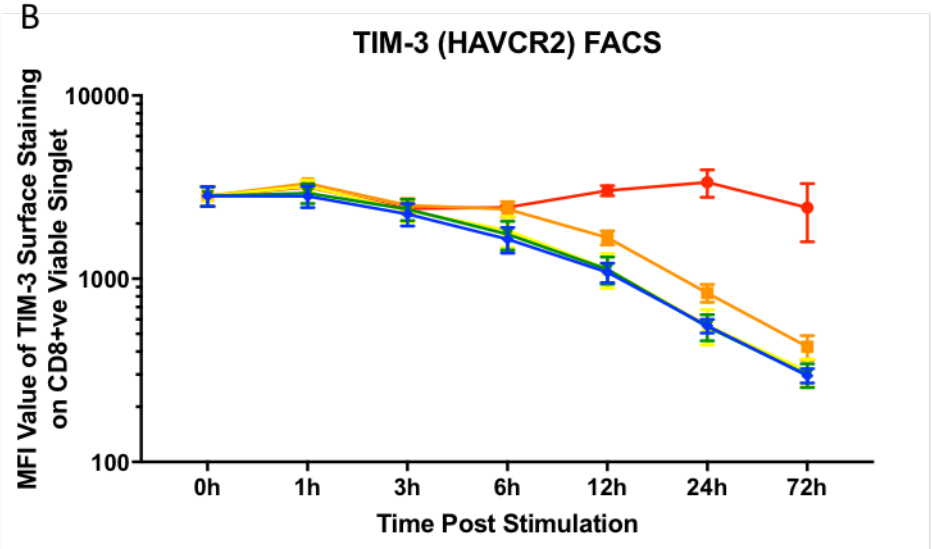
B
TIM-3 (HAVCR2) FACS
MFI Value of TIM-3 Surface Staining on CD8+ve Viable Singlet
10000
1000
100
0h
1h
3h
6h
12h
24h
72h
Time Post Stimulation

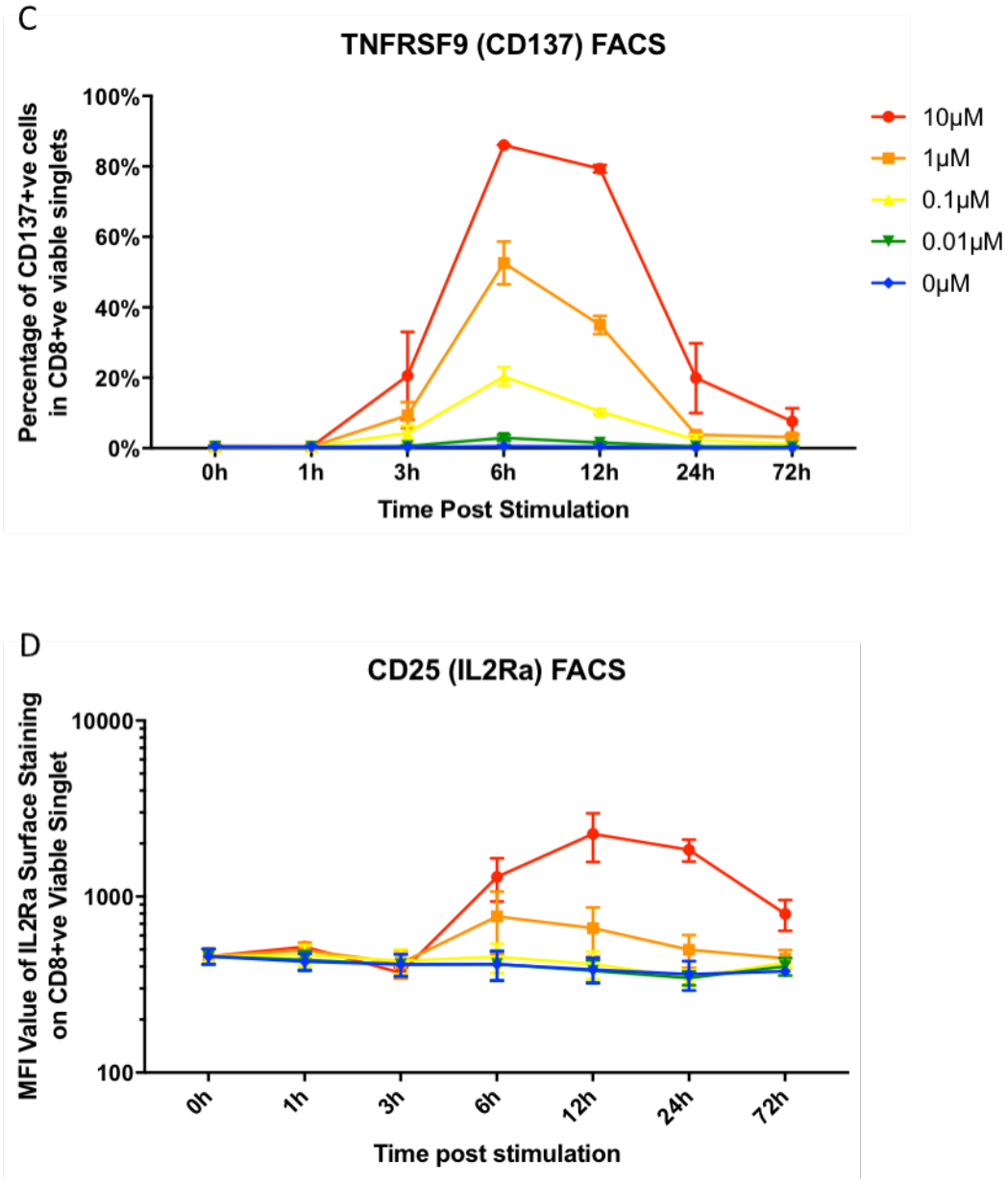

Figure 4-8 PD-1, TIM-3, 4-1BB, IL2Ra expressions by time course and dose course on clone A3.

The surface expressions (bimodal distribution) of PD-1 and 4-1BB were quantified by percentage over dose and time; the expressions of TIM-3 and TIGIT (normal or unimodal distribution) were quantified by median fluorescence intensity (MFI) over dose and time. The lines are coloured by antigen dose, the error bars stand for standard deviations (SD). (n=3)

To visualise the co-expression of these four activation-related surface receptors, SPICE algorithm was again applied to each sample. Summarised pie charts representing each group (dose/time, mean value) were shown in Figure 4-8 to depict the expressions of these four receptors simultaneously. Different from inhibitory receptors TIM-3 and PD-1, the IL2 receptor α-chain expression before 12h post stimulation time point was tightly correlated with 4-1BB expression (inclusion relationship). The 4-1BB expression decreased afterwards, while IL2 receptor α-chain expression lasted longer till 24h-72h. The expression of 4-1BB and IL2 receptor α-chain on PD-1+ve and PD-1-ve cells were comparable, probably due to the lack of PD-1 ligand expression on the target cells, with consequently no PD-1 inhibition on the effector cells.

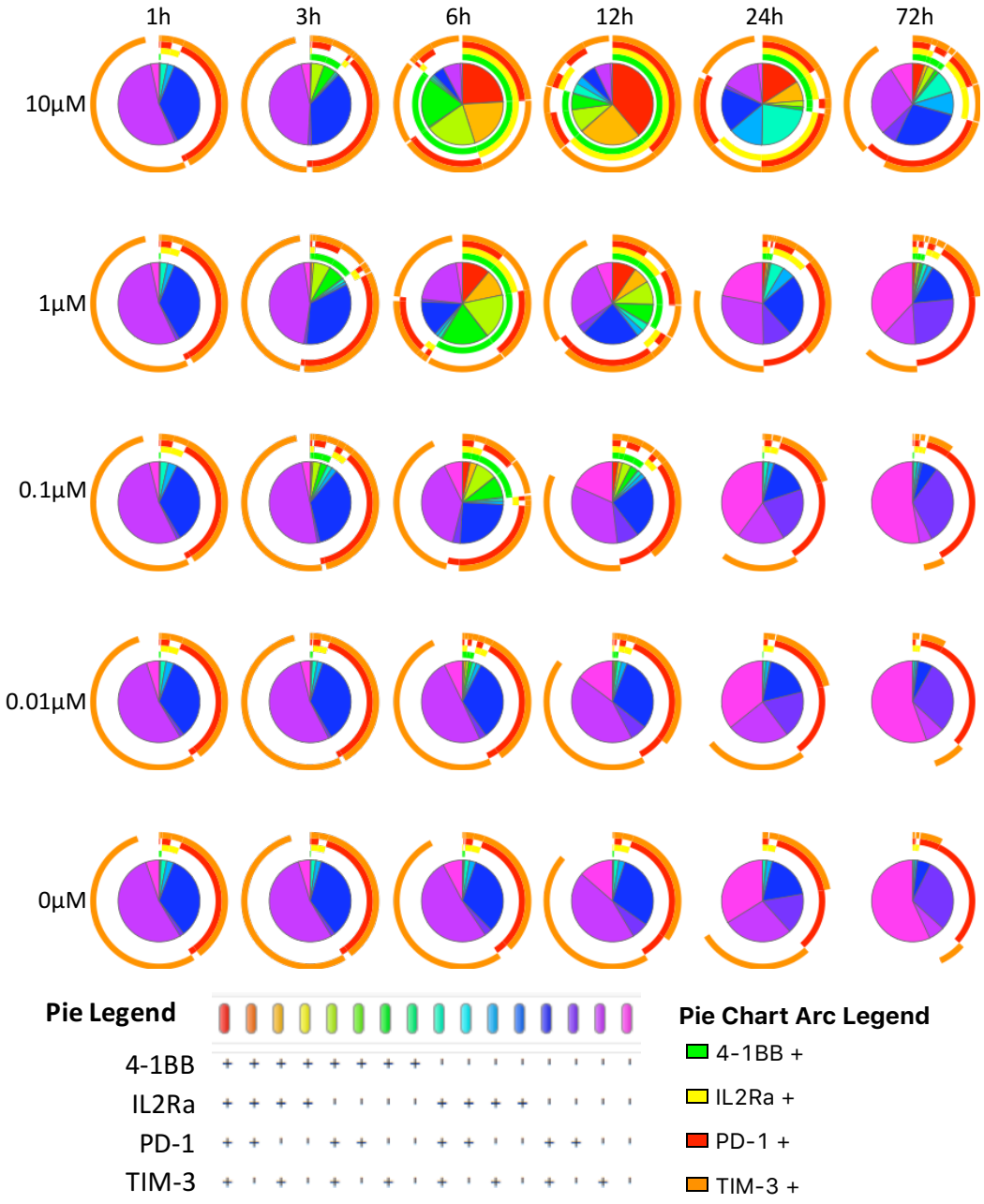

Figure 4-9 Combinatorial expression analysis of PD-1, TIM-3, 4-1BB and IL2Ra on clone A3.

Pie chart depicts the percentage of different subsets in CD8 CTLs characterized by 4 activation markers (PD-1, TIM-3, 4-1BB and CD25). The outer arcs illustrated the single activation markers expression in different subsets. Each row represents an antigen dose group (top to bottom: 10μM, 1μM, 0.1μM, 0.01μM and 0μM); each column represents a time point group (left to right: 1h, 3h, 6h, 12h, 24h and 72h). (n=3)

4.2.5 *Ex vivo* Expressions of Four Major Inhibitory Immune Checkpoint Receptors on Circulating Viral Epitope-Specific Cytotoxic T Cells.

In the peripheral blood, the CD8 cells compose a variety of heterogeneous cell populations. Influenza A virus (acute infection) is a common respiratory pathogen causing frequent epidemics and occasional pandemics associated with considerable morbidity and mortality. EBV and CMV (chronic infections) are herpesviruses and share with other herpesviruses the property of initial infection of young hosts, establishment of latency, and reactivation later in life with varied consequences. Hence, in the circulating blood of healthy donors, flu epitope-specific CTLs represent more of a status of 'memory', while EBV and CMV epitope-specific CTLs represent more of a status of 'exhaustion', due to the constant low dose antigen stimulation. Therefore, the immune checkpoint receptor phenotype of these three different types of viral epitope-specific CTLs could provide clues on the impact of antigen stimulation on immune checkpoint receptor expression.

To evaluate the expressions of major checkpoint molecules (CTLA-4, PD-1, TIM-3 and TIGIT) on circulating viral epitope-specific CTLs as well as total CD8+ T cells, the frozen PBMC samples from four previously recruited HLA-A*0201 healthy donors were investigated by multi-colour flow cytometry. Dumping channel, including viability dye, CD14, CD19 and CD56, guaranteed that the CD3 positive cells were pure T lymphocytes. The four individuals' immune check point expressions on CD3 positive dumping channel negative cells were shown in Figure 4-10.

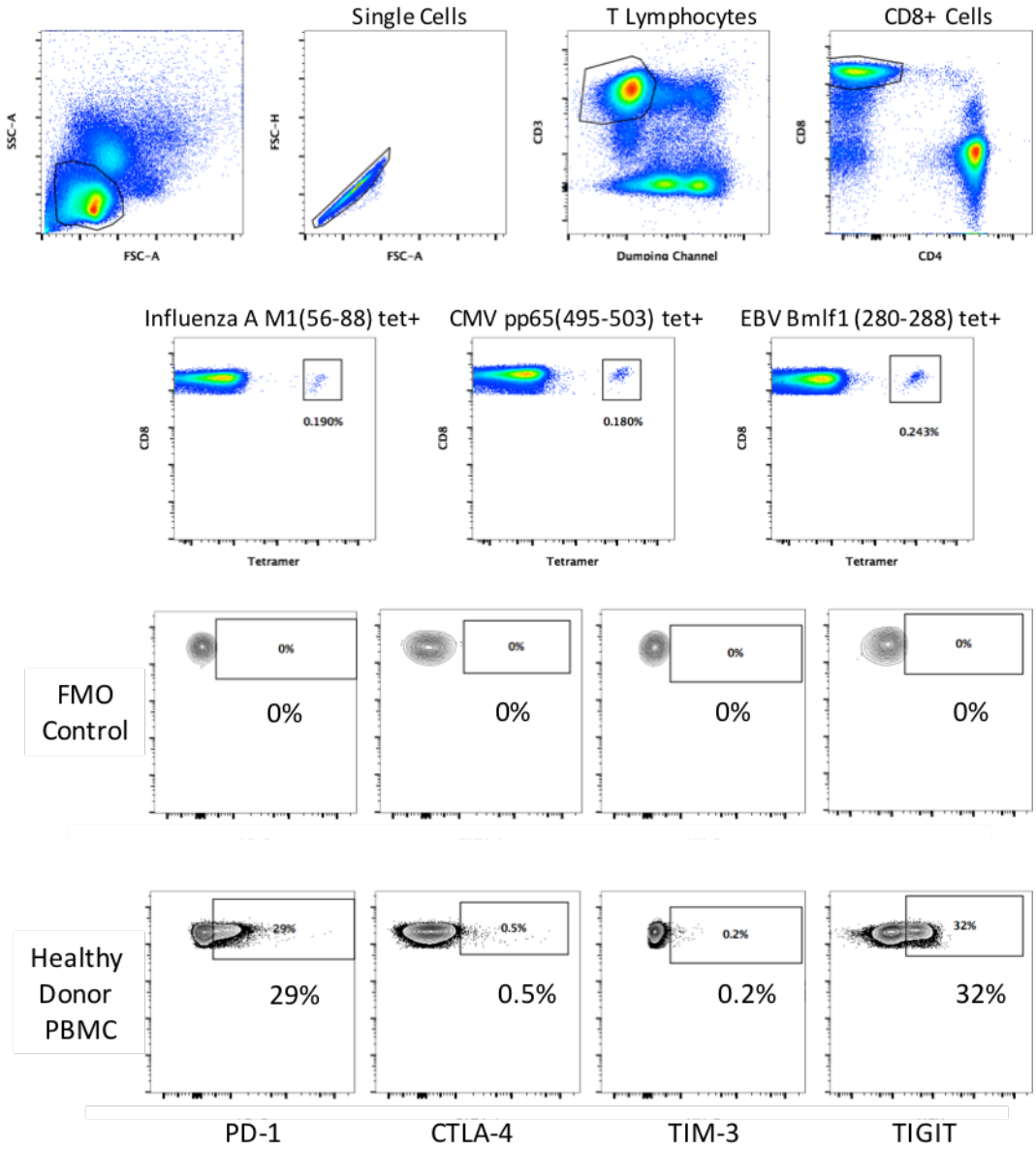

Figure 4-10 Gating strategy example from representative PBMC samples.

Top row: flow cytometry plots were first gated on live, single, CD3, CD8 double positive cells. Dumping channel includes CD14, CD19, CD56 and Aqua viability dye. Middle upper row: representative tetramer staining on PBMC samples. Middle lower row: FMO control was applied to localize the gating position of inhibitory receptor on CD8+T cells. Bottom row: positive staining from the samples.

To better visualize the flow cytometric data, a web-based Cytobank was used to analyse the data. The core algorithm of viSNE (known as t-Distributed Stochastic Neighbour Embedding, t-SNE) was developed in 2008 with continuous improvements and can reduce high dimensional flow cytometric data into 2-D categorized map representation of complex multi-parameter data. (Amir el et al., 2013; Maaten, 2008) Seven markers (CD4, CD8, tetramer, PD-1, CTLA-4, TIGIT and TIM-3) were used here to calculate the viSNE maps. The expression levels of these four immune check points on CD4 positive and CD8 positive cells were quite different. CTLA-4 was predominantly expressed on CD4+ T cells. There were certain overlapping regions of PD-1 expressing cells and TIGIT expressing cells. However, this co-expression trend was only observed in 30-50% among the PD-1 or TIGIT positive cells. For Tim-3, the overall expression was low. Similar to CTLA-4, a fraction of CD4+ cell expressed TIM-3, but these cells did not overlap with CTLA-4 cells (Figure 4-11).

Figure 4-11 Dot plots of viSNE maps from four healthy donor PBMC samples.

viSNE maps from one healthy donor. Each viSNE map was gated on population of singlets from $CD3^{+}CD14^{-}CD19^{-}CD56^{-}$ live cells. Each dot in the map represents one single cell from the samples. Median fluorescent expressions of CD4, CD8, PD-1, CTLA-4, TIGIT and TIM-3 are depicted in colour gradient manner. $CD8^{+}$ cells were circled in black to highlight. The positive cells were determined by FMO controls for PD-1, TIM-3, CTLA-4 and TIGIT.

Healthy Donor 2 CD3+ cells

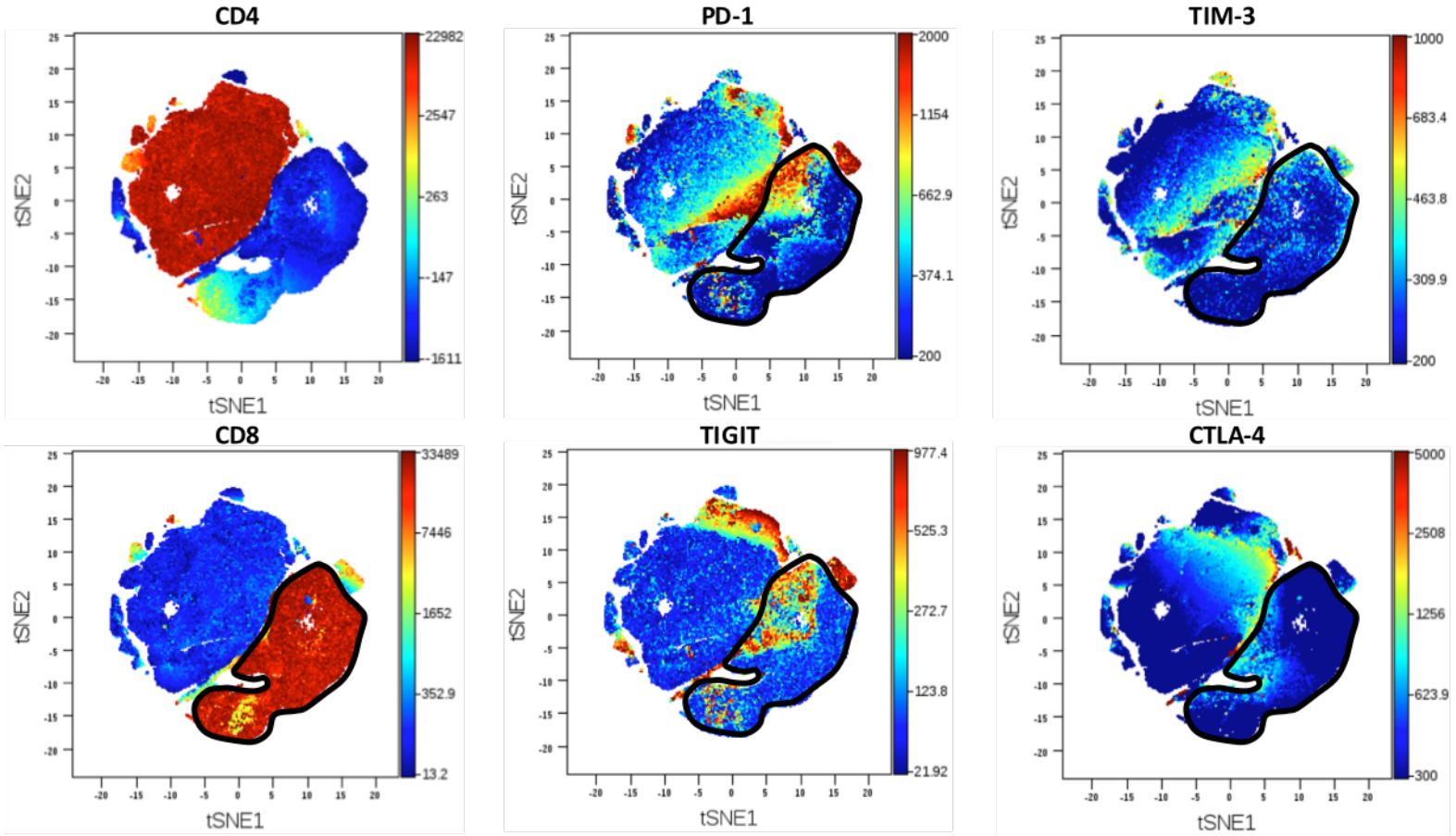

The Flu (Influenza virus A M1:58-66), CMV (cytomegalovirus pp65:495-503) and EBV (Epstein–Barr virus BMLF1:280-288) epitope-specific CD8+ T cell were further identified by homemade MHC-I tetramer among these 4 HLA-A*0201 positive healthy donors. Representative detailed immune check point expressions on individual epitope-specific CD8+ T cells were again shown as viSNE maps in Figure 4-12 and summarised expressions were shown in Figure 4-13. The expression patterns of these four immune checkpoints were fairly interesting, TIGIT highly expressed on CMV and EBV epitope-specific CD8+ T cells, PD-1 highly expressed on EBV epitope-specific CD8+ T cells, while CTLA-4 and TIM-3 were low in all three epitope-specific CD8+ T cells.

Figure 4-12 Immune checkpoint expressions on circulating viral-specific CTL populations.

First column of each group depicts the tetramer staining. (upper: total $CD3^+$ cells, lower: $tetramer^+$ cells only). Maps in second and third columns are gated on population of singlets from $CD3^+CD8^+CD14^-CD19^-CD56^-$ live tetramer positive cells. Median fluorescent expressions of PD-1, CTLA-4, TIGIT and TIM-3 are depicted in colour gradient manner. t-SNE: t-distributed stochastic neighbour embedding. The positive cells were determined by FMO controls for PD-1, TIM-3, CTLA-4 and TIGIT.

Healthy Donor 2 Influenza tet+ Cells

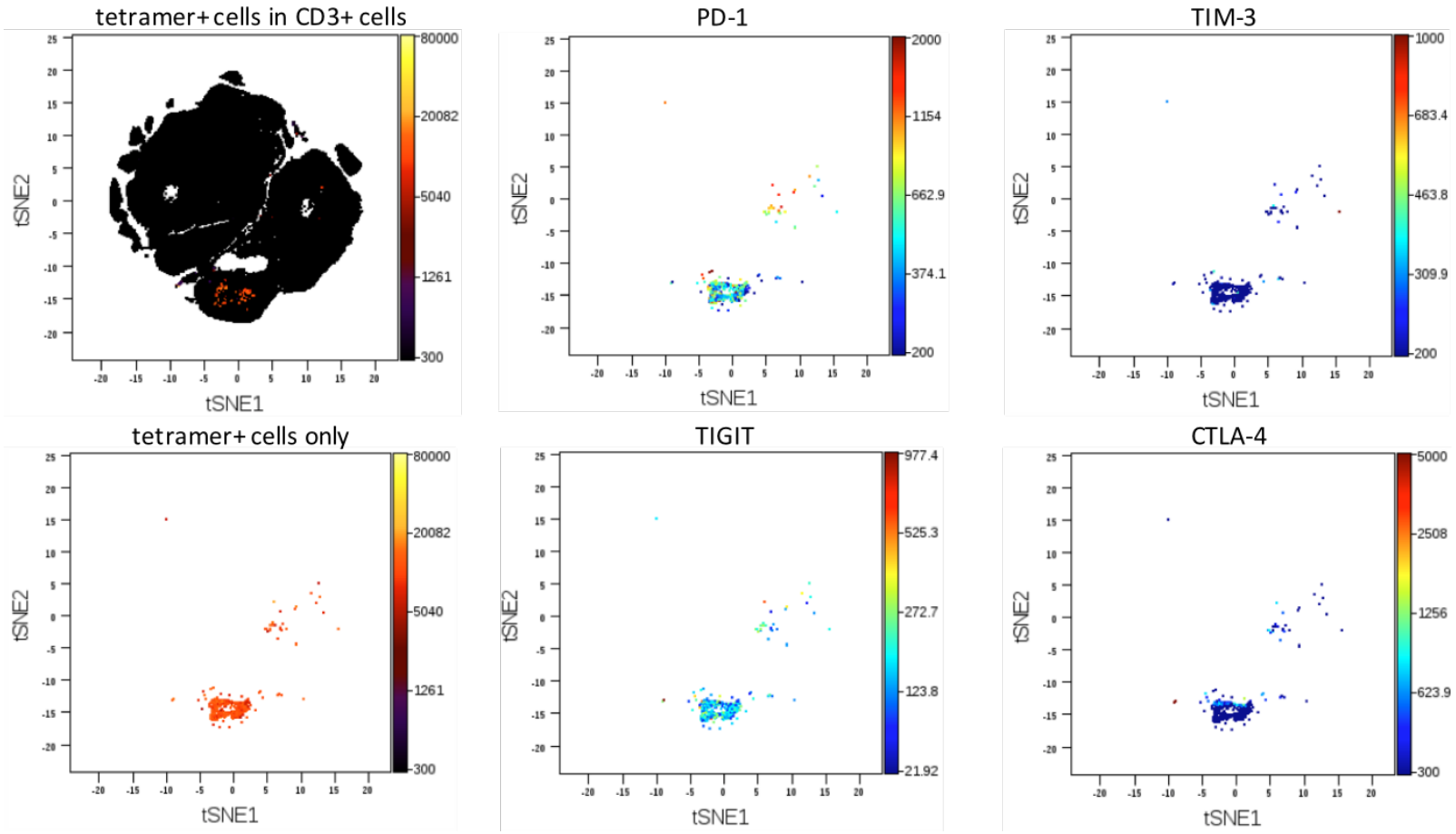

Healthy Donor 3 CMV tet+ Cells

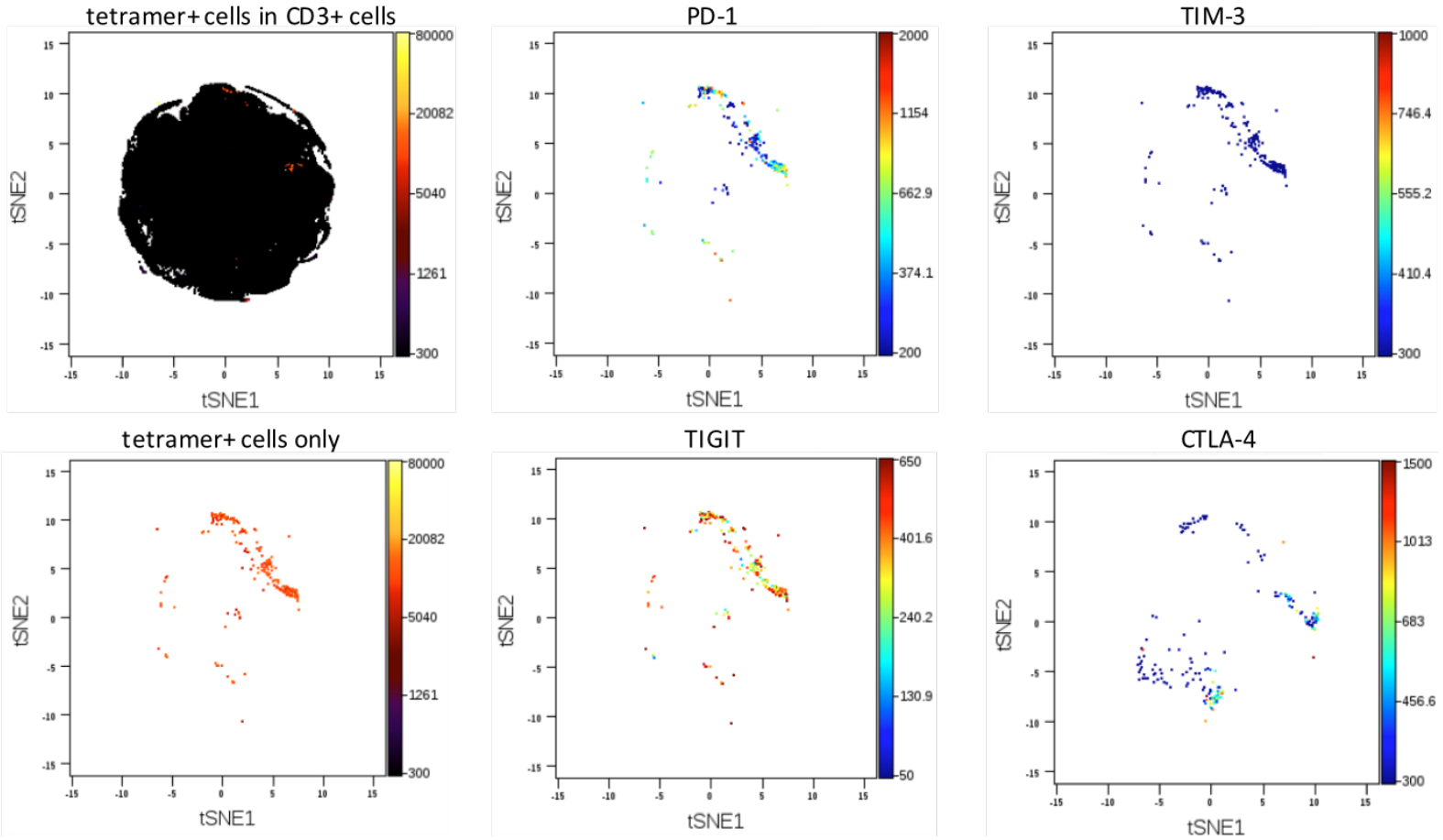

Healthy Donor 4 EBV tet+ Cells

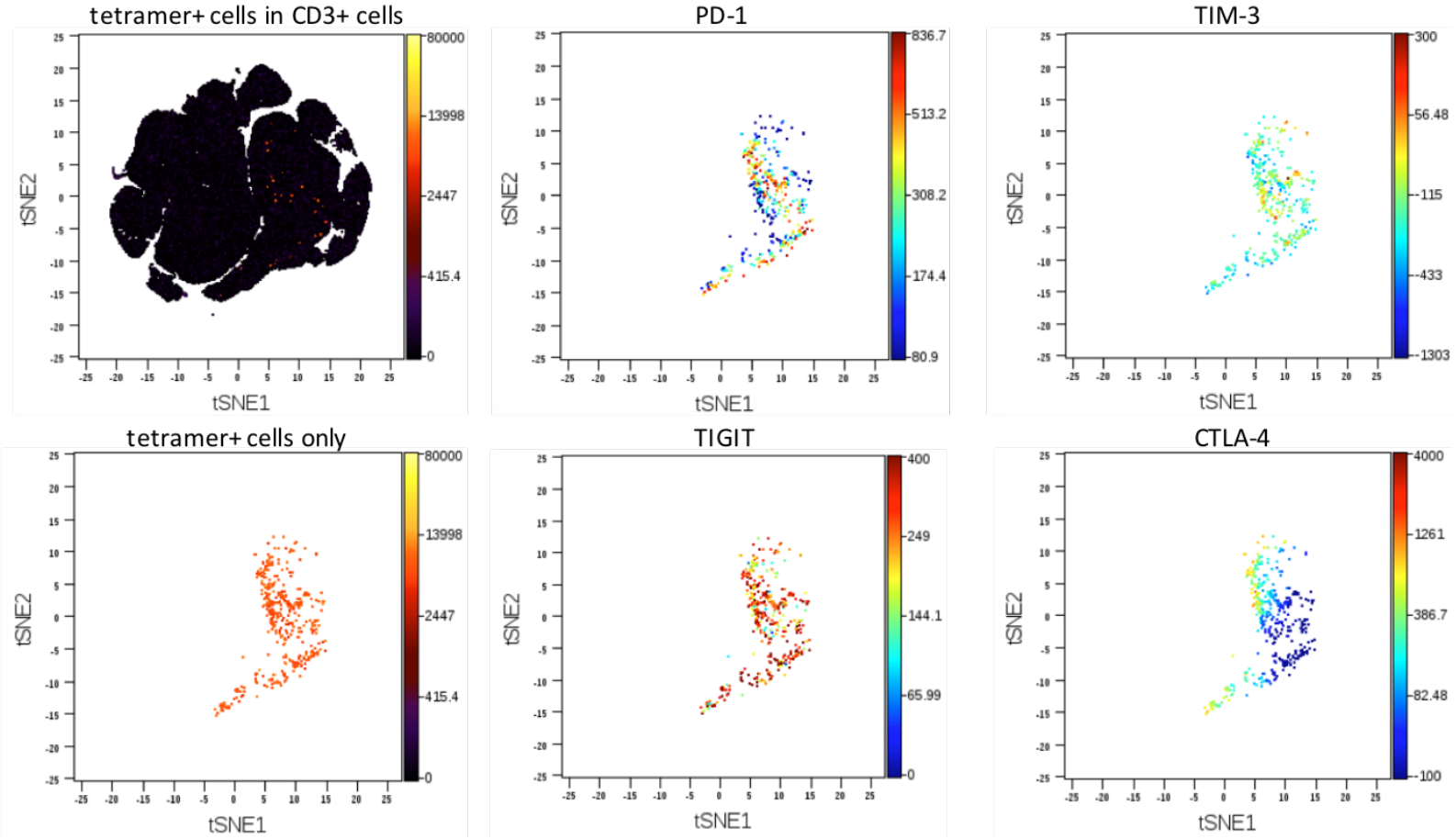

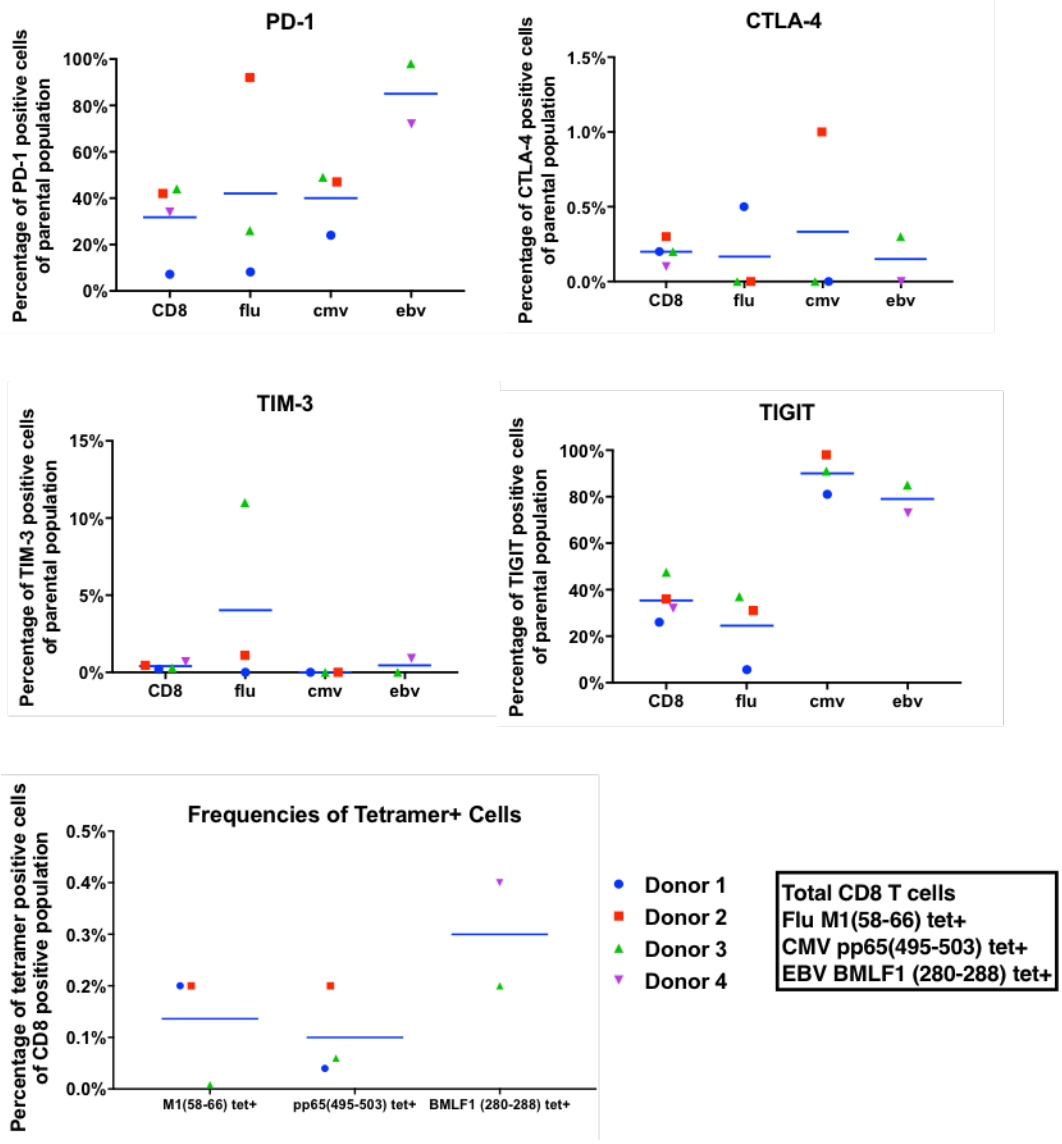

Figure 4-13 Heterogenity of immune checkpoint expressions on circulating viral-specific CTL populations.

The expressions of PD-1, CTLA-4, TIM-3 and TIGIT on total CD8 and three viral-specific circulating CTLs are summarized. Different donors are indicated by different colours.

4.3 Discussion.

In this chapter, we focused on the expression patterns of immune checkpoint receptors on antigen-specific CTLs. We started with the study on an *in vitro* cultured HIV epitope-specific CTL clone A3. A3 is a multi-functional CTL clone with an intermediate antigen sensitivity (EC_{50}= 0.025μM) among the CTL clones generated from an HIV patient LTNP005. Based on a high-dimension genomic analysis we had conducted to screen the candidate key immune regulator genes described in the last chapter, a panel of 45 immune checkpoint receptors were checked simultaneously in terms of mRNA expression level with five different doses of antigen stimulation and mock antigen stimulation. Interestingly, the expression patterns were heterogeneous and could be grouped into three categories: (A) up-regulation at high dose stimulation, genes include CD226, VISTA, 4-1BB, TIM-3, TIM-4, CTLA-4, PD-1, LAG-3 and CD160; (B) down-regulation at high dose stimulation, genes include 2B4, BTLA, TIGIT and CD96; and (C) 'unchanged' genes. The trend of CD226, VISTA, 4-1BB, TIM-3, TIM-4, CTLA-4, PD-1 and LAG-3 could also be reproduced on clone C23 (Figure 4-14). However, the data generated from clone C23 was somewhat restricted, as EC_{50} of this clone is 1.1μM, and the highest dose we stimulated was only 2μM, which may not be an adequately high dose to trigger full T cell activation.

4.3.1 4-1BB, a 'Master' Co-Stimulatory Receptor for Antigen-Experienced Cytotoxic T Cells?

A few interesting points were clearly shown in the microarray data. Unlike other co-stimulatory immune checkpoint receptors, 4-1BB was one of the most potent up-regulated genes in response to antigen stimulation. It seems that A3

clone (as well as C23 clone) favours up-regulating 4-1BB upon TCR engagement, as compared to CD28. This may due to the fact that A3 clones were *in vitro* cultured for passages, lost CD28 expression as antigen-experienced and terminally differentiated T cells, but could be reactivated without CD28 engagement (Mou et al., 2014). One recent study on chimeric antigen receptor (CAR) T has also shown that 4-1BB in the CAR architecture promoted the outgrowth of $CD8^+$ central memory T cells that had significantly enhanced respiratory capacity, increased fatty acid oxidation and enhanced mitochondrial biogenesis, in contrast to CD28 (Kawalekar et al., 2016). Trials conducted with CARs incorporating CD28 or 4-1BB costimulatory domains have shown that the clinical efficacy of CAR T cells with 4-1BB costimulatory domains (Porter et al., 2015) appears superior to that of CD28 domains (Brentjens et al., 2011). In addition, 4-1BB, together with LAG-3, has also been reported as a marker of dysfunctional T cells within tumours. And combined 4-1BB ligation added to LAG-3 blockade further rescues TILs from a paucity of 4-1BB signalling (Williams et al., 2017). Both LAG-3 and 4-1BB were reported to be driven by EGR-2, which was also among the most potent up-regulated genes in response to antigen stimulation from the microarray data, together with 4-1BB and CCL1. Apart from 4-1BB, other major co-stimulatory immune checkpoint receptors (CD28, CD27, ICOS, GITR and OX40) remained basically unchanged.

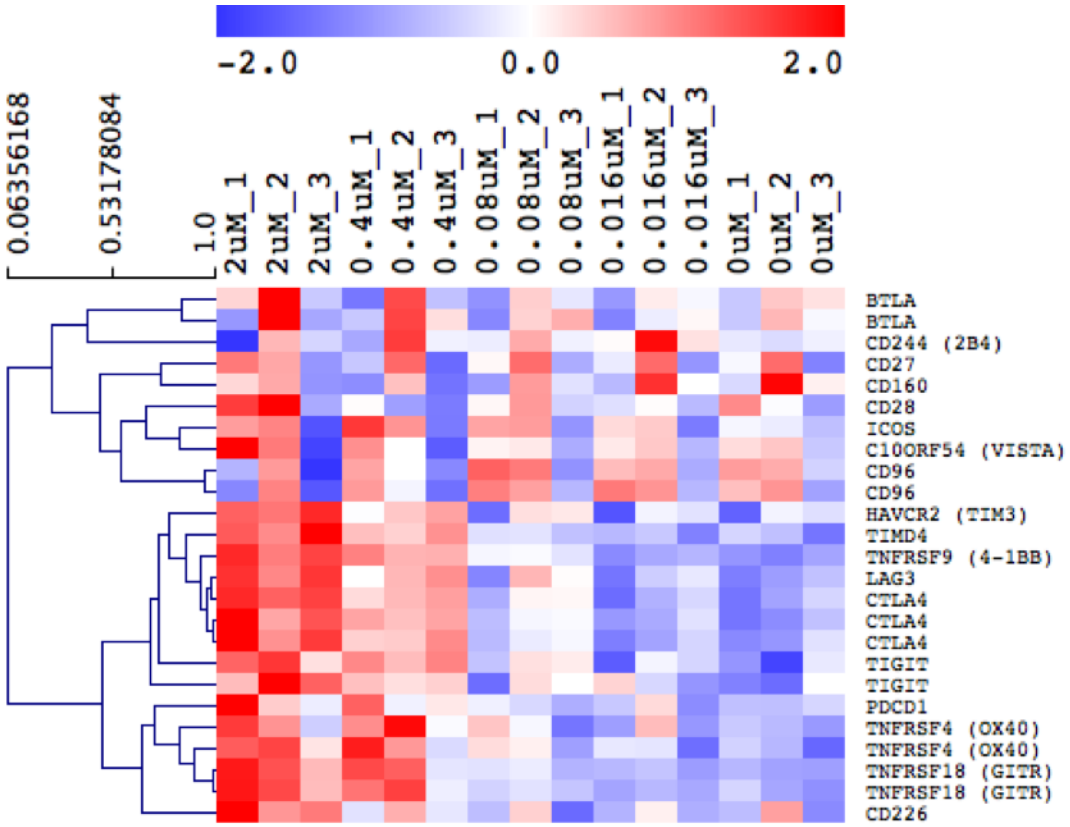

Figure 4-14 Differential expressions of most well-known immune check points in different antigen stimulations (C23).

Hierarchy clusters (HCL) of immune check point genes (both stimulatory and inhibitory) among different antigen dose groups. Each column represents a separate mRNA sample for each clone from three replicate experiments. Each row represents a probe from the bead array that maps to a gene in the Ensembl database. The colour represents the relative quantity of complementary RNA directly hybridised to each probe for each sample and is scaled within each row, to range from -2 (blue) to +2 (red). Some genes were represented by multiple probes.

4.3.2 Hierarchy of T Cell Inhibition in a Complexed Way.

Major inhibitory immune checkpoint receptors (PD-1, CTLA-4, TIM-3, LAG-3 and TIGIT) up-regulated with increased strength of antigen stimulation. Thus, there seems to be a much stronger negative feedback to down-regulate TCR signalling up T cell activation. The microarray data could only tell us the mRNA transcription changes of each individual genes; however, the real functional molecules are on the cell plasma membranes. Thus, the surface CTLA-4, PD-1, TIM-3, LAG3 and TIGIT expression level were checked via flow cytometry on clone A3.

CTLA-4 expression was the lowest among these five inhibitory receptors. The microarray identified CTLA-4 up-regulation by three different probes, while the FACS data showed only a small percentage increase of CTLA-4 positive cells. However, the CTLA-4 surface expression was really low on A3 as well as the peripheral CD8+ T cells from four healthy donors. There was a clear increased surface CTLA-4 staining shift on A3 in a dose-dependent way, which might be meaningful enough to modulate T cell functions. However, intracellular CTLA-4 staining revealed a much greater number of CTLA-4 molecules stored in the intracellular vesicles; this corresponds to the fact that the majority of CTLA-4 molecules on a T cell are actually located in intracellular compartments, from where they could be transported to the cell surface and rapidly internalised (Buchbinder and Desai, 2016).

PD-1 expression was the second lowest on clone A3. At resting stage, A3 clone expresses PD-1 (about 20-40% of the cells depending on the cell condition) in contrast to its sister clone A20 (no obvious PD-1 expression), even though they

are both generated from the same PBMC sample and shared identical TCR sequence (previous lab data). The percentage of PD-1 positive cells in the A3 population remained about 40% from d14 to d17 post feeder expansion. It is well-known that PD-1 is an inducible immune modulatory receptor. Upon interaction with its ligands PD-L1 and PD-L2, PD-1 plays important roles in negative regulation of T cell responses to antigen stimulation and maintaining peripheral tolerance (Yao and Chen, 2014). Upon activation by 10μM cognate peptide, PD-1 expressing proportion increased from about 40% to 60% of the A3 cell population. Unlike 4-1BB, TIM-3 and TIGIT which expressed on at least 90% of the cells with this strength of stimulation, only 20% of the cells increased PD-1 expression. PD-1 expression can be fully up-regulated by co-culturing with anti-CD3/CD28 magnetic beads (data not shown). Therefore, similar to CTLA-4, A3 cells are prone to restrict PD-1 expression but with a less strict regulation. In addition, it is interesting to see that the PD-1 positive cells expressed a higher level of TIM-3, but not TIGIT, compared to PD-1 negative cells. It has been shown in chronic LCMV infection that dual expressing cells (PD-1 and TIM-3 double positive) and PD-1 single-positive cells could be found on antigen-specific CD8+ T cells, but TIM-3 single-positive cells were relatively rare, which indicated a hierarchic expression of PD-1 and TIM-3 (Jin et al., 2010). Another study reported that TIGIT and PD-1 co-expression only appears in tumour antigen (TA)-specific (NY-ESO-1) CTLs in contrast to viral-specific CTLs (Flu and CMV). The authors claim that TIGIT might be an early T cell activation marker that is further up-regulated by dysfunctional TA-specific CD8+ T cells upon chronic stimulation (Chauvin et al., 2015). Nevertheless, both co-blockade of PD-1 and TIM-3 or TIGIT resulted in substantial better rescue of the CTL proliferation and cytokine

productions than blocking any pathway alone in the both studies. Clearly, the data of others and our data indicate a diversity of the expression patterns of these inhibitory immune checkpoint receptors; a deeper understanding of the underlying mechanisms will be helpful for rational drug and regimen designs.

LAG3 showed an intermediate expression level on clone A3, increased from 10% to 60% upon full activation. TIM-3 expression was higher than LAG-3 in general. On fresh cultured T cell clone cells (from feeder expansion), TIM-3 expression was high (more than 50% at resting stage) and could be induced to up-regulate to express on all the cells with strong antigen stimulation. Interestingly, we observed that fresh cultured A3 cells expressed much more TIM-3 molecules on the surface than frozen samples (thawed d10 A3 stock), indicating that TIM-3 expression was also influenced by the cell condition, similar to PD-1. This may explain the low expression of TIM-3 on the frozen PBMC samples from the healthy donors (Figure 4-11), as PBMC samples were defrosted and rested in growth medium overnight and the cell conditions were much poorer than T cell clones or fresh cells. In addition, TIM-3 expression on clone A3 gradually down-regulated over time (d14 to d17), during which the cells gradually underwent apoptosis. In contrast, stimulating cells with 10μM peptide kept cells active and TIM-3 expressions were also maintained. Thus, it seems that TIM-3 expression could indicate the status of T cells - active cells express high level of TIM-3, while apoptotic and resting cells express low level of TIM3. Unlike TIM-3, TIGIT expressed on about 40% of the total CD8+ T cells on frozen PBMC samples. TIGIT expressions on T cell clones were the highest among these five inhibitory receptors (100% positive on clone A3 in any stimulation strength). Interestingly, it seemed that TIGIT up-regulated in low dose stimulation, and down-regulated after

reaching a certain dose based on FACS data. The watershed dose for clone A3 was near 0.4μM and for C23 was near 2μM (Figure 4-15) and probably had a certain relationship with the antigen sensitivity of each clone (0.025μM for A3 and 1.1μM for C23). The down-regulation at protein level also linked to the TIGIT mRNA down-regulation on clone A3. It has been shown elsewhere that TIGIT expression is modulated by T-bet and Eomes (Tauriainen et al., 2017), so the change of TIGIT surface expression may link to the intracellular transcription factors. In addition, TIGIT is competing with CD226 on the cell surface (similar to CTLA-4 and CD28) for the ligands and both molecules are highly expressed on CD8+ T cells. The down-regulation of TIGIT after reaching certain dose may accompany with the up-regulation of CD226, although this requires further validation.

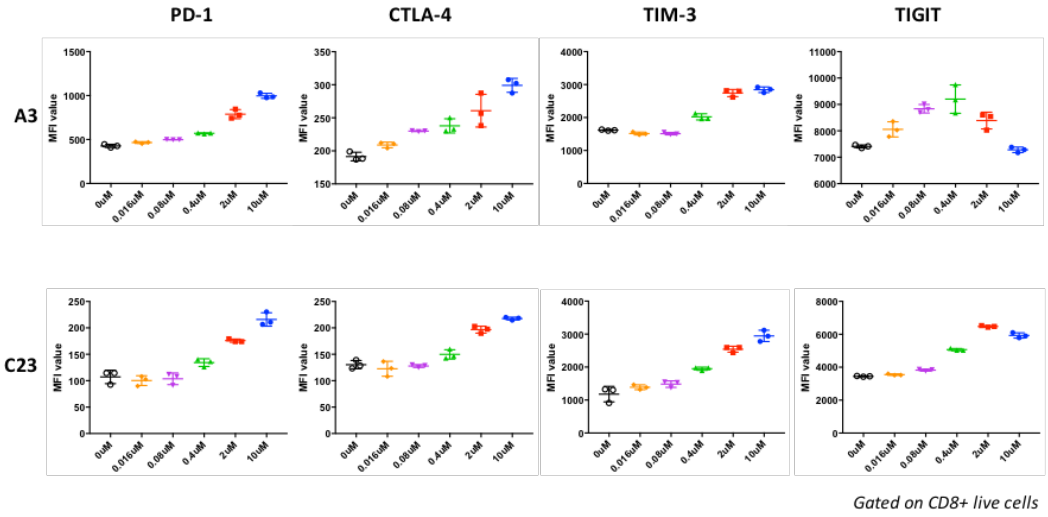

Figure 4-15 PD-1, CTLA-4, TIM-3 and TIGIT expression on CTL clones.

The surface expressions of each immune checkpoint receptor were quantified by flow cytometry and plotted with median fluorescent value to show the differences between each antigen dose stimulation. (0μM, 0.016μM, 0.08μM, 0.4μM, 2μM and 10μM).

These findings suggested that the level of surface expression of each inhibitory receptor might correlate inversely with its respective inhibitory potency. However, there was no clear hierarchic association (inclusion or exclusion relationship) between each inhibitory receptor indicated by the co-expression pattern. The complexed underlying regulatory mechanism highlighted the importance of a more detailed understanding of the interactions between each inhibitory receptor for a more rational regimen for cancer treatment. Based on these findings we propose that the level of surface expression of the inhibitory receptors might correlate inversely with their inhibitory potency (Figure 4-16).

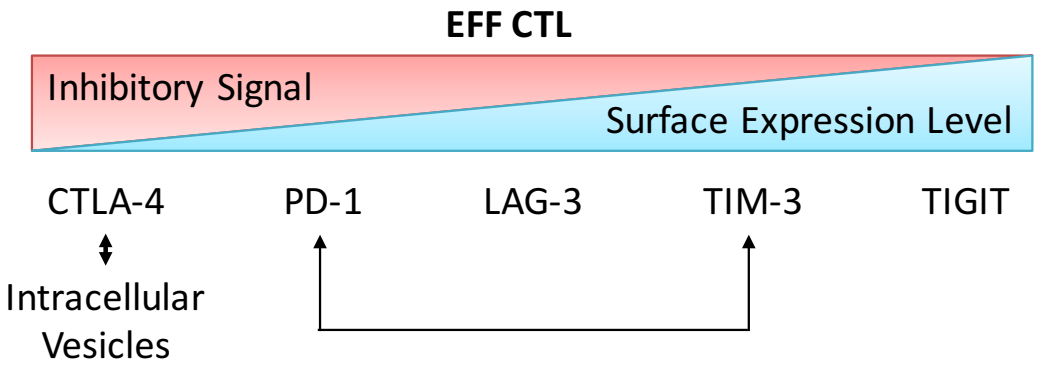

Figure 4-16 Proposed Model of CD8+ T Cell Inhibition Hierarchy.

By stimulating effector CTL clone A3 with a range of antigen stimulation (0-10μM of cognate epitope), the surface expression levels of each individual immune checkpoint receptor are: CTLA-4 (remains marginal, but is much more abundant intracellularly), PD-1 (from 30% to 50%, 20% increase), LAG-3 (from 20% to 60%, 40% increase), TIM-3 (from 25% to 80%, 55% increase) and TIGIT (remain 100% positive). As CTLA-4 mediates the highest CTL TCR inhibition, then comes with PD-1. The level of surface expression of the inhibitory receptors might correlate inversely with their inhibitory potency. In addition, PD-1 and TIM-3 were observed to be positively correlated, but there was not such correlation between TIGIT and PD-1 or TIGIT and TIM-3.

4.3.3 Co-stimulation Leverages with Co-inhibition.

Apart from inhibitory immune checkpoint receptors, co-stimulatory receptors are also promising therapeutic targets. 4-1BB engagement induces proliferation and production of IFNγ and IL-2, as well as augments the cytotoxicity of CTLs. (Giuroiu and Weber, 2017) It has been shown that 4-1BB has very strong correlation with PD-1 and LAG-3 on CD8+ T cells (Blackburn et al., 2009), and from our microarray data, this molecule was the only co-stimulatory receptor showing strong increased expressions in response to the increment of antigen dose, similar to other major inhibitory receptors (PD-1, LAG-3, TIM-3 and CTLA-4). From the FACS data, unlike other immune checkpoint receptors, 4-1BB expression perfectly fit the bimodal mode. And almost all the cells expressed 4-1BB upon stimulating the cells with 10μM antigen loaded APCs. Inside tumour microenvironment, although TA-specific CTLs may up-regulate 4-1BB, there may not be enough 4-1BB ligands for binding. All these facts highlighted the potential of 4-1BB as a therapeutic target. The initial attempt of 4-1BB agonist antibody for cancer treatment failed due to liver toxicity (Dubrot et al., 2010); however, the antibody re-entered the clinical study as significantly lower dose could achieve therapeutic activity without the previously toxicity. Currently, there are more than ten clinical trials with 4-1BB-mediated cancer immunotherapy in progress (Makkouk et al., 2016).

In the CTL clone data, although the cells expressed high level of different inhibitory receptors, the cells could still degranulate and secrete cytokines to kill the target cells. However, whether the 4-1BB up-regulation (to overcome the inhibitory signals by PD-1, TIM-3, CTLA-4, LAG-3 and TIGIT) contributed to the successful T cell functionalities remains unclear. Nevertheless, the surface

expression of 4-1BB appears at 3h and peaks at about 6h post TCR engagement, earlier than IL-2 receptor α-chain and PD-1 and sensitive to low strength of antigen stimulation; this may thus play a pivotal role in the overall late-stage T cell functionalities.

In summary, we have described herein several major immune checkpoint receptors' expression patterns on antigen-specific CTLs, with particular focus on co-stimulatory receptor 4-1BB and inhibitory receptor PD-1, TIM-3, LAG-3, CLTA-4 and TIGIT. CTL clones with the same TCR expressing different inhibitory receptors and co-stimulatory receptors, indicating that apart from the specificity of the TCR, which is the major determinant of the T cell function (Almeida et al., 2007; Chen et al., 2012), varied patterns of inhibitory receptor expression may also determine the outcome of a TCR signalling reaction.

5 Chapter 5: Optimisation of Gene Delivery into Human Antigen-Specific Cytotoxic T Cells.

5.1 Introduction.

T cells are pivotal components of human adaptive immune system. Despite that the magnificent advances of T cell immunology in the past few decades, many of the proteins and signalling transductions that regulate these cells have yet to be fully defined.

A considerable amount of progress has been made on the manipulation of T cell function-related proteins (such as co-stimulatory receptors or immune checkpoints), which offers the opportunity to functionally correct malfunctioning T cells into "good" T cells, and consequently to benefit T cell-mediated diseases, such as utilizing genetic tools to knockout (KO) specific genes for the study T cell development and functions in disease settings. For ethical reasons, most of studies are limited to murine animal models, however, owing to the complexity of human disease and different anatomical and cellular properties between rodents and human, it is becoming increasingly important to translate and test the finding from the murine studies to more relevant human cells (Mestas and Hughes, 2004; Shay et al., 2013). One approach is to study isolated T cell from human circulation. The major advantage to study human peripheral blood T cells is that those cells are easily accessible as well as can be isolated in relatively high amounts and further expanded, which offers the possibility for scientific study or clinic applications in a human setting.

5.1.1 Broad Application of T Cell-Based Therapy.

In the past two decades, gene therapy has proven to be one solution for several inherited diseases. ADA-deficient SCID (adenosine deaminase deficient severe combined immunodeficiency) was the first such disease to utilize T cell gene therapy, patients received functional ADA-expressing autologous retroviral transduced T lymphocytes and showed immune reconstitution. Moreover, functional ADA-expressing T lymphocytes had an advantage and eventually replaced the non-transduced T lymphocytes population to nearly 100% post therapy (Aiuti et al., 2002). There have also been reports on T cell gene therapy, such as lentivirus-based therapy on Wiskott-Aldrich Syndrome (WAS) (Dupre et al., 2004). In the treatment of cancers, Chimeric antigen receptor (CAR) transgenic T cells technology has shown great potential for treating CD19 positive B cell malignancies (Grupp et al., 2013; Porter et al., 2011). In some cases, patients who received multiple infusions of CAR transduced autologous T cells have been cured with many fewer side effects compared to traditional therapy. Similar concepts have also been applied onto NY-ESO-1 TCR transgenic T cells for treating melanoma or other solid tumours and have shown promising objective responses (Rapoport et al., 2015b; Robbins et al., 2015). Furthermore, T cell gene therapy might be an option for acquired diseases such as AIDS; possible therapies include transdominant *rev* and *tat*, CRISPR-Cas9 based CXCR4 or CCR5 knock out. By and large, it is becoming more and more clear that T cell based gene therapy holds great opportunities to offer alternatives for many current therapies.

5.1.2 The Mechanisms of siRNAs and CRISPR/Cas9.

RNA interference (RNAi) is a biological process in which RNA molecules inhibit gene expression, typically by causing the destruction of specific mRNA molecules. The RNAi pathway is initiated by Dicer, which cleaves long double-stranded RNAs into short (about 20 nucleotides) double-stranded small interfering RNAs (siRNAs). Each siRNA is then disassembled into two single-stranded RNAs - the passenger strand and the guide strand. Next, the guide strand is incorporated into the RNA-induced silencing complex, while the passenger strand is degraded. When the guide strand pairs with a complementary sequence in an mRNA, the RNA-induced silencing complexes (RISC) cleave the mRNA and cause post-transcriptional gene silencing (Hannon, 2002). The discovery of siRNAs led to a surge in interest for biomedical research and drug development. Many developments in siRNA therapy have been made in the past decade, however, the challenges to a successful siRNA therapy (such as biological barriers, toxicities of RNAi, tissue specificity and monitoring delivery) remain significant (Pecot et al., 2011).

CRISPR (Clustered regularly interspaced short palindromic repeats) is a microbial nuclease system, which confers bacteria with immunity against invading phages and plasmids. Cas9 (CRISPR associated protein 9) is an RNA-guided nuclease found in *Streptococcus pyogenes* and is now adapted for inducing sequence-specific DSBs (double-stranded break) and target genome editing. In the simplest and most widely used form of this system, two components must be introduced to the cells: the Cas9 nuclease and a guide RNA (gRNA), consisting of a fusion of a crRNA (CRISPR RNA) and a fixed tracrRNA (trans-activating

crRNA). The 20 nucleotides at the 5' end of the gRNA direct Cas9 to a specific target DNA site (must lie immediately 5' of a PAM (protospacer adjacent motif, which canonically is a NGG) sequence) using standard RNA-DNA complementarity base-paring rules (Ran et al., 2013; Sander and Joung, 2014). Nuclease-induced DSBs can be repaired by one of at least two different pathways: non-homologous end-joining (NHEJ) and homology-directed repair (HDR). NHEJ can lead to the introduction of insertion or deletion, which can cause a frameshift and thus may disrupt the expression of the gene. HDR can be used for introducing specific point mutation and inserting or deleting desired sequences through recombination of exogenously supplied donor DNA (Charpentier and Marraffini, 2014). Using synthetic single RNA guides, Cas9 can be reprogrammed to create specific DNA mutagenesis in the human genome, thus can be used as a therapeutic approach for a variety of diseases and disorders with limited biological toxicity and better histocompatibility. CRISPR/Cas9 technology has been widely tested and applied to many different mammalian cell types including some human primary cells such as T lymphocytes (Schumann et al., 2015; Su et al., 2016). Due to its simplicity to design and high efficiency to cause mutation, this system is becoming the most powerful genetic tool and provides great promise to medicine in the future.

5.1.3 The Aim of This Chapter.

T cells from peripheral blood are a pool of heterogeneous cells, which are distinguished by the differential expressions of surface or intracellular molecules, such as CD4 and CD8, T cell receptors, co-signalling receptors, chemokine and cytokine receptors, transcription factors, etc. Therefore, it can be difficult to study a certain function of a specific T cell population. The option of generating a specific population of T cells deriving from the progenitors that recognize same antigen (such as some viral protein) or same epitope or with identical phenotype and function (from one mother cell) can be helpful, as in T cell engineering. Modifying non-selected human primary T cells renders the risk of targeting the wrong cells. As the goal of such T cell based therapy is usually to treat patients with certain diseases, like cancers, it becomes very important to develop a method to manipulate T cells with specificity to offer real benefits. Continuous efforts have been made to optimize the methods to deliver foreign nucleotides into human primary T cells. However, those studies are mainly targeting CD4+ T lymphocytes. Perhaps the reason is that the CD4 cells are more proliferative compared to the CD8 cells and thus easier to be cultured *in vitro*. Primary CD8+ T cells are a promising cell source to be engineered to target tumour cells. In contrast to primary T cells study, there have been very few optimization efforts on introducing foreign nucleotides into *in vitro* cultured antigen specific CD8+ T cells (T cell clones). Therefore, optimisations of transfection/transduction methods on those T cells will be required and helpful to enable effective applications of genetic manipulation techniques on antigen specific T cells and in-depth study afterwards.

5.2 Results.

5.2.1 Knocking Down Genes by siRNA on Antigen-Specific T Cell Clone.

Primary CTLs are generally refractory to lipid-based transfection methods and thus require viral vector delivery system or electroporation. Nucleofection is an electroporation-based procedure that was developed by Lonza as described in the introduction. A recent article on Journal of Immunological Methods reports an improved two-hits nucleofection for siRNA-mediated gene silencing in stimulated primary human T cells (Freeley and Long, 2013). Based on this method, we performed optimisation experiments on one well-studied CD8+ T cell clone A3, generated from an HLA-B*08 HIV-1 patient.

Human antigen specific T cell clones are more difficult to culture than T cells directly isolated from blood. To grow T cell clones, cells are co-cultured with irradiated allogenic PBMCs from at least two healthy donors (feeder cells) and PHA. Cells are highly activated in the first 5 days and rapidly expand from day6 to day10. From day11 to day14, the cells become relatively stable. After day15, cells start dying even with IL-2 in the culture medium, and need another round of stimulation to proliferate. Different CTL clones have different rates of proliferation. Cells, which grow faster, are usually tougher and can stay alive in the culture medium up to 20 days' post stimulation. Previous experience of culturing T cell clones showed that 10 days post feeder expansion (d10), T cells became relatively stable. For this reason, T cells were electroporated twice using Nucleofector program T7 on d10 and d12, then incubated for 48h or 72h prior to lysis for Western blotting. The target gene here was GAPDH, a house keeping gene with good commercially available antibody.

Cell cultures were checked routinely under microscopy during the incubation. Noticeably, T cells that received electroporation underwent significant morphological change. 3h post each electroporation and prior to each harvest, the viability of cells was checked by flow cytometry of an aliquot of cell culture. The percentage of the viable cells dropped from 80% before electroporation to less than 20% after 72h post the second electroporation. (Figure 5-1 A,C) Although the electroporation caused such a big impact on cell survival, the knock down efficiency using this method was very good (Figure 5-1B). However, as the T cell clones are unlike cancer cell lines, which can quickly recover from electroporation and keep proliferating; T cell clones received electroporation became very apoptotic (Figure 5-1C). Since we were trying to engineer CTLs with physiological function and siRNAs only provided a short time knock down effect, therefore use of RNAi via electroporation might not be an ideal approach.

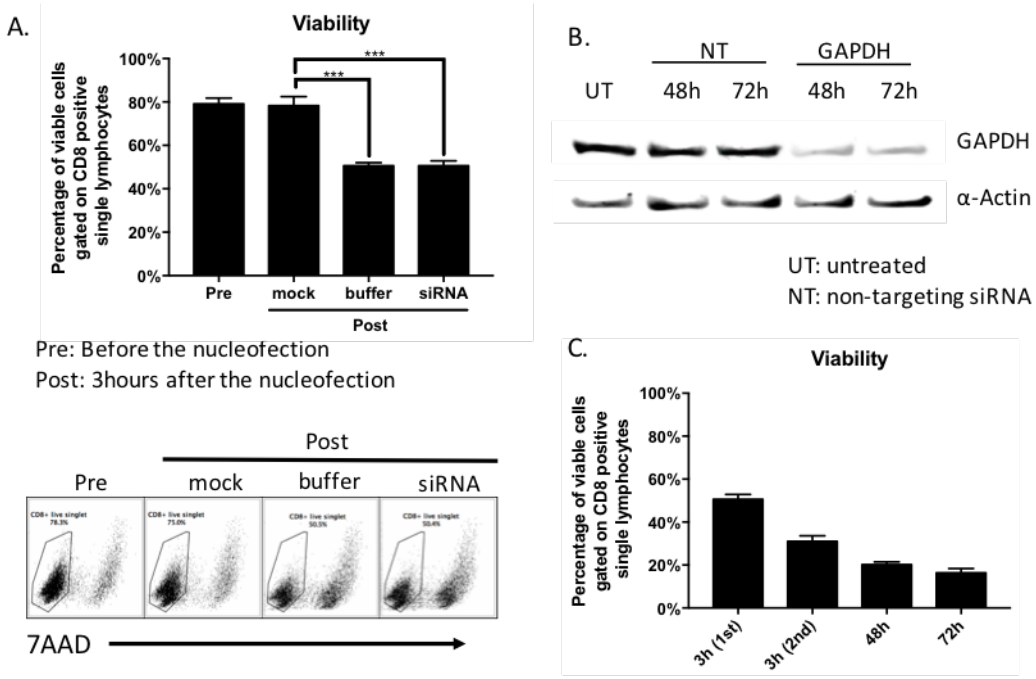

Figure 5-1 Electroporation based siRNA delivery could effectively knock down targeting genes but results in poor cell viability.

(A) Percentages of live cells before and 3h after electroporation. To quantify the cell damage of the electroporation method, the antigen specific T cell clone A3 cells were counted, washed, suspended in Nucleofector solution and transferred into a Nucleocuvette according to manufacturer's instructions, mock group did not receive pulse, buffer group received the pulse without NT siRNA, siRNA group received the pulse with NT siRNA. Cells were them immediately transferred into pre-warmed culture medium, after a brief spin-down, cells were cultured in 96-well U-bottom plate until being lysed to extract protein. An aliquot of the cells was stained with LIVE/DEAD Cell Viability Assays and acquired by a Cyan flow cytometer. (B) Western blot of the protein from the cell lysis, GAPDH was the target gene, α-Actin was the loading control gene. **C.** Percentages of live cells at different time points.

Another siRNAs method tested was using Accell siRNA (GE Dharmacon, UK), which was advertised to be able to deliver siRNA without transfection reagents, virus, or instrumentation into difficult-to-transfect cells efficiently. In contrast to the electroporation test, the knock down efficiency achieved was only up to 20% according to the manufacturer's instruction (Figure 5-2).

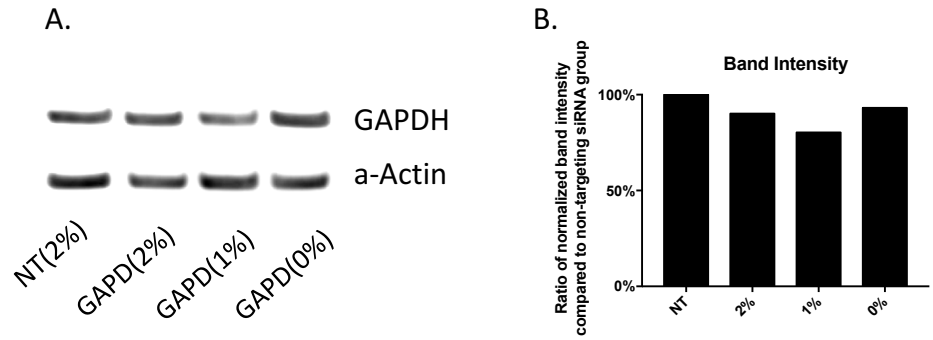

n% means delivery medium supplemented with n% human serum.

Figure 5-2 Accell siRNA works poorly on CD8 antigen-specific T cell clone.

(A) Western blotting of the protein from the cell lysis from *in vitro* cultured A3 CD8 antigen specific T cell clones. The antigen specific T cell clones were counted on day12 post feeder expansion and seeded in 96-well U-bottom plate at a concentrated of 100,000cells/well in serum free delivery medium. siRNA targeting of GAPDH were added into each well with the combination of different concentrations of human serum according to manufacturer's instruction. 24 hours later, cells were washed and cultured in fresh H10 medium supplemented with 100 U/ml IL2 for another 2 days prior being lysed to extract protein. Universal non-targeting (NT) siRNA were used as the negative control. (B) Knock down efficiencies were calculated by comparing the band intensity of GAPDH (siRNA targeting gene) versus α-Actin (loading control) and normalized by comparing to the negative control group, the band intensities were quantified using Fiji software.

RNAi has many good properties, though it also comes along with certain disadvantages, such as the variability and incompleteness of knockdowns and the potential off-target effects. When using siRNAs to target specific genes, the efficiency varies from cell type to cell type. Also, siRNAs are easily degraded by RNases, which renders the molecules of poor chemical stability and low half-life. Thus, the assays usually give transient inhibition only and targeting transcripts with high turnover is challenging. The applications of siRNAs on human antigen specific CD8+ T cells here showed either poor viability caused by delivery method or limited knock down efficiency. The methods may be able to be possible to improve, however, this will be costly both in money and time. Again, techniques need to be suitable for the experiment, as we are trying to establish a way to offer long term gene editing effects, siRNA is not the best option that we should choose.

5.2.2 Knocking Out Genes by the Electroporation-based CRISPR/Cas9 Technique on Antigen-Specific T Cell Clone.

CRISPR/Cas systems have evolved within bacterial and archaeal organisms as a defence against invading viruses and plasmids. Recently, the type II CRISPR/Cas system from *S. pyogenes* has been engineered to function in eukaryotic cells using two molecular components: a single Cas9 protein and a non-coding guide RNA (gRNA) (Ran et al., 2013). The most two common ways for CRISPR delivery are by lentiviral vectors and by plasmid. The advantages of lentiviral vectors are the high efficiency in many cell types and much lower genotoxicity compared to retroviral vectors. However, the random viral integrations still could cause unfavourable mutations and lead to cell dysfunctions. For such reason, we started with plasmid transfection to deliver CRISPR/Cas9 by electroporation. The plasmids pulsed into cells will most likely only transiently express Cas9s and sgRNAs, which can form complexes to recognize its target site and induce DNA double strand break in the genome. Unlike viral-based CRISPR/Cas9 system, the foreign DNAs only exist in the target cells in a short period usually three to five days but enough for gene editing effects, thus make this method safer for T cell therapy.

To validate this method, we chose HLA-*A02 as our positive control. The HLA molecules are constantly expressed on somatic cell membrane. PD1 is the gene that we want to target, which is an immunosuppressive receptor. We first designed two sgRNA from the CRISPRscreen, a prediction platform developed by CBRG (Oxford) for designing sgRNAs. For each gene, target sequences were selected according to the ranking given by CRISPRscreen and number of

additional genomic hit. The CRISPR/Cas9 plasmid construction is described in the Method section by inserting the annealed complementary sgRNAs into the pX330 plasmid. The transfection was done using program T20 or T23 on a Nucleofector.

Table 5-1 CRISPR/Cas9 target sequence predicted by CRISPRscreen.

Target Gene	Target Genomic Coordinates	Genome Sequence	Additional Genomic Hit
HLA-A*02	chr6: 31324127-31324149	CCTTGCCGTCGTAGG CGTACTGG	0
PD-1	chr2: 242797656-242797678	CTCGGATCCACGTA GGATCGTGG	0

To start with, we tried to knock out HLA-A*02 on A3 clone. This was an experiment to prove the concept. After the initial Nucleofection, noticeable clumps floating in the Nucleofector cuvette were observed, which should be the cell debris caused by electroporation. 3h post the electroporation, the cell viabilities were check by viability dye, in both T20 and T23 group, most cells became dead. The KO efficiency was checked after one round feeder expansion in the hope of altering the cells to a better status. However, the electroporated cells showed limited proliferation during the cell culture and were mostly dead at 12 days (Figure 5-3).

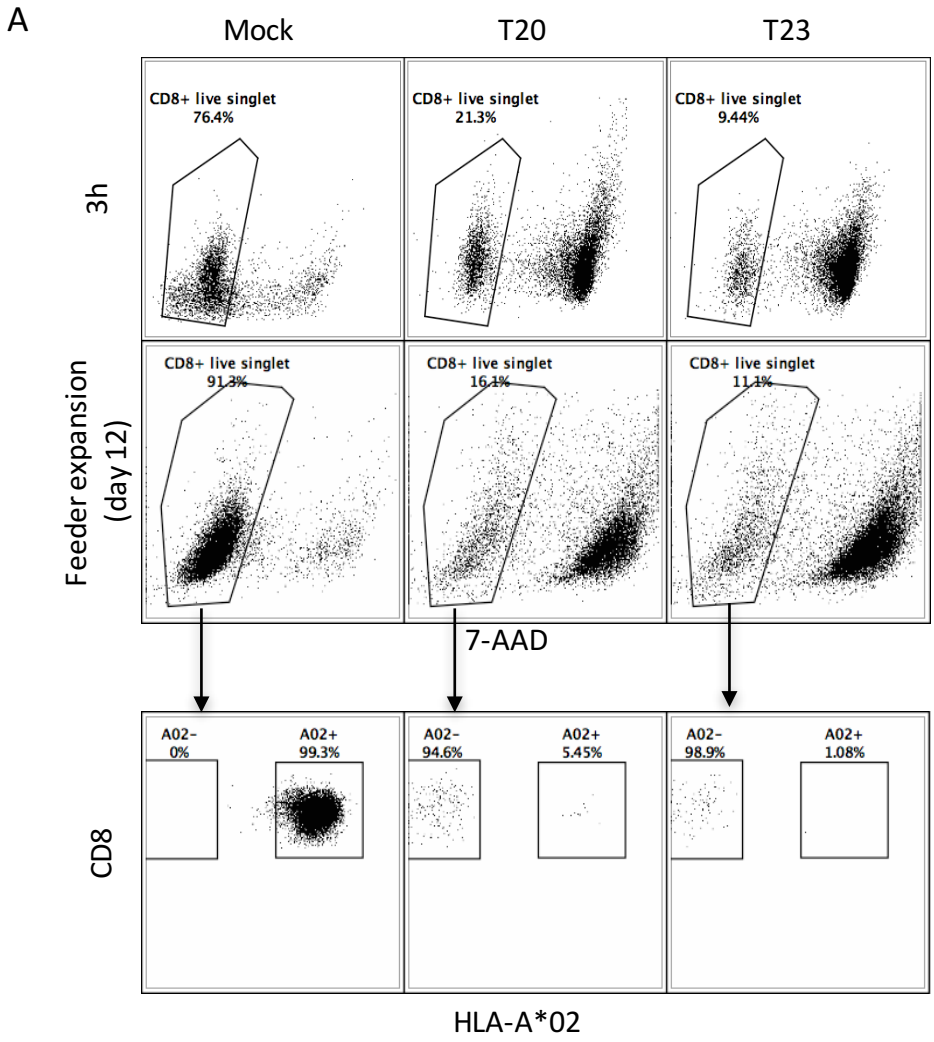

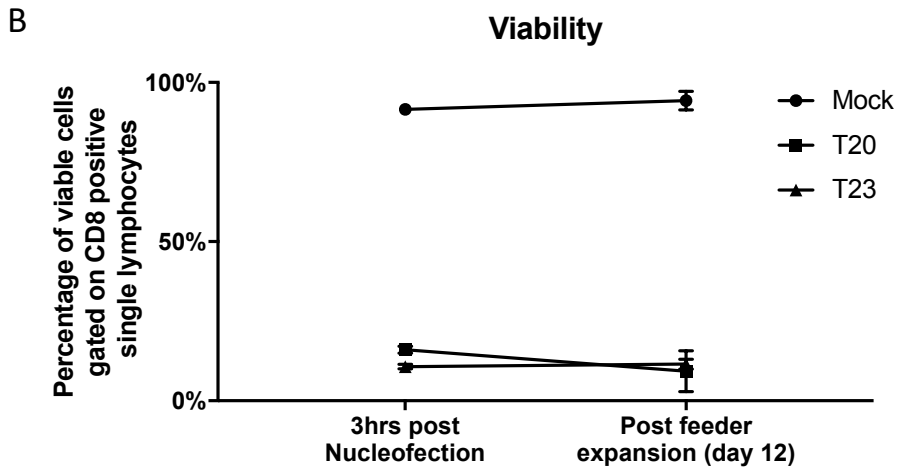

Figure 5-3 Electroporation based plasmid delivery results in poor cell viability also the evidence of knock down effect by CRISRP/Cas9 has been observed.

(A)(B) Percentage of live cells 3h after electroporation. The antigen specific T cell clone A3 cells were counted, washed, suspended in Nucleofector solution and transferred into a Nucleocuvette according to manufacturer's instructions, mock group did not receive pulse, T20 group received the pulse by T20 programme, T23 group received the pulse by T23 programme. Cells were them immediately transferred into pre-warmed culture medium, after a brief spin-down, cells were cultured in 96-well U-bottom plate and fed with feeder cells and PHA for expansion. An aliquot of the cells was stained with LIVE/DEAD Cell Viability Assays and acquired by a Cyan flow cytometer. The program for nucleofection was T20 and T23, which are two recommended nucleofection program for transfecting human primary T cells. 14 days after feeder expansion, the cells were stained again with LIVE/DEAD Cell Viability Assays and HLA-A*02 antibody (the target gene of the CRISPR/Cas9 plasmid), although there is a good knock out effect on the target genes, the electroporated cells could not be reinvigorated as indicated by the viability staining.

The viability issue encountered in both siRNAs and plasmid transfections raised the concerns that the Nucleofection is too harsh for *in vitro* cultured T cell clones, although it has been utilized broadly in human primary T cells for plasmid transfection. Since *in vitro* cultured T cell clones were forced to proliferate with high dose of T cell stimuli, cells may be in an apoptotic prone state. Electroporation damages the cell membrane and can disrupt cellular metabolism. However, further optimisations will be needed to draw a firm conclusion, such as by trying to use a different electroporator, different electric pulses, different voltages to apply the electroporation methods to the T cell clones.

5.2.3 CRISPR/Cas9 via Lentivirus for Antigen-Specific T Cell Clone.

Stepping backward, we switched to lentivirus-based CRISPR/Cas9 delivery. The packaging system that we currently used was the three plasmids based system with pMD.2G as the envelope plasmid and psPAX2 as the packaging plasmid. The TLA-HEK293T cells were used for optimal viral production. The envelope and packaging plasmids were verified by enzyme digestion followed by gel electrophoresis (Figure 5-4A). Co-transfections of the plasmids with an lenti-vector containing a GFP cassette into TLA cells can be monitored by fluorescent microscopy (Figure 5-4B). The titres of packaged lentivirus were quantified by infecting Jurkat T cell line (Figure 5-4C) in a serial dilution, and the infectious particle concentrating were calculated according to the formula described in the method chapter (Figure 5-4D). The pL-CRISRP.SFFV.GFP vector, which was most successfully packaged indicated by the highest viral titre among the three vectors, was picked for the following optimization experiment.

The lentiviral-based DNA delivery into primary human T cells is more broadly utilized than electroporation in both laboratory and clinical studies. To simulate the lentiviral transduction on human antigen specific T cells, primary T cells from three different donors were used to optimize the lentiviral transduction conditions. The binding of viral particles to target cell is mediated by several factors, such as pH, physical co-localization, affinity between receptors on the cell surface and viral envelope proteins. The efficiency of this initial binding and, consequently, lentiviral transduction also varied depending on the electrostatic repulsion between the negatively charged cell membrane and the virus.

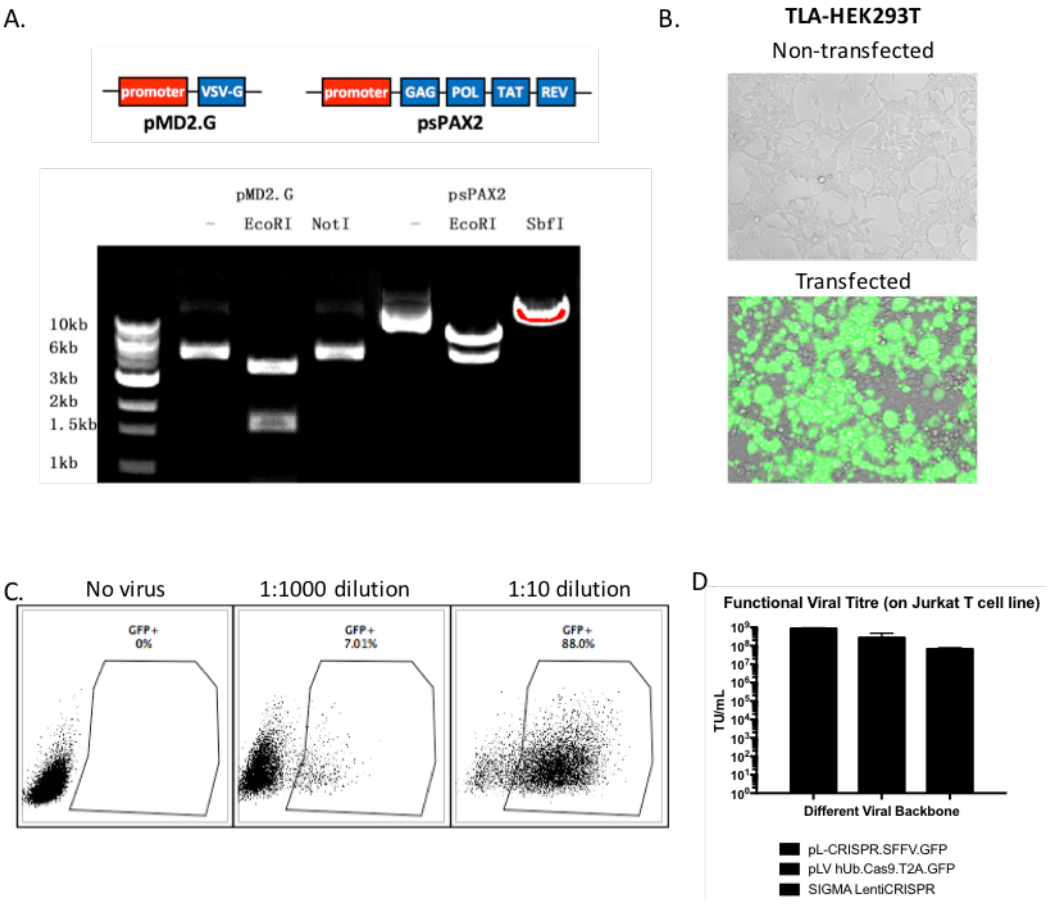

Figure 5-4 Validation of lentivirus packaging system and measurement of packaged lentivirus.

(A) Maxiprep purified plasmids of pMD2.G and psPAX2 vectors were digested by restriction enzymes and resolved on 1% TAE agarose gel. Expected band size are 1.7kb+4.1kb (pMD.2G EcoRI) and 4.4kb+6.3kb (psPAX2 EcoRI) (B) TLA-HEK293T cells were co-transfected with pMD2.G, psPAX2 and GFP expressing lenti-vector, 48 hours after transfection, GFP expression can be visualized under fluorescent microscope. (C) Exemplified GFP expression of Jurkat cells with serial diluted lentiviral transduction. Concentrated lentiviruses were diluted to transduce Jurkat cells, GFP expression were checked 72 hours post transduction. Suitable dilution (GFP expression with 5-20%) will be used to determined function viral titre. (D) Different titres were observed among different CRISPR/Cas9 expressing backbones. Packaged lentivirus were aliquoted and stored in -80 ℃ freezer prior to use.

Several methods have been developed to increase lentiviral transduction efficiency, including centrifugation of target cells with virus at low speed, co-localization of cells and virus on immobilized proteins such as fibronectin, performing multiple rounds of transductions and the addition of positively charged polycations. Polybrene, DEAE-dextran, protamine sulphate are commonly used polycations which can reduce the repulsion forces between cells and viruses, facilitate the binding of viruses and cell resulting in a more efficient lentiviral transduction. RetroNectin (recombinant human fibronectin fragments), which composes three functional domains, the fibronectin cell-binding domain, heparin-binding domain and CS-1 sequence, is a recombinant protein utilized to co-localize cells and viral particle. Specifically, the viral particles bind the reagent via interaction with the heparin-binding domain, and target cells bind through the interaction of cell surface integrin receptor VLA-5 and VLA-4 with the fibronectin C-domain and CS-1 site, respectively.

The optimisations here included the centrifugation to co-localise cells and viruses, testing different polycations and the use of RetroNectin. PBMCs were isolated from healthy donors and the T lymphocytes were activated by anti-CD3/CD28 magnetic beads in the presence of IL-2. The same number of cells were seeded into RetroNectin-coated Flat-bottom or uncoated U-bottom 96-well plates in the presence of polybrene, protamine sulphate or DEAE-dextran. One RetroNectin-coated plate and U-bottom plate was spun for 2 hours at low speed. In general, CD4 and CD8+ T cells showed similar transduction efficiencies in all twelve conditions. T cells transduced in the condition with DEAE-dextran, RetroNectin and centrifugation provided the highest transduction efficiency. However, DEAE-dextran, in contrast to the other two polycations, showed some

toxicity to cells, indicated by 7-AAD staining (Figure 5-5 A). The highest efficient lentiviral transduction was the combination of centrifugation, DEAE-dextran and RetroNectin Coating, where roughly 50% transduction efficiency was achieved on both CD4 cells and CD8 cells (Figure 5-5 B, C).

A.

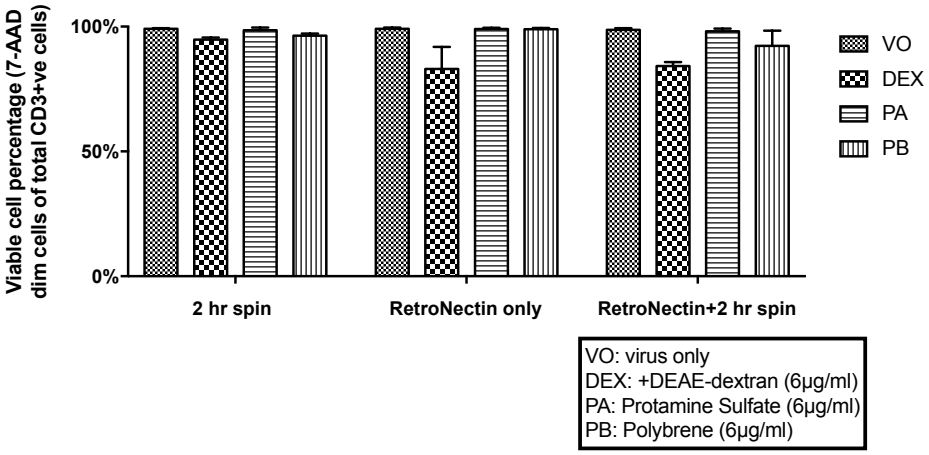

B.

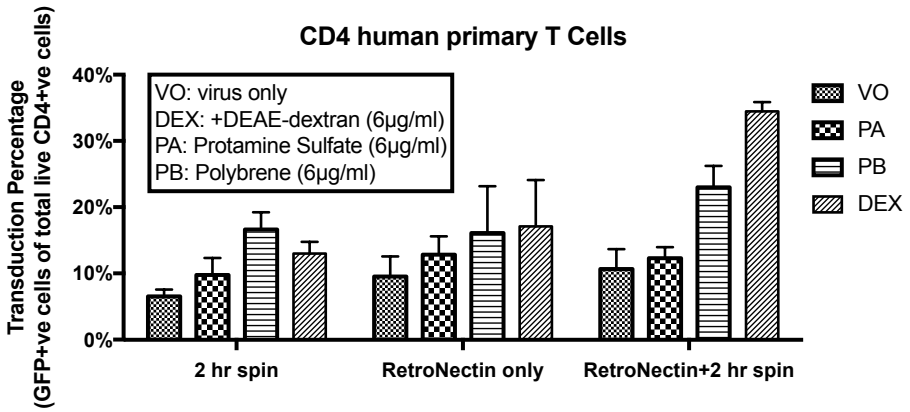

C.

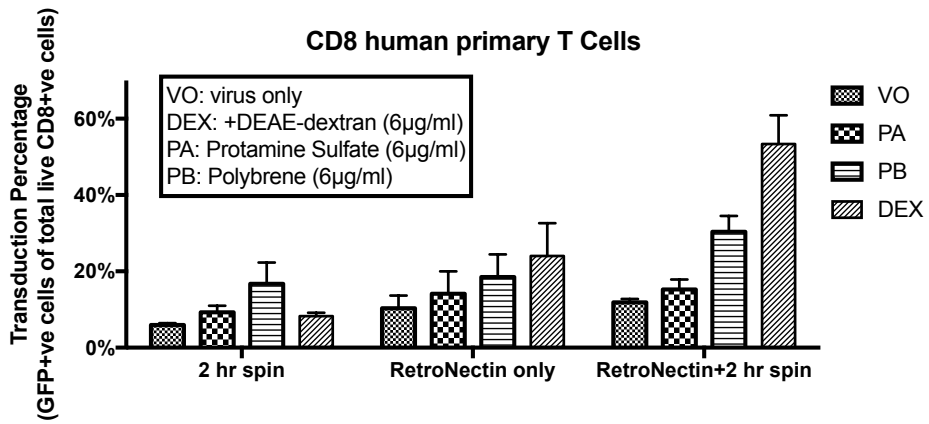

Figure 5-5 Optimization of lentiviral transduction efficiency of human primary T cells by comparing different polycations and transduction methods.

Different kinds of polycations combined with different transduction methods were compared in terms of the facilitating effect of lentiviral transduction on human primary T cells, both on CD4+ T cells and CD8+ T cells. The PBMCs from different donors were separated from the whole blood and activated by co-culturing with aCD3/CD28 Dynabeads (in beads to cells ration of 1:1) for 2 days prior to be lentiviral transduced. 3 days later, cells were then stained with proper surface marker and acquired on a Cyan flow cytometer. MOI=10. (A) Evaluation of cell viabilities after lentiviral transductions. (B)(C) Lentiviral transduction efficiency on CD4 or CD8 primary T cells in different conditions.

In the primary T cell lentiviral transduction optimization, resting primary T cells need to be stimulated with anti-CD3/CD28 magnetic beads to allow the cells entering mitosis from the resting G_0 phase, which is an essential step for successful lentiviral genome reverse transcriptions and following integration into host genome. The *in vitro* cultured T cell clones are proliferating cells for about 10days after stimulations with feeder cells, PHA and IL2. Thus theoretically, those cells are receptive to the lentiviral transductions. To test this hypothesis, we first lentiviral transduced two CD4+ T cell clones (UK001 C22, C28), two CD8+ T cell clones (LTNP005 A3, G3) and one CD8+ T cell line (UK001 GL9 bulk), utilizing spinoculation with DEAE-dextran (MOI=10) at two time points during the feeder expansion, specifically, day 7 and day11. According to our experience in culturing T cell clones, in the first 4-5 days' post feeder expansion, T cells are highly activated and then started to proliferate. This peaks at day 6-7 and lasts to day 10-12. In the following two days, the cells become stable in terms of T cell activation and gradually start apoptosis. Thus day 7 clones represent proliferating

cells and day 11 clones represent the resting cells. Interestingly, both *in vitro* cultured CD4 and CD8 antigen specific T cells showed low efficiency of transduction by lentivirus. (Figure 5-6)

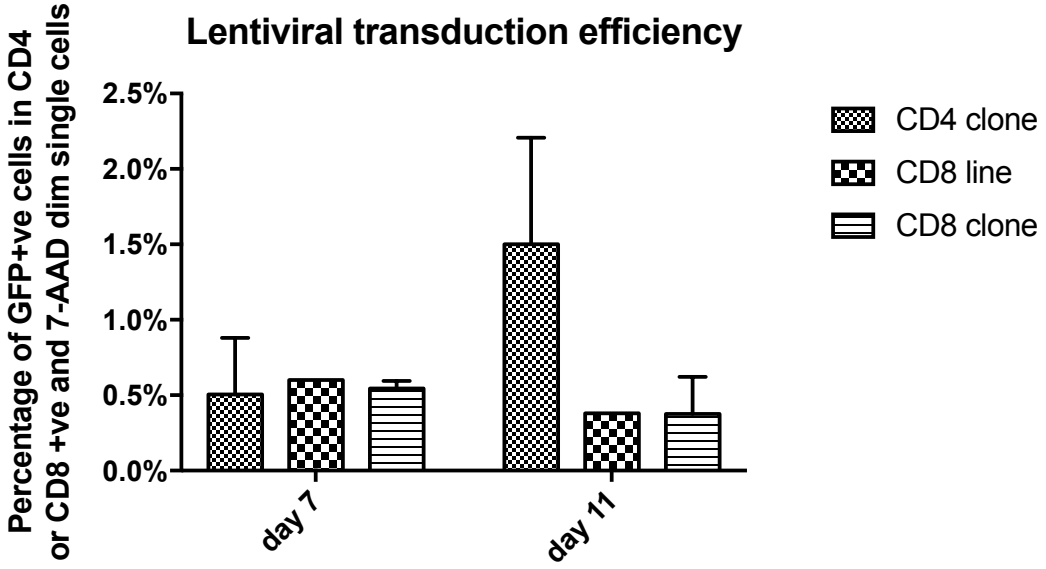

Figure 5-6 T cell clones were refractory to lentiviral transduction.

Two CD4+ T cell clones, UK001 HA-45 C22 and C28, two CD8+ T cell clones, LTNP005 A3 and G3, and one flu specific CD8 bulk T lines were feeder expanded for 7 days or 11 days prior to be lentiviral transduced with 6μg/ml polybrene and centrifugation at 600 g for 2hours at 32°C. MOI used here was 10. After 4 days, GFP and viability of the cells were checked by Cyan flow cytometer.

To test if the low efficiency came from the differences between feeder/PHA activation versus CD3/CD28 activation, a panel of d11 T cell clones were activated by anti-CD3/CD28 magnetic beads, similar to the previous co-cultural with primary T cells. From previous laboratory experience, feeder/PHA is a better way to grow T cell clones than CD3/CD28 stimulation. In addition, it is also well known that CD3/CD28 stimulation could induce activation-induced cell death. To address this problem, cell status was constantly monitored by 7-AAD/Annexin V. PBMCs were stimulated at same time as the positive control.

For the lentiviral transductions of the primary T cells, cells are usually stimulated with Dynabeads for 48h. The viability of CD4 and CD8 primary T cells at 48h (Figure 5-7A) were very good, although in the FACS plot, there was noticeable increased shift for the Annexin V staining, which might indicate the cells were undergoing active metabolism. Unlike primary CD4+ T cells, CD4+ T cell clones here shown different cell status changes in terms of viability and apoptosis - CD4 clones underwent a highly apoptotic stage and gradually recovered to a viable status after 96 hours. Under T cell stimulation, CD3-TCR complexes are down-regulated at cell surface, thus, the surface CD3 staining intensity correlates to the activation status of the T cells. 48h post CD3/CD28 stimulation, the CD3 expression on activated primary T cell down-regulated to about 60% (CD4) and 70% (CD8) of the expression on unstimulated control cells. For the CD4 clone C22, CD3 started to down-regulate after CD3/CD28 stimulation, then recovered to 50% after 96h and 100% after 120h (Figure 5-7 B). Thus, we hypothesized that four days post CD3/CD28 stimulation is the optimal time point for lentiviral transduction of CD4+ T cell clone. However, the CD8+ T cell clones became very apoptotic after the treatment with CD3/CD28

stimulations and did not show any sign of recovery post 6 days (Figure 5-7 C). For this reason, the lentiviral transduction efficiency cannot be increased by stimulating CD8 clones with CD3/CD28 Dynabeads. Perhaps the only way to overcome the low efficiency issue will be sorting the cells by flow cytometry and further culture and expansion.

The optimization of lentiviral transduction was continued on CD4+ T cell clone C22. To our surprise, activation via CD3/CD28 or transduction with RetroNectin coated plates did not facilitate lentiviral transduction on this CD4+ T cell clone. Additionally, although the three polycations tested provide marginal increase on lentiviral transduction efficiency, the overall efficiencies were very low. One approach to address this low efficiency issue is to further enrich the GFP positive population by FACS. Indeed, although we could not conduct high efficient lentiviral transductions on T cell clones, the T cell cloning technology enabled the re-cloning of lentiviral transduced T cells. Further information on sorting and expanding lentiviral transduced *in vitro* cultured antigen-specific T cells will be detailed in the next chapter.

Figure 5-7 Screening of apoptosis and viability between two CD4+ T cell clones and seven CD8+ T cell clones.

(A) Fresh PBMCs or T cell clones (d10 post feeder stimulations) were counted and mixed with aCD3/CD28 Dynabeads (bead:cell=1:1) in H10 medium supplemented with 100U/ml IL2. Cells were them aliquoted into 96-well flat-bottom plates for activation and expansion. On each given day, a well of cells were suspended and stained with proper surface marker, 7-AAD and Annexin V (AV). Cells status were determined by 7AAD/AV quadrants, $7AAD^-/AV^-$ are viable cells, $7AAD^-/AV^+$ are early apoptotic cells, $7AAD^+/AV^+$ are late apoptotic or dead cells. (B) The CD3 expression levels on primary T cells and CD4 clone C22 were quantified by MFI value from FACS staining. (C) Summary of two CD4+ T cell clones and seven CD8+ T cell clones, each dot represents the percentage of $7AAD^-/AV^-$ cells in the total population.

A.

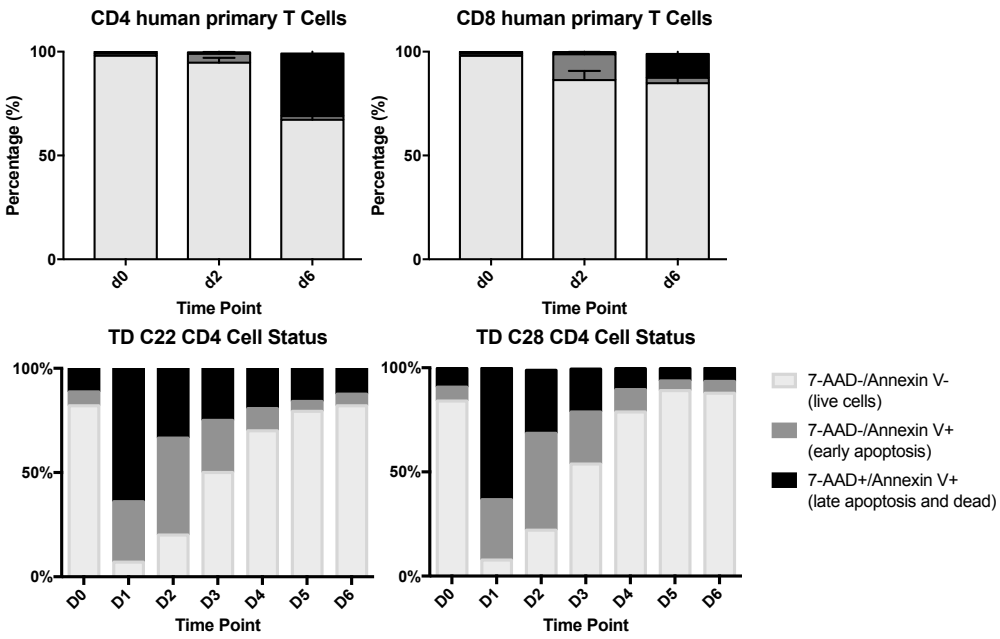
CD4 human primary T Cells
CD8 human primary T Cells
Percentage (%)
100
50
0
d0
d2
d6
Time Point
TD C22 CD4 Cell Status
TD C28 CD4 Cell Status
100%
50%
0%
D0
D1
D2
D3
D4
D5
D6
Time Point
7-AAD-/Annexin V- (live cells)
7-AAD-/Annexin V+ (early apoptosis)
7-AAD+/Annexin V+ (late apoptosis and dead)

B.

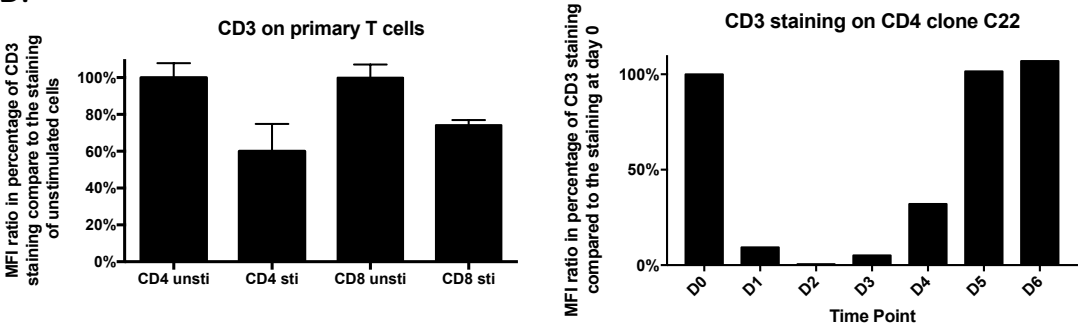
CD3 on primary T cells
MFI ratio in percentage of CD3 staining compare to the staining of unstimulated cells
100%
80%
60%
40%
20%
0%
CD4 unsti
CD4 sti
CD8 unsti
CD8 sti
CD3 staining on CD4 clone C22
MFI ratio in percentage of CD3 staining compared to the staining at day 0
100%
50%
0%
D0
D1
D2
D3
D4
D5
D6
Time Point

C.

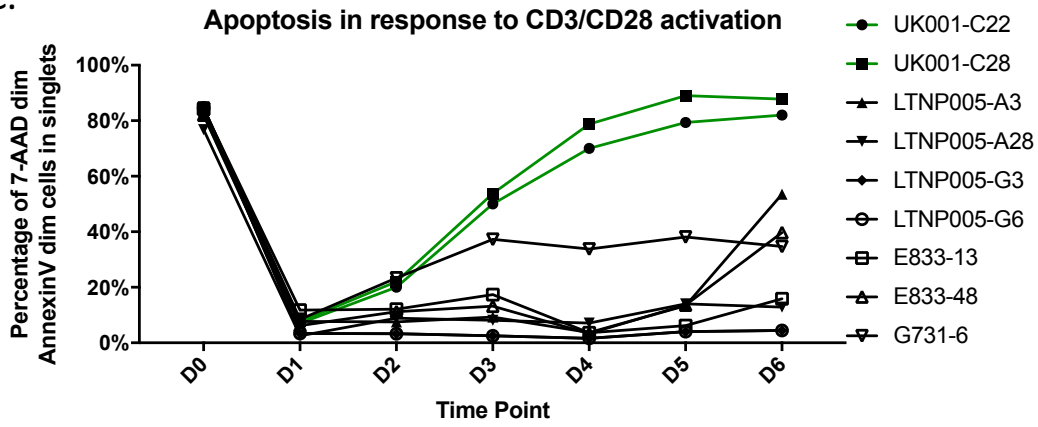
Apoptosis in response to CD3/CD28 activation
Percentage of 7-AAD dim AnnexinV dim cells in singlets
100%
80%
60%
40%
20%
0%
D0
D1
D2
D3
D4
D5
D6
Time Point
UK001-C22
UK001-C28
LTNP005-A3
LTNP005-A28
LTNP005-G3
LTNP005-G6
E833-13
E833-48
G731-6

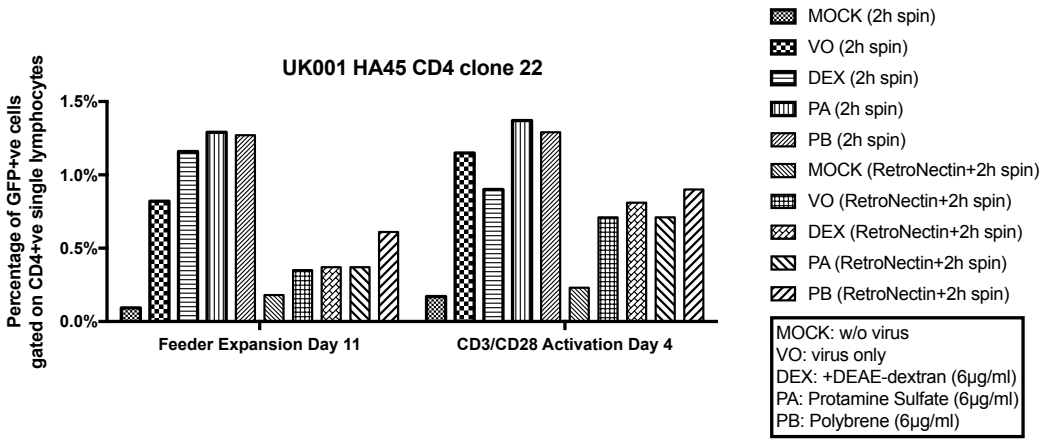

Figure 5-8 Optimization of lentiviral transduction efficiency on a CD4+ T cell clone.

Clone 22 were either pre-stimulated with Dynabeads (bead:cell=1:1) at day 11 post feeder expansion for 4 days or re-stimulated with feeder cells for 11 days prior to be lentiviral transduced or mock transduced with different combinations of polycations and transduction methods. MOI used here was 10. After 4 days, GFP expression was checked by Cyan flow cytometer.

5.3 Discussion.

With the development of cancer immunotherapy, human immune system has been shown to be highly important for the cancer development and disease control. Cytotoxic T lymphocytes, which kill their targets specifically by TCR-p-MHC I recognition, are becoming the best candidate for cell-based anti-tumour 'drug'. So far, the attempts to arm CTLs with higher functionalities, such as antigen specificity like CARs or TCRs, have achieved several breakthroughs in patients with different cancers. Efforts are being made to continuously improve the biosafety and effectiveness of such cell therapy.

The T cell clone technique enables us to study certain T cell clonotype in detail and gives out clear-cut results that may be diluted in total T cells or even a T cell subtype. However, in-depth studies on certain candidate genes, such as surface proteins with differential expressions among different T cell clones, have been restricted due to the limited tools to modulate the expression levels of one specific candidate gene on T cell clones. The attempts to knock down and knock out gene expressions on T cell clones have lasted for several years in our group, and even so it has remained challenging to up-regulate or down-regulate gene expression in T cell clones. In this chapter, we have test several common gene engineering techniques in T cell clone system, including temporary knock down siRNAs and everlasting CRISRP/Cas9.

5.3.1 The Application of siRNAs Method on T Cell Clone System.

siRNAs have been utilized for gene modulation for over a decade now and were shown to be functional in different cell types across species. Upon entry into the cytoplasm, the siRNAs bind to their target mRNAs and induce mRNA degradation and thus downregulate certain gene expression. For its applications on T cell clones, the first barrier is the delivery. siRNAs are commonly delivered into cells by the Lipofectamine reagent, which is made up of cationic lipid subunits that can form liposomes in an aqueous environment to entrap the transfection payload, negatively charged nucleic acid molecules, to overcome the negative electrostatic repulsion of the cell membrane. Although this deliver method works well in many adherent cells, only low efficiency can be achieved on suspension cells. The most widely used siRNA deliver method into non-adherent T cells is electroporation-based methods. In the first part of the result section, we have tested a reported optimized electroporation method to transfect siRNAs into a HIV-specific CD8+ T cell clone A3. Although we observed a good knock down effect for the positive control gene GAPDH, poor viability and noticeable morphological changes of the cells indicated that this method was not an ideal way to modulate T cell functions. We then tested another chemical engineered siRNAs technique, the Accell siRNA system from GE Dharmacon. In contrast to the previous attempt, this method provided a very marginal knock down efficiency although it preserved the cell viability. Other concerns for siRNA are the off-target effects and the short period of knock down effect which can last. Therefore, all things considered, the siRNA gene knock down method was not proven to be a good way for manipulation gene expression on T cell clone system.

5.3.2 What is the best way to deliver CRISPR/Cas9 to a T cell clone?

The CRISPR/Cas9 gene editing system, firstly reported in 2013, is replacing other gene silencing systems, such as siRNA, shRNA, Zinc fingers and TALENs. This system was adapted from the bacteria immune system and utilized to work on editing genomes via the Watson-Crick base pairing rule. It has been proved to be the most effective and efficient gene editing tool currently. Similar to siRNAs, the CRISPR/Cas9 can be delivered into cell via electroporation in a plasmid form. The pX330 (pX330-U6-Chimeric_BB-CBh-hSpCas9), an early version of the CRISPR/Cas9 all-in-one plasmid from Feng Zhang's lab, was tested on the T cell clone system shortly after its release in 2014. sgRNAs targeting PD-1 and HLA-A*02 were designed and cloned into the pX330 vector, and were electroporated into A3 clones. As the size of the plasmids are much larger than the siRNAs, the electroporation programs used for delivering plasmids caused even bigger impact on viability of the T cell clone. In contrast to the siRNAs, the CRISPR/Cas9 directly mutate genomic DNA sequences which be passed from the mother cells to the daughter cells, conferring a permanent gene-editing effect. Thus, the viability issue can be potentially overcome if the electroporated cells could be further cultured and expanded. Nevertheless, T cell clones are more difficult to culture than many other primary cells and damage caused by Nucleofection cannot be reversed by the feeder/PHA with H10 medium culture. Consequently, a better method suitable for electroporating hard-to-transfect T cell clones is needed. It is worth mentioning the Nucleofector that we used was an old machine (Nucleofector I) which has been recently replaced by new versions. In the newer Nucleofector version, the Nucleofection program for primary T cell has been optimised for a better delivery, causes less damage and higher efficiency, which

may also work for T cell clone system. Therefore, further experiments will be needed before ruling out the possible application of Nucleofection on T cell clones. Apart from Nucleofection, Schumann and colleagues conducted electroporation of ribonucleoprotein format of CRISPR/Cas9 to primary CD4+ T cells via a Neon device, and showed effective gene editing on CXCR4 and PD-1 (Schumann et al., 2015). Therefore, electroporation via Neon device may also be an option to deliver CRISPR/Cas9 T cell clones.

The major effort we made in this chapter was optimising the lentiviral transduction method for *in vitro* cultured antigen specific T cells. As a viral-based gene delivery, it has served as the major tool in T cell engineering and has been applied in clinical usage for decades. Particularly, lentiviral vectors have shown promise in the transduction of several resting cell types such as retinal cells, pancreatic islets, cells of the central nervous system, or progenitor and differentiated hematopoietic cells (Vigna and Naldini, 2000). It is still not fully understood why resting T cells are refractory to lentiviral vectors, this may be attributed to defects in initiation and completion of the reverse-transcription process (Korin and Zack, 1998; Stevenson et al., 1990; Zack et al., 1992), lack of ATP-dependent nuclear import (Bukrinsky et al., 1993a), and lack of integration of the pro-viral genome.

However, by activating human primary T cells via the CD3/CD28 pathway, high efficiency of lentiviral transduction can be achieved. To our surprise, although the T cell clones were activated (in the first 10 days, cells were rapidly proliferating), those cells were refractory to transduction by lentivirus via published methods, which is unlike activated primary T cells. The mechanisms

behind the different responsiveness between primary T cells and *in vitro* cultured T cell clones remain elusive. One possible reason is that T cell clones were cultured in high dose of PHA, which is a lectin that binds to sugars on glycosylated surface proteins, including T cell receptor (TCR), and triggers calcium-dependent signalling pathways leading to T cell activation, instead of being activated by TCR-pMHC ligation. Such PHA cultural may result in different surface protein expressions on T cell clones compared to CD3/CD28 activated primary T cells. Other evidence that PHA cultural could change T cell functions comes from that the *in vitro* cultured T cell clones were unable to secrete IFNγ after PHA stimulation indicated by Elispot (data not shown). Moreover, in the result chapter, the activation of CD4 or CD8+ T cell clones via anti-CD3/CD28 magnetic beads resulted an apoptotic status as T cell clones may already lose the CD28 expression (at least for the case on clone A3). In contrast, primary T cells could rapidly turnover this status and start to proliferate in contrast to CD4 or CD8+ T cell clones. This may come from a weaker survival signalling or an enhanced apoptotic signalling within T cell clones, either of which could make impact on the cell response to lentiviral transduction. One the other hand, the primary T cells were a mixture of cells with different functions and differentiation stages, while T cell clones are mainly memory T cells that have undergone multiple mitoses. The difference may also come from the differences of the responsiveness of lentiviral transduction between different T cell types and numbers of cell division.

The lentiviral system that we have utilized was VSV-G pseudotyped, which infects most cell types. Different to this most widely used envelope, Agosto and colleagues introduced an CXCR4-tropic HIV envelope that can promote more

efficient gene delivery to resting CD4+ T cells than VSV-G envelope. (Agosto et al., 2009) This amendment may be also helpful for transducing CD4+ T cell clones and the concept can be potentially utilized to develop a different envelope to target CD8+ T cells. Polycations are commonly used to improve lentiviral transduction, which are capable if neutralizing the negative changes on the target cell membrane and viral particles. Indeed, the presence of polycations was observed to increase lentiviral transduction on Jurkat and human primary T cells. However, owing to the low efficiency of lentiviral transductions on T cell clones, the benefit of polycations was very marginal and could be even toxic to T cell clones. Coating the surface with RetroNectin in T cell culture is another way to increase T cell transduction, as the protein can bind to both viral particle and target cells to facilitate the viral entry. Nevertheless, similar to polycations, this benefit was not significant enough on T cell clone systems. The imperfect strategy adopted currently was to make a compromise to the low transduction efficiency by the enrichment of the transduced cell, for example, FACS sorting GFP positive cells. This requires the lentiviral vector include CRISPR/Cas9 components and the EGFP gene, which are quite big cargos for a virus to take. A drug resistance gene could also be considered; nonetheless, the T cell clones are very fastidious in their culture requirements, optimisation should be conducted beforehand. What is more, due to the nature of *in vitro* culture of antigen specific T cells, the number of cell divisions available is limited. Therefore, transducing early passages of the antigen specific T cells would be desirable for generating enough number of cells for experiment or therapy.

Taken together, in this chapter, we have explored different methods and optimisations for modulating the levels of gene expressions on T cell clones and

positive control cells (primary T cells). None of the methods provide a one-step high efficiency way to introduce foreign nucleotides into *in vitro* cultured T cell clones. For all that, we have concluded that a feasible way to achieve the aim is to transduce T cell clones in early passages, followed by GFP sorting and further expansion. We have applied this strategy to different T cell clones and lines to knock out the PD1 gene via CRISPR/Cas9, which will be described in detail in the next chapter.

6 Chapter 6: Boosting Human Antigen-Specific Cytotoxic T Cell Responses by CRISPR/Cas9-Mediated PD1 Disruption.

6.1 Introduction.

In response to the constant antigenic stimulation caused by tumours or chronic viral infections, T cells usually suffer from over stimulation and induced cell death (Wherry, 2011). Tumour cells hijack certain immune checkpoint pathways as a way to induce immune resistance, particularly with respect to T cell interactions that are specific for tumour (Baitsch et al., 2011; Fourcade et al., 2010). The ability to restore these interactions in a disease may be vital for treatment, making the modulation of T cell immunity one of the most exciting areas of cancer research in recent years. Since 2011, a series of antibody therapies that act on immune checkpoint receptors (*i.e.* cytotoxic T-lymphocyte-associated protein 4 (CTLA-4), and the programmed cell death protein 1 (PD-1) and their ligands (*i.e.* PD-L1) have been approved by the FDA and have achieved substantial success in treating various malignancies (Brahmer et al., 2012; Hodi et al., 2010; Topalian et al., 2012a). Simultaneously, engineering patient autologous T cells to express chimeric antigen receptors (CARs) using replication-deficient viruses has been reported to cure some lymphoma patients (Grupp et al., 2013; Porter et al., 2011). In light of these developments, immunotherapy is playing an ever-greater role in the cancer treatment, alongside traditional treatment, such as surgery, radiotherapy and chemotherapy (Ascierto and Marincola, 2015).

Cytotoxic T cells are distinguished from other blood cells by their capacity to directly kill target cells, using cytolytic molecules (Andersen et al., 2006). The

latter specificity is granted by the somatic gene rearrangement of T cell receptors (TCRs) during T cell maturation in thymus, which is potentially able to produce an array of different TCRs that can recognise an almost infinite variety of non-host targets (Davis and Bjorkman, 1988). TCRs recognize and bind to specific major histocompatibility complex (MHC) peptide complexes that are expressed on host cells, resulting in the destruction of the target cell. In a disease setting, such as infection or cancer, only a small proportion of total peripheral T cells recognize the viral or cancer antigens, while the majority of T cells act as 'bystanders'. The systemic administration of antibodies that interfere with immune checkpoint pathways may lead to a breakdown in the discrimination of self and non-self by T cells, resulting in the onset of autoimmune disorders (Michot et al., 2016). Immune-related adverse events (iRAEs) are frequently observed in patients who receive antibodies that act on immune checkpoints, occurring in up to 90% and 70% of patients that are treated with anti-CTLA4 (Hodi et al., 2010) or anti-PD-1/PD-L1 antibodies (Topalian et al., 2012b; Weber et al., 2015), respectively. Steroids can be used to relieve iRAEs, but the anti-tumour responses induced by antibody therapies can in turn be compromised by the generalized immune-suppression that is associated with steroid use (Michot et al., 2016). Thus, the specific and intrinsic disruption of immune checkpoints in T cells through genetic targeting is likely to result in a better safety profile than current systemic administration of antibody-based immune checkpoints blockade (Su et al., 2016).

Replication-deficient pseudotyped lentiviral vectors are widely used as basic tools in basic research (Young et al., 2006), as well as for treatment of some human diseases such as inherited genetic disorders (Brenner and Malech, 2003;

Charrier et al., 2007), and more recently, cancers (Liechtenstein et al., 2013; Oldham et al., 2015). CRISPR associated protein 9 (Cas9) is an RNA-guided endonuclease, which is widely used as a simple and affordable way to edit mammalian cell genome (Gaj et al., 2013; Kim and Kim, 2014; Sander and Joung, 2014).

6.1.1 The Aim of This Chapter.

Given the fact that systemic administrations of PD-1 blocking antibodies carries the risk of breaking peripheral tolerance, here we incorporate CRISPR/Cas9 genome editing and lentiviral delivery to disrupt PD-1 gene expression only on selected human antigen-specific CTLs, which should confer a better safety profile than current immunotherapy. Herein, we conducted a proof-of-concept study to ascertain the feasibility of knocking-out the PD-1 gene using lentivirus in antigen-specific CTLs for potential alternative adoptive therapy. Functional improvements in the methodology and evaluation of the knock-outs were monitored by cytokine production and degranulation. Our results underscore the potential application of isolating antigen-specific CTLs from patients, their *in vitro* gene editing/expansion, and transfusion back into patients for treatments of cancers and/or chronic infections.

Schematic representation of generating human antigen-specific T cells and CRISPR/Cas9 gene modification delivered by lentivirus, followed by genetic and functional evaluation.

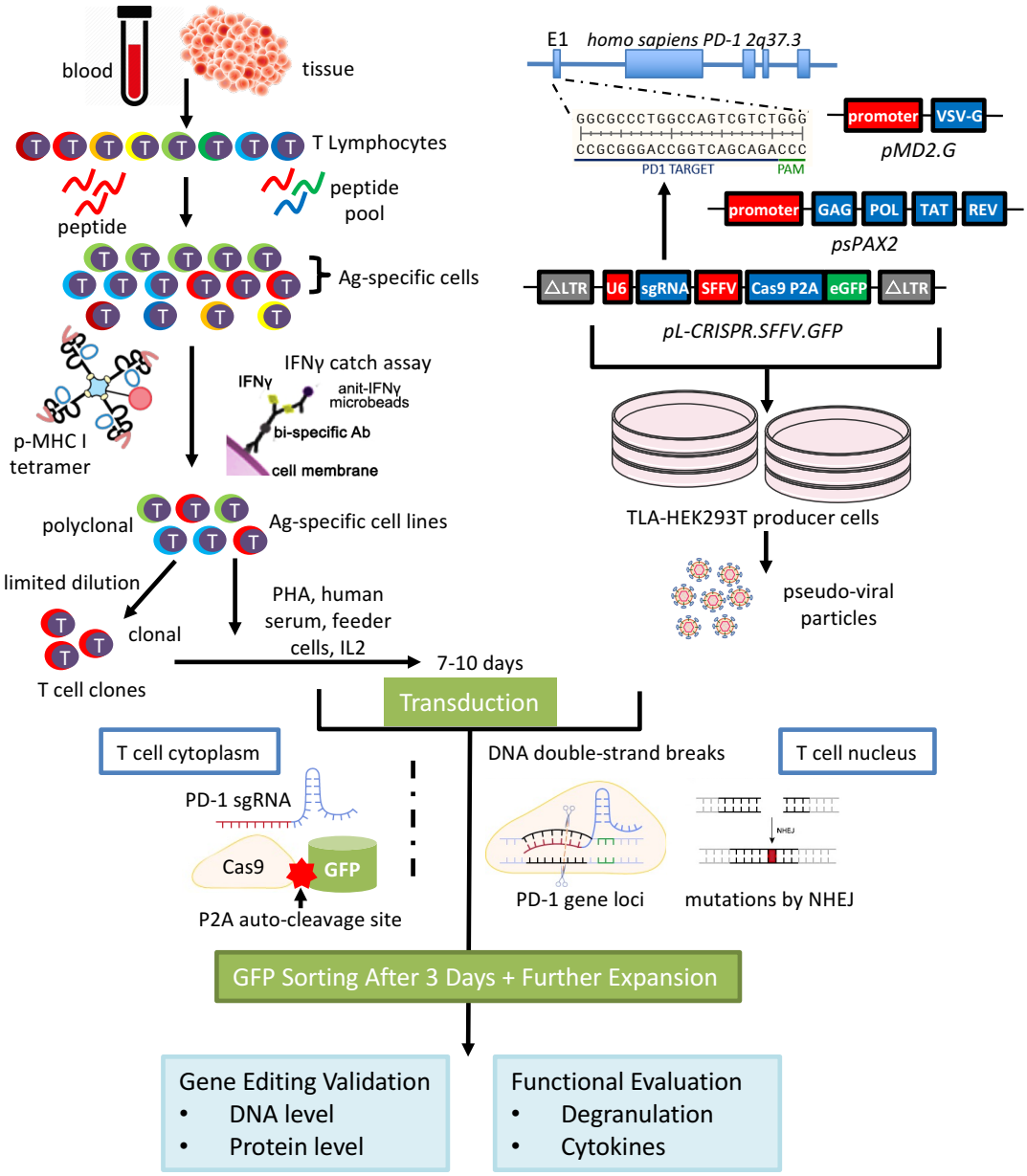

6.2 Results.

6.2.1 Validation of PD-1 sgRNA and Lentiviral Gene Transfer.

Human PD-1 gene locates at Chr2q37.3 (Shinohara et al., 1994) and contains 6 exons. Previous work by other groups has shown that CRISPR/Cas9 targets DNA with specificity (Ran et al., 2013) and could be utilized for PD-1 disruption on human T cells (Gwiazda et al., 2016; Schumann et al., 2015; Su et al., 2016). Three PD-1 targeting sgRNAs were designed and cloned into pL-CRISPR.SFFV.GFP vector, which delivers Cas9, GFP and PD-1 targeting sgRNA (Cas9:GFP:PD1sgRNA) simultaneously (Heckl et al., 2014). (Figure 6-1A) To validate the sgRNA effect on loss-of-function of PD-1 gene, we first lentiviral transduced Jurkat E6 T cells. The PD-1 expressions are inducible upon T cell activation. Thus, we first optimized the condition to stimulate Jurkat cells for higher PD-1 upregulation by testing different combinations of T cell activators. Jurkat PD-1 expressions were then checked by flow cytometry. PMA and ionomycin has been shown to most effectively up-regulate PD-1 expressions on Jurkat cells. (Figure 6-2 A) The pL-CRISPR.SFFV.GFP vector used here contains *Streptococcus pyogenes* cas9 gene co-expresses eGFP via P2A cleavage site from SFFV promoter and a chimeric sgRNA from U6 promoter, thus enabling the Cas9 and sgRNA delivery in only one step (Heckl et al., 2014). Jurkat T cells were transduced with the lentiviruses that contain all the PD-1 targeting CRISPR/Cas9 components (MOI=10) with low speed centrifugation at 32 °C and then transferred to complete growth medium for further cultural. PMA and ionomycin were supplemented after 48 hours and the GFP and PD-1 expression was checked by FACS 24 hours after the stimulation. Cells with lentiviral transduction

expressed high amount of GFP and lower PD-1 compared to the control cells (mock transduced cells). The sgRNA#1 targeting PD-1 exon1 was picked in the following experiment as it mediated strongest PD-1 down-regulation among the three. (Figure 6-1B) Genomic DNA harvested from these Jurkat T cells was checked for the presence of site-specific gene disruptions by Sanger sequencing of the PCR amplicon surrounding the target site. Indel mutations were detected within the sgRNA targeting site, indicated successful CRISPR/Cas9-mediated DNA double-strand break formation. (Figure 6-2B) To further validate the lentiviral delivery method, pre-stimulated human primary T cells (with anti-CD3/CD28 magnetic beads) were transduced with Cas9:GFP:PD1sgRNA virus at different MOIs, cells were cultured for three days, and the GFP expression monitored by flow cytometry. Both CD4 and CD8+ T cells were efficiently transduced, as indicated by GFP expression. T7E1 cleavage assays revealed mismatches within the PCR amplicon. (Figure 6-2C) These data demonstrate that the selected sgRNA worked effectively with Cas9 to disrupt the PD-1 gene, and the lentiviral transduction method delivered Cas9:GFP:PD1sgRNA into human T cells.

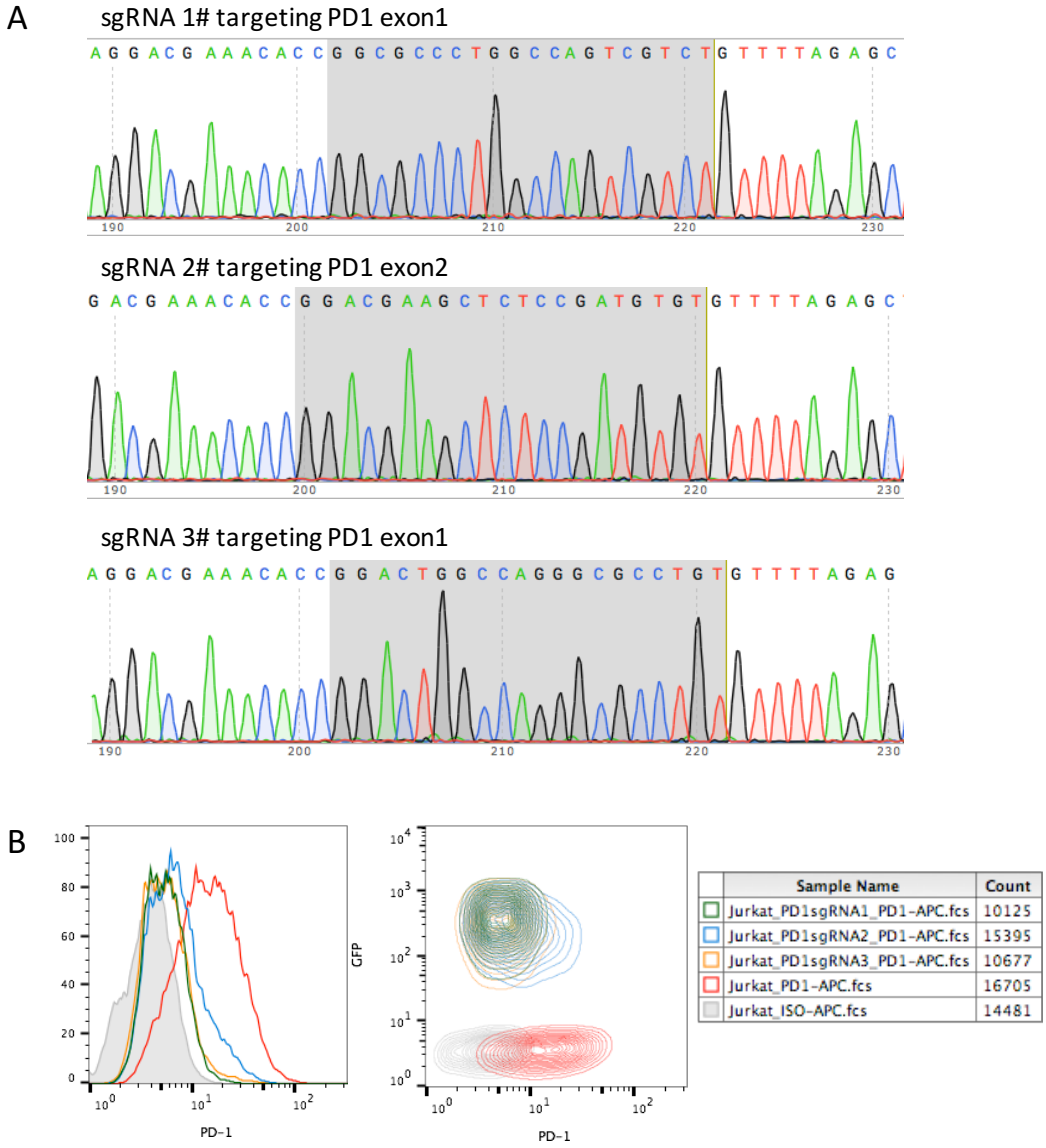

Figure 6-1 Design of sgRNAs to target PD-1.

(A) Sequencing results indicate successful insertions of the sgRNAs into pL-CRISPR.SFFV.GFP lentiviral backbone. (B) sgRNA mediated PD-1 disruptions were evaluated by transducing Jurkat T cells (MOI=10) with the three lentiviruses at same condition. The GFP and PD-1 expressions were checked after three days. sgRNA 1# and 3# (targeting exon1) mediated more efficient PD-1 down-regulations than 2# (targeting exon2). sgRNA 1# was picked to continue in the following experiments.

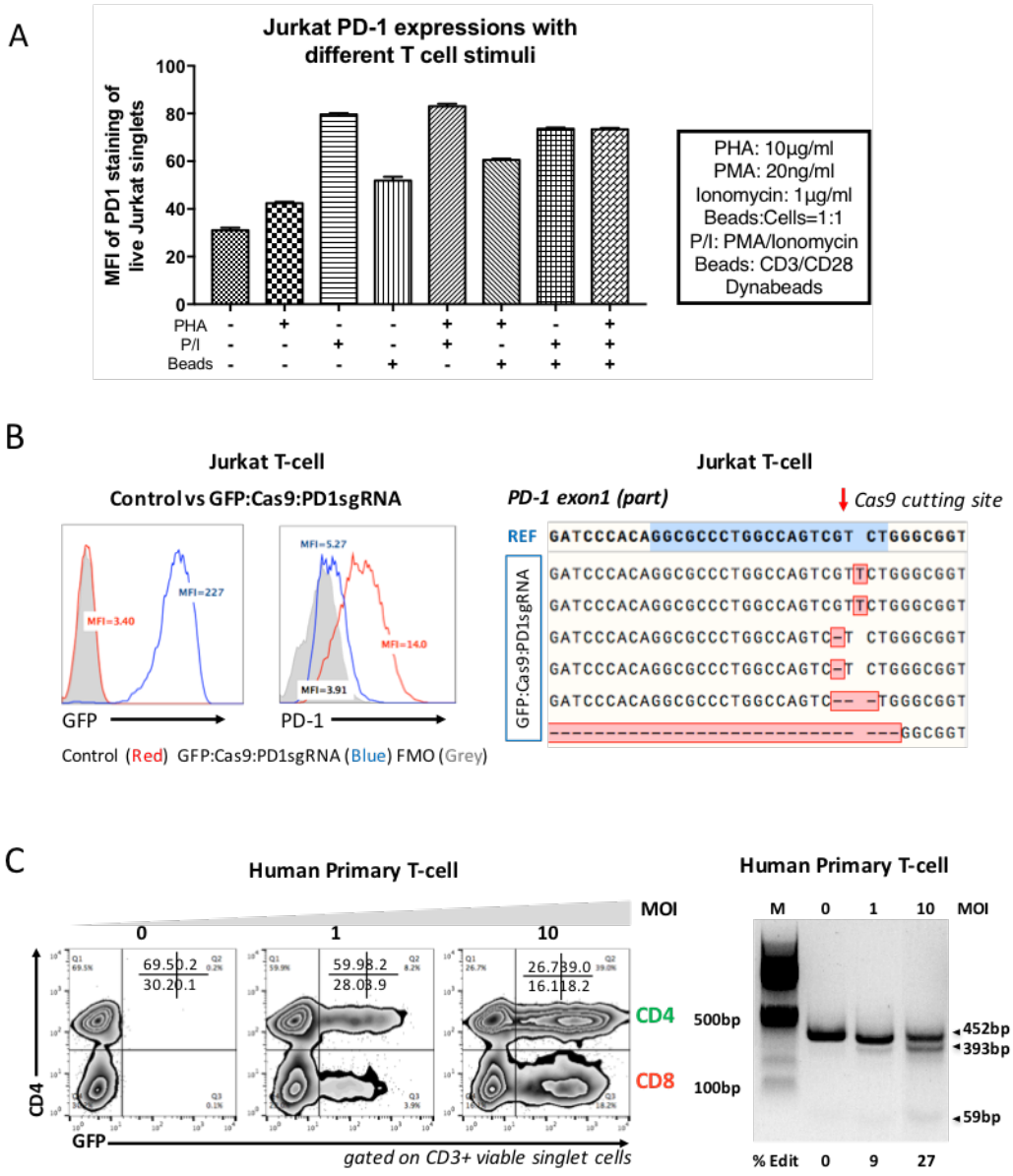

Figure 6-2 The validation of PD-1 sgRNA/Cas9-mediated PD-1 knock-out via lentivirus on Jurkat T cells and human primary T cells.

(A) Jurkat cells were counted and seeded in to 96-well U-bottom plates in a concentration of 1,000,000 cells/mL. Cells were co-cultured with the presence of different T cell stimulatory reagents in triplicate. PD-1 expressions of the cells were checked after 24 hours by flow cytometer. (B) Examples of GFP and PD1 expressions on non-transduced (control) and GFP:Cas9:PD1sgRNA transduced Jurkat T cells. (MOI=10) Jurkat with lentiviral transduction has a significant lower expression of PD1 compared to non-transduced cells. FMO control was shown in grey tinted area. Sanger sequencing confirmed the PD-1 down-regulation was due to site-specific mutations caused by sgRNA/Cas9. (C) The transduction method was further validated on pre-stimulated human primary T cells. Viruses with MOI of 0, 1 and 10 were used to transduce cells, the PCR amplicon were tested for T7E1 cleavage assay. The above experiments have been repeated 3 times with similar results.

6.2.2 Generation of PD-1 KO Human Antigen-Specific CTL Clones/Lines.

Each T cell clone has a specific rearrangement of its TCR genes and each clone recognizes a different epitope or antigen. Thus, in many experimental settings, it may be difficult to attribute a certain function to a defined T cell population by studying the overall population of T cells (Mariotti and Nisini, 2009). Using MHC-peptide tetramers, T cells with TCRs that recognize a certain epitope can be isolated from the peripheral blood T cell pool and further expanded by feeder cells for detailed study (Dong et al., 2004). Previously, we have accumulated a bank of both CD4 and CD8 antigen-specific polyclonal CTL lines and CTL clones (further cloned from lines), the antigen specificities range from acute infections (such as influenza), chronic infections (such as hepatitis C, and AIDS), and cancers (such as tumour-associated antigen (TAA) specific cells). Lentiviral transductions were performed unitizing those pre-established antigen-specific cells (Table 6-1). After initial viral transduction, the frequency of GFP-positive (and also Cas9-positive, due to co-transcription of the Cas9 and GFP cassettes, which separate via an auto-cleavage site) T cells in the population was less than 5%, although those cells were also PD-1 negative, which may indicate successful PD-1 gene disruptions (Figure 6-3A). In contrast to the stimulated human primary T cells (Figure 6-2C), *in vitro* cultured antigen specific T cell clones were quite refractory to lentiviral transductions. The low efficiency could not be overcome by using polycations, or further CD3/CD28 stimulation (Figure 5-7). Thus, another round of fluorescence-activated cell sorting was applied to enrich the GFP-positive cells. After GFP enrichment and further expansion, the frequency of GFP-positive cells within the total population was as high as 80%. (Figure 6-3B)

Table 6-1 Information of lentiviral transduced antigen-specific CTL cells.			
CTL ID	**Nature**	**Pathogen**	**HLA Restriction**
UK001 C22	CD4 clone	H3 HA	DRB1*0901
UK001 C28	CD4 clone	H3 HA	DRB1*0901
LTNP005 A28	CD8 clone	HIV FL8	B*0801
UK001 influenza bulk	CD8 line	M1 GL9	A*0201
SM021 HIV bulk	CD8 line	HIV Nef Pool	Multiple
SM021 HCV bulk	CD8 line	HCV NS3 pool	Multiple
GC001 SSX-2 TAA bulk	CD8 line	SSX-2 KV9	A*0201

Figure 6-3 Lentiviral transductions on *in vitro* cultured antigen-specific CTL lines.

(A) Representative PD1-GFP plots of one CD4 (left) and one CD8 (right) antigen-specific T cell clone. For each group, the control cells (mock lentiviral transduction) are on the left and the GFP:Cas9:PD1sgRNA transduced cells are on the right. In general, three days after transduction, only a small proportion of virally transduced cells became GFP positive. (B) CD4-GFP plot of one CD4 antigen-specific T cell clone and CD8-GFP plot of five antigen-specific CD8 CTL lines. Lentiviral transduced cells (GFP positive cells, left) could be enriched by GFP sorting and further expanded by feeder cells plus PHA (right). GFP positive cells comprised up to 80% of the cells after one round of sorting plus the expansion procedure. Summaries of GFP expression sorting patterns are plotted at the bottom.

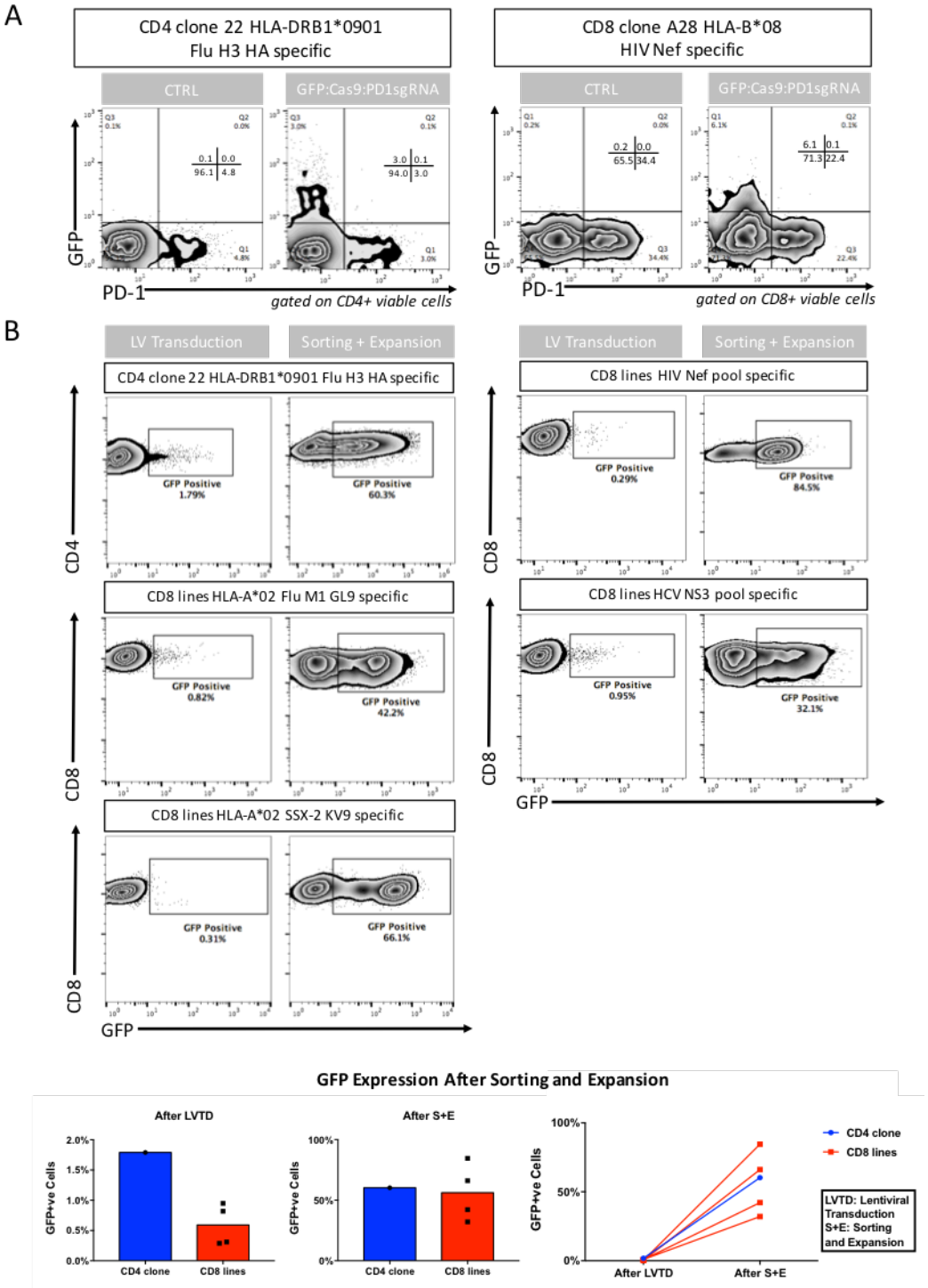
A
CD4 clone 22 HLA-DRB1*0901
Flu H3 HA specific
CD8 clone A28 HLA-B*08
HIV Nef specific
CTRL
GFP:Cas9:PD1sgRNA
GFP
PD-1
gated on CD4+ viable cells
gated on CD8+ viable cells
B
LV Transduction
Sorting + Expansion
CD4 clone 22 HLA-DRB1*0901 Flu H3 HA specific
CD8 lines HIV Nef pool specific
CD8 lines HLA-A*02 Flu M1 GL9 specific
CD8 lines HCV NS3 pool specific
CD8 lines HLA-A*02 SSX-2 KV9 specific
GFP Positive
CD4
CD8
GFP
GFP Expression After Sorting and Expansion
After LVTD
After S+E
GFP+ve Cells
CD4 clone
CD8 lines
LVTD: Lentiviral Transduction
S+E: Sorting and Expansion

6.2.3 Efficient Cas9-mediated PD-1 Disruption in Selected Antigen-Specific T Cells of Patients.

PD-1 expression on T cells is tightly and dynamically regulated. PD-1 is up-regulated in response to immune challenges and is rapidly down-regulated in acute settings to allow normal immune responses. Its expression remains high in chronic settings leading to an impaired immune response to stimuli (Bally et al., 2016). The expression of PD-1 in *in vitro* cultured antigen-specific CTL cells is low unless they are stimulated by co-culturing with anti-CD3/CD28 magnetic beads. To further characterize the GFP-sorted and expanded cells, and validate that GFP selection could distinguish PD-1 knock-out cells from the population, four pairs of lentiviral-transduced and GFP-sorted antigen-specific CTL cells were stimulated and their PD-1 expression was determined after 24 hours (Figure 6-4A). In general, cells transduced with PD-1-targeting lentivirus that were GFP positive expressed much lower levels of PD-1 on their cell surface compared to their control pairs. To validate that PD-1 down-regulation on these antigen-specific T cells was caused by site-specific mutations, genomic DNA was extracted from the three CD8 antigen-specific CTL cell-line pairs, and PCR amplicons of the surrounding region were cloned for sequencing. T7E1 assays and sanger sequencing of the three control pairs detected no mutations in the region around sgRNA target site. However, a heterogeneous collection of mutations was identified in all three GFP:Cas9:PD1sgRNA transduced pairs (Figure 6-4 B, C). The detailed PD-1 MFI value and mutation rate for each group were summarized in Table 6-2. Taken together, these results demonstrate the efficient disruption of the PD-1 gene at both DNA and protein level.

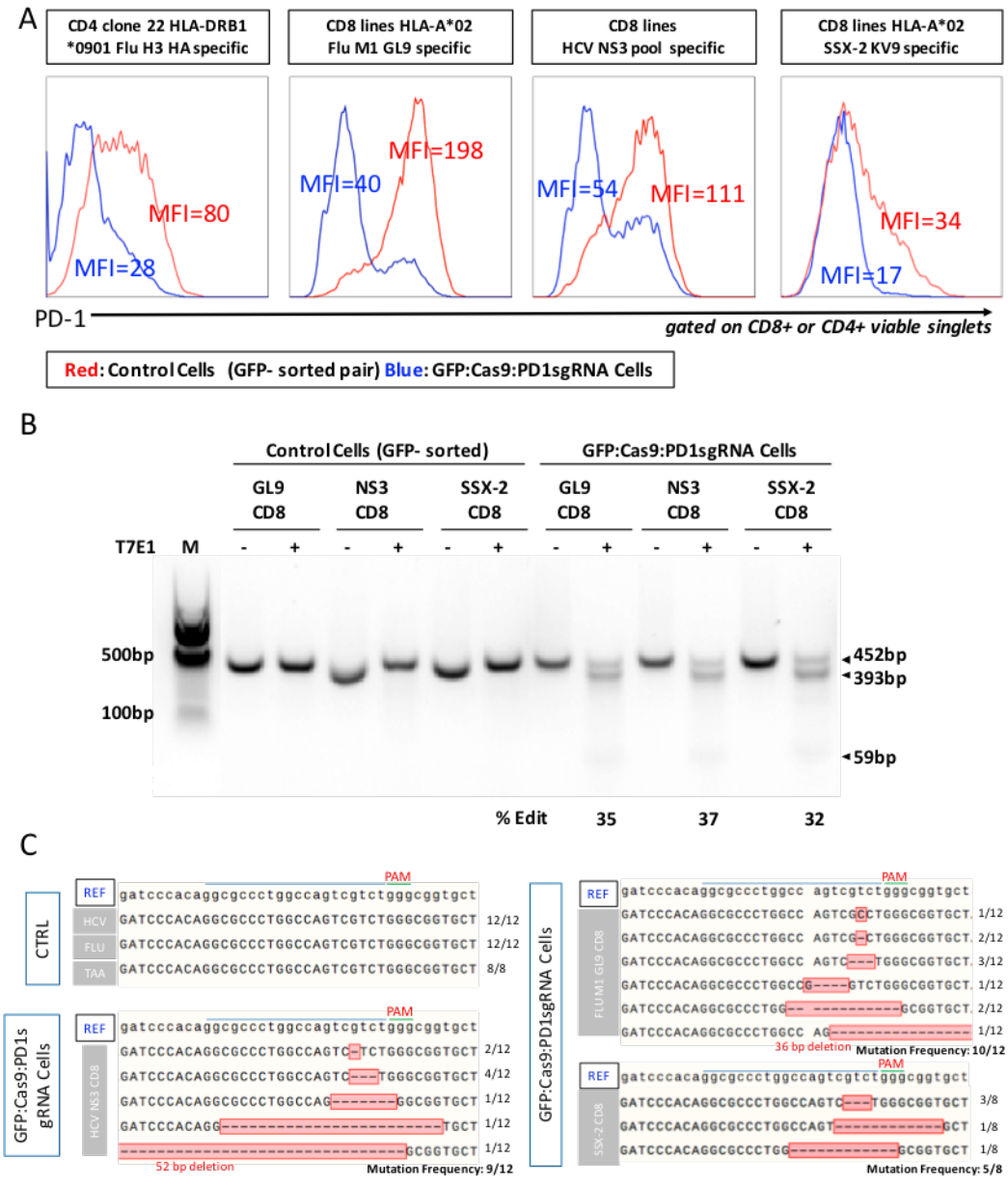

Figure 6-4 Validation of PD1 knock out effect on antigen specific CTL cell lines.

(A) PD1 expression in lentiviral transduced (GFP:Cas9:PD1sgRNA) and non-transduced (control) antigen specific T cell lines. PD1 expression in T cells was checked 24 hours post anti-CD3/anti-CD28 stimulation. With stimulation, almost all the control cells express PD1, but in the majority of GFP:Cas9:PD1sgRNA cells PD1 expression declines (both in terms of MFI and percentage). (B) T7E1 cleavage assays were conducted to reveal the indel mutation within the sgRNA targeting region in the GFP:Cas9:PD1sgRNA cells. Total editing frequency is shown at the bottom. (C) Sanger sequencing of the PCR product flanking the sgRNA site. No indel mutations were detected in control cells, in contrast to GFP:Cas9:PD1sgRNA cells where the sgRNA targeting sites were heavily mutated.

Table 6-2 Summary of PD-1 levels on different PD-1 knock out groups						
CTL ID	Control Cells		GFP:Cas9:PD1sgRNA cells			
	PD1+ PCT	PD-1 MFI	PD1+ PCT	PD-1 MFI	T7E1	Sequencing
CD4 Influenza clone22	66.5%	79.4	25.9%	27.8	-	-
CD8 Influenza GL9 line	87.6%	198	20.8%	39.3	35%	10/12
CD8 HCV HS3 pool line	71.2%	111	34.3%	54.4	37%	9/12
CD8 SSX-2 KV9 line	37.6%	33.6	11.2%	16.9	32%	5/8
PCT: percentage, MFI: median fluorescent intensity.						

6.2.4 Inhibition of T Cell Function by the Ligand of PD-1.

PD-L1 induces T cell apoptosis and functional exhaustion (Jiang et al., 2015). Under physiological condition, few normal human tissues express PD-L1. In contrast, PD-L1 protein is highly expressed on the cell surface in various human cancers, as indicated by immunohistochemistry in frozen human tumour sections (Chen and Han, 2015). To validate that high levels of PD-L1 expression result in the inhibition of antigen-specific CTL cell, we overexpressed PD-L1, using our lentivirus expression system, in EBV-transformed HLA-A*02 B lymphoblastoid cell lines (BCLs). Compared to non-transduced BCLs, lentiviral-transduced BCLs show a dramatic increase in PD-L1 protein levels on the cell surface, with no change in expression of CD19, CD20 and HLA-A*02 molecules, nor any change in viability (Figure 6-5A).

GL9 ($M1_{58-66}$) is an immunodominant HLA-A*02-restricted CTL epitope in influenza infections (Stewart-Jones et al., 2003). KV9 ($SSX\text{-}2_{41-49}$) is a tumour-specific HLA-A*02-restricted epitope within the SSX-2 gene, which is expressed in neoplasms of various histological types (Ayyoub et al., 2003). To evaluate PD-L1 inhibition of T cell functions, supernatant from the co-culture of effector cells (wild-type M1- or SSX2-specific CTL bulk lines) and target cells (epitope-loaded

PDL1-lo or PDL1-hi BCLs) was collected for cytokine quantification by Luminex multiplex assay. Among the CTL cytokines, Interleukin 2 (IL-2) is important for the proliferation of T lymphocytes (Gaffen and Liu, 2004); Interferon γ (IFNγ) has anti-viral, anti-tumour and immunoregulatory properties (Ikeda et al., 2002; McNab et al., 2015; Schroder et al., 2004), while tumour necrosis factor α (TNFα) is a multi-functional pro-inflammatory cytokine that is involved in the regulation of a wide spectrum of biological processes (Kalliolias and Ivashkiv, 2016). By co-culturing antigen-specific CTL cells with PD-L1 low BCL or PD-L1 high BCL (target cells), T cells showed decreased production of cytokines, especially when stimulated with lower amount of antigen. In particular, IL-2 production was substantially reduced (Figure 6-5B, 6-5C).

Figure 6-5 PD-L1 can inhibit T cell cytokine secretions.

(A) PDL1, CD19 and viability on non-transduced and PDL1 ORF virus transduced HLA-A*0201/ DRB1*0901 BCLs (target cells). (B). Influenza A M1 specific and SSX-2 specific CD8 CTL lines were co-cultured with peptide-pulsed PDL1-low or PDL1-high BCL target cells with corresponding amount of peptide, cells were cultured for 24 hours and the supernatants were harvested and went through Luminex assay for cytokine quantifications. (C) H3 HA specific CD4+ T cell clone 22 (left) and M1 specific CD8 CTL lines (right) were treated with Golgi Stop/Plug and co-cultured with peptide-pulsed PDL1-lo or PDL1-hi (lentiviral overexpressed) HLA-matched BCL (target cells) with corresponding amount of peptide for four hours respectively, and stained for CD107a and IL2, IFNγ, TNFα. Effector cells co-cultured with PDL1-hi target cells showed decreased degranulation (indicated by CD107a staining) and IL2 productions on both CD8 line and CD4 clone. Data shown are mean ± SD of three independent experiments and we depicted a representative out of three experiments yielding similar results. * indicates p-value<0.05. ** indicates p-value<0.01. *** indicates p-value<0.001. **** indicates p-value<0.0001. p-values were calculated using two-tail unpaired student's t-test.

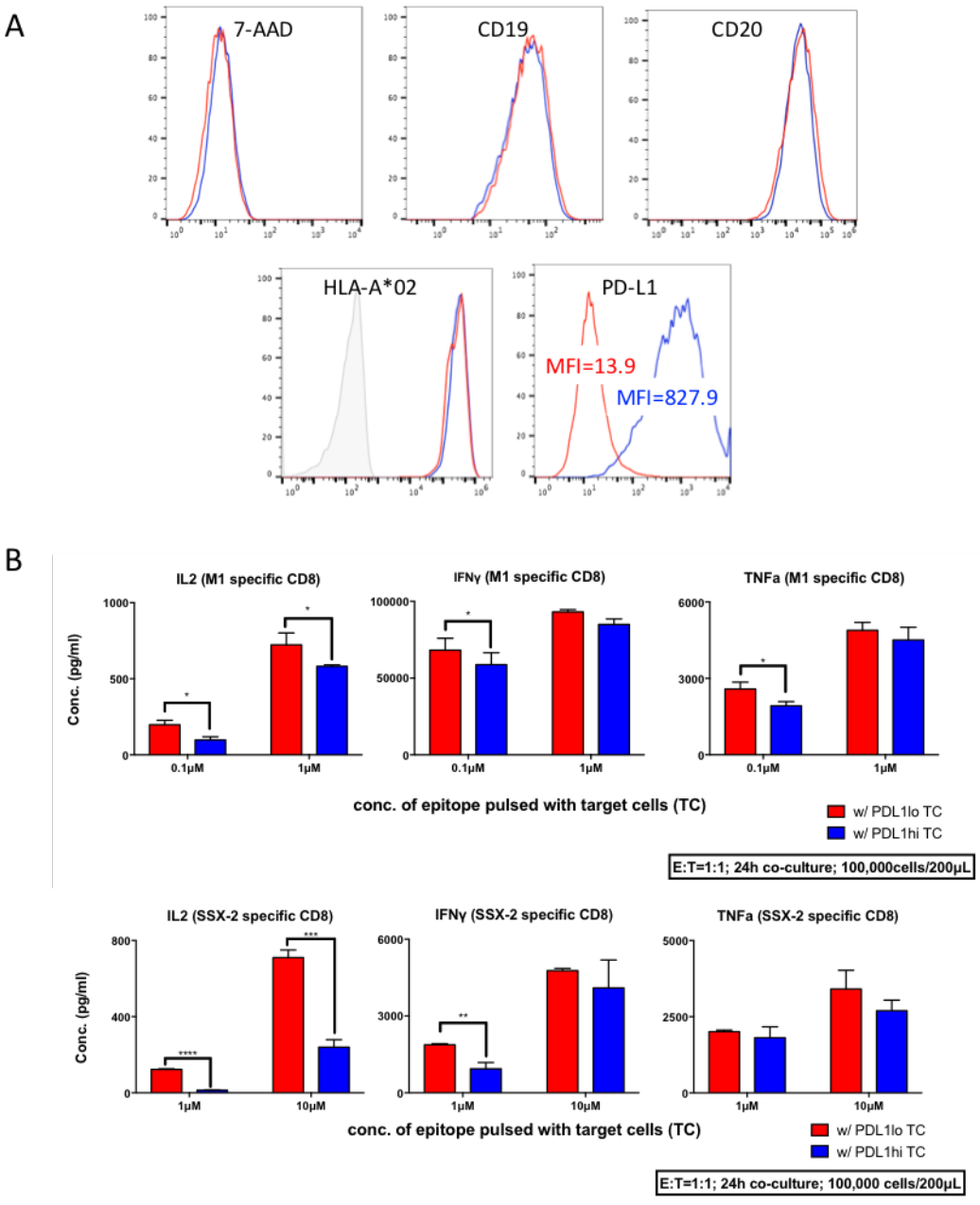
A
7-AAD
CD19
CD20
HLA-A*02
PD-L1
MFI=13.9
MFI=827.9
B
IL2 (M1 specific CD8)
IFNγ (M1 specific CD8)
TNFa (M1 specific CD8)
Conc. (pg/ml)
0.1μM
1μM
conc. of epitope pulsed with target cells (TC)
w/ PDL1lo TC
w/ PDL1hi TC
E:T=1:1; 24h co-culture; 100,000cells/200μL
IL2 (SSX-2 specific CD8)
IFNγ (SSX-2 specific CD8)
TNFa (SSX-2 specific CD8)
Conc. (pg/ml)
1μM
10μM
conc. of epitope pulsed with target cells (TC)
w/ PDL1lo TC
w/ PDL1hi TC
E:T=1:1; 24h co-culture; 100,000 cells/200μL

C

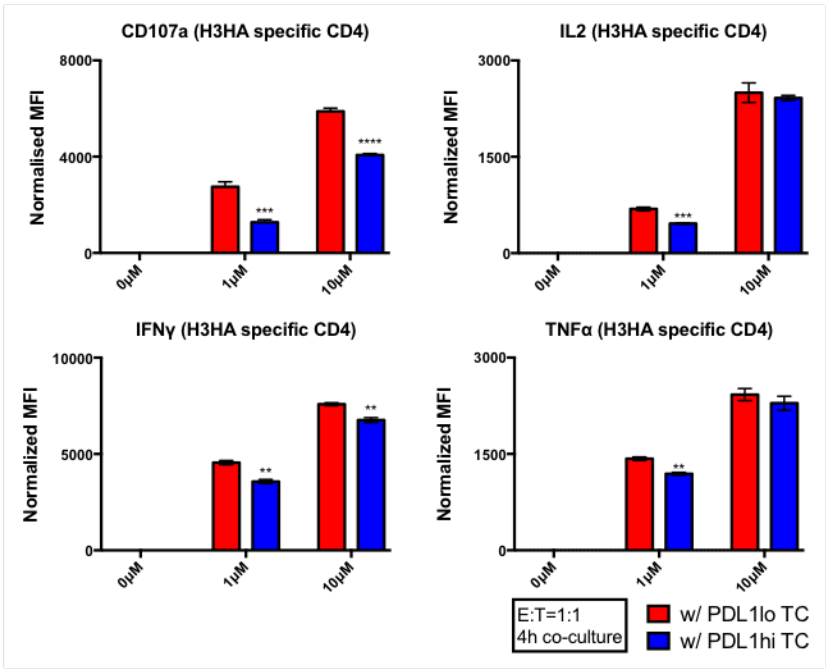
CD107a (H3HA specific CD4)
Normalised MFI
8000
4000
0
0μM
1μM
10μM
IL2 (H3HA specific CD4)
Normalized MFI
3000
1500
0
IFNγ (H3HA specific CD4)
10000
5000
TNFα (H3HA specific CD4)
E:T=1:1
4h co-culture
w/ PDL1lo TC
w/ PDL1hi TC

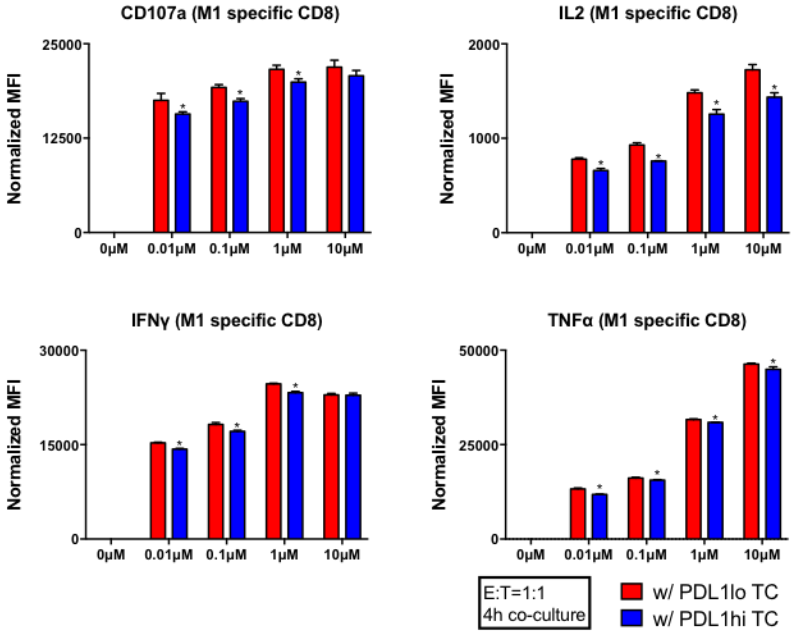
CD107a (M1 specific CD8)
Normalized MFI
25000
12500
0
0μM
0.01μM
0.1μM
1μM
10μM
IL2 (M1 specific CD8)
2000
1000
IFNγ (M1 specific CD8)
30000
15000
TNFα (M1 specific CD8)
50000
25000
E:T=1:1
4h co-culture
w/ PDL1lo TC
w/ PDL1hi TC

6.2.5 Invigoration of T Cells by Ablating PD-1 in Immune-Suppressive Microenvironment.

We tested if the loss of function of PD-1 can invigorate T cell functions in the presence of high levels of PD-L1. PD-L1 inhibition is known to be more effective when lower amounts of antigen are presented to the antigen-specific CTLs (Figure 6-5B). Thus, 0.1μM and 1μM of epitope was used to stimulate M1-specific CD8 CTLs and SSX2-specific CD8 CTLs, respectively. Lentiviral-transduced CTL pairs (GFP:Cas9:PD1sgRNA and control cells) were co-cultured with PDL1-hi or -lo HLA-matched target cells (HLA-A*02 BCL) with or without antigen, and the supernatants were collected and analysed. In both antigen-specific CTL lines, GFP:Cas9:PD1sgRNA cells produced comparable levels of IL-2, IFNγ, and TNFα in the presence of high-level or low-level PD-L1, which is in contrast to the control cells. TNFα is less significant than IL2 and IFNγ, but with similar trend (Figure 6-6A). In a similar experimental setting, the M1-specific CD8 cells and H3 HA-specific CD4 clone22 cells were co-cultured with the proper target cells in the presence of Golgi transporter blockers, and then stained to determine intercellular level of cytokines, and surface levels of CD107a, which is present in the membranes of cytotoxic granules and is transported onto the cell surface as a result of degranulation (Betts et al., 2003), and represents T cell degranulation status. CTL cells lentiviral-transduced to ablate the PD-1 gene produced comparable amount of IL2, IFNγ and TNFα with PDL1-lo target cells but significant higher amounts of these cytokines with PDL1-hi target cells. In addition, the GFP:Cas9:PD1sgRNA-transduced T cells exerted similar level of degradation with the control T cells in the PDL1-lo BCL group, in contrast to the higher expressions in the PDL1-hi BCL group (Figure 6-6 B, C).

These findings confirm our hypothesis that the ablation of PD-1 on antigen-specific CTL cells can overcome PD-L1 inhibition and allow the CTLs to improve the control of the target cells, as indicated by the higher level of degranulation and cytokine production.

A

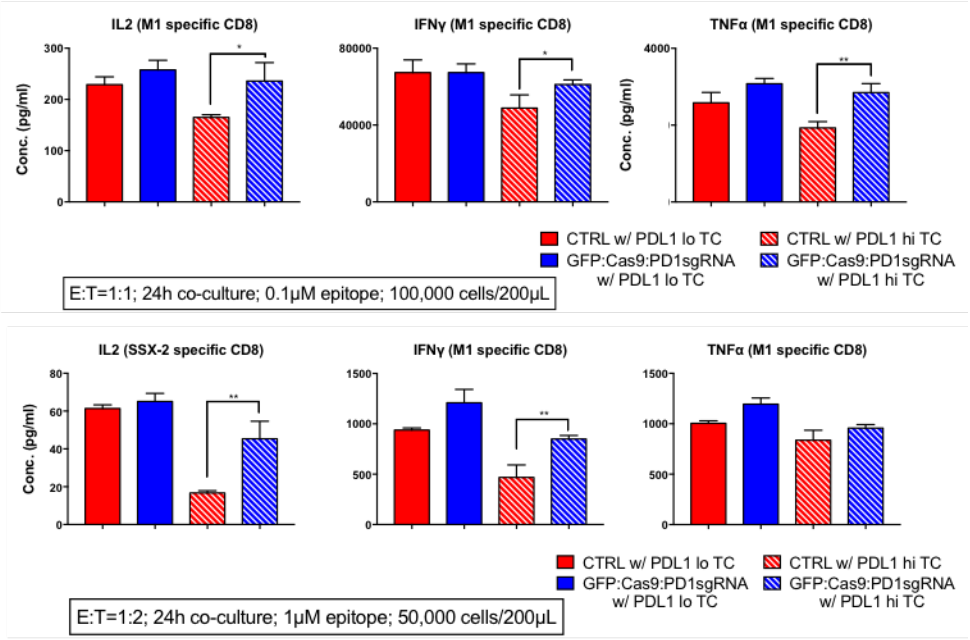
IL2 (M1 specific CD8)
IFNγ (M1 specific CD8)
TNFα (M1 specific CD8)
Conc. (pg/ml)
CTRL w/ PDL1 lo TC
GFP:Cas9:PD1sgRNA w/ PDL1 lo TC
CTRL w/ PDL1 hi TC
GFP:Cas9:PD1sgRNA w/ PDL1 hi TC
E:T=1:1; 24h co-culture; 0.1μM epitope; 100,000 cells/200μL
IL2 (SSX-2 specific CD8)
IFNγ (M1 specific CD8)
TNFα (M1 specific CD8)
Conc. (pg/ml)
CTRL w/ PDL1 lo TC
GFP:Cas9:PD1sgRNA w/ PDL1 lo TC
CTRL w/ PDL1 hi TC
GFP:Cas9:PD1sgRNA w/ PDL1 hi TC
E:T=1:2; 24h co-culture; 1μM epitope; 50,000 cells/200μL

B

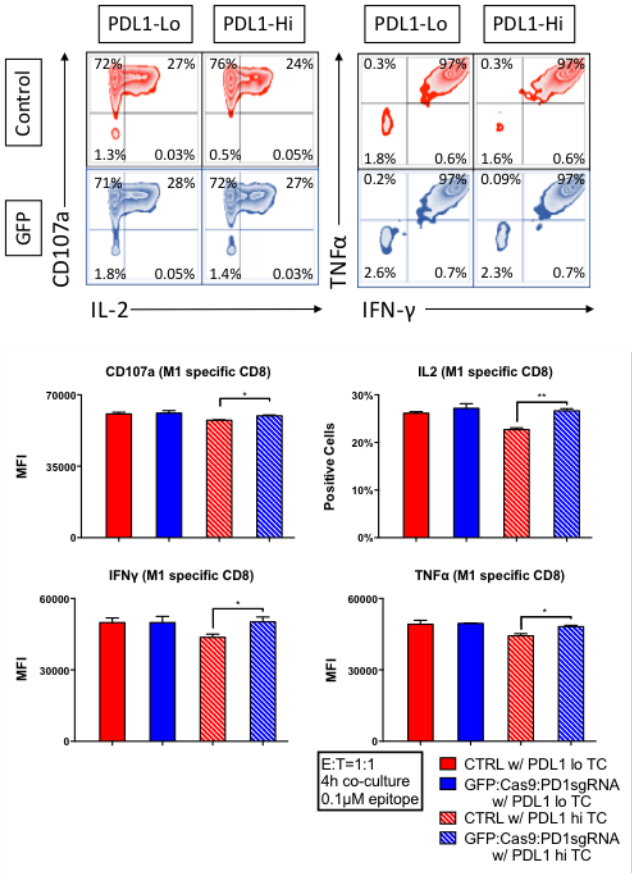
PDL1-Lo
PDL1-Hi
PDL1-Lo
PDL1-Hi
Control
GFP
CD107a
IL-2
TNFα
IFN-γ
72%
27%
76%
24%
1.3%
0.03%
0.5%
0.05%
71%
28%
72%
27%
1.8%
0.05%
1.4%
0.03%
0.3%
97%
0.3%
97%
1.8%
0.6%
1.6%
0.6%
0.2%
97%
0.09%
97%
2.6%
0.7%
2.3%
0.7%
CD107a (M1 specific CD8)
IL2 (M1 specific CD8)
MFI
Positive Cells
IFNγ (M1 specific CD8)
TNFα (M1 specific CD8)
MFI
MFI
E:T=1:1
4h co-culture
0.1μM epitope
CTRL w/ PDL1 lo TC
GFP:Cas9:PD1sgRNA w/ PDL1 lo TC
CTRL w/ PDL1 hi TC
GFP:Cas9:PD1sgRNA w/ PDL1 hi TC

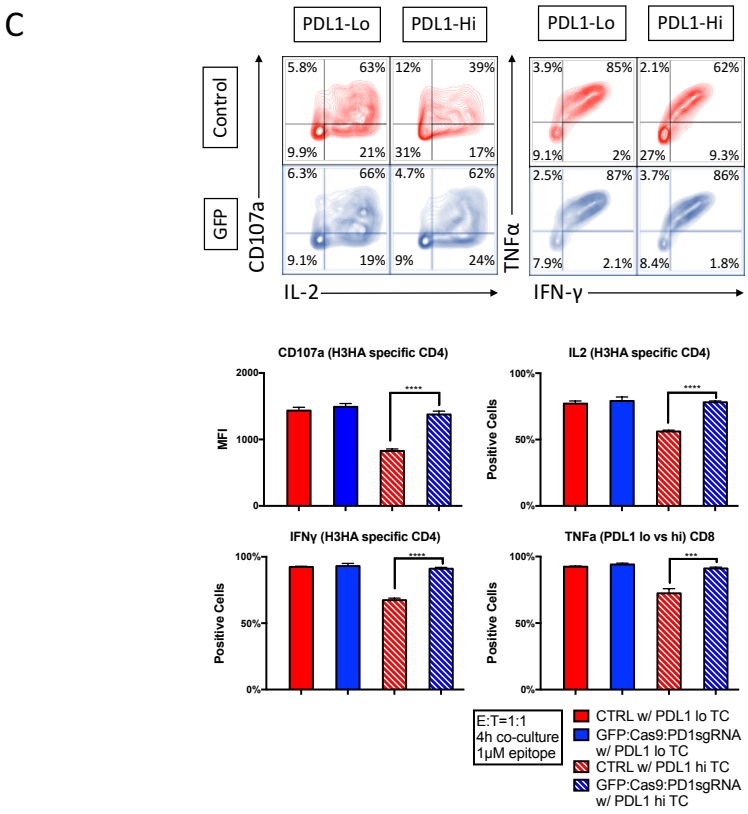

Figure 6-6 Knocking out PD-1 to release PD-L1 inhibition on T cell degranulation and cytokine secretion.

(A) IL2, IFNγ, TNFa cytokine production of effector cells and target cell co-cultures (24h) were quantified by Luminex assay for M1-specific and SSX-2-specific CD8 CTL lines. Control effector cells co-cultured with PDL1-hi target cells showed decreased IL2, IFNγ, and TNFα production compared to co-culture with PDL1-lo target cells, while GFP:Cas9:PD1sgRNA effector cells produced comparable amount of these cytokines with both PDL1-lo and –hi groups. (B) FACS plot (left) and bar chart (right) for M1-specific CD8+ T cell lines. The effector cells were co-cultured with peptide-pulsed PDL1-low or PDL1-hi target cells together with 0.1μM peptide for 4 hours in the presence of Golgi blockers. Control effector cells co-cultured with PDL1-hi target cells showed decreased degranulation (indicated by CD107a staining) and cytokine production. GFP:Cas9:PD1sgRNA effector cells showed only marginal inhibition, indicating PD-1 ablation restores PD-L1 inhibition. (C) Similar results were observed in the H3 HA specific CD4+ T clone 22 cell pair. Control: control T cells, GFP negative sorted control lentiviral transduced cells. GFP: GFP:Cas9:PD1sgRNA T cells, GFP positive sorted PD1sgRNA inserted CRISPR lentiviral transduced cells. Normalized MFI equals the frequency of positive cells times the median fluorescent intensity (MFI) of the positive cells. Data shown are mean ± SD of three independent experiments and we depicted a representative out of three experiments yielding similar results. * indicates p-value<0.05. ** indicates p-value<0.01. *** indicates p-value<0.001. **** indicates p-value<0.0001. p-values were calculated using two-tail unpaired student's t-test.

6.3 Discussion.

The introduction of CAR or TCR transgenic T cells has revolutionised the field of immunotherapy and provided evidence for the feasibility of cell-based strategies to treat cancers. However, targeting solid tumours using CAR T cells remains problematic (Newick et al., 2016). Unlike circulating blood, the tumour microenvironment is, in many cases, immunosuppressive; transformed cells and local immune cells express high-levels of the PD-1 ligand. PD-L1 binding to PD-1 results in the phosphorylation of tyrosine on the cytoplasmic tail of PD-1, which recruits SHP2 (SH2-domain containing tyrosine phosphatase 2) and dephosphorylate PI3K (phosphatidylinositol-4,5-bisphosphate 3-kinase). The inactivation of PI3K dampens downstream Akt signalling, and hampers T cell activation, proliferation, and survival (Keir et al., 2008). One strategy to counter PD-1 restriction is by the systemic administration of anti-PD1 or anti-PDL1 blocking antibodies, which has already been approved by the FDA for treating different cancers (Ascierto and Marincola, 2015; Chen and Han, 2015), although patients may suffer the risk of developing autoimmune disorders. Combination use of PD-1-blocking antibodies and CAR T cells in mice has been reported to enhance the anti-tumour efficacy (John et al., 2013b), however, this will make the treatment more costly and carries a higher risk of breaking peripheral immune tolerance.

Thus, autologous tumour-specific T cells with a loss-of-function mutation in the PD1 gene could provide an alternative cancer treatment. The CRISPR/Cas9 has been adapted to engineer genome in many species (Charpentier and Marraffini, 2014; Gaj et al., 2013; Ran et al., 2013). Several studies have reported the

successful engineering of the PD-1 gene in primary T cells using CRISRP/Cas9 (Gwiazda et al., 2016; Schumann et al., 2015; Su et al., 2016). Nevertheless, those studies engineered the PD-1 gene in T cells that did not target a specific antigen, which, in a similar fashion to antibody therapy, could induce T cells to target self-antigens. Here, we described the first PD-1 knock out on antigen-specific CTL lines. This approach, together with the identification of new tumour antigens, could provide alternatives to T cell-based therapy, especially in those cases where no appropriate antibodies are available for constructing chimeric receptors. Furthermore, PD-1 disruption can be used in combination with other immune checkpoint knock-outs, such as T cell immunoglobulin and mucin-domain containing-3 (TIM-3), as blocking PD-1 can induce compensatory TIM-3 up-regulation (Romero, 2016), and genes that promote T cell death, such as FAS, may together with PD-1 blockade, be more effective in anti-tumour responses.

In addition, the expression of the PD-1 ligand on the target cells and PD-1 on the effector cells should be considered for a proper outcome to reveal PD-1 inhibition. It is well established that the PD-1 pathway provides major inhibitory regulation for T cell activation (Chen and Han, 2015). Nevertheless, the extent of PD-1 inhibition depends on many factors, including PD-1/L1expression, the effector cell to target cell (E:T) ratio, the effector cell's nature, and its surrounding environment, etc. For instance, we initially evaluated T cell function at an E:T ratio of 10:1. No differences were detected between PDL1-lo target cells and PDL1-hi target cells until we decreased the ratio to 1:1, or 1:2. PD-L1 inhibition was marginal on our CD8 influenza virus specific T cell lines, probably due to the high antigen sensitivity and avidity (potent killing happens within minutes for antigen-experienced T cells (de la Roche et al., 2016)) and low PD-1

expression on the T cells (Figure 6-7). Furthermore, as flu infection is usually acute, the influenza virus-specific T cells generated from blood are resting memory T cells, instead of tumour-specific T cells which are usually in a status of exhaustion due to constant stimulation.

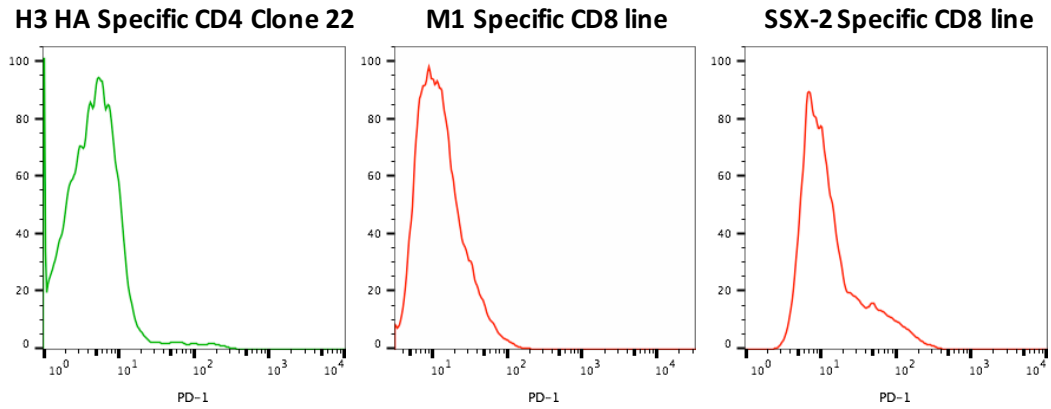

Figure 6-7 PD-1 expressions at resting stage in vitro cultured antigen-specific CTL lines.

Cells were gated on live single CD4 or CD8 positive cells. At leave three independent experiments were conducted and we depicted a representative out of three experiments yielding similar results.

Blockade of the PD-1 pathway is already known to improve effector cell IFN-γ production, as well as cytotoxicity, both *in vitro* and *in vivo* (Blank et al., 2006; John et al., 2013a). Here we also demonstrated that the GFP:Cas9:PD1sgRNA-modified antigen-specific CTL cells from patients exhibited enhanced IFN-γ production, by co-culturing with the related antigen-loaded target cells. At the same time, we also detected enhanced degranulation potency and production of cytokine IL-2. Our observations that PD-L1 inhibition could only be observed in PDL1-hi groups and not PDL1-lo group indicate that the improved T cell functions seen in GFP:Cas9:PD1sgRNA cells in the PD-L1 high environment was indeed due to the CRISPR/Cas9 mediated PD-1 mutations.

Nonetheless, the GFP:Cas9:PD1sgRNA cells we have generated became resistant to proliferate after multiple rounds of expansion, particular after manipulations such as lentiviral transduction and GFP sorting. In addition, TIM-3 was up-regulated (compensatory mechanism) in T cells from animals that developed resistance to the anti-PD-1 treatment (Romero, 2016).Thus, we are currently exploring the possibility of knocking out apoptosis genes or other immune checkpoint genes together with PD-1 to make the cells both more sustainable and functionally capable of lysing antigen. A single lenti-vector has been reported that can carry up to four different sgRNAs simultaneous (Kabadi et al., 2014). We have successfully constructed dual knock-out lenti-vectors that combine a PD-1-targeting sgRNA with a CTLA-4-targeting sgRNA, or a TIM-3-targeting sgRNA, or a TIGIT-targeting sgRNA. However, it is still unclear how long those cells can survive outside the human body, and how their proliferation would be affected if transfused back. Additionally, all the antigen-specific CTL cells in this study were generated from peripheral blood, thus the frequency of

antigen-specific CTL cells could be lower compared to cells from the diseased site. We have attempted to generate antigen-specific T cells directly from tissues or tumours, which may provide us higher numbers of the antigen-specific T cells, as well as a proportion of PD-1 positive cells. Lentiviral transduction of those cells, followed by GFP sorting at an early time point, together with reduced rounds of feeder expansion are more favourable for cell proliferation and should facilitate future applications. However, the difficulties of culturing and expanding these cells indicate we need to further optimize the procedure.

In conclusion, we have established a platform for disrupting an immune check-point gene in human antigen-specific CTL cells. The technique could be widely used and easily applied to other immune checkpoint genes. Our gene editing method is suitable for functional studies of single or combined mutations in immune checkpoint receptors, more importantly, has the potential to be adapted for clinical applications such as the treatment of infection, autoimmunity, and cancer.

7 Summary

This D.Phil. thesis focuses on human antigen-specific cytotoxic T lymphocytes. In the first part of the thesis, the impact of antigen stimulation strength on CTL activation was investigated by evaluating the global transcriptomes of a well-characterized CTL clone and some of its surface protein expressions, with particular focus on immune checkpoint receptors. Based on the gene differentiations, an 'EGR2-CCL1-4-1BB' pathway, which is sensitive to very low-strength antigen stimulation, was identified. We proposed to block CCL1/CCR8 for future cancer therapeutic treatment as this could be a key mechanism for attracting immune-suppressive cells to local tumour-specific CTLs. Further, an 'inverse correlation of inhibitory signal and expression level' model was developed to explain the expression patterns of dominant inhibitory immune checkpoint receptors (CTLA-4, PD-1, LAG-3, TIM-3 and TIGIT). These findings throw lights on the understanding of CTL functions and the future design of T cell-based cancer immunotherapy. In the second half the thesis, the potential use of CRISPR/Cas9 technology was explored in manipulating antigen-specific CTLs and the antigen-specific CTL clone gene delivery method was optimised. Successful disruption of PD-1 gene by CRISPR/Cas9 via lentivirus has been achieved on several antigen-specific CTL lines and clones. After disrupting PD-1 gene, CTLs function better when the target cells express high level of PD-1 ligand. This part of work is the first study to knock out PD-1 gene on human antigen-specific primary CD8+ T cells and has the potential for clinical applications such as the treatment of infection, autoimmunity and cancer.

7.1 The Impact of Antigen Stimulation Strength on CTL Functions.

Human CD8+ cytotoxic T lymphocytes, which play a pivotal role in the cell-mediated immunity for the protection of the human body. The 'qualities' of CTLs that specific to antigens determine the outcome of viral infections as well as different types of cancers. Thus, understanding how CTL re-programmes its functions after TCR engagement could provide insights into future development of CTL-based therapy. However. the heterogeneity of the antigen-specific CTL in the circulation system confounds the investigation of the pathways that regulate CTL functions. In order to address this question, in the first half of this thesis, we reduced the heterogeneity of CTLs into single units by studying T cell clones that all the cells were derived from a single mother T cell isolated from the patient. Different to human primary T cells, studying homogenous T cell clones reduced the complexity of the system and provide more clear-cut data presentation. In tumour micro-environment (TME), due to down-regulation of MHC- I, it is likely the amount of tumour antigen presented on cancer cells is low, leading to suboptimal antigen presentation. In this situation, the triggered CTL effector functions may not be enough to eliminate the cancer cells but enough for T cell to survive and proliferate. As a proof of concept study, by making use the antigen (HIV) specific CTL clones available in our laboratory, we evaluated the strength of antigen stimulation required for CTL in triggering key molecular signalling events required for cell survival, cell interaction, proliferation and effector functions.

Previous T cell clone studies in our group focused on comparing sister T cell clones to identify protective correlates, with less emphasis on utilizing this system

as a model to study T cell properties. As the current available lab strains of human T cells are mainly CD4 transformed T lymphoma cells, such as Jurkat E6-1, the availability of proliferative clonal human CD8+ T cells provides exclusive opportunity for studying CTL functions. Although systematic analyses of lymphocyte transcriptomes have already yielded important insights on lymphocyte functions and development (Heng and Painter, 2008), almost all of them were using heterogeneous T cells, bearing different types of TCRs. In the Chapter 3, a transcriptome study of clonal antigen-specific CTLs that received six different strengths of antigen stimulation (10^{1}μM – 10^{-3}μM of cognate peptide) was conducted. Around 1,000 genes have been observed to be differentially expressed by more than 2-fold at 10μM peptide stimulation (highest dose group), and most of them have been identified to either up-regulate or down-regulate in a dose-dependent way. Among them, the most noticeable differentiation was from those genes related to cellular metabolism, which agreed with the current understanding that metabolic reprogramming is the hallmark of T cell activation (Dimeloe et al., 2017). Based on this global expression dataset, we have further characterized the expression of cytokine/chemokine, solute carriers and co-signalling molecules at different strengths of antigen stimulation. SLC3A2 and its dimer partner SLC7A5 (form LAT1) are the dominant transporters expressed on CTL surface (5.5×10^{5} and 4.7×10^{5} copies respectively), with GLUT3 (7.2×10^{4} copies), GLUT1 (6.2×10^{4} copies) and SLC1A5 (3×10^{4} copies) coming after (Hukelmann et al., 2016). In our data, LAT1 and its sub units are the most sensitive transporter genes to antigen stimulation (10^{-2}-10^{-1}μM level), with ZIP8/ZIP14 coming after (10^{-1}μM level). The majority of transporter genes up-regulated at 1μM level. This finding extends our understanding of the nutrient

transporter on the surface of CTLs and highlighted the importance of LAT1 in the T cell activation. In addition, we observed that several pairs of functional related genes swapped in response to antigen stimulation, such as CCR4 (up) and CCR3 (down), IL2RA (up) and IL10RA (down), CCL1 (up) and CCL22 (down), CAT1 (up) and CAT2 (down). Furthermore, based on our microarray data, EGR2, CCL1 and 4-1BB are the most sensitive genes for the CTL clone in response to antigen stimulation (10^{-2}μM level). It has been reported that overexpression of EGR2 on mice T cells leads to the up-regulation of both CCL1 and 4-1BB (Williams et al., 2017). Based on the data of others and our findings, we proposed an EGR2-4-1BB-CCL1 pathways – TCR engagement (sensitive to very low strength of antigen stimulation) activates EGR2 expression which further promotes the transcriptions of 4-1BB and CCL1. In TME, low concentration of tumor antigen peptide-MHC-I complexes are presented on tumour cells, which could not trigger optimal killing by tumour antigen specific CTLs. However, this low strength of stimulation might be enough to induce CTLs to secrete CCL1 molecules, which bind to CCR8 (a chemokine receptor dominantly expressed on regulatory T cells and CCR8+/CD11b+ myeloid cell subset in cancer patients). We hypothesize that up-regulation of CCL1 could attracts surrounding Treg and myeloid cells, and further compromises the immune surveillance. Therefore, blocking CCL1/CCR8 might offer a new therapeutic strategy for cancer treatment (Hoelzinger et al., 2010), and antagonizing 4-1BB could be an additional approach. Although it's still too early to draw a firm conclusion, it's an interesting direction for future study to investigate whether this pathway could be shared in a broader scope on different CTLs and functionally important. It is arguable how representative of using a limited number of viral-specific T cell clones to predict

in vivo tumour-specific T cell responses. Therefore, further experiments are planned, including: 1) to validate top genes identified in the microarray on different tumour-specific CTL lines using single cell Fluidigm; 2) flow-based detection of CCR8 in tumour infiltrating immune cells from cancer patients; 3) establish *in vitro* assay to test if CCL1 blockade could be an approach for better CTL functions.

7.2 Heterogeneity of Immune Checkpoint Receptors.

Immune checkpoint receptors fine-balance the TCR signalling and are particularly interesting as they have been showing tremendous potentials for therapeutic applications. The microarray dataset described in Chapter 3 enabled us to simultaneously detect the mRNA levels of about 45 immune checkpoint genes at different strengths of antigen stimulation. In parallel, we characterized the surface expression patterns of major co-stimulatory and inhibitory immune checkpoint receptors (and intracellular expression pattern for CTLA-4), and proposed a model to explain our observations - inhibitory signal strength of the immune checkpoint receptor inversely correlates with its surface expression level. We observed a positive expression correlation between PD-1 with TIM-3 but not TIGIT and each immune checkpoint receptor does not inclusive or exclusive correlates with each other. Our findings indicated that apart from the specificity of the TCR, which is the major determinant of the T cell function (Almeida et al., 2007; Chen et al., 2012), varied patterns of inhibitory receptor expression may also determine the outcome of a TCR signalling reaction.

7.3 Manipulation of the Cytotoxic T Cell Functions.

Enhancing the body's own immune responses against cancer is the goal of immunotherapy. One strategy is to immunize cancer patients with specific antigens to utilise patient's own immune system to do the screening for immunogenicity and generate the appropriate effector cells. Alternatively, adoptive transfer of *in vitro* expanded TILs, which could overcome the difficulty of generating a strong response in vaccination. For example, through the *ex vivo* selection, expansion and re-infusion of antigen-specific T cells. However, these efforts have achieved only limited success. The most successful cell-based clinical trials on immunotherapy so far is using CAR-T cells to treat haematological malignancies (Brentjens et al., 2011; Jensen et al., 2010; Kalos et al., 2011; Kochenderfer et al., 2012). The approach is based on the genetic modifications of the autologous T cells by infecting them with replication-deficient viruses, which can insert part of their genome into the host genome, to provide these cells with extra antigen specificities. Similarly, in Chapter 5, we described the efforts that we made to manipulate certain gene expression on selected antigen-specific CTLs. The optimisation was first on the gene delivery method, including siRNA, electroporation based plasmid transfection and lentiviral transduction, for *in vitro* cultured antigen-specific T cells. The former two methods were ruled out owing to the low efficiency and poor viability issues. The lentiviral transduction was continued in the subsequent studies. We have further compared different lentiviral backbones, polycations and transduction methods for facilitating gene delivery into T cell clones. Despite the limited improvements on T cell clone transduction efficiency, these optimizations worked well on human primary T cells. In Chapter 6, we continued with the best available approach tested in Chapter 5 and have

established a platform for disrupting immune checkpoint gene (PD-1) on several human antigen-specific CTL cells.

Instead of simply amplifying certain T cell population from the patient, CAR-T or TCR-T provide T cells with extra optimized antigen specificity. Because a single T cell clone is not sufficient to cure the disease, it may be necessary to improve the function of the T cell clone, and to combine T cell clones of different specificities. Hence, in the Chapter 6, we described a viral-based delivery using CRISPR/Cas9 system to disrupt specific gene expression on *in vitro* cultured antigen-specific CTL lines and clones, and it was evident that disrupting PD-1 could improve T cell functions in the presence of PD-1 ligand. In the future, we will further optimise this platform and extend to disrupt multiple genes. For instance, knocking out of TIM-3 in combination of PD-1 may provide extra functional benefit for exhausted antigen-specific T cells, as it has been reported that TIM-3 was up-regulated in T cells in compensation to the anti-PD-1 treatment (Romero, 2016).

References

Acuto, O., V. Di Bartolo, and F. Michel. 2008. Tailoring T-cell receptor signals by proximal negative feedback mechanisms. *Nature reviews. Immunology* 8:699-712.

Acuto, O., R.E. Hussey, K.A. Fitzgerald, J.P. Protentis, S.C. Meuer, S.F. Schlossman, and E.L. Reinherz. 1983. The human T cell receptor: appearance in ontogeny and biochemical relationship of alpha and beta subunits on IL-2 dependent clones and T cell tumors. *Cell* 34:717-726.

Agosto, L.M., J.J. Yu, M.K. Liszewski, C. Baytop, N. Korokhov, L.M. Humeau, and U. O'Doherty. 2009. The CXCR4-tropic human immunodeficiency virus envelope promotes more-efficient gene delivery to resting CD4+ T cells than the vesicular stomatitis virus glycoprotein G envelope. *Journal of virology* 83:8153-8162.

Ahmadzadeh, M., L.A. Johnson, B. Heemskerk, J.R. Wunderlich, M.E. Dudley, D.E. White, and S.A. Rosenberg. 2009. Tumor antigen-specific CD8 T cells infiltrating the tumor express high levels of PD-1 and are functionally impaired. *Blood* 114:1537-1544.

Aiuti, A., S. Vai, A. Mortellaro, G. Casorati, F. Ficara, G. Andolfi, G. Ferrari, A. Tabucchi, F. Carlucci, H.D. Ochs, L.D. Notarangelo, M.G. Roncarolo, and C. Bordignon. 2002. Immune reconstitution in ADA-SCID after PBL gene therapy and discontinuation of enzyme replacement. *Nature medicine* 8:423-425.

Akari, H., S. Arold, T. Fukumori, T. Okazaki, K. Strebel, and A. Adachi. 2000. Nef-induced major histocompatibility complex class I down-regulation is functionally dissociated from its virion incorporation, enhancement of viral infectivity, and CD4 down-regulation. *Journal of virology* 74:2907-2912.

Alexander-Miller, M.A., G.R. Leggatt, A. Sarin, and J.A. Berzofsky. 1996. Role of antigen, CD8, and cytotoxic T lymphocyte (CTL) avidity in high dose antigen induction of apoptosis of effector CTL. *The Journal of experimental medicine* 184:485-492.

Almeida, J.R., D.A. Price, L. Papagno, Z.A. Arkoub, D. Sauce, E. Bornstein, T.E. Asher, A. Samri, A. Schnuriger, I. Theodorou, D. Costagliola, C. Rouzioux, H. Agut, A.G. Marcelin, D. Douek, B. Autran, and V. Appay. 2007. Superior control of HIV-1 replication by CD8+ T cells is reflected by their avidity, polyfunctionality, and clonal turnover. *The Journal of experimental medicine* 204:2473-2485.

Almeida, J.R., D. Sauce, D.A. Price, L. Papagno, S.Y. Shin, A. Moris, M. Larsen, G. Pancino, D.C. Douek, B. Autran, A. Saez-Cirion, and V. Appay. 2009.

Antigen sensitivity is a major determinant of CD8+ T-cell polyfunctionality and HIV-suppressive activity. *Blood* 113:6351-6360.

Amir el, A.D., K.L. Davis, M.D. Tadmor, E.F. Simonds, J.H. Levine, S.C. Bendall, D.K. Shenfeld, S. Krishnaswamy, G.P. Nolan, and D. Pe'er. 2013. viSNE enables visualization of high dimensional single-cell data and reveals phenotypic heterogeneity of leukemia. *Nat Biotechnol* 31:545-552.

Andersen, M.H., D. Schrama, P. thor Straten, and J.C. Becker. 2006. Cytotoxic T Cells. *J Invest Dermatol* 126:32-41.

Anderson, A.C., N. Joller, and V.K. Kuchroo. 2016. Lag-3, Tim-3, and TIGIT: co-inhibitory receptors with specialized functions in immune regulation. *Immunity* 44:989-1004.

Appay, V., D.C. Douek, and D.A. Price. 2008. CD8+ T cell efficacy in vaccination and disease. *Nature medicine* 14:623-628.

Armand, P., M.A. Shipp, V. Ribrag, J.-M. Michot, P.L. Zinzani, J. Kuruvilla, E.S. Snyder, A.D. Ricart, A. Balakumaran, S. Rose, and C.H. Moskowitz. 2016. Programmed Death-1 Blockade With Pembrolizumab in Patients With Classical Hodgkin Lymphoma After Brentuximab Vedotin Failure. *Journal of Clinical Oncology* 34:3733-3739.

Ascierto, P.A., and F.M. Marincola. 2015. 2015: The Year of Anti-PD-1/PD-L1s Against Melanoma and Beyond. *EBioMedicine* 2:92-93.

Au-Yeung, B.B., J. Zikherman, J.L. Mueller, J.F. Ashouri, M. Matloubian, D.A. Cheng, Y. Chen, K.M. Shokat, and A. Weiss. 2014. A sharp T-cell antigen receptor signaling threshold for T-cell proliferation. *Proceedings of the National Academy of Sciences of the United States of America* 111:E3679-3688.

Ayyoub, M., D. Rimoldi, P. Guillaume, P. Romero, J.C. Cerottini, D. Valmori, and D. Speiser. 2003. Tumor-reactive, SSX-2-specific CD8+ T cells are selectively expanded during immune responses to antigen-expressing tumors in melanoma patients. *Cancer research* 63:5601-5606.

Baitsch, L., P. Baumgaertner, E. Devevre, S.K. Raghav, A. Legat, L. Barba, S. Wieckowski, H. Bouzourene, B. Deplancke, P. Romero, N. Rufer, and D.E. Speiser. 2011. Exhaustion of tumor-specific CD8(+) T cells in metastases from melanoma patients. *J Clin Invest* 121:2350-2360.

Baitsch, L., A. Legat, L. Barba, S.A. Fuertes Marraco, J.P. Rivals, P. Baumgaertner, C. Christiansen-Jucht, H. Bouzourene, D. Rimoldi, H. Pircher, N. Rufer, M. Matter, O. Michielin, and D.E. Speiser. 2012. Extended co-expression of inhibitory receptors by human CD8 T-cells depending on differentiation, antigen-specificity and anatomical localization. *PloS one* 7:e30852.

Bally, A.P., J.W. Austin, and J.M. Boss. 2016. Genetic and Epigenetic Regulation of PD-1 Expression. *Journal of immunology (Baltimore, Md. : 1950)* 196:2431-2437.

Barrett, D.M., N. Singh, D.L. Porter, S.A. Grupp, and C.H. June. 2014. Chimeric antigen receptor therapy for cancer. *Annual review of medicine* 65:333-347.

Barry, M., and R.C. Bleackley. 2002. Cytotoxic T lymphocytes: all roads lead to death. *Nature reviews. Immunology* 2:401-409.

Beatriz Mothe, A.L., Javier Ibarrondo, Jennifer Zamarren, Mattia Schiaulini, Cristina Miranda, Marta Ruiz-Riol, Christoph T. Berger, M. Jose´ Herrero, Eduard Palou, Montse Plana, Morgane Rolland, Ashok Khatri, David Heckerman, Florencia Pereyra, Bruce D. Walker, David Weiner, Roger Paredes, Bonaventura Clotet, Barbara K. Felber, George N. Pavlakis, James I. Mullins, Christian Brander. 2012. CTL Responses of High Functional Avidity and Broad Variant Cross-Reactivity Are Associated with HIV Control. *PloS one* 7:1-9.

Becker, J.C., M.H. Andersen, D. Schrama, and P. thor Straten. 2013. Immune-suppressive properties of the tumor microenvironment. *Cancer Immunology, Immunotherapy* 62:1137-1148.

Bengsch, B., B. Martin, and R. Thimme. 2014. Restoration of HBV-specific CD8+ T-cell function by PD-1 blockade in inactive carrier patients is linked to T-cell differentiation. *Journal of hepatology*

Berger, C.T., N. Frahm, D.A. Price, B. Mothe, M. Ghebremichael, K.L. Hartman, L.M. Henry, J.M. Brenchley, L.E. Ruff, and V. Venturi. 2011. High-functional-avidity cytotoxic T lymphocyte responses to HLA-B-restricted Gag-derived epitopes associated with relative HIV control. *Journal of virology* 85:9334-9345.

Betts, M.R., J.M. Brenchley, D.A. Price, S.C. De Rosa, D.C. Douek, M. Roederer, and R.A. Koup. 2003. Sensitive and viable identification of antigen-specific CD8+ T cells by a flow cytometric assay for degranulation. *Journal of immunological methods* 281:65-78.

Betts, M.R., M.C. Nason, S.M. West, S.C. De Rosa, S.A. Migueles, J. Abraham, M.M. Lederman, J.M. Benito, P.A. Goepfert, M. Connors, M. Roederer, and R.A. Koup. 2006. HIV nonprogressors preferentially maintain highly functional HIV-specific CD8+ T cells. In Blood. United States. 4781-4789.

Bilal, M.Y., A. Vacaflores, and J.C. Houtman. 2015. Optimization of methods for the genetic modification of human T cells. *Immunol Cell Biol* 93:896-908.

Blackburn, S.D., H. Shin, W.N. Haining, T. Zou, C.J. Workman, A. Polley, M.R. Betts, G.J. Freeman, D.A. Vignali, and E.J. Wherry. 2009. Coregulation of CD8+ T cell exhaustion by multiple inhibitory receptors during chronic viral infection. *Nature immunology* 10:29-37.

Blank, C., J. Kuball, S. Voelkl, H. Wiendl, B. Becker, B. Walter, O. Majdic, T.F. Gajewski, M. Theobald, and R. Andreesen. 2006. Blockade of PD‐L1 (B7‐H1) augments human tumor‐specific T cell responses in vitro. *International journal of cancer* 119:317-327.

Borghaei, H., L. Paz-Ares, L. Horn, D.R. Spigel, M. Steins, N.E. Ready, L.Q. Chow, E.E. Vokes, E. Felip, E. Holgado, F. Barlesi, M. Kohlhäufl, O. Arrieta, M.A. Burgio, J. Fayette, H. Lena, E. Poddubskaya, D.E. Gerber, S.N. Gettinger, C.M. Rudin, N. Rizvi, L. Crinò, G.R.J. Blumenschein, S.J. Antonia, C. Dorange, C.T. Harbison, F. Graf Finckenstein, and J.R. Brahmer. 2015. Nivolumab versus Docetaxel in Advanced Nonsquamous Non–Small-Cell Lung Cancer. *New England Journal of Medicine* 373:1627-1639.

Brahmer, J., K.L. Reckamp, P. Baas, L. Crinò, W.E.E. Eberhardt, E. Poddubskaya, S. Antonia, A. Pluzanski, E.E. Vokes, E. Holgado, D. Waterhouse, N. Ready, J. Gainor, O. Arén Frontera, L. Havel, M. Steins, M.C. Garassino, J.G. Aerts, M. Domine, L. Paz-Ares, M. Reck, C. Baudelet, C.T. Harbison, B. Lestini, and D.R. Spigel. 2015. Nivolumab versus Docetaxel in Advanced Squamous-Cell Non–Small-Cell Lung Cancer. *New England Journal of Medicine* 373:123-135.

Brahmer, J.R., S.S. Tykodi, L.Q. Chow, W.-J. Hwu, S.L. Topalian, P. Hwu, C.G. Drake, L.H. Camacho, J. Kauh, and K. Odunsi. 2012. Safety and activity of anti–PD-L1 antibody in patients with advanced cancer. *New England Journal of Medicine* 366:2455-2465.

Brenner, S., and H.L. Malech. 2003. Current developments in the design of onco-retrovirus and lentivirus vector systems for hematopoietic cell gene therapy. *Biochimica et Biophysica Acta (BBA)-Molecular Cell Research* 1640:1-24.

Brentjens, R.J., I. Riviere, J.H. Park, M.L. Davila, X. Wang, J. Stefanski, C. Taylor, R. Yeh, S. Bartido, O. Borquez-Ojeda, M. Olszewska, Y. Bernal, H. Pegram, M. Przybylowski, D. Hollyman, Y. Usachenko, D. Pirraglia, J. Hosey, E. Santos, E. Halton, P. Maslak, D. Scheinberg, J. Jurcic, M. Heaney, G. Heller, M. Frattini, and M. Sadelain. 2011. Safety and persistence of adoptively transferred autologous CD19-targeted T cells in patients with relapsed or chemotherapy refractory B-cell leukemias. *Blood* 118:4817-4828.

Buchbinder, E.I., and A. Desai. 2016. CTLA-4 and PD-1 Pathways: Similarities, Differences, and Implications of Their Inhibition. *Am J Clin Oncol* 39:98-106.

Buck, M.D., D. O'Sullivan, and E.L. Pearce. 2015. T cell metabolism drives immunity. *The Journal of experimental medicine* 212:1345-1360.

Bukrinsky, M.I., S. Haggerty, M.P. Dempsey, N. Sharova, A. Adzhubei, L. Spitz, P. Lewis, D. Goldfarb, M. Emerman, and M. Stevenson. 1993a. A nuclear

localization signal within HIV-1 matrix protein that governs infection of non-dividing cells.

Bukrinsky, M.I., S. Haggerty, M.P. Dempsey, N. Sharova, A. Adzhubel, L. Spitz, P. Lewis, D. Goldfarb, M. Emerman, and M. Stevenson. 1993b. A nuclear localization signal within HIV-1 matrix protein that governs infection of non-dividing cells. *Nature* 365:666-669.

Bunce, M., C.M. O'Neill, M.C. Barnardo, P. Krausa, M.J. Browning, P.J. Morris, and K.I. Welsh. 1995. Phototyping: comprehensive DNA typing for HLA-A, B, C, DRB1, DRB3, DRB4, DRB5 & DQB1 by PCR with 144 primer mixes utilizing sequence-specific primers (PCR-SSP). *Tissue antigens* 46:355-367.

Castelli, C., L. Rivoltini, G. Andreola, M. Carrabba, N. Renkvist, and G. Parmiani. 2000. T-cell recognition of melanoma-associated antigens. *J Cell Physiol* 182:323-331.

Catakovic, K., E. Klieser, D. Neureiter, and R. Geisberger. 2017. T cell exhaustion: from pathophysiological basics to tumor immunotherapy. *Cell Commun Signal* 15:1.

Chakraborty, A.K., and A. Weiss. 2014. Insights into the initiation of TCR signaling. *Nature immunology* 15:798-807.

Cham, C.M., G. Driessens, J.P. O'Keefe, and T.F. Gajewski. 2008. Glucose deprivation inhibits multiple key gene expression events and effector functions in CD8+ T cells. *Eur J Immunol* 38:2438-2450.

Chang, C.H., and E.L. Pearce. 2016. Emerging concepts of T cell metabolism as a target of immunotherapy. *Nature immunology* 17:364-368.

Charpentier, E., and L.A. Marraffini. 2014. Harnessing CRISPR-Cas9 immunity for genetic engineering. *Current opinion in microbiology* 19:114-119.

Charrier, S., L. Dupre, S. Scaramuzza, L. Jeanson-Leh, M. Blundell, O.a. Danos, F. Cattaneo, A. Aiuti, R. Eckenberg, and A. Thrasher. 2007. Lentiviral vectors targeting WASp expression to hematopoietic cells, efficiently transduce and correct cells from WAS patients. *Gene therapy* 14:415-428.

Chauvin, J.M., O. Pagliano, J. Fourcade, Z. Sun, H. Wang, C. Sander, J.M. Kirkwood, T.H. Chen, M. Maurer, A.J. Korman, and H.M. Zarour. 2015. TIGIT and PD-1 impair tumor antigen-specific CD8(+) T cells in melanoma patients. *J Clin Invest* 125:2046-2058.

Chen, H., Z.M. Ndhlovu, D. Liu, L.C. Porter, J.W. Fang, S. Darko, M.A. Brockman, T. Miura, Z.L. Brumme, A. Schneidewind, A. Piechocka-Trocha, K.T. Cesa, J. Sela, T.D. Cung, I. Toth, F. Pereyra, X.G. Yu, D.C. Douek, D.E. Kaufmann, T.M. Allen, and B.D. Walker. 2012. TCR clonotypes modulate the protective effect of HLA class I molecules in HIV-1 infection. *Nature immunology* 13:691-700.

Chen, L., and D.B. Flies. 2013. Molecular mechanisms of T cell co-stimulation and co-inhibition. *Nature reviews. Immunology* 13:227-242.

Chen, L., and X. Han. 2015. Anti-PD-1/PD-L1 therapy of human cancer: past, present, and future. *J Clin Invest* 125:3384-3391.

Chicaybam, L., A.L. Sodre, B.A. Curzio, and M.H. Bonamino. 2013. An efficient low cost method for gene transfer to T lymphocytes. *PloS one* 8:e60298.

Cole, D.K., B. Laugel, M. Clement, D.A. Price, L. Wooldridge, and A.K. Sewell. 2012. The molecular determinants of CD8 co-receptor function. *Immunology* 137:139-148.

Cong, L., F.A. Ran, D. Cox, S. Lin, R. Barretto, N. Habib, P.D. Hsu, X. Wu, W. Jiang, L.A. Marraffini, and F. Zhang. 2013. Multiplex genome engineering using CRISPR/Cas systems. *Science* 339:819-823.

Costello, E., M. Munoz, E. Buetti, P. Meylan, H. Diggelmann, and M. Thali. 2000. Gene transfer into stimulated and unstimulated T lymphocytes by HIV-1-derived lentiviral vectors. *Gene therapy* 7:596-604.

Cretenet, G., I. Clerc, M. Matias, S. Loisel, M. Craveiro, L. Oburoglu, S. Kinet, C. Mongellaz, V. Dardalhon, and N. Taylor. 2016. Cell surface Glut1 levels distinguish human CD4 and CD8 T lymphocyte subsets with distinct effector functions. *Sci Rep* 6:24129.

Croft, M. 2009. The role of TNF superfamily members in T-cell function and diseases. *Nature reviews. Immunology* 9:271-285.

Davis, M.M., and P.J. Bjorkman. 1988. T-cell antigen receptor genes and T-cell recognition. *Nature* 334:395-402.

Day, C.L., D.E. Kaufmann, P. Kiepiela, J.A. Brown, E.S. Moodley, S. Reddy, E.W. Mackey, J.D. Miller, A.J. Leslie, C. DePierres, Z. Mncube, J. Duraiswamy, B. Zhu, Q. Eichbaum, M. Altfeld, E.J. Wherry, H.M. Coovadia, P.J. Goulder, P. Klenerman, R. Ahmed, G.J. Freeman, and B.D. Walker. 2006. PD-1 expression on HIV-specific T cells is associated with T-cell exhaustion and disease progression. *Nature* 443:350-354.

Dayton, T.L., T. Jacks, and M.G. Vander Heiden. 2016. PKM2, cancer metabolism, and the road ahead. *EMBO Rep* 17:1721-1730.

de la Roche, M., Y. Asano, and G.M. Griffiths. 2016. Origins of the cytolytic synapse. *Nature reviews. Immunology* 16:421-432.

De Ravin, S.S., X. Wu, S. Moir, S. Anaya-O'Brien, N. Kwatemaa, P. Littel, N. Theobald, U. Choi, L. Su, M. Marquesen, D. Hilligoss, J. Lee, C.M. Buckner, K.A. Zarember, G. O'Connor, D. McVicar, D. Kuhns, R.E. Throm, S. Zhou, L.D. Notarangelo, I.C. Hanson, M.J. Cowan, E. Kang, C. Hadigan, M. Meagher, J.T. Gray, B.P. Sorrentino, and H.L. Malech. 2016. Lentiviral hematopoietic stem cell gene therapy for X-linked severe combined immunodeficiency. *Science translational medicine* 8:335ra357.

Dimeloe, S., A.V. Burgener, J. Grahlert, and C. Hess. 2017. T-cell metabolism governing activation, proliferation and differentiation; a modular view. *Immunology* 150:35-44.

Dong, T., D. Boyd, W. Rosenberg, N. Alp, M. Takiguchi, A. McMichael, and S. Rowland‐Jones. 1996. An HLA‐B35‐restricted epitope modified at an anchor residue results in an antagonist peptide. *European journal of immunology* 26:335-339.

Dong, T., E. Moran, N. Vinh Chau, C. Simmons, K. Luhn, Y. Peng, B. Wills, N. Phuong Dung, L. Thi Thu Thao, T.T. Hien, A. McMichael, J. Farrar, and S. Rowland-Jones. 2007. High pro-inflammatory cytokine secretion and loss of high avidity cross-reactive cytotoxic T-cells during the course of secondary dengue virus infection. *PloS one* 2:e1192.

Dong, T., G. Stewart-Jones, N. Chen, P. Easterbrook, X. Xu, L. Papagno, V. Appay, M. Weekes, C. Conlon, C. Spina, S. Little, G. Screaton, A. van der Merwe, D.D. Richman, A.J. McMichael, E.Y. Jones, and S.L. Rowland-Jones. 2004. HIV-specific cytotoxic T cells from long-term survivors select a unique T cell receptor. *The Journal of experimental medicine* 200:1547-1557.

Dotti, G., S. Gottschalk, B. Savoldo, and M.K. Brenner. 2014. Design and development of therapies using chimeric antigen receptor-expressing T cells. *Immunol Rev* 257:107-126.

Du, P., W.A. Kibbe, and S.M. Lin. 2008. lumi: a pipeline for processing Illumina microarray. *Bioinformatics (Oxford, England)* 24:1547-1548.

Dubrot, J., F. Milheiro, C. Alfaro, A. Palazon, I. Martinez-Forero, J.L. Perez-Gracia, A. Morales-Kastresana, J.L. Romero-Trevejo, M.C. Ochoa, S. Hervas-Stubbs, J. Prieto, M. Jure-Kunkel, L. Chen, and I. Melero. 2010. Treatment with anti-CD137 mAbs causes intense accumulations of liver T cells without selective antitumor immunotherapeutic effects in this organ. *Cancer immunology, immunotherapy : CII* 59:1223-1233.

Dupre, L., S. Trifari, A. Follenzi, F. Marangoni, T. Lain de Lera, A. Bernad, S. Martino, S. Tsuchiya, C. Bordignon, L. Naldini, A. Aiuti, and M.G. Roncarolo. 2004. Lentiviral vector-mediated gene transfer in T cells from Wiskott-Aldrich syndrome patients leads to functional correction. *Molecular therapy : the journal of the American Society of Gene Therapy* 10:903-915.

Dustin, M.L., and T.A. Springer. 1989. T-cell receptor cross-linking transiently stimulates adhesiveness through LFA-1. *Nature* 341:619-624.

Duval, L., H. Schmidt, K. Kaltoft, K. Fode, J.J. Jensen, S.M. Sorensen, M.I. Nishimura, and H. von der Maase. 2006. Adoptive transfer of allogeneic cytotoxic T lymphocytes equipped with a HLA-A2 restricted MART-1 T-cell receptor: a phase I trial in metastatic melanoma. *Clinical cancer*

research : an official journal of the American Association for Cancer Research 12:1229-1236.

Ebert, O., S. Finke, A. Salahi, M. Herrmann, B. Trojaneck, P. Lefterova, E. Wagner, R. Kircheis, D. Huhn, and F. Schriever. 1997. Lymphocyte apoptosis: induction by gene transfer techniques. *Gene therapy* 4:296-302.

Eide, D.J. 2004. The SLC39 family of metal ion transporters. *Pflugers Arch* 447:796-800.

Eyquem, J., J. Mansilla-Soto, T. Giavridis, S.J. van der Stegen, M. Hamieh, K.M. Cunanan, A. Odak, M. Gonen, and M. Sadelain. 2017. Targeting a CAR to the TRAC locus with CRISPR/Cas9 enhances tumour rejection. *Nature* 543:113-117.

Fehres, C.M., W.W.J. Unger, J.J. Garcia-Vallejo, and Y. van Kooyk. 2014. Understanding the Biology of Antigen Cross-Presentation for the Design of Vaccines Against Cancer. *Frontiers in immunology* 5:149.

Felice, B., C. Cattoglio, D. Cittaro, A. Testa, A. Miccio, G. Ferrari, L. Luzi, A. Recchia, and F. Mavilio. 2009. Transcription factor binding sites are genetic determinants of retroviral integration in the human genome. *PloS one* 4:e4571.

Ferris, R.L., G. Blumenschein, Jr., J. Fayette, J. Guigay, A.D. Colevas, L. Licitra, K. Harrington, S. Kasper, E.E. Vokes, C. Even, F. Worden, N.F. Saba, L.C. Iglesias Docampo, R. Haddad, T. Rordorf, N. Kiyota, M. Tahara, M. Monga, M. Lynch, W.J. Geese, J. Kopit, J.W. Shaw, and M.L. Gillison. 2016. Nivolumab for Recurrent Squamous-Cell Carcinoma of the Head and Neck. *The New England journal of medicine* 375:1856-1867.

Finlay, D., and D.A. Cantrell. 2011. Metabolism, migration and memory in cytotoxic T cells. *Nature reviews. Immunology* 11:109-117.

Fourcade, J., Z. Sun, M. Benallaoua, P. Guillaume, I.F. Luescher, C. Sander, J.M. Kirkwood, V. Kuchroo, and H.M. Zarour. 2010. Upregulation of Tim-3 and PD-1 expression is associated with tumor antigen-specific CD8+ T cell dysfunction in melanoma patients. *The Journal of experimental medicine* 207:2175-2186.

Fox, C.J., P.S. Hammerman, and C.B. Thompson. 2005. Fuel feeds function: energy metabolism and the T-cell response. *Nature reviews. Immunology* 5:844-852.

Frecha, C., C. Costa, D. Negre, E. Gauthier, S.J. Russell, F.L. Cosset, and E. Verhoeyen. 2008. Stable transduction of quiescent T cells without induction of cycle progression by a novel lentiviral vector pseudotyped with measles virus glycoproteins. *Blood* 112:4843-4852.

Freeley, M., and A. Long. 2013. The two hit hypothesis: an improved method for siRNA-mediated gene silencing in stimulated primary human T cells. *Journal of immunological methods* 396:116-127.

Gaffen, S.L., and K.D. Liu. 2004. Overview of interleukin-2 function, production and clinical applications. *Cytokine* 28:109-123.

Gaj, T., C.A. Gersbach, and C.F. Barbas, 3rd. 2013. ZFN, TALEN, and CRISPR/Cas-based methods for genome engineering. *Trends Biotechnol* 31:397-405.

Garon, E.B., N.A. Rizvi, R. Hui, N. Leighl, A.S. Balmanoukian, J.P. Eder, A. Patnaik, C. Aggarwal, M. Gubens, L. Horn, E. Carcereny, M.-J. Ahn, E. Felip, J.-S. Lee, M.D. Hellmann, O. Hamid, J.W. Goldman, J.-C. Soria, M. Dolled-Filhart, R.Z. Rutledge, J. Zhang, J.K. Lunceford, R. Rangwala, G.M. Lubiniecki, C. Roach, K. Emancipator, and L. Gandhi. 2015. Pembrolizumab for the Treatment of Non–Small-Cell Lung Cancer. *New England Journal of Medicine* 372:2018-2028.

Gett, A.V., F. Sallusto, A. Lanzavecchia, and J. Geginat. 2003. T cell fitness determined by signal strength. *Nature immunology* 4:355-360.

Giuroiu, I., and J. Weber. 2017. Novel Checkpoints and Cosignaling Molecules in Cancer Immunotherapy. *Cancer J* 23:23-31.

Gresch, O., F.B. Engel, D. Nesic, T.T. Tran, H.M. England, E.S. Hickman, I. Körner, L. Gan, S. Chen, and S. Castro-Obregon. 2004. New non-viral method for gene transfer into primary cells. *Methods* 33:151-163.

Gruener, N.H., F. Lechner, M.-C. Jung, H. Diepolder, T. Gerlach, G. Lauer, B. Walker, J. Sullivan, R. Phillips, and G.R. Pape. 2001. Sustained dysfunction of antiviral CD8+ T lymphocytes after infection with hepatitis C virus. *Journal of virology* 75:5550-5558.

Grupp, S.A., M. Kalos, D. Barrett, R. Aplenc, D.L. Porter, S.R. Rheingold, D.T. Teachey, A. Chew, B. Hauck, J.F. Wright, M.C. Milone, B.L. Levine, and C.H. June. 2013. Chimeric antigen receptor-modified T cells for acute lymphoid leukemia. *The New England journal of medicine* 368:1509-1518.

Gwiazda, K.S., A.E. Grier, J. Sahni, S.M. Burleigh, U. Martin, J.G. Yang, N.A. Popp, M.C. Krutein, I.F. Khan, K. Jacoby, M.C. Jensen, D.J. Rawlings, and A.M. Scharenberg. 2016. High efficiency CRISPR/Cas9-mediated gene editing in primary human T-cells using mutant adenoviral E4orf6/E1b55k "helper" proteins. *Molecular therapy : the journal of the American Society of Gene Therapy*

Hacein-Bey-Abina, S., C. Von Kalle, M. Schmidt, M.P. McCormack, N. Wulffraat, P. Leboulch, A. Lim, C.S. Osborne, R. Pawliuk, E. Morillon, R. Sorensen, A. Forster, P. Fraser, J.I. Cohen, G. de Saint Basile, I. Alexander, U. Wintergerst, T. Frebourg, A. Aurias, D. Stoppa-Lyonnet, S. Romana, I. Radford-Weiss, F. Gross, F. Valensi, E. Delabesse, E. Macintyre, F. Sigaux, J. Soulier, L.E. Leiva, M. Wissler, C. Prinz, T.H. Rabbitts, F. Le Deist, A. Fischer, and M. Cavazzana-Calvo. 2003. LMO2-associated clonal T cell proliferation in two patients after gene therapy for SCID-X1. *Science* 302:415-419.

Hamid, O., C. Robert, A. Daud, F.S. Hodi, W.J. Hwu, R. Kefford, J.D. Wolchok, P. Hersey, R.W. Joseph, J.S. Weber, R. Dronca, T.C. Gangadhar, A. Patnaik, H. Zarour, A.M. Joshua, K. Gergich, J. Elassaiss-Schaap, A. Algazi, C. Mateus, P. Boasberg, P.C. Tumeh, B. Chmielowski, S.W. Ebbinghaus, X.N. Li, S.P. Kang, and A. Ribas. 2013. Safety and tumor responses with lambrolizumab (anti-PD-1) in melanoma. *The New England journal of medicine* 369:134-144.

Hamm, A., N. Krott, I. Breibach, R. Blindt, and A.K. Bosserhoff. 2002. Efficient transfection method for primary cells. *Tissue engineering* 8:235-245.

Hannon, G.J. 2002. RNA interference. *Nature* 418:244-251.

Hatzoglou, M., J. Fernandez, I. Yaman, and E. Closs. 2004. Regulation of cationic amino acid transport: the story of the CAT-1 transporter. *Annu Rev Nutr* 24:377-399.

Hayashi, K., and N. Anzai. 2014. Role of LAT1 in the Promotion of Amino Acid Incorporation in Activated T Cells. *Critical Reviews™ in Immunology* 34:

Hayashi, K., and N. Anzai. 2017. Novel therapeutic approaches targeting L-type amino acid transporters for cancer treatment. *World J Gastrointest Oncol* 9:21-29.

Heberle, H., G.V. Meirelles, F.R. da Silva, G.P. Telles, and R. Minghim. 2015. InteractiVenn: a web-based tool for the analysis of sets through Venn diagrams. *BMC bioinformatics* 16:169.

Heckl, D., M.S. Kowalczyk, D. Yudovich, R. Belizaire, R.V. Puram, M.E. McConkey, A. Thielke, J.C. Aster, A. Regev, and B.L. Ebert. 2014. Generation of mouse models of myeloid malignancy with combinatorial genetic lesions using CRISPR-Cas9 genome editing. *Nature biotechnology* 32:941-946.

Heng, T.S., and M.W. Painter. 2008. The Immunological Genome Project: networks of gene expression in immune cells. *Nature immunology* 9:1091-1094.

Hicklin, D.J., F.M. Marincola, and S. Ferrone. 1999. HLA class I antigen downregulation in human cancers: T-cell immunotherapy revives an old story. *Molecular Medicine Today* 5:178-186.

Hodi, F.S., S.J. O'Day, D.F. McDermott, R.W. Weber, J.A. Sosman, J.B. Haanen, R. Gonzalez, C. Robert, D. Schadendorf, J.C. Hassel, W. Akerley, A.J.M. van den Eertwegh, J. Lutzky, P. Lorigan, J.M. Vaubel, G.P. Linette, D. Hogg, C.H. Ottensmeier, C. Lebbé, C. Peschel, I. Quirt, J.I. Clark, J.D. Wolchok, J.S. Weber, J. Tian, M.J. Yellin, G.M. Nichol, A. Hoos, and W.J. Urba. 2010. Improved Survival with Ipilimumab in Patients with Metastatic Melanoma. *New England Journal of Medicine* 363:711-723.

Hoelzinger, D.B., S.E. Smith, N. Mirza, A.L. Dominguez, S.Z. Manrique, and J. Lustgarten. 2010. Blockade of CCL1 inhibits T regulatory cell suppressive

function enhancing tumor immunity without affecting T effector responses. *Journal of immunology (Baltimore, Md. : 1950)* 184:6833-6842.

Howe, S.J., M.R. Mansour, K. Schwarzwaelder, C. Bartholomae, M. Hubank, H. Kempski, M.H. Brugman, K. Pike-Overzet, S.J. Chatters, D. de Ridder, K.C. Gilmour, S. Adams, S.I. Thornhill, K.L. Parsley, F.J. Staal, R.E. Gale, D.C. Linch, J. Bayford, L. Brown, M. Quaye, C. Kinnon, P. Ancliff, D.K. Webb, M. Schmidt, C. von Kalle, H.B. Gaspar, and A.J. Thrasher. 2008. Insertional mutagenesis combined with acquired somatic mutations causes leukemogenesis following gene therapy of SCID-X1 patients. *J Clin Invest* 118:3143-3150.

Huang, J., M. Brameshuber, X. Zeng, J. Xie, Q.J. Li, Y.H. Chien, S. Valitutti, and M.M. Davis. 2013. A single peptide-major histocompatibility complex ligand triggers digital cytokine secretion in CD4(+) T cells. *Immunity* 39:846-857.

Hukelmann, J.L., K.E. Anderson, L.V. Sinclair, K.M. Grzes, A.B. Murillo, P.T. Hawkins, L.R. Stephens, A.I. Lamond, and D.A. Cantrell. 2016. The cytotoxic T cell proteome and its shaping by the kinase mTOR. *Nature immunology* 17:104-112.

Hyatt, G., R. Melamed, R. Park, R. Seguritan, C. Laplace, L. Poirot, S. Zucchelli, R. Obst, M. Matos, E. Venanzi, A. Goldrath, L. Nguyen, J. Luckey, T. Yamagata, A. Herman, J. Jacobs, D. Mathis, and C. Benoist. 2006. Gene expression microarrays: glimpses of the immunological genome. *Nature immunology* 7:686-691.

Ikeda, H., L.J. Old, and R.D. Schreiber. 2002. The roles of IFN gamma in protection against tumor development and cancer immunoediting. *Cytokine Growth Factor Rev* 13:95-109.

Jackson, H.J., S. Rafiq, and R.J. Brentjens. 2016. Driving CAR T-cells forward. *Nature reviews. Clinical oncology* 13:370-383.

Jensen, M.C., L. Popplewell, L.J. Cooper, D. DiGiusto, M. Kalos, J.R. Ostberg, and S.J. Forman. 2010. Antitransgene rejection responses contribute to attenuated persistence of adoptively transferred CD20/CD19-specific chimeric antigen receptor redirected T cells in humans. *Biology of blood and marrow transplantation : journal of the American Society for Blood and Marrow Transplantation* 16:1245-1256.

Jiang, Y., Y. Li, and B. Zhu. 2015. T-cell exhaustion in the tumor microenvironment. *Cell Death Dis* 6:e1792.

Jin, H.T., A.C. Anderson, W.G. Tan, E.E. West, S.J. Ha, K. Araki, G.J. Freeman, V.K. Kuchroo, and R. Ahmed. 2010. Cooperation of Tim-3 and PD-1 in CD8 T-cell exhaustion during chronic viral infection. *Proceedings of the National Academy of Sciences of the United States of America* 107:14733-14738.

Joffre, O.P., E. Segura, A. Savina, and S. Amigorena. 2012. Cross-presentation by dendritic cells. *Nature reviews. Immunology* 12:557-569.

John, L.B., C. Devaud, C.P. Duong, C.S. Yong, P.A. Beavis, N.M. Haynes, M.T. Chow, M.J. Smyth, M.H. Kershaw, and P.K. Darcy. 2013a. Anti-PD-1 antibody therapy potently enhances the eradication of established tumors by gene-modified T cells. *Clinical cancer research* 19:5636-5646.

John, L.B., C. Devaud, C.P. Duong, C.S. Yong, P.A. Beavis, N.M. Haynes, M.T. Chow, M.J. Smyth, M.H. Kershaw, and P.K. Darcy. 2013b. Anti-PD-1 antibody therapy potently enhances the eradication of established tumors by gene-modified T cells. *Clinical cancer research : an official journal of the American Association for Cancer Research* 19:5636-5646.

June, C.H., B.R. Blazar, and J.L. Riley. 2009. Engineering lymphocyte subsets: tools, trials and tribulations. *Nature reviews. Immunology* 9:704-716.

Kabadi, A.M., D.G. Ousterout, I.B. Hilton, and C.A. Gersbach. 2014. Multiplex CRISPR/Cas9-based genome engineering from a single lentiviral vector. *Nucleic acids research* 42:e147.

Kaech, S.M., S. Hemby, E. Kersh, and R. Ahmed. 2002. Molecular and functional profiling of memory CD8 T cell differentiation. *Cell* 111:837-851.

Kalliolias, G.D., and L.B. Ivashkiv. 2016. TNF biology, pathogenic mechanisms and emerging therapeutic strategies. *Nat Rev Rheumatol* 12:49-62.

Kalos, M., B.L. Levine, D.L. Porter, S. Katz, S.A. Grupp, A. Bagg, and C.H. June. 2011. T cells with chimeric antigen receptors have potent antitumor effects and can establish memory in patients with advanced leukemia. *Science translational medicine* 3:95ra73.

Karwacz, K., C. Bricogne, D. MacDonald, F. Arce, C.L. Bennett, M. Collins, and D. Escors. 2011. PD-L1 co-stimulation contributes to ligand-induced T cell receptor down-modulation on CD8(+) T cells. *EMBO Molecular Medicine* 3:581-592.

Kawalekar, O.U., R.S. O'Connor, J.A. Fraietta, L. Guo, S.E. McGettigan, A.D. Posey, Jr., P.R. Patel, S. Guedan, J. Scholler, B. Keith, N.W. Snyder, I.A. Blair, M.C. Milone, and C.H. June. 2016. Distinct Signaling of Coreceptors Regulates Specific Metabolism Pathways and Impacts Memory Development in CAR T Cells. *Immunity* 44:380-390.

Keir, M.E., M.J. Butte, G.J. Freeman, and A.H. Sharpe. 2008. PD-1 and its ligands in tolerance and immunity. *Annu. Rev. Immunol.* 26:677-704.

Kershaw, M.H., J.A. Westwood, and P.K. Darcy. 2013. Gene-engineered T cells for cancer therapy. *Nature reviews. Cancer* 13:525-541.

Kim, H., and J.S. Kim. 2014. A guide to genome engineering with programmable nucleases. *Nature reviews. Genetics* 15:321-334.

Klenerman, P., and R. Thimme. 2012. T cell responses in hepatitis C: the good, the bad and the unconventional. *Gut* 61:1226-1234.

Kochenderfer, J.N., M.E. Dudley, S.A. Feldman, W.H. Wilson, D.E. Spaner, I. Maric, M. Stetler-Stevenson, G.Q. Phan, M.S. Hughes, R.M. Sherry, J.C. Yang, U.S. Kammula, L. Devillier, R. Carpenter, D.A. Nathan, R.A. Morgan, C. Laurencot, and S.A. Rosenberg. 2012. B-cell depletion and remissions of malignancy along with cytokine-associated toxicity in a clinical trial of anti-CD19 chimeric-antigen-receptor-transduced T cells. *Blood* 119:2709-2720.

Korin, Y.D., and J.A. Zack. 1998. Progression to the G1b phase of the cell cycle is required for completion of human immunodeficiency virus type 1 reverse transcription in T cells. *Journal of virology* 72:3161-3168.

Korin, Y.D., and J.A. Zack. 1999. Nonproductive human immunodeficiency virus type 1 infection in nucleoside-treated G0 lymphocytes. *Journal of virology* 73:6526-6532.

Kuvibidila, S., R.P. Warrier, and B. Surendra Baliga. 2003. An overview of the role of iron in T cell activation. *The Journal of Trace Elements in Experimental Medicine* 16:219-225.

Lakshmi Narendra, B., K. Eshvendar Reddy, S. Shantikumar, and S. Ramakrishna. 2013. Immune system: a double-edged sword in cancer. *Inflammation research : official journal of the European Histamine Research Society ... [et al.]* 62:823-834.

Lamers, C.H., R.A. Willemsen, B.A. Luider, R. Debets, and R.L. Bolhuis. 2002. Protocol for gene transduction and expansion of human T lymphocytes for clinical immunogene therapy of cancer. *Cancer gene therapy* 9:613-623.

Larkin, J., V. Chiarion-Sileni, R. Gonzalez, J.J. Grob, C.L. Cowey, C.D. Lao, D. Schadendorf, R. Dummer, M. Smylie, P. Rutkowski, P.F. Ferrucci, A. Hill, J. Wagstaff, M.S. Carlino, J.B. Haanen, M. Maio, I. Marquez-Rodas, G.A. McArthur, P.A. Ascierto, G.V. Long, M.K. Callahan, M.A. Postow, K. Grossmann, M. Sznol, B. Dreno, L. Bastholt, A. Yang, L.M. Rollin, C. Horak, F.S. Hodi, and J.D. Wolchok. 2015. Combined Nivolumab and Ipilimumab or Monotherapy in Untreated Melanoma. *New England Journal of Medicine* 373:23-34.

Leishman, A.J., O.V. Naidenko, A. Attinger, F. Koning, C.J. Lena, Y. Xiong, H.C. Chang, E. Reinherz, M. Kronenberg, and H. Cheroutre. 2001. T cell responses modulated through interaction between CD8alphaalpha and the nonclassical MHC class I molecule, TL. *Science* 294:1936-1939.

Li, S., T. Miao, M. Sebastian, P. Bhullar, E. Ghaffari, M. Liu, A.L. Symonds, and P. Wang. 2012. The transcription factors Egr2 and Egr3 are essential for the control of inflammation and antigen-induced proliferation of B and T cells. *Immunity* 37:685-696.

Liechtenstein, T., N. Perez-Janices, and D. Escors. 2013. Lentiviral vectors for cancer immunotherapy and clinical applications. *Cancers (Basel)* 5:815-837.

Lin, L., S.W. Yee, R.B. Kim, and K.M. Giacomini. 2015. SLC transporters as therapeutic targets: emerging opportunities. *Nat Rev Drug Discov* 14:543-560.

Lipson, E.J., P.M. Forde, H.J. Hammers, L.A. Emens, J.M. Taube, and S.L. Topalian. 2015. Antagonists of PD-1 and PD-L1 in Cancer Treatment. *Semin Oncol* 42:587-600.

Liu, H., M. Rhodes, D.L. Wiest, and D.A. Vignali. 2000. On the dynamics of TCR:CD3 complex cell surface expression and downmodulation. *Immunity* 13:665-675.

Liu, L., C. Johnson, S. Fujimura, F. Teque, and J.A. Levy. 2011. Transfection optimization for primary human CD8+ cells. *Journal of immunological methods* 372:22-29.

Maaten, L.v.d. 2008. Visualizing Data using t-SNE. *Journal of Machine Learning Research*

Makkouk, A., C. Chester, and H.E. Kohrt. 2016. Rationale for anti-CD137 cancer immunotherapy. *Eur J Cancer* 54:112-119.

Mariotti, S., and R. Nisini. 2009. Generation of human T cell clones. *Methods in molecular biology (Clifton, N.J.)* 514:65-93.

Matherly, L.H., Z. Hou, and Y. Deng. 2007. Human reduced folate carrier: translation of basic biology to cancer etiology and therapy. *Cancer metastasis reviews* 26:111-128.

Mattson, E., L. Xu, L. Li, G.E. Liu, and Z. Xiao. 2014. Transcriptome profiling of CTLs regulated by rapamycin using RNA-Seq. *Immunogenetics* 66:625-633.

McElrath, M.J., S.C. De Rosa, Z. Moodie, S. Dubey, L. Kierstead, H. Janes, O.D. Defawe, D.K. Carter, J. Hural, R. Akondy, S.P. Buchbinder, M.N. Robertson, D.V. Mehrotra, S.G. Self, L. Corey, J.W. Shiver, and D.R. Casimiro. 2008. HIV-1 vaccine-induced immunity in the test-of-concept Step Study: a case-cohort analysis. *Lancet* 372:1894-1905.

McMichael, A.J. 2003. Principles of immunology. In Oxford Textbook of Medicine. D.A. In Warrell, Cox, T. M., Firth, J. D. and Benz, E. J. (Ed.), editor Oxford University Press, Oxford. 131–144.

McMichael, A.J., P. Borrow, G.D. Tomaras, N. Goonetilleke, and B.F. Haynes. 2010. The immune response during acute HIV-1 infection: clues for vaccine development. *Nature reviews. Immunology* 10:11-23.

McMichael, A.J., A. Ting, H.J. Zweerink, and B.A. Askonas. 1977. HLA restriction of cell-mediated lysis of influenza virus-infected human cells. *Nature* 270:524-526.

McNab, F., K. Mayer-Barber, A. Sher, A. Wack, and A. O'Garra. 2015. Type I interferons in infectious disease. *Nature reviews. Immunology* 15:87-103.

Mestas, J., and C.C. Hughes. 2004. Of mice and not men: differences between mouse and human immunology. *The Journal of Immunology* 172:2731-2738.

Mi, H., X. Huang, A. Muruganujan, H. Tang, C. Mills, D. Kang, and P.D. Thomas. 2017. PANTHER version 11: expanded annotation data from Gene Ontology and Reactome pathways, and data analysis tool enhancements. *Nucleic acids research* 45:D183-189.

Mi, H., A. Muruganujan, J.T. Casagrande, and P.D. Thomas. 2013. Large-scale gene function analysis with the PANTHER classification system. *Nature protocols* 8:1551-1566.

Michot, J.M., C. Bigenwald, S. Champiat, M. Collins, F. Carbonnel, S. Postel-Vinay, A. Berdelou, A. Varga, R. Bahleda, A. Hollebecque, C. Massard, A. Fuerea, V. Ribrag, A. Gazzah, J.P. Armand, N. Amellal, E. Angevin, N. Noel, C. Boutros, C. Mateus, C. Robert, J.C. Soria, A. Marabelle, and O. Lambotte. 2016. Immune-related adverse events with immune checkpoint blockade: a comprehensive review. *Eur J Cancer* 54:139-148.

Miller, D.G., M.A. Adam, and A.D. Miller. 1990. Gene transfer by retrovirus vectors occurs only in cells that are actively replicating at the time of infection. *Mol Cell Biol* 10:4239-4242.

Moebius, U., G. Kober, A.L. Griscelli, T. Hercend, and S.C. Meuer. 1991. Expression of different CD8 isoforms on distinct human lymphocyte subpopulations. *Eur J Immunol* 21:1793-1800.

Montini, E., D. Cesana, M. Schmidt, F. Sanvito, M. Ponzoni, C. Bartholomae, L. Sergi Sergi, F. Benedicenti, A. Ambrosi, C. Di Serio, C. Doglioni, C. von Kalle, and L. Naldini. 2006. Hematopoietic stem cell gene transfer in a tumor-prone mouse model uncovers low genotoxicity of lentiviral vector integration. *Nature biotechnology* 24:687-696.

Motzer, R.J., B. Escudier, D.F. McDermott, S. George, H.J. Hammers, S. Srinivas, S.S. Tykodi, J.A. Sosman, G. Procopio, E.R. Plimack, D. Castellano, T.K. Choueiri, H. Gurney, F. Donskov, P. Bono, J. Wagstaff, T.C. Gauler, T. Ueda, Y. Tomita, F.A. Schutz, C. Kollmannsberger, J. Larkin, A. Ravaud, J.S. Simon, L.-A. Xu, I.M. Waxman, and P. Sharma. 2015. Nivolumab versus Everolimus in Advanced Renal-Cell Carcinoma. *New England Journal of Medicine* 373:1803-1813.

Motzer, R.J., B.I. Rini, D.F. McDermott, B.G. Redman, T.M. Kuzel, M.R. Harrison, U.N. Vaishampayan, H.A. Drabkin, S. George, and T.F. Logan.

2014. Nivolumab for metastatic renal cell carcinoma: results of a randomized phase II trial. *Journal of clinical oncology* 33:1430-1437.

Mou, D., J. Espinosa, D.J. Lo, and A.D. Kirk. 2014. CD28 negative T cells: is their loss our gain? *Am J Transplant* 14:2460-2466.

Murphy, K., C. Janeway, P. Travers, M. Walport, A. Mowat, and C. Weaver. 2012a. Antigen Presentation to T Lymphocytes. In Janeway's immunobiology. Garland Science, New York. 207.

Murphy, K., C. Janeway, P. Travers, M. Walport, A. Mowat, and C. Weaver. 2012b. Antigen Recognition by B-cell and T-cell Receptors. In Janeway's immunobiology. Garland Science, New York. 139.

Murphy, K., C. Janeway, P. Travers, M. Walport, A. Mowat, and C. Weaver. 2012c. The Generation of Lymphocyte Antigen Receptors. In Janeway's immunobiology. Garland Science, New York. 169-172.

Murphy, K., C. Janeway, P. Travers, M. Walport, A. Mowat, and C. Weaver. 2012d. T Cell-Mediated Immunity. In Janeway's immunobiology. Garland Science, New York. 335-337.

Naldini, L., U. Blomer, P. Gallay, D. Ory, R. Mulligan, F.H. Gage, I.M. Verma, and D. Trono. 1996. In vivo gene delivery and stable transduction of nondividing cells by a lentiviral vector. *Science* 272:263-267.

Neumann, E., M. Schaefer-Ridder, Y. Wang, and P. Hofschneider. 1982. Gene transfer into mouse lyoma cells by electroporation in high electric fields. *The EMBO journal* 1:841.

Newick, K., E. Moon, and S.M. Albelda. 2016. Chimeric antigen receptor T-cell therapy for solid tumors. *Mol Ther Oncolytics* 3:16006.

Nirschl, C.J., and C.G. Drake. 2013. Molecular pathways: coexpression of immune checkpoint molecules: signaling pathways and implications for cancer immunotherapy. *Clinical cancer research : an official journal of the American Association for Cancer Research* 19:4917-4924.

Norment, A.M., and D.R. Littman. 1988. A second subunit of CD8 is expressed in human T cells. *Embo j* 7:3433-3439.

Okazaki, T., S. Chikuma, Y. Iwai, S. Fagarasan, and T. Honjo. 2013. A rheostat for immune responses: the unique properties of PD-1 and their advantages for clinical application. *Nature immunology* 14:1212-1218.

Okazaki, T., A. Maeda, H. Nishimura, T. Kurosaki, and T. Honjo. 2001. PD-1 immunoreceptor inhibits B cell receptor-mediated signaling by recruiting src homology 2-domain-containing tyrosine phosphatase 2 to phosphotyrosine. *Proceedings of the National Academy of Sciences of the United States of America* 98:13866-13871.

Oldham, R.A., E.M. Berinstein, and J.A. Medin. 2015. Lentiviral vectors in cancer immunotherapy. *Immunotherapy* 7:271-284.

Pardoll, D.M. 2012. The blockade of immune checkpoints in cancer immunotherapy. *Nature reviews. Cancer* 12:252-264.

Pecot, C.V., G.A. Calin, R.L. Coleman, G. Lopez-Berestein, and A.K. Sood. 2011. RNA interference in the clinic: challenges and future directions. *Nature reviews. Cancer* 11:59-67.

Pinilla-Tenas, J.J., B.K. Sparkman, A. Shawki, A.C. Illing, C.J. Mitchell, N. Zhao, J.P. Liuzzi, R.J. Cousins, M.D. Knutson, and B. Mackenzie. 2011. Zip14 is a complex broad-scope metal-ion transporter whose functional properties support roles in the cellular uptake of zinc and nontransferrin-bound iron. *Am J Physiol Cell Physiol* 301:C862-871.

Porter, D.L., W.T. Hwang, N.V. Frey, S.F. Lacey, P.A. Shaw, A.W. Loren, A. Bagg, K.T. Marcucci, A. Shen, V. Gonzalez, D. Ambrose, S.A. Grupp, A. Chew, Z. Zheng, M.C. Milone, B.L. Levine, J.J. Melenhorst, and C.H. June. 2015. Chimeric antigen receptor T cells persist and induce sustained remissions in relapsed refractory chronic lymphocytic leukemia. *Science translational medicine* 7:303ra139.

Porter, D.L., B.L. Levine, M. Kalos, A. Bagg, and C.H. June. 2011. Chimeric antigen receptor-modified T cells in chronic lymphoid leukemia. *The New England journal of medicine* 365:725-733.

Rabinovich, G.A., D. Gabrilovich, and E.M. Sotomayor. 2007. Immunosuppressive strategies that are mediated by tumor cells. *Annual review of immunology* 25:267-296.

Ran, F.A., P.D. Hsu, J. Wright, V. Agarwala, D.A. Scott, and F. Zhang. 2013. Genome engineering using the CRISPR-Cas9 system. *Nature protocols* 8:2281-2308.

Rapoport, A.P., E.A. Stadtmauer, G.K. Binder-Scholl, O. Goloubeva, D.T. Vogl, S.F. Lacey, A.Z. Badros, A. Garfall, B. Weiss, J. Finklestein, I. Kulikovskaya, S.K. Sinha, S. Kronsberg, M. Gupta, S. Bond, L. Melchiori, J.E. Brewer, A.D. Bennett, A.B. Gerry, N.J. Pumphrey, D. Williams, H.K. Tayton- Martin, L. Ribeiro, T. Holdich, S. Yanovich, N. Hardy, J. Yared, N. Kerr, S. Philip, S. Westphal, D.L. Siegel, B.L. Levine, B.K. Jakobsen, M. Kalos, and C.H. June. 2015a. NY-ESO-1-specific TCR-engineered T cells mediate sustained antigen-specific antitumor effects in myeloma. *Nature medicine* 21:914-921.

Rapoport, A.P., E.A. Stadtmauer, G.K. Binder-Scholl, O. Goloubeva, D.T. Vogl, S.F. Lacey, A.Z. Badros, A. Garfall, B. Weiss, J. Finklestein, I. Kulikovskaya, S.K. Sinha, S. Kronsberg, M. Gupta, S. Bond, L. Melchiori, J.E. Brewer, A.D. Bennett, A.B. Gerry, N.J. Pumphrey, D. Williams, H.K. Tayton-Martin, L. Ribeiro, T. Holdich, S. Yanovich, N. Hardy, J. Yared, N. Kerr, S. Philip, S. Westphal, D.L. Siegel, B.L. Levine, B.K. Jakobsen, M.

Kalos, and C.H. June. 2015b. NY-ESO-1-specific TCR-engineered T cells mediate sustained antigen-specific antitumor effects in myeloma. *Nature medicine* 21:914-921.

Ren, W., G. Liu, J. Yin, B. Tan, G. Wu, F.W. Bazer, Y. Peng, and Y. Yin. 2017. Amino-acid transporters in T-cell activation and differentiation. *Cell Death Dis* 8:e2757.

Restifo, N.P. 2014. Big bang theory of stem-like T cells confirmed. *Blood* 124:476-477.

Ritchie, M.E., B. Phipson, D. Wu, Y. Hu, C.W. Law, W. Shi, and G.K. Smyth. 2015. limma powers differential expression analyses for RNA-sequencing and microarray studies. *Nucleic acids research* 43:e47.

Robbins, P.F., S.H. Kassim, T.L. Tran, J.S. Crystal, R.A. Morgan, S.A. Feldman, J.C. Yang, M.E. Dudley, J.R. Wunderlich, R.M. Sherry, U.S. Kammula, M.S. Hughes, N.P. Restifo, M. Raffeld, C.C. Lee, Y.F. Li, M. El-Gamil, and S.A. Rosenberg. 2015. A pilot trial using lymphocytes genetically engineered with an NY-ESO-1-reactive T-cell receptor: long-term follow-up and correlates with response. *Clinical cancer research : an official journal of the American Association for Cancer Research* 21:1019-1027.

Robbins, P.F., R.A. Morgan, S.A. Feldman, J.C. Yang, R.M. Sherry, M.E. Dudley, J.R. Wunderlich, A.V. Nahvi, L.J. Helman, C.L. Mackall, U.S. Kammula, M.S. Hughes, N.P. Restifo, M. Raffeld, C.C. Lee, C.L. Levy, Y.F. Li, M. El-Gamil, S.L. Schwarz, C. Laurencot, and S.A. Rosenberg. 2011. Tumor regression in patients with metastatic synovial cell sarcoma and melanoma using genetically engineered lymphocytes reactive with NY-ESO-1. *J Clin Oncol* 29:917-924.

Robert, C., G.V. Long, B. Brady, C. Dutriaux, M. Maio, L. Mortier, J.C. Hassel, P. Rutkowski, C. McNeil, E. Kalinka-Warzocha, K.J. Savage, M.M. Hernberg, C. Lebbe, J. Charles, C. Mihalcioiu, V. Chiarion-Sileni, C. Mauch, F. Cognetti, A. Arance, H. Schmidt, D. Schadendorf, H. Gogas, L. Lundgren-Eriksson, C. Horak, B. Sharkey, I.M. Waxman, V. Atkinson, and P.A. Ascierto. 2015a. Nivolumab in previously untreated melanoma without BRAF mutation. *The New England journal of medicine* 372:320-330.

Robert, C., J. Schachter, G.V. Long, A. Arance, J.J. Grob, L. Mortier, A. Daud, M.S. Carlino, C. McNeil, M. Lotem, J. Larkin, P. Lorigan, B. Neyns, C.U. Blank, O. Hamid, C. Mateus, R. Shapira-Frommer, M. Kosh, H. Zhou, N. Ibrahim, S. Ebbinghaus, A. Ribas, and K.-. investigators. 2015b. Pembrolizumab versus Ipilimumab in Advanced Melanoma. *The New England journal of medicine* 372:2521-2532.

Robinson, J., A. Malik, P. Parham, J.G. Bodmer, and S.G. Marsh. 2000. IMGT/HLA database--a sequence database for the human major histocompatibility complex. *Tissue antigens* 55:280-287.

Roe, T., T.C. Reynolds, G. Yu, and P.O. Brown. 1993. Integration of murine leukemia virus DNA depends on mitosis. *Embo j* 12:2099-2108.

Roederer, M., J.L. Nozzi, and M.C. Nason. 2011. SPICE: exploration and analysis of post-cytometric complex multivariate datasets. *Cytometry A* 79:167-174.

Romero, D. 2016. Immunotherapy: PD-1 says goodbye, TIM-3 says hello. *Nature reviews. Clinical oncology* 13:202-203.

Rosenberg, J.E., J. Hoffman-Censits, T. Powles, M.S. van der Heijden, A.V. Balar, A. Necchi, N. Dawson, P.H. O'Donnell, A. Balmanoukian, Y. Loriot, S. Srinivas, M.M. Retz, P. Grivas, R.W. Joseph, M.D. Galsky, M.T. Fleming, D.P. Petrylak, J.L. Perez-Gracia, H.A. Burris, D. Castellano, C. Canil, J. Bellmunt, D. Bajorin, D. Nickles, R. Bourgon, G.M. Frampton, N. Cui, S. Mariathasan, O. Abidoye, G.D. Fine, and R. Dreicer. 2016. Atezolizumab in patients with locally advanced and metastatic urothelial carcinoma who have progressed following treatment with platinum-based chemotherapy: a single-arm, multicentre, phase 2 trial. *Lancet* 387:1909-1920.

Rosenberg, S.A., B.S. Packard, P.M. Aebersold, D. Solomon, S.L. Topalian, S.T. Toy, P. Simon, M.T. Lotze, J.C. Yang, C.A. Seipp, and et al. 1988. Use of tumor-infiltrating lymphocytes and interleukin-2 in the immunotherapy of patients with metastatic melanoma. A preliminary report. *The New England journal of medicine* 319:1676-1680.

Rosenberg, S.A., and N.P. Restifo. 2015. Adoptive cell transfer as personalized immunotherapy for human cancer. *Science* 348:62-68.

Rosenblum, M.D., K.A. Remedios, and A.K. Abbas. 2015. Mechanisms of human autoimmunity. *J Clin Invest* 125:2228-2233.

Saeed, A.I., V. Sharov, J. White, J. Li, W. Liang, N. Bhagabati, J. Braisted, M. Klapa, T. Currier, M. Thiagarajan, A. Sturn, M. Snuffin, A. Rezantsev, D. Popov, A. Ryltsov, E. Kostukovich, I. Borisovsky, Z. Liu, A. Vinsavich, V. Trush, and J. Quackenbush. 2003. TM4: a free, open-source system for microarray data management and analysis. *BioTechniques* 34:374-378.

Saez-Cirion, A., C. Lacabaratz, O. Lambotte, P. Versmisse, A. Urrutia, F. Boufassa, F. Barre-Sinoussi, J.F. Delfraissy, M. Sinet, G. Pancino, A. Venet, and E.P.H.I.V.C.S.G. Agence Nationale de Recherches sur le Sida. 2007. HIV controllers exhibit potent CD8 T cell capacity to suppress HIV infection ex vivo and peculiar cytotoxic T lymphocyte activation phenotype. *Proceedings of the National Academy of Sciences of the United States of America* 104:6776-6781.

Safford, M., S. Collins, M.A. Lutz, A. Allen, C.T. Huang, J. Kowalski, A. Blackford, M.R. Horton, C. Drake, R.H. Schwartz, and J.D. Powell. 2005. Egr-2 and Egr-3 are negative regulators of T cell activation. *Nature immunology* 6:472-480.

Saito, T., T. Yokosuka, and A. Hashimoto-Tane. 2010. Dynamic regulation of T cell activation and co-stimulation through TCR-microclusters. *FEBS Lett* 584:4865-4871.

Sander, J.D., and J.K. Joung. 2014. CRISPR-Cas systems for editing, regulating and targeting genomes. *Nature biotechnology* 32:347-355.

Schneider, H., and C.E. Rudd. 2014. Diverse mechanisms regulate the surface expression of immunotherapeutic target ctla-4. *Frontiers in immunology* 5:619.

Schroder, K., P.J. Hertzog, T. Ravasi, and D.A. Hume. 2004. Interferon-gamma: an overview of signals, mechanisms and functions. *J Leukoc Biol* 75:163-189.

Schumann, K., S. Lin, E. Boyer, D.R. Simeonov, M. Subramaniam, R.E. Gate, G.E. Haliburton, C.J. Ye, J.A. Bluestone, J.A. Doudna, and A. Marson. 2015. Generation of knock-in primary human T cells using Cas9 ribonucleoproteins. *Proceedings of the National Academy of Sciences of the United States of America*

Shay, T., V. Jojic, O. Zuk, K. Rothamel, D. Puyraimond-Zemmour, T. Feng, E. Wakamatsu, C. Benoist, D. Koller, and A. Regev. 2013. Conservation and divergence in the transcriptional programs of the human and mouse immune systems. *Proceedings of the National Academy of Sciences* 110:2946-2951.

Shinohara, T., M. Taniwaki, Y. Ishida, M. Kawaichi, and T. Honjo. 1994. Structure and chromosomal localization of the human PD-1 gene (PDCD1). *Genomics* 23:704-706.

Sinclair, L.V., J. Rolf, E. Emslie, Y.B. Shi, P.M. Taylor, and D.A. Cantrell. 2013. Control of amino-acid transport by antigen receptors coordinates the metabolic reprogramming essential for T cell differentiation. *Nature immunology* 14:500-508.

Snell, L.M., G.H. Lin, A.J. McPherson, T.J. Moraes, and T.H. Watts. 2011. T-cell intrinsic effects of GITR and 4-1BB during viral infection and cancer immunotherapy. *Immunol Rev* 244:197-217.

Stanley, J.S., D.M. Mock, J.B. Griffin, and J. Zempleni. 2002. Biotin Uptake into Human Peripheral Blood Mononuclear Cells Increases Early in the Cell Cycle, Increasing Carboxylase Activities. *The Journal of nutrition* 132:1854-1859.

Stein, S., M.G. Ott, S. Schultze-Strasser, A. Jauch, B. Burwinkel, A. Kinner, M. Schmidt, A. Kramer, J. Schwable, H. Glimm, U. Koehl, C. Preiss, C. Ball, H. Martin, G. Gohring, K. Schwarzwaelder, W.K. Hofmann, K. Karakaya, S. Tchatchou, R. Yang, P. Reinecke, K. Kuhlcke, B. Schlegelberger, A.J. Thrasher, D. Hoelzer, R. Seger, C. von Kalle, and M. Grez. 2010. Genomic instability and myelodysplasia with monosomy 7 consequent to

EVI1 activation after gene therapy for chronic granulomatous disease. *Nature medicine* 16:198-204.

Stemberger, C., P. Graef, M. Odendahl, J. Albrecht, G. Dössinger, F. Anderl, V.R. Buchholz, G. Gasteiger, M. Schiemann, G.U. Grigoleit, F.R. Schuster, A. Borkhardt, B. Versluys, T. Tonn, E. Seifried, H. Einsele, L. Germeroth, D.H. Busch, and M. Neuenhahn. 2014. Lowest numbers of primary CD8 T cells can reconstitute protective immunity upon adoptive immunotherapy. *Blood* 124:628.

Stevenson, M., T. Stanwick, M. Dempsey, and C. Lamonica. 1990. HIV-1 replication is controlled at the level of T cell activation and proviral integration. *The EMBO journal* 9:1551.

Stewart-Jones, G.B., A.J. McMichael, J.I. Bell, D.I. Stuart, and E.Y. Jones. 2003. A structural basis for immunodominant human T cell receptor recognition. *Nature immunology* 4:657-663.

Su, S., B. Hu, J. Shao, B. Shen, J. Du, Y. Du, J. Zhou, L. Yu, L. Zhang, F. Chen, H. Sha, L. Cheng, F. Meng, Z. Zou, X. Huang, and B. Liu. 2016. CRISPR-Cas9 mediated efficient PD-1 disruption on human primary T cells from cancer patients. *Sci Rep* 6:20070.

Takeuchi, A., Y. Itoh, A. Takumi, C. Ishihara, N. Arase, T. Yokosuka, H. Koseki, S. Yamasaki, Y. Takai, J. Miyoshi, K. Ogasawara, and T. Saito. 2009. CRTAM confers late-stage activation of CD8+ T cells to regulate retention within lymph node. *Journal of immunology (Baltimore, Md. : 1950)* 183:4220-4228.

Tauriainen, J., L. Scharf, J. Frederiksen, A. Naji, H.G. Ljunggren, A. Sonnerborg, O. Lund, G. Reyes-Teran, F.M. Hecht, S.G. Deeks, M.R. Betts, M. Buggert, and A.C. Karlsson. 2017. Perturbed CD8+ T cell TIGIT/CD226/PVR axis despite early initiation of antiretroviral treatment in HIV infected individuals. *Sci Rep* 7:40354.

Timosenko, E., H. Ghadbane, J.D. Silk, D. Shepherd, U. Gileadi, L.J. Howson, R. Laynes, Q. Zhao, R.L. Strausberg, L.R. Olsen, S. Taylor, F.M. Buffa, R. Boyd, and V. Cerundolo. 2016. Nutritional Stress Induced by Tryptophan-Degrading Enzymes Results in ATF4-Dependent Reprogramming of the Amino Acid Transporter Profile in Tumor Cells. *Cancer research* 76:6193-6204.

Tomiyama, H., T. Matsuda, and M. Takiguchi. 2002. Differentiation of human CD8(+) T cells from a memory to memory/effector phenotype. *Journal of immunology (Baltimore, Md. : 1950)* 168:5538-5550.

Topalian, S.L., F.S. Hodi, J.R. Brahmer, S.N. Gettinger, D.C. Smith, D.F. McDermott, J.D. Powderly, R.D. Carvajal, J.A. Sosman, and M.B. Atkins. 2012a. Safety, activity, and immune correlates of anti–PD-1 antibody in cancer. *New England Journal of Medicine* 366:2443-2454.

Topalian, S.L., F.S. Hodi, J.R. Brahmer, S.N. Gettinger, D.C. Smith, D.F. McDermott, J.D. Powderly, R.D. Carvajal, J.A. Sosman, M.B. Atkins, P.D. Leming, D.R. Spigel, S.J. Antonia, L. Horn, C.G. Drake, D.M. Pardoll, L. Chen, W.H. Sharfman, R.A. Anders, J.M. Taube, T.L. McMiller, H. Xu, A.J. Korman, M. Jure-Kunkel, S. Agrawal, D. McDonald, G.D. Kollia, A. Gupta, J.M. Wigginton, and M. Sznol. 2012b. Safety, activity, and immune correlates of anti-PD-1 antibody in cancer. *The New England journal of medicine* 366:2443-2454.

Topalian, S.L., M. Sznol, D.F. McDermott, H.M. Kluger, R.D. Carvajal, W.H. Sharfman, J.R. Brahmer, D.P. Lawrence, M.B. Atkins, J.D. Powderly, P.D. Leming, E.J. Lipson, I. Puzanov, D.C. Smith, J.M. Taube, J.M. Wigginton, G.D. Kollia, A. Gupta, D.M. Pardoll, J.A. Sosman, and F.S. Hodi. 2014. Survival, durable tumor remission, and long-term safety in patients with advanced melanoma receiving nivolumab. *J Clin Oncol* 32:1020-1030.

Topalian, S.L., J.M. Taube, R.A. Anders, and D.M. Pardoll. 2016. Mechanism-driven biomarkers to guide immune checkpoint blockade in cancer therapy. *Nature reviews. Cancer* 16:275-287.

Townsend, A.R., J. Rothbard, F.M. Gotch, G. Bahadur, D. Wraith, and A.J. McMichael. 1986. The epitopes of influenza nucleoprotein recognized by cytotoxic T lymphocytes can be defined with short synthetic peptides. *Cell* 44:959-968.

Trautmann, L., L. Janbazian, N. Chomont, E.A. Said, S. Gimmig, B. Bessette, M.R. Boulassel, E. Delwart, H. Sepulveda, R.S. Balderas, J.P. Routy, E.K. Haddad, and R.P. Sekaly. 2006. Upregulation of PD-1 expression on HIV-specific CD8+ T cells leads to reversible immune dysfunction. *Nature medicine* 12:1198-1202.

Tscharke, D.C., N.P. Croft, P.C. Doherty, and N.L. La Gruta. 2015. Sizing up the key determinants of the CD8(+) T cell response. *Nature reviews. Immunology* 15:705-716.

Unutmaz, D., V.N. KewalRamani, S. Marmon, and D.R. Littman. 1999. Cytokine signals are sufficient for HIV-1 infection of resting human T lymphocytes. *The Journal of experimental medicine* 189:1735-1746.

Vacchelli, E., F. Aranda, N. Bloy, A. Buque, I. Cremer, A. Eggermont, W.H. Fridman, J. Fucikova, J. Galon, R. Spisek, L. Zitvogel, G. Kroemer, and L. Galluzzi. 2016. Trial Watch-Immunostimulation with cytokines in cancer therapy. *Oncoimmunology* 5:e1115942.

Valsecchi, M.E. 2015. Combined Nivolumab and Ipilimumab or Monotherapy in Untreated Melanoma. *The New England journal of medicine* 373:1270.

Vander Heiden, M.G., L.C. Cantley, and C.B. Thompson. 2009. Understanding the Warburg effect: the metabolic requirements of cell proliferation. *Science* 324:1029-1033.

Vantourout, P., and A. Hayday. 2013. Six-of-the-best: unique contributions of gammadelta T cells to immunology. *Nature reviews. Immunology* 13:88-100.

Verrey, F., E.I. Closs, C.A. Wagner, M. Palacin, H. Endou, and Y. Kanai. 2004. CATs and HATs: the SLC7 family of amino acid transporters. *Pflugers Arch* 447:532-542.

Vigna, E., and L. Naldini. 2000. Lentiviral vectors: excellent tools for experimental gene transfer and promising candidates for gene therapy. *The journal of gene medicine* 2:308-316.

Vremec, D., J. Pooley, H. Hochrein, L. Wu, and K. Shortman. 2000. CD4 and CD8 expression by dendritic cell subtypes in mouse thymus and spleen. *Journal of immunology (Baltimore, Md. : 1950)* 164:2978-2986.

Wang, C.Y., S. Jenkitkasemwong, S. Duarte, B.K. Sparkman, A. Shawki, B. Mackenzie, and M.D. Knutson. 2012. ZIP8 is an iron and zinc transporter whose cell-surface expression is up-regulated by cellular iron loading. *J Biol Chem* 287:34032-34043.

Wang, J., B. Chmielowski, J. Pellissier, R. Xu, K. Stevinson, and F.X. Liu. 2017. Cost-Effectiveness of Pembrolizumab Versus Ipilimumab in Ipilimumab-Naive Patients with Advanced Melanoma in the United States. *J Manag Care Spec Pharm* 23:184-194.

Wang, R., and D.R. Green. 2012. Metabolic checkpoints in activated T cells. *Nature immunology* 13:907-915.

Waugh, C., L. Sinclair, D. Finlay, J.R. Bayascas, and D. Cantrell. 2009. Phosphoinositide (3,4,5)-triphosphate binding to phosphoinositide-dependent kinase 1 regulates a protein kinase B/Akt signaling threshold that dictates T-cell migration, not proliferation. *Mol Cell Biol* 29:5952-5962.

Weber, J.S., S.J. Antonia, S.L. Topalian, D. Schadendorf, J.M. Larkin, M. Sznol, H.Y. Liu, I. Waxman, and C. Robert. 2015. Safety profile of nivolumab (NIVO) in patients (pts) with advanced melanoma (MEL): A pooled analysis. In American Society of Clinical Oncology.

Wherry, E.J. 2011. T cell exhaustion. *Nature immunology* 12:492-499.

Wherry, E.J., and M. Kurachi. 2015. Molecular and cellular insights into T cell exhaustion. *Nature reviews. Immunology* 15:486-499.

Williams, J.B., B.L. Horton, Y. Zheng, Y. Duan, J.D. Powell, and T.F. Gajewski. 2017. The EGR2 targets LAG-3 and 4-1BB describe and regulate dysfunctional antigen-specific CD8+ T cells in the tumor microenvironment. *The Journal of experimental medicine* 214:381-400.

Woo, S.R., M.E. Turnis, M.V. Goldberg, J. Bankoti, M. Selby, C.J. Nirschl, M.L. Bettini, D.M. Gravano, P. Vogel, C.L. Liu, S. Tangsombatvisit, J.F.

Grosso, G. Netto, M.P. Smeltzer, A. Chaux, P.J. Utz, C.J. Workman, D.M. Pardoll, A.J. Korman, C.G. Drake, and D.A. Vignali. 2012. Immune inhibitory molecules LAG-3 and PD-1 synergistically regulate T-cell function to promote tumoral immune escape. *Cancer research* 72:917-927.

Wu, Z., A.J. Macneil, R. Junkins, B. Li, J.N. Berman, and T.J. Lin. 2013. Mast cell FcepsilonRI-induced early growth response 2 regulates CC chemokine ligand 1-dependent CD4+ T cell migration. *Journal of immunology (Baltimore, Md. : 1950)* 190:4500-4507.

Xu, D., and M.E. Hemler. 2005. Metabolic activation-related CD147-CD98 complex. *Mol Cell Proteomics* 4:1061-1071.

Yao, S., and L. Chen. 2014. PD-1 as an immune modulatory receptor. *Cancer J* 20:262-264.

Yeh, J.H., S.S. Sidhu, and A.C. Chan. 2008. Regulation of a late phase of T cell polarity and effector functions by Crtam. *Cell* 132:846-859.

Yi, G., J.G. Choi, P. Bharaj, S. Abraham, Y. Dang, T. Kafri, O. Alozie, M.N. Manjunath, and P. Shankar. 2014. CCR5 Gene Editing of Resting CD4+ T Cells by Transient ZFN Expression From HIV Envelope Pseudotyped Nonintegrating Lentivirus Confers HIV-1 Resistance in Humanized Mice. *Molecular Therapy - Nucleic Acids* 3:e198.

Yokosuka, T., M. Takamatsu, W. Kobayashi-Imanishi, A. Hashimoto-Tane, M. Azuma, and T. Saito. 2012. Programmed cell death 1 forms negative costimulatory microclusters that directly inhibit T cell receptor signaling by recruiting phosphatase SHP2. *The Journal of experimental medicine* 209:1201-1217.

Young, L.S., P.F. Searle, D. Onion, and V. Mautner. 2006. Viral gene therapy strategies: from basic science to clinical application. *J Pathol* 208:299-318.

Yu, M., W.W. Lee, D. Tomar, S. Pryshchep, M. Czesnikiewicz-Guzik, D.L. Lamar, G. Li, K. Singh, L. Tian, C.M. Weyand, and J.J. Goronzy. 2011. Regulation of T cell receptor signaling by activation-induced zinc influx. *The Journal of experimental medicine* 208:775-785.

Zack, J., A. Haislip, P. Krogstad, and I. Chen. 1992. Incompletely reverse-transcribed human immunodeficiency virus type 1 genomes in quiescent cells can function as intermediates in the retroviral life cycle. *Journal of virology* 66:1717-1725.

Zhao, S., W.P. Fung-Leung, A. Bittner, K. Ngo, and X. Liu. 2014. Comparison of RNA-Seq and microarray in transcriptome profiling of activated T cells. *PloS one* 9:e78644.

Zhu, Y., S. Yao, and L. Chen. 2011. Cell surface signaling molecules in the control of immune responses: a tide model. *Immunity* 34:466-478.

Zinkernagel, R.M., and P.C. Doherty. 1974. Immunological surveillance against altered self components by sensitised T lymphocytes in lymphocytic choriomeningitis. *Nature* 251:547-548.

Appendix

1. Microarray sample sheet.			
Sample Name	**Sample Group**	**Sentrix ID**	**Sentrix Position**
A1	1	200053700003	A
B1	2	200053700003	B
C1	3	200053700003	C
D1	4	200053700003	D
E1	5	200053700003	E
F1	6	200053700003	F
G1	7	200053700003	G
H1	8	200053700003	H
A2	9	200053700003	I
B2	10	200053700003	J
C2	11	200053700003	K
D2	12	200053700003	L
E2	1	200053700033	A
F2	2	200053700033	B
G2	3	200053700033	C
H2	4	200053700033	D
A3	5	200053700033	E
B3	6	200053700033	F
C3	7	200053700033	G
D3	8	200053700033	H
E3	9	200053700033	I
F3	10	200053700033	J
G3	11	200053700033	K
H3	12	200053700033	L
A4	1	200053700013	A
B4	2	200053700013	B
C4	3	200053700013	C
D4	4	200053700013	D
E4	5	200053700013	E
F4	6	200053700013	F
G4	7	200053700013	G
H4	8	200053700013	H
A5	9	200053700013	I
B5	10	200053700013	J
C5	11	200053700013	K
D5	12	200053700013	L

2. Gene IDs of up-regulated (2-fold) genes in Venn diagram, (fold change>2, *p*-value<0.05), LTNP005 A3

[10μM]&[1μM]&[0.1μM]&[0.01μM]:
CCL1

[10μM]&[1μM]&[0.1μM]:
TNFRSF9, EGR2, ZBED2, TIMD4, C12ORF48, HAVCR2;
[1μM]&[0.1μM]:
HBA2

[10μM]&[1μM]:
RRS1, NME1, EBNA1BP2, TNIP3, LOC642956, NOLC1, FABP5L2, METTL1, FABP5, ECE2, GPATCH4, WDR12, SLC7A5, PAICS, BOLA2, DCTPP1, RRP12, SLC39A14, BATF, C3ORF26, AK3L1, MTP18, IL2RA, SLC3A2, MRPS17, TIMM8A, PUS7, C10ORF61, BOP1, POLD2, NHP2, PHLDA1, PFAS, MRTO4, NAMPT, SFXN4, TFB2M, CDK4, PRDX4, DPH2, FASLG, CTXN1, PTRH2, HS.390407, EXOSC5, AK2, NOL6, NTRK2, TCTN3, ZDHHC9, NPM3, WDR74, MRPL12, DDX10, WDR4, ALG3, C7ORF40, SRM, WDR46, EXOSC7, PPP2R1B, PHB, SRPRB, NR2C2AP, IFNG, POLR1C, ATAD3A, RRP15, EIF3B, ZNF593, CSF2, TSPAN17, TBC1D4, CYCSL1, AIMP2, MAF, TRAP1, LOC391811, IMP4, TRMT1, NDFIP2, MPP6, SERTAD1, NOP16, AHCY, DHX37, HSPC111, GADD45G, MYB, PPAN, IQCG, CD151, KCNK1, TOMM40, YIF1A, FKBP11, NOP2, PUS1, NCLN, MIR155HG, HSPE1, ARD1A, HMBS, SDF2L1, LOC653506, ARG2, C19ORF10, SEMA4A, AGPAT9, CD160, CENPV, UPP1;
[1μM]:
MTHFD1L

[10μM]:
LYST, GLT25D1, GAR1, NDUFAF2, KIAA0020, CTLA4, VARS, CTPS, SEH1L, BZW2, PIP5K1B, CCDC86, LOC100132139, DUSP5, IARS, PIGW, NXT1, FAM3C, DUSP4, UBIAD1, MAMLD1, WDR43, SLC1A5, HSP90AB1, BYSL, SLC7A1, HS.10862, SIAH2, TSEN2, PPARG, GART, LOC642780, FLJ16793, C1QBP, UTP14A, NCL, NARG1, SLC27A2, TFRC, SLC25A19, BCCIP, SLC25A22, C17ORF79, SLC39A8, EMG1, MARS, SLC35F2, IFRD2, TIMM23, NCBP2, RPIA, SLC35B1, WDR77, MRPL24, RGS16, CELSR3, ATIC, RPF2, SLC29A1, SRFBP1, POLR3H, PIM3, LOC728698, FARSA, IPO4, PRPF19, CIRH1A, HS.25892, LOC729608, PRMT5, WDR36,

FAM89A, TTLL12, C10ORF2, GTPBP4, NR4A2, LARS, URB2, TTC27, DDX21, PRDX1, AHSA1, TIMM10, POLR2H, C17ORF96, BEND3, CCT2, RCL1, PINX1, MRPL4, GNL3, ALDH18A1, MKI67IP, MAP1LC3A, HNRNPAB, MAK16, PPRC1, PMF1, EXOSC2, RPL34, RBPJ, DDX56, MRPS7, NME2, UBE2F, SIGMAR1, MRPS12, RANBP1, PRMT1, FAM86B1, GADD45B, EIF4G1, WBSCR22, CDK6, CCL3L1, TSR1, LOC648024, C8ORF33, APEX1, PA2G4, RIOK1, LOC729535, GNL2, FAM86A, BATF3, NETO2, PRR5, LOC100130919, ABCE1, C3ORF21, HSPC171, TSPAN5, NAT10, UCHL5IP, TNFRSF1B, PNO1, LARP1B, HRB, LRP8, PLD6, PMM2, IMPAD1, FAM195A, NAT5, NUDC, PMCH, FASN, DNAJB11, GEMIN4, MRPL32, LOC652481, HSPA5, UBQLN4, MTHFD2, ODC1, EIF2C2, ABCF2, KIAA0133, PDCD2L, LOC100133328, GSPT1, PEX5, MRPS26, PITX1, FKBP4, MGC4677, LYAR, PELP1, RAN, LOC647150, C21ORF70, NHP2L1, RRP1, LOC652864, CRLS1, NOP56, SERPINB9, GCSH, MRPS23, LOC727803, C17ORF70, SNHG3, RCC1, UCK2, PYCR1, VARS2, NANS, C12ORF45, RANGAP1, IER3, RRP7A, XCL1, GEMIN6, C6ORF66, METRNL, MLLT6, DNLZ, IL5, SSSCA1, TMEM138, BRIX1, LOC100128266, PGAM4, SFRS7, PMPCA, CHCHD8, CECR5, CCT3, TMEM97, STIP1, DDX31, PER2, HYOU1, NT5DC3, FLOT1, DDX39, PAPD1, CHCHD4, GFOD1, MAT2A, DDX55, SNAPC2, LAS1L, LMNA, PES1, LOC100134393, LOC345041, FAM136A, IRAK1, CSF1, ANKRD37, PDIA5, C10ORF128, MCM6, ZBTB32, PTGES2, LOC653566, HK2, SNRPB, C13ORF15, LOC644422, CXORF64, ARMET, CD320, MAGMAS, DIMT1L, HIST2H2AA3, FVT1, C12ORF24, HEATR1, ADAM15, HIST2H2AA4, EIF4A1, ZMYND19, C19ORF48, GMPPB, IMPDH1, GJB2, FEN1, KHSRP, C9ORF114, AXUD1, SCO2, TXNDC5, STRA13

3. Gene IDs of down-regulated (2-fold) genes in Venn diagram, (fold change>2, *p*-value<0.05), LTNP005 A3

[10μM]&[1μM]&[0.1μM]:
C14ORF4, FSCN1, IL23A, MFGE8, CCL22, ASS1, BASP1, MARCKS, PLS3, CCDC106, FAM43A, SPRYD5, DPY19L1, LOC283116, SERPINB2, PRKCDBP, LOC642362, RXRA, LOC653111, LOC340274, MYH10, KIF1A, TRIM48, ANKRD57, IGSF3, ATP9A;
[0.1μM]:
CCR7

[10μM&[1μM]:
CDKN2D, ZBP1, VNN2, SRPK2, TC2N, BIN1, SORL1, STK38, ABLIM1, CNN2, ARHGAP9, CCM2, FBXO32, BNIP3, SNURF, ADD3, FAIM3, TSC22D3, AHNAK, LOC100130516, MKNK2, KRT81, FYB, KRT86, PIK3IP1, TP53INP1, DSE, CD5, TTC3, DPYSL2, LOC100134006, TNNI2, FCGBP, SNAP25, CADM1, NOXO1, HS.579631, ANXA8;
[1μM]:
IRF4, PDX1

[10μM]:
C5ORF39, SLAMF8, ADRB2, NMT2, MGST3, GYPC, GLIPR2, STMN3, RGL4, CAT, TMX4, CD8A, C4ORF34, ADA, BNIP3L, ALDH6A1, UNC84B, PAQR8, TMEM71, CYFIP2, FAM8A1, LIME1, RBL2, PPP2R5C, HS.356079, PECR, ICAM3, ATM, SIDT2, PRKCB1, ITM2C, PRKCB, STAT4, PPP2R2B, AKAP7, CCDC28A, SLFN5, CMIP, MAP4K1, NDRG3, LIPA, SUSD3, WDR54, TNFSF12, CLIC3, FLOT2, YPEL1, TIAF1, PDLIM1, SPN, RHOU, DDIT4L, KIAA1949, LOC100188949, LOC730455, LOC728661, YPEL3, ABR, RNASET2, FAM113B, PITPNC1, SMYD3, TMEM154, PYCARD, PLCG1, MT1F, AKTIP, CERK, GCHFR, LOC644988, NTAN1, SGSM2, FAM62B, RAB37, CXCR4, POLR3GL, DYRK2, PLEKHF1, TBC1D10C, KLF6, SEP09, ERMP1, CECR1, CTDSP2, MXD4, DCK, LOC653438, MT1E, KIAA1370, SLAMF6, RHOC, STOM, GIMAP1, VEZF1, ZFP36L2, NPC1, GIMAP6, CBR4, GNS, LOC100129502, IDH2, GLRX, UBL3, HSD17B11, MAP4K2, CDC2L6, SNRPN, ECH1, LBA1, TMEM14C, MAN2B2, SAMD9, LOC729495, ANKDD1A, SAMD3, PTPRC, ARHGEF3, GIMAP8, BTN3A2, IL7R, CPNE3, ERAP2, CD37, PSIP1, TMEM14D, NIN, MAP1LC3B, PDGFD, TMEM14A, EVI2B, SH3BGRL, OSTF1, C12ORF35, MYH9, ACAP1, GPSM3, BTN3A3, ZMAT3, GNAI2, LOC728855, CCR3, RPS29, JAKMIP2, TRIM38, CATSPER2, APAF1, IL16, BCL11B, HS.296031, FAM108A2, HS.371609, ARHGAP30, HIST1H2BD, CCDC23, GAB3, HERC1, LRRC37B, NUDT14, ZNF217, RARRES3, SYTL2, SAMD9L, PLCG2,

KIAA1128, RASGRP3, FGD3, IL10RA, APOL3, HS.436879, KIAA1147, ITM2B, C5ORF41, FGR, C17ORF44, KIAA1671, SH2D3C, RCSD1, SYT11, LOC90586, CDC14A, DAPK2, CNPY4, FAM190B, GIMAP2, FLJ36131, ACAT2, KLHL24, ARL6IP6, ARHGAP15, BLZF1, LOC100132391, CCNG2, RPL13A, ALPP, RAB5B, KIAA0240, PTPN4, FHL2, PTPN12, PSCD1, TXNIP, LOC730313, FLJ46309, FAM65B, ILK, MGAT4A, ARHGAP25, GVIN1, OPTN, PERP, RASSF2, NFKBIZ, SMC4, HS.163752, MLLT11, IRAK2, LOC728809, SPG11, DOCK8, MACF1, IQGAP1, HCG2P7, WASPIP, PRKCA, F2R, FAM125B, ROD1, BTLA, RAB7L1, HMGB2, MAST3, IFIH1, DOCK11, PYHIN1, C14ORF85, TPP1, ZNF14, ZBTB4, PDCD4, LOC100190938, IL17RD, LOC399900, KIAA1751, CEBPD, E2F3, PHF21A, EID2B, ZNF394, PHF15, KIAA0430, WIPF1, CDKN2AIPNL, AKNA, NR5A2, LOC100129362, ST6GAL1, CDKN1B, CDC42SE2, XRCC6BP1, PJA2, LBH, FAM84B, MBNL1, RGS12, CAPZB, RAB8B, ATP6V1A, PAG1, MYL12A, LOC728903, CHCHD6, CBS, CYTH4, SLC25A23, SLC44A2

4. Clone A3 Gene Differential Expressions Table (fold change greater than 2 at 10μM, 409 probes ↑, 289 probes ↓)

(Descending order)		log2 (fold change value, mean)					p-value (two-tailed t test)				
Gene ID	**Probe ID**	**10^{1}μM**	**10^{0}μM**	**10^{-1}μM**	**10^{-2}μM**	**10^{-3}μM**	**10^{1}μM**	**10^{0}μM**	**10^{-1}μM**	**10^{-2}μM**	**10^{-3}μM**
C12ORF48	ILMN_1813379	3.75	3.01	1.22	0.15	0.23	0.00	0.00	0.02	0.64	0.44
TNFRSF9	ILMN_1743199	3.46	3.00	2.21	0.99	0.31	0.00	0.00	0.00	0.03	0.15
ZBED2	ILMN_1767658	3.35	2.50	1.15	0.18	0.00	0.04	0.02	0.04	0.35	0.98
EGR2	ILMN_1663131	2.96	2.81	1.89	0.72	0.22	0.00	0.00	0.01	0.03	0.40
HAVCR2	ILMN_2414399	2.88	2.64	1.65	0.62	0.29	0.00	0.00	0.00	0.05	0.27
CCL1	ILMN_1727043	2.81	3.04	2.53	1.52	0.53	0.01	0.00	0.01	0.00	0.07
METTL1	ILMN_1768127	2.56	2.02	0.58	0.16	0.23	0.00	0.00	0.00	0.21	0.06
IL2RA	ILMN_1707591	2.51	1.80	0.37	0.21	0.21	0.05	0.02	0.06	0.38	0.41
CSF2	ILMN_2412549	2.49	1.65	0.74	0.47	0.31	0.02	0.03	0.18	0.35	0.43
TNIP3	ILMN_3210741	2.46	1.49	0.52	0.17	0.09	0.03	0.01	0.16	0.39	0.60
METTL1	ILMN_2184640	2.42	1.70	0.42	0.06	0.24	0.00	0.00	0.01	0.64	0.02
DCTPP1	ILMN_3178258	2.35	1.69	0.34	0.22	0.33	0.00	0.00	0.22	0.41	0.22
MIR155HG	ILMN_3306997	2.35	1.85	0.45	-0.13	-0.32	0.00	0.00	0.29	0.49	0.17
NAMPT	ILMN_1741133	2.33	1.36	0.45	0.23	0.11	0.01	0.01	0.01	0.07	0.28
IQCG	ILMN_2146761	2.30	1.72	0.44	0.08	0.04	0.00	0.00	0.03	0.54	0.77
PUS7	ILMN_1682857	2.30	1.72	0.61	-0.05	-0.18	0.00	0.00	0.03	0.75	0.28
TIMD4	ILMN_1748883	2.25	2.19	1.38	0.39	0.13	0.00	0.00	0.00	0.08	0.46
BATF3	ILMN_2275248	2.25	0.90	-0.46	0.33	0.52	0.03	0.02	0.16	0.23	0.11
SLC7A5	ILMN_3266606	2.18	1.42	0.47	0.53	0.33	0.00	0.01	0.18	0.09	0.20
PHLDA1	ILMN_1665483	2.16	1.57	0.77	0.08	-0.04	0.00	0.01	0.02	0.70	0.61

SLC39A14	ILMN_2383306	2.14	1.67	0.89	0.16	0.01	0.00	0.01	0.01	0.24	0.94
BOP1	ILMN_1815190	2.14	1.52	0.33	0.27	0.37	0.00	0.00	0.17	0.05	0.02
NDFIP2	ILMN_2045729	2.12	1.88	0.90	0.32	0.13	0.00	0.00	0.03	0.27	0.63
MAF	ILMN_1747197	2.10	1.26	0.62	0.09	0.14	0.00	0.01	0.10	0.82	0.68
GPATCH4	ILMN_2098616	2.08	1.42	0.30	0.19	0.22	0.00	0.00	0.13	0.10	0.09
RRS1	ILMN_2261627	2.04	1.37	0.31	0.03	0.01	0.00	0.00	0.06	0.69	0.92
PUS1	ILMN_1667224	2.04	1.33	0.24	0.27	0.31	0.00	0.01	0.11	0.00	0.01
MRTO4	ILMN_1696601	2.04	1.50	0.34	0.12	0.24	0.00	0.00	0.00	0.15	0.09
HSPC111	ILMN_1695590	2.04	1.12	0.09	0.22	0.32	0.00	0.00	0.40	0.26	0.03
IFNG	ILMN_1763487	2.02	1.28	0.49	-0.11	-0.25	0.04	0.02	0.22	0.56	0.05
WDR4	ILMN_1773760	2.00	1.48	0.41	0.08	0.06	0.00	0.00	0.06	0.60	0.68
ZNF593	ILMN_1783285	1.99	1.44	0.11	0.14	0.24	0.00	0.00	0.56	0.59	0.26
ZDHHC9	ILMN_2381138	1.98	1.45	0.33	0.09	0.12	0.01	0.02	0.13	0.66	0.46
DPH2	ILMN_1659343	1.96	1.59	0.37	-0.07	0.10	0.01	0.00	0.01	0.30	0.17
FKBP11	ILMN_1763129	1.95	1.49	0.48	0.25	0.38	0.00	0.00	0.03	0.20	0.06
POLR1C	ILMN_1803811	1.93	1.29	0.24	0.14	0.35	0.00	0.00	0.07	0.24	0.04
SRPRB	ILMN_1767253	1.92	1.29	0.33	0.20	0.25	0.00	0.00	0.03	0.18	0.07
NPM3	ILMN_1805807	1.92	1.44	0.33	0.22	0.38	0.00	0.00	0.13	0.33	0.03
DCTPP1	ILMN_1676548	1.91	1.64	0.44	0.26	0.49	0.02	0.00	0.01	0.15	0.00
SLC3A2	ILMN_1668822	1.91	1.45	0.86	0.48	0.27	0.00	0.01	0.00	0.05	0.09
PAICS	ILMN_1705753	1.89	1.41	0.42	-0.03	-0.03	0.01	0.00	0.06	0.80	0.86
GPATCH4	ILMN_2338038	1.86	1.28	0.32	-0.02	0.04	0.00	0.00	0.01	0.88	0.32
WDR74	ILMN_1734478	1.85	1.19	0.16	0.13	0.27	0.00	0.00	0.31	0.49	0.10
NOLC1	ILMN_1792681	1.85	1.16	0.27	0.01	0.06	0.00	0.01	0.00	0.87	0.49

CYCSL1	ILMN_2355665	1.85	1.14	0.12	0.00	0.10	0.00	0.00	0.40	0.98	0.24
PAICS	ILMN_1683774	1.84	1.43	0.49	0.06	0.07	0.00	0.01	0.06	0.78	0.74
MTP18	ILMN_3236694	1.84	1.42	0.40	0.28	0.24	0.00	0.00	0.05	0.09	0.13
IMP4	ILMN_1726456	1.84	1.26	0.26	0.11	0.32	0.00	0.00	0.10	0.60	0.06
NHP2	ILMN_1804851	1.84	1.42	0.54	0.25	0.43	0.00	0.00	0.06	0.25	0.09
WDR12	ILMN_1656378	1.83	1.31	0.36	0.06	0.07	0.00	0.00	0.17	0.72	0.64
WDR12	ILMN_2392546	1.83	1.25	0.36	-0.04	0.04	0.00	0.00	0.04	0.69	0.31
NME1	ILMN_1733956	1.82	1.51	0.52	0.07	0.22	0.00	0.00	0.01	0.16	0.03
SDF2L1	ILMN_1743397	1.81	1.31	0.50	0.39	0.30	0.00	0.01	0.08	0.04	0.13
PPP2R1B	ILMN_1722239	1.79	1.09	0.21	-0.04	0.06	0.00	0.04	0.01	0.73	0.41
C3ORF26	ILMN_1760280	1.79	1.37	0.46	0.11	0.14	0.01	0.01	0.02	0.13	0.24
AGPAT9	ILMN_2368773	1.78	1.65	0.93	0.41	0.15	0.04	0.05	0.17	0.54	0.81
BATF	ILMN_1808391	1.78	1.47	0.50	0.42	0.44	0.00	0.00	0.14	0.02	0.01
NOP16	ILMN_1779353	1.78	1.10	-0.03	0.22	0.29	0.00	0.00	0.80	0.19	0.08
LOC653506	ILMN_2383305	1.77	1.09	0.49	0.11	0.20	0.04	0.00	0.11	0.45	0.25
ECE2	ILMN_1768077	1.77	1.23	0.25	0.13	0.12	0.00	0.00	0.04	0.10	0.14
LOC642956	ILMN_1715583	1.77	1.24	0.15	0.25	0.39	0.02	0.01	0.48	0.06	0.00
ECE2	ILMN_1751956	1.77	1.35	0.21	0.05	0.26	0.00	0.00	0.02	0.51	0.07
TBC1D4	ILMN_1651872	1.76	1.09	0.50	0.02	-0.12	0.02	0.03	0.16	0.79	0.13
C3ORF26	ILMN_1680856	1.75	1.30	0.34	-0.06	-0.01	0.01	0.01	0.12	0.65	0.90
EXOSC5	ILMN_1671442	1.75	1.37	0.53	0.23	0.26	0.01	0.00	0.01	0.04	0.04
RRP12	ILMN_1777261	1.75	1.29	0.27	0.05	0.04	0.01	0.00	0.06	0.56	0.68
PTRH2	ILMN_1652631	1.74	1.25	0.18	0.17	0.17	0.00	0.01	0.35	0.21	0.32
NOL6	ILMN_3305304	1.73	1.07	0.32	0.04	0.05	0.00	0.02	0.01	0.72	0.70

NAMPT	ILMN_3244117	1.73	0.89	0.23	0.16	0.10	0.01	0.02	0.34	0.32	0.55
PHB	ILMN_2281069	1.71	1.13	0.36	0.19	0.39	0.00	0.00	0.04	0.25	0.03
TOMM40	ILMN_1673711	1.71	1.09	0.06	0.09	0.19	0.00	0.00	0.68	0.35	0.13
HS.25892	ILMN_1663422	1.70	0.95	-0.22	0.08	0.21	0.00	0.04	0.40	0.77	0.43
CCDC86	ILMN_1651705	1.70	0.97	-0.07	-0.13	0.04	0.00	0.00	0.65	0.53	0.77
UPP1	ILMN_2365544	1.69	1.19	0.36	0.35	0.38	0.01	0.02	0.21	0.24	0.24
FASLG	ILMN_1682792	1.68	1.27	0.65	0.34	0.28	0.00	0.00	0.05	0.08	0.10
GALR2	ILMN_3242459	1.68	0.71	0.16	-0.03	-0.04	0.07	0.01	0.12	0.74	0.60
ATAD3A	ILMN_1687978	1.67	1.05	0.24	0.02	0.06	0.01	0.03	0.11	0.71	0.20
FABP5	ILMN_1741054	1.67	1.03	0.19	0.17	0.21	0.01	0.00	0.36	0.19	0.13
PPRC1	ILMN_1755862	1.66	0.93	0.10	0.18	0.07	0.00	0.00	0.49	0.12	0.63
C17ORF96	ILMN_1689800	1.66	0.91	-0.02	0.11	0.12	0.01	0.02	0.86	0.34	0.38
ALG3	ILMN_1653871	1.66	1.14	0.24	0.20	0.23	0.00	0.00	0.35	0.24	0.21
HMBS	ILMN_2363361	1.66	1.25	0.29	0.24	0.39	0.01	0.00	0.24	0.09	0.02
AK3L1	ILMN_1760374	1.65	1.25	0.23	0.00	0.08	0.00	0.00	0.06	1.00	0.55
TRMT1	ILMN_1772521	1.65	1.15	0.14	0.14	0.22	0.02	0.02	0.57	0.13	0.02
WDR74	ILMN_1843198	1.64	0.89	0.23	0.11	0.08	0.00	0.00	0.07	0.13	0.37
MPP6	ILMN_1801313	1.63	1.02	0.37	0.05	0.03	0.00	0.02	0.00	0.29	0.59
NHP2	ILMN_1746393	1.63	1.35	0.51	0.09	0.12	0.00	0.00	0.05	0.61	0.54
WDR46	ILMN_1770692	1.62	1.20	0.40	0.18	0.28	0.00	0.00	0.05	0.20	0.09
PRDX4	ILMN_3226807	1.62	1.32	0.37	0.10	0.27	0.00	0.00	0.04	0.46	0.07
TFB2M	ILMN_1800225	1.62	1.05	0.17	-0.01	-0.01	0.00	0.04	0.44	0.95	0.91
MRPS17	ILMN_1713892	1.61	1.01	0.07	0.03	0.25	0.00	0.01	0.48	0.77	0.09
TRAP1	ILMN_1718672	1.61	1.06	0.33	0.02	0.18	0.01	0.01	0.10	0.83	0.18

GLT25D1	ILMN_1679476	1.61	0.97	0.15	0.08	0.10	0.00	0.00	0.14	0.19	0.26
GEMIN4	ILMN_1752798	1.59	0.97	0.06	0.10	0.12	0.00	0.00	0.73	0.35	0.23
HS.390407	ILMN_2067708	1.59	1.40	0.55	0.07	0.25	0.02	0.04	0.19	0.81	0.46
NOP2	ILMN_2184575	1.59	1.04	0.13	0.15	0.22	0.01	0.01	0.39	0.31	0.26
SFXN4	ILMN_1658437	1.59	1.26	0.22	0.06	0.25	0.00	0.00	0.22	0.56	0.00
MRPL12	ILMN_1668996	1.59	1.14	0.55	0.14	0.07	0.00	0.02	0.07	0.12	0.38
METRNL	ILMN_1689001	1.58	0.85	0.46	0.08	-0.05	0.03	0.01	0.05	0.49	0.65
DDX21	ILMN_2095820	1.58	0.94	0.45	0.09	0.02	0.03	0.04	0.36	0.26	0.80
RRP15	ILMN_2222234	1.57	1.08	0.27	-0.08	0.06	0.00	0.00	0.26	0.70	0.69
PPAN	ILMN_2375418	1.56	1.04	0.38	0.12	0.20	0.00	0.01	0.00	0.20	0.01
CD151	ILMN_2372040	1.56	1.19	0.28	0.17	0.21	0.00	0.00	0.12	0.23	0.20
CENPV	ILMN_1781824	1.55	1.38	0.30	0.26	0.32	0.00	0.00	0.43	0.20	0.15
AK2	ILMN_1695422	1.55	1.12	0.23	0.05	0.17	0.00	0.00	0.17	0.79	0.27
NHP2	ILMN_1765994	1.55	1.28	0.52	0.15	0.25	0.00	0.00	0.03	0.36	0.18
C7ORF40	ILMN_1759766	1.54	1.04	-0.17	0.13	0.26	0.00	0.02	0.47	0.65	0.31
SRM	ILMN_1669142	1.54	1.12	0.37	0.16	0.25	0.01	0.01	0.15	0.54	0.30
CD160	ILMN_1683859	1.54	1.12	0.16	-0.18	-0.04	0.01	0.00	0.30	0.37	0.83
AIMP2	ILMN_2215545	1.53	1.02	0.05	0.14	0.20	0.00	0.00	0.82	0.25	0.08
KIAA0020	ILMN_1762883	1.53	0.79	0.06	-0.11	-0.11	0.00	0.03	0.42	0.36	0.13
NME1	ILMN_2311548	1.53	1.10	0.19	0.01	0.11	0.00	0.00	0.01	0.86	0.02
MAMLD1	ILMN_1906423	1.52	0.96	0.32	0.15	0.07	0.03	0.04	0.15	0.37	0.65
C17ORF79	ILMN_2317658	1.52	0.97	0.17	0.06	0.27	0.00	0.02	0.22	0.79	0.16
EBNA1BP2	ILMN_1764629	1.52	1.13	0.11	0.04	0.15	0.01	0.00	0.42	0.73	0.10
SLC7A1	ILMN_1674243	1.52	0.97	0.21	0.09	0.07	0.00	0.01	0.30	0.48	0.53

CIRH1A	ILMN_1659725	1.51	0.96	0.08	0.05	0.17	0.00	0.03	0.40	0.69	0.03
EIF3B	ILMN_1716053	1.51	1.04	0.22	0.19	0.19	0.01	0.02	0.41	0.21	0.14
UBIAD1	ILMN_1805561	1.51	0.84	-0.03	-0.03	0.00	0.00	0.05	0.72	0.84	0.95
LOC391811	ILMN_1771966	1.50	1.17	0.33	0.11	0.28	0.00	0.00	0.23	0.50	0.17
NAT10	ILMN_1670542	1.50	0.89	0.16	0.23	0.17	0.00	0.02	0.63	0.08	0.20
UCK2	ILMN_2320250	1.50	0.82	0.19	0.11	0.23	0.00	0.00	0.13	0.08	0.05
KCNK1	ILMN_1651365	1.50	1.10	0.41	-0.02	0.01	0.00	0.03	0.10	0.88	0.93
POLR3H	ILMN_2357855	1.50	1.00	0.08	0.06	0.09	0.02	0.01	0.73	0.34	0.13
MTHFD1L	ILMN_1732410	1.49	1.35	0.40	0.05	0.07	0.08	0.01	0.06	0.64	0.45
NHP2	ILMN_1752947	1.49	1.11	0.45	0.01	0.07	0.00	0.01	0.08	0.95	0.72
SFRS7	ILMN_3244526	1.49	0.82	0.13	-0.01	0.05	0.00	0.02	0.27	0.89	0.70
SLC3A2	ILMN_1803824	1.49	1.12	0.87	0.27	0.15	0.00	0.00	0.01	0.07	0.24
DDX10	ILMN_1700831	1.48	1.02	0.42	0.10	0.14	0.00	0.00	0.05	0.54	0.35
CTXN1	ILMN_1718961	1.48	1.05	0.34	-0.02	0.01	0.02	0.03	0.09	0.67	0.92
TMEM97	ILMN_1793220	1.48	0.87	0.14	0.02	0.03	0.00	0.03	0.50	0.93	0.85
PINX1	ILMN_1797074	1.48	0.85	0.20	0.07	0.18	0.00	0.00	0.29	0.45	0.08
GART	ILMN_1799819	1.47	0.90	0.28	0.11	0.02	0.01	0.01	0.23	0.45	0.92
SLC3A2	ILMN_1785284	1.47	1.21	0.78	0.52	0.29	0.00	0.01	0.09	0.00	0.01
FKBP4	ILMN_2338963	1.46	0.93	0.12	0.18	0.23	0.00	0.01	0.61	0.34	0.24
MTHFD2	ILMN_1678939	1.46	0.75	-0.07	0.03	0.19	0.01	0.03	0.64	0.91	0.30
DHX37	ILMN_2110252	1.45	1.01	0.18	0.17	0.18	0.01	0.02	0.32	0.19	0.02
POLR1C	ILMN_1789775	1.45	0.96	0.15	0.00	0.12	0.00	0.00	0.20	0.97	0.32
EIF4A1	ILMN_1742031	1.45	0.73	-0.04	0.27	0.39	0.00	0.03	0.90	0.28	0.13
CDK6	ILMN_1657451	1.45	0.93	0.21	0.12	-0.02	0.04	0.01	0.47	0.42	0.90

CDK4	ILMN_1699603	1.45	1.12	0.12	-0.04	0.07	0.00	0.00	0.36	0.73	0.56
KCNK1	ILMN_1753249	1.45	1.04	0.43	-0.18	-0.15	0.00	0.00	0.20	0.10	0.14
IARS	ILMN_1664231	1.45	0.92	0.29	0.09	0.10	0.00	0.00	0.02	0.42	0.36
SLC27A2	ILMN_2412564	1.45	0.98	0.47	0.08	-0.02	0.01	0.02	0.11	0.77	0.94
MAT2A	ILMN_1782633	1.44	0.85	0.15	0.23	0.13	0.00	0.01	0.43	0.21	0.43
NCLN	ILMN_1714809	1.44	1.00	0.23	0.23	0.27	0.02	0.01	0.47	0.22	0.07
SLC25A19	ILMN_1679041	1.43	0.92	0.08	0.16	0.19	0.02	0.00	0.58	0.07	0.05
DNLZ	ILMN_1742889	1.43	0.98	0.13	0.25	0.39	0.01	0.02	0.59	0.48	0.20
HSPE1	ILMN_2398995	1.43	1.12	0.55	-0.04	-0.23	0.02	0.02	0.32	0.92	0.55
IFRD2	ILMN_1656628	1.43	0.97	0.23	0.06	0.10	0.01	0.01	0.07	0.58	0.54
BZW2	ILMN_1691290	1.42	0.97	0.10	-0.02	0.00	0.01	0.01	0.53	0.87	0.98
NETO2	ILMN_3231390	1.42	0.91	0.30	-0.10	-0.17	0.00	0.05	0.25	0.53	0.28
GNL3	ILMN_1673991	1.42	0.79	0.05	-0.01	0.14	0.00	0.00	0.71	0.91	0.25
EXOSC7	ILMN_1664167	1.42	1.01	0.29	0.13	0.17	0.00	0.00	0.18	0.09	0.08
C12ORF24	ILMN_1698996	1.42	0.71	0.15	0.20	0.21	0.03	0.01	0.36	0.09	0.07
PRMT5	ILMN_1694589	1.42	0.91	0.28	0.08	0.06	0.01	0.00	0.05	0.20	0.33
FAM3C	ILMN_1721024	1.41	0.86	0.38	0.00	-0.08	0.00	0.02	0.11	0.98	0.72
NR2C2AP	ILMN_1786024	1.41	1.10	0.27	0.03	0.18	0.00	0.00	0.17	0.84	0.31
PA2G4	ILMN_1711886	1.41	0.93	0.67	0.13	0.23	0.00	0.01	0.08	0.37	0.14
NOP56	ILMN_3248773	1.40	0.98	-0.08	-0.03	0.01	0.01	0.03	0.66	0.91	0.97
C19ORF10	ILMN_1661337	1.40	1.11	0.44	0.29	0.24	0.02	0.03	0.08	0.06	0.17
XCL1	ILMN_1674402	1.40	0.84	0.32	0.09	-0.01	0.05	0.04	0.15	0.40	0.88
PRMT5	ILMN_1778255	1.40	0.99	0.16	0.04	0.01	0.00	0.00	0.31	0.67	0.95
TIMM10	ILMN_1798172	1.40	0.94	0.09	0.25	0.33	0.00	0.01	0.42	0.00	0.00

SFXN4	ILMN_2212354	1.39	0.99	0.23	-0.03	0.02	0.01	0.00	0.18	0.84	0.78
MAGMAS	ILMN_2354478	1.38	0.86	0.10	0.08	0.35	0.03	0.01	0.16	0.31	0.01
HEATR1	ILMN_1734596	1.38	0.96	0.20	0.53	0.57	0.00	0.00	0.59	0.01	0.03
BOLA2	ILMN_1769545	1.37	1.20	0.52	0.23	0.28	0.01	0.00	0.03	0.08	0.09
BOLA2	ILMN_2055477	1.37	1.11	0.38	0.11	0.17	0.00	0.00	0.14	0.42	0.08
HNRNPAB	ILMN_1796235	1.37	0.87	0.25	0.14	0.00	0.00	0.01	0.21	0.29	0.97
TIMM8A	ILMN_1898124	1.36	1.01	0.25	0.00	0.09	0.00	0.00	0.18	0.99	0.49
PMM2	ILMN_3226392	1.36	0.84	-0.04	0.07	0.08	0.01	0.00	0.79	0.35	0.28
NOP56	ILMN_1709247	1.36	0.87	-0.05	-0.04	0.24	0.01	0.04	0.86	0.90	0.42
ALDH18A1	ILMN_2309245	1.34	0.91	0.24	0.17	0.14	0.01	0.02	0.42	0.46	0.54
NCL	ILMN_2403889	1.34	0.67	0.27	0.20	0.12	0.00	0.02	0.30	0.24	0.55
POLD2	ILMN_1692651	1.34	1.06	0.32	0.00	0.04	0.00	0.01	0.02	0.98	0.62
PDCD2L	ILMN_1807448	1.34	0.71	0.18	0.18	0.25	0.00	0.00	0.19	0.22	0.16
EMG1	ILMN_1727184	1.34	0.95	0.34	0.22	0.20	0.00	0.00	0.02	0.06	0.14
TXNDC5	ILMN_2285817	1.33	0.80	0.11	0.02	0.01	0.01	0.01	0.53	0.88	0.95
CCT3	ILMN_1663113	1.33	0.81	0.14	0.18	0.26	0.01	0.05	0.57	0.48	0.33
RRP1	ILMN_1708619	1.33	0.82	0.26	0.08	0.11	0.00	0.00	0.02	0.32	0.15
SERTAD1	ILMN_1756999	1.33	1.03	0.27	0.21	0.25	0.00	0.00	0.40	0.28	0.04
AK3L1	ILMN_2364971	1.33	0.78	0.13	0.04	-0.01	0.00	0.00	0.54	0.85	0.92
PPARG	ILMN_1811188	1.33	0.93	0.27	0.11	0.04	0.02	0.00	0.18	0.35	0.73
POLR2H	ILMN_1875342	1.33	0.87	0.18	0.11	0.24	0.01	0.00	0.07	0.42	0.03
MRPL4	ILMN_1751072	1.32	0.85	0.39	0.16	0.08	0.01	0.00	0.07	0.13	0.44
MYB	ILMN_2135798	1.32	1.17	0.46	0.10	0.08	0.03	0.04	0.30	0.82	0.81
FABP5L2	ILMN_2207291	1.32	1.13	0.08	-0.23	-0.16	0.01	0.01	0.74	0.07	0.14

LOC648024	ILMN_1701243	1.32	0.84	0.24	0.13	0.11	0.00	0.03	0.37	0.53	0.57
IPO4	ILMN_1742577	1.32	0.86	0.32	-0.07	-0.02	0.01	0.01	0.05	0.15	0.90
FABP5	ILMN_1767219	1.32	1.12	0.24	0.02	0.00	0.01	0.02	0.55	0.96	0.99
CTPS	ILMN_1782305	1.32	0.87	0.11	-0.06	0.07	0.00	0.00	0.39	0.49	0.46
LOC727803	ILMN_1757317	1.31	1.00	0.35	0.15	0.27	0.01	0.04	0.24	0.65	0.38
TSPAN17	ILMN_1738530	1.31	1.40	0.67	0.26	0.24	0.00	0.02	0.20	0.06	0.01
TSPAN17	ILMN_1757730	1.30	1.34	0.49	0.16	0.16	0.01	0.01	0.18	0.09	0.02
PES1	ILMN_1735461	1.30	0.85	0.12	0.17	0.18	0.00	0.00	0.53	0.15	0.13
MRPL24	ILMN_1685661	1.30	0.97	0.43	0.03	0.08	0.01	0.01	0.01	0.79	0.27
TSEN2	ILMN_1791912	1.30	0.93	0.19	0.04	-0.06	0.00	0.00	0.04	0.71	0.31
CD320	ILMN_1806908	1.30	0.85	0.17	0.09	0.13	0.02	0.03	0.30	0.41	0.21
MTHFD2	ILMN_2366391	1.30	0.55	-0.09	0.16	0.24	0.00	0.02	0.43	0.05	0.02
LOC345041	ILMN_1703617	1.29	0.72	0.02	-0.06	0.18	0.00	0.02	0.89	0.69	0.24
HNRNPAB	ILMN_1750678	1.29	0.71	0.25	0.22	0.24	0.00	0.00	0.14	0.05	0.04
NTRK2	ILMN_1765332	1.28	1.00	0.46	0.21	0.07	0.01	0.00	0.00	0.11	0.31
GNL3	ILMN_1689445	1.28	0.72	-0.07	0.03	0.14	0.00	0.01	0.61	0.78	0.06
PITX1	ILMN_1715636	1.28	0.76	0.23	0.06	0.08	0.00	0.01	0.11	0.57	0.44
BYSL	ILMN_2366041	1.28	0.52	-0.19	0.00	0.01	0.01	0.00	0.27	0.97	0.88
ARMET	ILMN_3247139	1.28	0.89	0.19	0.19	0.18	0.01	0.03	0.39	0.39	0.39
RCL1	ILMN_1678652	1.28	0.64	0.05	0.04	0.10	0.00	0.01	0.38	0.53	0.01
SEMA4A	ILMN_1798249	1.28	1.01	0.34	-0.05	-0.07	0.01	0.04	0.18	0.65	0.58
HS.10862	ILMN_3299520	1.28	0.65	-0.03	0.03	-0.01	0.00	0.02	0.87	0.85	0.96
HSPC171	ILMN_1703441	1.27	0.98	0.27	0.19	0.22	0.00	0.01	0.22	0.29	0.25
WDR43	ILMN_1661861	1.26	0.75	0.20	0.02	-0.01	0.00	0.02	0.05	0.70	0.89

DKC1	ILMN_2375032	1.26	0.82	0.28	-0.05	-0.03	0.05	0.02	0.18	0.64	0.89
UTP14A	ILMN_1679382	1.26	0.83	0.30	0.25	0.20	0.01	0.03	0.01	0.13	0.04
HSPE1	ILMN_1813766	1.26	0.95	0.30	0.19	0.26	0.01	0.01	0.09	0.01	0.00
C17ORF70	ILMN_1695576	1.26	0.84	0.21	0.15	0.25	0.00	0.00	0.45	0.40	0.07
YIF1A	ILMN_1785202	1.26	1.03	0.23	0.26	0.35	0.01	0.01	0.40	0.28	0.19
PEX5	ILMN_1790309	1.25	0.79	0.22	0.01	0.08	0.01	0.04	0.11	0.97	0.36
NXT1	ILMN_2352042	1.25	0.80	-0.08	0.11	0.21	0.00	0.01	0.55	0.51	0.17
GART	ILMN_1806106	1.25	0.88	0.37	0.13	0.08	0.00	0.01	0.04	0.29	0.63
APEX1	ILMN_1660732	1.25	0.82	0.21	0.13	0.22	0.00	0.00	0.22	0.09	0.03
RRP7A	ILMN_2060115	1.25	0.87	0.18	0.20	0.25	0.01	0.01	0.18	0.11	0.07
BCCIP	ILMN_2302716	1.24	0.92	0.22	0.01	0.12	0.00	0.00	0.14	0.97	0.38
GEMIN6	ILMN_2374383	1.24	0.78	0.13	0.22	0.29	0.01	0.01	0.39	0.23	0.09
FAM3C	ILMN_1786189	1.24	0.90	0.42	0.06	-0.09	0.01	0.01	0.11	0.84	0.70
AK2	ILMN_1776188	1.23	0.88	0.20	0.14	0.27	0.01	0.00	0.08	0.27	0.03
SEH1L	ILMN_1716563	1.23	0.73	0.04	0.11	0.07	0.00	0.01	0.86	0.41	0.55
NUDC	ILMN_1688098	1.23	0.73	-0.03	0.13	0.26	0.00	0.04	0.87	0.48	0.15
BOLA2	ILMN_2152581	1.22	1.19	0.36	0.03	0.08	0.01	0.00	0.11	0.90	0.72
PFAS	ILMN_2335718	1.22	1.06	0.32	-0.05	-0.03	0.00	0.00	0.18	0.73	0.76
CTLA4	ILMN_1654429	1.22	0.86	0.56	0.15	0.05	0.02	0.01	0.05	0.42	0.74
FASN	ILMN_1777139	1.22	0.77	0.31	0.13	0.22	0.00	0.01	0.12	0.56	0.10
NDUFAF2	ILMN_1798659	1.22	0.94	0.18	-0.01	0.10	0.00	0.00	0.12	0.90	0.25
NR4A2	ILMN_1796210	1.22	0.93	0.50	0.13	-0.10	0.02	0.04	0.13	0.46	0.50
C12ORF45	ILMN_1756445	1.21	0.61	0.13	0.21	0.20	0.00	0.01	0.23	0.08	0.10
C21ORF70	ILMN_2396672	1.21	0.68	-0.04	0.15	0.14	0.01	0.05	0.84	0.00	0.05

PIP5K1B	ILMN_1764090	1.21	0.70	0.44	0.19	0.02	0.02	0.04	0.02	0.14	0.89
C10ORF2	ILMN_1738075	1.21	0.74	0.13	0.12	0.12	0.01	0.00	0.14	0.17	0.15
UBE2F	ILMN_1697736	1.21	0.97	0.49	0.17	0.29	0.02	0.01	0.10	0.49	0.28
MRPS12	ILMN_1696302	1.20	0.96	0.18	0.21	0.20	0.02	0.00	0.04	0.02	0.23
BRIX1	ILMN_1738229	1.20	0.63	-0.09	-0.07	0.10	0.00	0.02	0.58	0.73	0.52
NANS	ILMN_1770290	1.20	0.78	0.25	0.16	0.19	0.00	0.03	0.15	0.11	0.03
CHCHD4	ILMN_1774823	1.20	0.81	0.17	0.20	0.24	0.00	0.01	0.37	0.20	0.13
MRPS26	ILMN_1663751	1.20	0.72	-0.04	0.04	0.12	0.00	0.00	0.77	0.84	0.32
LOC642780	ILMN_1718063	1.20	0.73	0.18	0.02	-0.01	0.00	0.01	0.04	0.45	0.94
AK3L1	ILMN_1673252	1.20	0.83	0.12	-0.07	-0.14	0.00	0.01	0.29	0.52	0.27
NOP2	ILMN_1719543	1.20	0.75	0.20	0.05	0.16	0.01	0.00	0.03	0.20	0.07
CRLS1	ILMN_1679405	1.20	0.84	0.14	0.03	0.19	0.01	0.02	0.55	0.87	0.42
NAT5	ILMN_1692546	1.19	0.80	0.14	0.07	0.16	0.00	0.00	0.25	0.41	0.11
RPF2	ILMN_1759818	1.19	0.69	-0.03	0.02	0.07	0.01	0.03	0.82	0.86	0.60
GADD45G	ILMN_1785570	1.19	1.15	0.38	0.08	0.21	0.01	0.01	0.22	0.77	0.39
TTC27	ILMN_1813389	1.19	0.87	0.29	0.22	0.20	0.00	0.00	0.06	0.13	0.14
HSP90AB1	ILMN_1658289	1.19	0.74	0.35	0.10	0.08	0.03	0.03	0.10	0.32	0.70
GPATCH4	ILMN_2234873	1.19	0.68	0.10	0.06	0.02	0.00	0.01	0.32	0.54	0.76
SLC25A22	ILMN_2164242	1.19	0.68	-0.01	0.21	0.30	0.02	0.00	0.96	0.05	0.02
RANGAP1	ILMN_1699737	1.19	0.78	0.14	0.20	0.25	0.02	0.04	0.73	0.06	0.12
GMPPB	ILMN_2398489	1.19	0.82	0.45	0.20	0.12	0.04	0.03	0.02	0.09	0.02
NCBP2	ILMN_1683700	1.18	0.66	0.17	0.07	0.08	0.01	0.00	0.18	0.47	0.38
PNO1	ILMN_1693826	1.18	0.69	0.10	-0.03	0.04	0.00	0.03	0.54	0.81	0.64
WBSCR22	ILMN_1746252	1.18	0.69	0.36	0.32	0.24	0.02	0.01	0.01	0.01	0.02

EIF3B	ILMN_1671257	1.18	0.79	0.42	0.10	-0.04	0.01	0.01	0.03	0.41	0.75
LOC100133328	ILMN_2156982	1.18	0.82	0.20	0.16	0.23	0.01	0.03	0.44	0.48	0.31
SIGMAR1	ILMN_2324056	1.18	0.76	0.18	-0.18	-0.14	0.01	0.04	0.03	0.01	0.16
SSSCA1	ILMN_1812940	1.17	0.50	0.16	0.09	0.19	0.01	0.02	0.21	0.47	0.16
SCO2	ILMN_1677396	1.17	0.73	-0.01	0.17	0.36	0.00	0.01	0.95	0.26	0.07
DDX56	ILMN_1726222	1.17	0.76	0.14	0.10	0.13	0.00	0.00	0.30	0.35	0.35
HSPA5	ILMN_1795338	1.17	0.87	0.42	0.16	0.07	0.01	0.01	0.09	0.42	0.68
DUSP4	ILMN_2055634	1.17	0.79	0.57	0.34	0.12	0.00	0.02	0.00	0.01	0.45
SNRPB	ILMN_1679995	1.16	0.84	0.23	0.38	0.49	0.02	0.03	0.35	0.17	0.11
GAR1	ILMN_1788955	1.16	0.68	0.09	0.04	-0.03	0.00	0.02	0.24	0.60	0.68
SLC39A8	ILMN_2371964	1.16	0.87	0.34	-0.25	-0.27	0.00	0.02	0.13	0.18	0.10
RANBP1	ILMN_1721457	1.16	0.80	0.22	-0.03	-0.01	0.01	0.04	0.36	0.91	0.98
LOC729608	ILMN_1688725	1.16	0.69	-0.07	-0.03	0.08	0.00	0.04	0.71	0.85	0.62
STRA13	ILMN_2347234	1.16	0.90	-0.04	0.03	0.25	0.00	0.01	0.83	0.86	0.23
ARD1A	ILMN_1655051	1.16	1.08	0.16	0.03	0.24	0.04	0.04	0.70	0.95	0.50
RIOK1	ILMN_1801040	1.16	0.52	0.06	0.00	0.11	0.00	0.04	0.50	0.98	0.22
TNFRSF1B	ILMN_1811955	1.16	0.93	0.52	0.26	0.21	0.00	0.03	0.16	0.11	0.12
C9ORF114	ILMN_1663916	1.15	0.72	0.13	0.33	0.50	0.00	0.01	0.65	0.06	0.02
LYAR	ILMN_3242586	1.15	0.71	0.10	-0.09	0.01	0.02	0.00	0.61	0.55	0.90
RPL34	ILMN_1696537	1.15	0.74	-0.04	0.15	0.24	0.02	0.01	0.40	0.09	0.04
CECR5	ILMN_1768470	1.15	0.78	0.06	0.07	0.21	0.01	0.02	0.77	0.57	0.15
C8ORF33	ILMN_1697348	1.15	0.84	0.09	0.15	0.33	0.00	0.00	0.52	0.17	0.02
CCT2	ILMN_1732967	1.15	0.86	0.14	0.08	0.11	0.00	0.00	0.38	0.43	0.32

AHCY	ILMN_1802615	1.15	1.02	0.21	0.03	0.09	0.00	0.01	0.19	0.83	0.59
IRAK1	ILMN_3249175	1.15	0.91	0.38	0.03	0.06	0.01	0.03	0.19	0.87	0.67
MAP1LC3A	ILMN_1801864	1.15	0.88	0.57	0.16	0.06	0.02	0.03	0.02	0.20	0.50
TIMM23	ILMN_1775761	1.14	0.83	0.35	0.04	0.11	0.01	0.01	0.13	0.86	0.55
TCTN3	ILMN_3300663	1.14	1.20	0.71	0.09	0.06	0.00	0.00	0.01	0.44	0.58
PTGES2	ILMN_1665736	1.14	0.83	0.24	0.25	0.42	0.01	0.04	0.46	0.21	0.07
TMEM138	ILMN_2098325	1.14	0.73	0.05	0.11	0.19	0.00	0.01	0.81	0.47	0.06
FAM86B1	ILMN_1791147	1.14	0.76	0.23	0.23	0.06	0.00	0.00	0.03	0.06	0.40
EIF3B	ILMN_1661886	1.14	0.68	0.35	0.13	0.00	0.01	0.03	0.07	0.43	0.97
EXOSC2	ILMN_1672878	1.14	0.87	0.08	0.01	0.00	0.00	0.01	0.59	0.91	0.96
MRPS12	ILMN_1728984	1.14	0.87	0.13	0.21	0.30	0.01	0.00	0.37	0.09	0.04
IMPDH1	ILMN_1797534	1.14	0.71	-0.04	0.07	0.19	0.02	0.03	0.88	0.62	0.22
LARP1B	ILMN_3306019	1.14	0.68	0.13	0.00	-0.04	0.02	0.00	0.15	0.98	0.82
CTLA4	ILMN_1785424	1.13	0.95	0.57	0.26	0.07	0.03	0.01	0.04	0.24	0.72
PIGW	ILMN_1761113	1.13	0.84	0.14	0.01	-0.05	0.00	0.00	0.40	0.89	0.56
MRPL24	ILMN_2400250	1.13	0.93	0.35	0.12	0.13	0.00	0.01	0.05	0.32	0.30
MKI67IP	ILMN_1763207	1.13	0.63	0.00	-0.03	0.11	0.00	0.03	1.00	0.76	0.23
TSPAN5	ILMN_1760849	1.13	0.81	0.53	0.15	-0.03	0.01	0.01	0.01	0.25	0.83
MARS	ILMN_1660017	1.12	0.81	0.14	-0.06	0.07	0.01	0.04	0.55	0.79	0.73
FAM195A	ILMN_1794017	1.12	0.94	0.21	0.06	0.04	0.02	0.04	0.04	0.13	0.37
C3ORF21	ILMN_3247723	1.12	0.73	0.14	0.14	0.17	0.00	0.01	0.53	0.40	0.32
HIST2H2AA3	ILMN_1651262	1.12	0.92	0.24	0.05	0.10	0.00	0.01	0.25	0.81	0.70
TSR1	ILMN_1657862	1.12	0.67	0.32	0.04	-0.02	0.00	0.01	0.15	0.71	0.83

PMF1	ILMN_3176090	1.11	0.76	0.20	0.14	0.16	0.00	0.01	0.28	0.39	0.38
C13ORF15	ILMN_1671565	1.11	0.77	0.32	0.07	0.05	0.00	0.01	0.13	0.47	0.55
DNAJB11	ILMN_2330267	1.11	0.59	0.20	0.08	0.03	0.00	0.01	0.18	0.40	0.73
ZMYND19	ILMN_1671116	1.11	0.56	0.06	0.06	0.19	0.01	0.04	0.64	0.73	0.17
NARG1	ILMN_2192683	1.11	0.56	0.11	-0.11	-0.08	0.00	0.01	0.30	0.28	0.39
AXUD1	ILMN_1810680	1.11	0.66	0.09	0.10	0.05	0.03	0.04	0.67	0.48	0.70
GNL2	ILMN_1712431	1.11	0.66	0.09	0.06	0.04	0.00	0.02	0.52	0.75	0.79
ABCF2	ILMN_1688279	1.11	0.66	0.42	0.09	0.03	0.00	0.01	0.13	0.42	0.75
CELSR3	ILMN_1700419	1.11	0.69	0.14	-0.03	-0.03	0.01	0.00	0.04	0.50	0.75
MCM6	ILMN_1741954	1.10	0.79	0.25	0.00	0.09	0.00	0.02	0.10	0.99	0.47
HNRNPAB	ILMN_2088124	1.10	0.71	0.23	0.05	0.00	0.00	0.00	0.23	0.61	0.96
GAR1	ILMN_1674160	1.10	0.63	0.11	0.15	0.14	0.02	0.04	0.68	0.46	0.47
DDX31	ILMN_1740160	1.10	0.58	0.06	0.11	0.16	0.01	0.02	0.62	0.24	0.16
FARSA	ILMN_1680453	1.10	0.66	0.30	0.16	0.09	0.01	0.00	0.00	0.24	0.09
LMNA	ILMN_1718766	1.10	0.83	-0.16	0.27	0.20	0.01	0.02	0.43	0.41	0.44
MTP18	ILMN_2377240	1.09	0.81	0.19	0.14	0.17	0.01	0.00	0.10	0.05	0.06
UTP14A	ILMN_1704055	1.09	0.70	0.13	-0.04	-0.01	0.01	0.01	0.41	0.81	0.92
ARG2	ILMN_1799028	1.09	1.18	0.60	0.15	0.04	0.01	0.01	0.04	0.43	0.84
PELP1	ILMN_1767475	1.09	0.66	0.42	0.06	0.26	0.02	0.03	0.18	0.64	0.07
RPIA	ILMN_3228585	1.09	0.77	0.19	0.06	-0.03	0.00	0.01	0.29	0.54	0.81
APEX1	ILMN_1705594	1.09	0.79	0.31	0.07	0.06	0.01	0.01	0.09	0.64	0.65
PAPD1	ILMN_3201485	1.09	0.69	0.28	0.22	0.13	0.01	0.03	0.24	0.33	0.50
GTPBP4	ILMN_2371700	1.09	0.59	0.01	-0.19	0.05	0.00	0.02	0.94	0.28	0.61
PYCR1	ILMN_1764788	1.09	0.62	0.10	-0.04	0.02	0.02	0.04	0.30	0.58	0.81

PRR5	ILMN_1753607	1.09	0.64	0.10	-0.06	0.04	0.00	0.05	0.36	0.33	0.43
RAN	ILMN_1815552	1.09	0.65	0.07	0.09	0.18	0.00	0.00	0.61	0.33	0.10
FAM89A	ILMN_1733390	1.08	0.56	0.21	0.14	0.08	0.01	0.02	0.38	0.07	0.20
LOC652481	ILMN_1779171	1.08	0.57	0.17	0.09	0.16	0.01	0.03	0.42	0.71	0.46
PRMT1	ILMN_2086965	1.08	0.67	0.09	0.22	0.35	0.03	0.00	0.41	0.40	0.16
C1QBP	ILMN_1677765	1.08	0.68	-0.02	-0.13	-0.06	0.00	0.01	0.92	0.39	0.65
SEH1L	ILMN_2057573	1.08	0.51	0.08	-0.01	0.05	0.00	0.01	0.39	0.89	0.63
FEN1	ILMN_1652198	1.08	0.69	0.15	0.12	0.21	0.01	0.02	0.45	0.52	0.31
FAM136A	ILMN_1714515	1.08	0.59	-0.07	0.13	0.21	0.01	0.01	0.33	0.27	0.02
ATIC	ILMN_1785336	1.08	0.82	0.24	0.00	-0.04	0.01	0.00	0.11	0.99	0.64
VARS2	ILMN_1696311	1.08	0.74	0.15	0.12	0.26	0.03	0.02	0.50	0.56	0.14
BEND3	ILMN_1651498	1.08	0.55	0.08	0.05	0.07	0.01	0.03	0.35	0.54	0.31
PRPF19	ILMN_2255579	1.08	0.79	0.31	0.09	0.17	0.00	0.00	0.05	0.17	0.10
GCSH	ILMN_1730523	1.08	0.59	0.03	0.04	0.11	0.02	0.00	0.63	0.36	0.19
DDX55	ILMN_1689097	1.07	0.82	0.17	0.07	0.15	0.01	0.00	0.08	0.50	0.17
FABP5L2	ILMN_1801584	1.07	0.84	0.19	-0.20	-0.08	0.00	0.00	0.36	0.24	0.32
PUS1	ILMN_1711894	1.07	0.67	0.13	0.05	0.00	0.00	0.00	0.16	0.42	0.93
LOC652864	ILMN_1760667	1.07	0.76	0.08	0.05	0.14	0.00	0.01	0.75	0.82	0.51
NHP2L1	ILMN_2097546	1.07	0.80	0.25	0.22	0.22	0.01	0.01	0.24	0.26	0.25
SLC35F2	ILMN_1798459	1.07	0.67	0.19	0.08	0.20	0.00	0.00	0.05	0.40	0.12
UCHL5IP	ILMN_2170095	1.07	0.83	0.18	0.08	0.17	0.01	0.02	0.42	0.40	0.09
SLC35B1	ILMN_1784871	1.07	0.67	0.18	0.09	0.07	0.01	0.02	0.29	0.60	0.68
TRIB1	ILMN_1753243	1.07	0.84	0.48	0.10	0.00	0.06	0.01	0.02	0.38	0.99
WDR77	ILMN_1770206	1.07	0.59	0.10	-0.04	-0.04	0.00	0.01	0.36	0.71	0.65

ADAM15	ILMN_2374249	1.06	0.77	0.21	0.07	0.02	0.01	0.03	0.45	0.47	0.84
LOC729535	ILMN_1749432	1.06	0.73	-0.04	0.03	0.16	0.00	0.00	0.71	0.59	0.02
HIST2H2AA4	ILMN_1777881	1.06	0.84	0.31	0.18	0.31	0.00	0.01	0.10	0.33	0.09
LYST	ILMN_1708605	1.06	0.86	0.71	0.43	0.19	0.02	0.03	0.05	0.14	0.41
C10ORF61	ILMN_1773865	1.06	1.20	0.78	0.20	0.02	0.00	0.00	0.01	0.15	0.85
PMPCA	ILMN_1789349	1.06	0.65	0.09	0.17	0.23	0.00	0.01	0.51	0.34	0.11
FLOT1	ILMN_2405521	1.06	0.44	0.20	0.22	0.25	0.04	0.01	0.08	0.15	0.05
CCT3	ILMN_1802377	1.06	0.74	0.19	0.32	0.37	0.01	0.02	0.36	0.14	0.10
LOC100130919	ILMN_1772359	1.06	0.63	0.28	0.23	0.12	0.00	0.02	0.30	0.12	0.53
MLLT6	ILMN_1737406	1.06	0.67	0.22	0.17	0.11	0.01	0.05	0.33	0.49	0.64
DDX39	ILMN_1661589	1.05	0.72	0.14	0.08	0.06	0.02	0.05	0.69	0.81	0.84
GSPT1	ILMN_1718863	1.05	0.53	0.14	0.14	0.07	0.01	0.01	0.46	0.38	0.59
FLJ16793	ILMN_1769118	1.05	0.46	0.00	0.02	-0.02	0.00	0.01	0.99	0.83	0.79
LOC100128266	ILMN_1683475	1.05	0.65	0.00	0.11	0.21	0.00	0.04	1.00	0.39	0.25
TTLL12	ILMN_1703955	1.05	0.60	0.03	-0.03	0.03	0.01	0.03	0.70	0.65	0.69
MRPL32	ILMN_2278729	1.05	0.64	0.06	-0.02	0.00	0.00	0.02	0.67	0.88	0.97
SERPINB9	ILMN_1751425	1.05	0.91	0.75	0.14	0.24	0.01	0.01	0.02	0.43	0.32
ABCE1	ILMN_1712975	1.05	0.71	0.30	-0.02	-0.08	0.00	0.05	0.34	0.83	0.32
SNHG3-RCC1	ILMN_1781999	1.04	0.60	0.02	0.02	-0.03	0.02	0.02	0.93	0.78	0.73
KIAA0133	ILMN_1696556	1.04	0.67	0.05	0.05	0.06	0.01	0.02	0.74	0.77	0.72
CXORF64	ILMN_1706149	1.04	0.60	0.11	0.18	0.21	0.03	0.01	0.39	0.05	0.11

C10ORF61	ILMN_3287266	1.04	1.17	0.90	0.33	0.00	0.03	0.00	0.01	0.22	0.99
WDR36	ILMN_1787345	1.04	0.74	0.24	0.13	0.07	0.01	0.02	0.07	0.35	0.60
ANKRD37	ILMN_1751851	1.04	0.61	0.23	0.05	0.06	0.00	0.03	0.22	0.31	0.23
SNAPC2	ILMN_1724658	1.04	0.67	0.26	0.30	0.28	0.00	0.02	0.35	0.04	0.05
CD151	ILMN_1746686	1.04	0.74	0.26	0.05	0.03	0.02	0.03	0.07	0.09	0.53
AHSA1	ILMN_1750130	1.04	0.73	0.34	0.14	0.26	0.00	0.02	0.06	0.07	0.08
NAT5	ILMN_1692962	1.03	0.79	0.15	0.22	0.13	0.01	0.01	0.41	0.33	0.47
EIF4G1	ILMN_1756541	1.03	0.68	0.29	0.12	0.05	0.01	0.05	0.16	0.56	0.83
KHSRP	ILMN_2173611	1.03	0.64	0.14	0.36	0.48	0.01	0.03	0.64	0.16	0.05
PMCH	ILMN_1660232	1.03	0.75	0.16	-0.04	-0.10	0.00	0.03	0.36	0.61	0.17
DIMT1L	ILMN_1676026	1.03	0.80	0.29	0.13	0.42	0.01	0.04	0.22	0.72	0.13
LARS	ILMN_1660000	1.03	0.73	0.32	0.08	0.03	0.01	0.01	0.08	0.67	0.80
SIGMAR1	ILMN_1674386	1.02	0.61	0.40	0.00	-0.05	0.03	0.04	0.06	0.99	0.66
BOLA2	ILMN_1782045	1.02	0.82	0.32	0.07	0.19	0.01	0.01	0.12	0.65	0.34
IMPAD1	ILMN_1700733	1.02	0.63	0.12	-0.13	-0.04	0.00	0.00	0.09	0.28	0.67
MRPS7	ILMN_1760109	1.02	0.86	0.27	0.23	0.28	0.01	0.01	0.17	0.25	0.17
FAM86A	ILMN_1764362	1.02	0.60	0.24	0.06	0.07	0.00	0.01	0.03	0.14	0.26
LOC100132139	ILMN_2313730	1.02	0.73	0.19	-0.04	-0.05	0.00	0.01	0.19	0.27	0.50
MRPS23	ILMN_1723158	1.01	0.58	0.02	0.02	0.04	0.03	0.00	0.76	0.71	0.30
CHCHD8	ILMN_2298511	1.01	0.64	0.13	0.14	0.18	0.00	0.00	0.32	0.34	0.24
SIAH2	ILMN_1674706	1.01	0.60	0.21	0.13	0.03	0.01	0.02	0.20	0.37	0.83
C19ORF48	ILMN_1766657	1.01	0.51	-0.24	0.07	0.30	0.03	0.00	0.18	0.31	0.01
LRP8	ILMN_1705310	1.01	0.57	0.00	0.00	-0.07	0.03	0.01	0.91	0.97	0.28

UBQLN4	ILMN_1728684	1.01	0.72	0.23	0.15	0.12	0.01	0.05	0.42	0.50	0.62
TFRC	ILMN_1716678	1.01	0.71	0.17	0.10	0.07	0.04	0.00	0.20	0.50	0.48
MAK16	ILMN_2326713	1.01	0.62	0.05	-0.13	-0.12	0.00	0.02	0.77	0.29	0.33
SRFBP1	ILMN_3307930	1.01	0.70	0.27	0.05	0.06	0.00	0.00	0.07	0.67	0.55
PRDX1	ILMN_2104924	1.01	0.65	0.13	0.11	0.19	0.00	0.01	0.19	0.08	0.05
C6ORF66	ILMN_1697614	1.00	0.49	0.10	0.16	0.26	0.01	0.00	0.22	0.19	0.03
BCCIP	ILMN_2150258	1.00	0.63	0.27	-0.06	-0.04	0.01	0.02	0.27	0.80	0.82
SLC29A1	ILMN_3235477	1.00	0.56	0.11	0.05	0.10	0.00	0.00	0.12	0.26	0.06
GFOD1	ILMN_1713505	1.00	0.79	0.26	0.16	0.03	0.05	0.01	0.41	0.42	0.90
VARS	ILMN_1688818	1.00	0.79	-0.03	-0.07	0.12	0.01	0.01	0.91	0.76	0.52
NME2	ILMN_2329429	1.00	0.72	0.16	0.04	0.18	0.02	0.00	0.09	0.60	0.18
CBS	ILMN_1737685	-1.00	-0.96	-0.81	0.07	0.26	0.01	0.01	0.02	0.80	0.31
MGST3	ILMN_1813400	-1.00	-0.66	-0.23	-0.12	0.02	0.00	0.01	0.16	0.36	0.90
GNS	ILMN_1744517	-1.01	-0.63	-0.09	0.04	0.02	0.00	0.00	0.62	0.65	0.81
KIAA1671	ILMN_2411559	-1.01	-0.51	-0.10	0.00	-0.14	0.01	0.02	0.65	0.98	0.37
SMYD3	ILMN_3265143	-1.01	-0.75	-0.53	-0.27	-0.10	0.02	0.02	0.05	0.23	0.59
ALDH6A1	ILMN_1787378	-1.01	-0.75	-0.26	-0.22	-0.30	0.01	0.01	0.18	0.23	0.14
ACAP1	ILMN_1810729	-1.02	-0.62	0.13	0.02	0.01	0.00	0.05	0.64	0.91	0.96
RGS12	ILMN_1705407	-1.02	-0.97	-0.84	-0.16	0.15	0.01	0.02	0.01	0.58	0.66
NPC2	ILMN_1742052	-1.02	-0.65	-0.29	0.00	0.09	0.06	0.03	0.27	0.97	0.48
CYFIP2	ILMN_1662658	-1.02	-0.60	-0.07	-0.07	-0.14	0.00	0.03	0.52	0.59	0.26
CHCHD6	ILMN_2090782	-1.03	-0.92	-0.72	0.06	0.28	0.02	0.03	0.05	0.85	0.37
IFIH1	ILMN_1687359	-1.03	-0.66	-0.15	-0.12	-0.16	0.00	0.01	0.45	0.32	0.28
PTPN12	ILMN_1676891	-1.03	-0.71	-0.15	-0.26	-0.31	0.00	0.00	0.52	0.16	0.04

LOC644988	ILMN_3212373	-1.03	-0.65	0.06	-0.05	-0.03	0.01	0.03	0.43	0.40	0.79
SNAP25	ILMN_2354140	-1.03	-1.06	-0.82	-0.20	-0.16	0.05	0.05	0.07	0.56	0.64
LOC100134006	ILMN_2328433	-1.03	-1.03	-0.84	-0.07	0.14	0.00	0.00	0.01	0.70	0.40
RPL13A	ILMN_3237632	-1.03	-0.76	-0.29	-0.14	-0.02	0.00	0.01	0.14	0.38	0.88
KIAA0430	ILMN_1750321	-1.03	-0.64	-0.16	0.05	-0.11	0.01	0.02	0.52	0.81	0.57
LOC730455	ILMN_1775542	-1.04	-0.65	-0.11	-0.14	-0.10	0.01	0.02	0.49	0.18	0.26
ITM2C	ILMN_1711823	-1.04	-0.90	-0.25	0.05	0.10	0.00	0.01	0.22	0.75	0.46
PTPN12	ILMN_1707493	-1.05	-0.75	-0.25	-0.10	-0.09	0.00	0.00	0.03	0.24	0.51
FAM84B	ILMN_1768662	-1.05	-0.62	-0.17	-0.18	-0.17	0.01	0.03	0.03	0.01	0.10
CXCR4	ILMN_3248910	-1.05	-0.66	-0.09	0.16	0.05	0.00	0.02	0.71	0.10	0.29
CDC14A	ILMN_2044832	-1.05	-0.68	-0.27	-0.05	-0.09	0.00	0.00	0.05	0.55	0.48
PERP	ILMN_1753111	-1.05	-1.00	-0.72	-0.31	-0.09	0.02	0.01	0.04	0.32	0.73
HS.436879	ILMN_1768510	-1.05	-0.70	-0.13	0.01	-0.05	0.00	0.01	0.61	0.97	0.75
KIAA1128	ILMN_1814305	-1.05	-0.67	-0.07	-0.07	-0.16	0.01	0.00	0.72	0.33	0.06
SAMD3	ILMN_3297510	-1.06	-0.46	-0.13	-0.01	0.05	0.03	0.01	0.29	0.91	0.72
PSIP1	ILMN_2376403	-1.06	-0.60	-0.17	-0.26	-0.27	0.01	0.03	0.28	0.23	0.07
WIPF1	ILMN_1813139	-1.06	-0.54	0.10	-0.27	-0.41	0.00	0.03	0.74	0.16	0.07
P2RY10	ILMN_1814526	-1.06	-0.45	0.03	-0.03	-0.15	0.12	0.05	0.89	0.87	0.38
MAN2B2	ILMN_1803775	-1.06	-0.72	-0.35	-0.20	-0.07	0.01	0.03	0.29	0.53	0.73
RAB7L1	ILMN_2311278	-1.07	-0.78	-0.06	-0.10	-0.08	0.02	0.05	0.87	0.75	0.76
RNASET2	ILMN_1796013	-1.07	-0.53	-0.35	0.10	0.28	0.00	0.01	0.15	0.52	0.06
DYRK2	ILMN_2102960	-1.07	-0.61	-0.28	-0.25	-0.18	0.00	0.00	0.17	0.05	0.12
ZFP36L2	ILMN_2258816	-1.07	-0.61	-0.08	0.20	0.10	0.00	0.01	0.53	0.32	0.53

KLF6	ILMN_1653652	-1.07	-0.78	-0.30	0.09	0.00	0.00	0.00	0.29	0.45	0.99
CDC2L6	ILMN_1737585	-1.08	-0.53	-0.14	0.00	0.06	0.00	0.01	0.44	0.97	0.48
PDGFD	ILMN_1815874	-1.08	-0.67	-0.13	0.02	-0.06	0.00	0.02	0.46	0.90	0.75
ROD1	ILMN_1728435	-1.08	-0.66	-0.16	-0.41	-0.48	0.01	0.01	0.39	0.00	0.00
PTPRC	ILMN_1781010	-1.08	-0.54	0.04	0.10	0.05	0.01	0.04	0.88	0.61	0.81
WDR54	ILMN_1656537	-1.08	-0.56	-0.19	0.01	0.07	0.04	0.05	0.37	0.89	0.20
RAB5B	ILMN_1747305	-1.08	-0.62	-0.12	0.07	-0.11	0.00	0.02	0.55	0.56	0.28
DSE	ILMN_1700067	-1.09	-1.06	-0.82	-0.30	-0.14	0.04	0.04	0.06	0.32	0.64
WBP2	ILMN_1662198	-1.09	-0.55	-0.02	-0.05	-0.07	0.06	0.01	0.89	0.37	0.32
BTN3A2	ILMN_1773576	-1.09	-0.83	-0.13	0.07	0.10	0.01	0.01	0.62	0.73	0.47
PRKCB1	ILMN_1743145	-1.09	-0.74	-0.23	-0.21	-0.17	0.01	0.02	0.12	0.40	0.27
CPNE3	ILMN_1688178	-1.09	-0.57	-0.04	-0.14	-0.15	0.00	0.00	0.76	0.04	0.03
SMC4	ILMN_1735014	-1.10	-0.66	-0.20	-0.33	-0.31	0.02	0.05	0.11	0.04	0.05
ZBTB4	ILMN_2224955	-1.10	-0.66	0.08	-0.17	-0.32	0.01	0.02	0.82	0.41	0.25
CCDC28A	ILMN_1707484	-1.10	-0.59	-0.12	-0.07	0.01	0.00	0.03	0.42	0.65	0.97
LOC729495	ILMN_1659524	-1.10	-0.64	0.10	0.08	0.04	0.00	0.05	0.31	0.42	0.69
CBR4	ILMN_1755415	-1.11	-0.74	-0.25	-0.20	-0.15	0.00	0.01	0.09	0.18	0.23
SLAMF6	ILMN_1696485	-1.11	-0.47	0.20	0.10	0.15	0.00	0.02	0.21	0.56	0.28
CCNG2	ILMN_1786176	-1.11	-0.63	-0.13	-0.17	-0.20	0.00	0.00	0.22	0.13	0.09
DAPK2	ILMN_1688775	-1.11	-0.54	0.16	0.05	0.12	0.01	0.02	0.59	0.75	0.43
AKTIP	ILMN_1809866	-1.11	-0.61	-0.04	-0.24	-0.25	0.00	0.04	0.91	0.23	0.25
MAP1LC3B	ILMN_1788701	-1.12	-0.74	-0.21	-0.04	-0.04	0.00	0.00	0.04	0.56	0.54
SLAMF8	ILMN_1718734	-1.12	-0.85	-0.31	-0.17	-0.04	0.01	0.00	0.07	0.25	0.80
CERK	ILMN_1714567	-1.13	-0.57	-0.25	-0.09	-0.04	0.00	0.04	0.37	0.31	0.58

FHL2	ILMN_2112049	-1.13	-0.70	-0.14	0.14	0.11	0.00	0.01	0.38	0.53	0.54
HS.163752	ILMN_1724753	-1.13	-0.77	-0.44	-0.24	-0.61	0.02	0.05	0.17	0.42	0.10
KIAA0240	ILMN_1703244	-1.13	-0.71	-0.11	-0.18	-0.24	0.01	0.02	0.52	0.36	0.25
PPP2R5C	ILMN_1733847	-1.13	-0.68	-0.06	-0.05	-0.05	0.02	0.02	0.64	0.62	0.65
JAKMIP2	ILMN_1803094	-1.13	-0.72	-0.12	-0.32	-0.28	0.01	0.02	0.62	0.09	0.12
CD37	ILMN_2376859	-1.13	-0.76	0.14	0.20	0.06	0.01	0.01	0.41	0.21	0.66
ARHGAP15	ILMN_1728714	-1.14	-0.75	-0.10	-0.14	-0.14	0.01	0.04	0.53	0.57	0.29
SAMD3	ILMN_3306742	-1.14	-0.52	-0.14	-0.08	-0.08	0.03	0.00	0.20	0.52	0.51
PDLIM1	ILMN_1708954	-1.14	-0.79	-0.34	0.04	0.18	0.01	0.03	0.35	0.86	0.48
KIAA1949	ILMN_1702835	-1.14	-0.76	-0.22	0.07	0.07	0.00	0.01	0.47	0.55	0.58
IL16	ILMN_1664761	-1.14	-0.59	-0.15	0.05	-0.02	0.00	0.01	0.49	0.85	0.93
FAM43A	ILMN_2319344	-1.14	-1.34	-1.25	-0.13	0.13	0.02	0.01	0.01	0.67	0.66
KIAA1147	ILMN_1726289	-1.15	-0.90	-0.26	0.01	-0.09	0.03	0.02	0.13	0.94	0.59
LOC100129502	ILMN_2155172	-1.15	-0.56	-0.08	0.06	0.03	0.02	0.04	0.63	0.75	0.86
TPP1	ILMN_2087702	-1.15	-0.78	-0.17	-0.06	-0.17	0.01	0.02	0.58	0.82	0.53
FAM62B	ILMN_1808395	-1.15	-0.85	-0.37	-0.11	-0.16	0.00	0.01	0.02	0.51	0.20
CMIP	ILMN_1662799	-1.15	-0.66	0.13	0.16	0.01	0.00	0.04	0.63	0.41	0.95
MT1E	ILMN_2379469	-1.15	-0.63	-0.55	-0.02	0.23	0.04	0.01	0.02	0.87	0.14
IQGAP1	ILMN_3191695	-1.15	-0.76	-0.08	-0.28	-0.32	0.00	0.00	0.82	0.06	0.06
C5ORF39	ILMN_2071641	-1.15	-0.53	-0.31	-0.05	0.04	0.00	0.03	0.14	0.84	0.83
ABR	ILMN_1778836	-1.15	-0.75	-0.43	0.07	0.13	0.01	0.04	0.29	0.71	0.50
BNIP3L	ILMN_2373831	-1.16	-0.76	-0.04	-0.05	-0.01	0.00	0.01	0.62	0.63	0.86
C4ORF34	ILMN_1654262	-1.16	-0.73	-0.16	0.02	0.05	0.01	0.02	0.51	0.94	0.77

WASPIP	ILMN_1764239	-1.17	-0.69	-0.11	-0.31	-0.44	0.01	0.01	0.62	0.13	0.05
SIDT2	ILMN_1732750	-1.17	-0.64	-0.12	0.07	0.06	0.01	0.00	0.33	0.55	0.57
TNFSF12	ILMN_1654690	-1.17	-0.77	-0.23	-0.08	-0.05	0.00	0.02	0.18	0.56	0.82
CD37	ILMN_3234142	-1.18	-0.81	0.21	0.13	0.02	0.01	0.01	0.43	0.50	0.90
CD8A	ILMN_1702320	-1.18	-0.73	0.09	0.08	0.04	0.02	0.00	0.56	0.50	0.75
KIAA1370	ILMN_2343618	-1.18	-0.60	-0.15	-0.31	-0.34	0.00	0.04	0.46	0.11	0.11
PYHIN1	ILMN_2092536	-1.18	-0.48	0.03	-0.02	0.02	0.01	0.03	0.84	0.92	0.82
APAF1	ILMN_2334989	-1.19	-0.73	-0.21	-0.23	-0.33	0.01	0.00	0.23	0.02	0.01
NOXO1	ILMN_1710962	-1.19	-1.15	-0.88	-0.07	0.16	0.02	0.02	0.03	0.75	0.60
TMEM154	ILMN_2286014	-1.20	-0.71	-0.28	-0.24	-0.22	0.01	0.02	0.02	0.07	0.01
NPC1	ILMN_1651828	-1.20	-0.72	-0.07	-0.11	-0.13	0.01	0.03	0.70	0.57	0.52
LOC728855	ILMN_1659463	-1.20	-0.62	-0.05	-0.05	-0.02	0.03	0.01	0.74	0.72	0.89
PRKCB1	ILMN_1813572	-1.20	-0.69	-0.22	-0.12	-0.06	0.00	0.01	0.22	0.52	0.70
TNNI2	ILMN_1665761	-1.20	-1.20	-0.92	0.09	0.41	0.01	0.01	0.02	0.76	0.09
NTAN1	ILMN_1721977	-1.21	-0.78	-0.12	-0.34	-0.29	0.00	0.02	0.45	0.02	0.03
CCDC106	ILMN_1827736	-1.21	-1.20	-1.02	-0.04	0.19	0.04	0.04	0.04	0.91	0.57
KLF6	ILMN_3231944	-1.21	-0.79	-0.20	-0.01	0.08	0.00	0.00	0.38	0.95	0.38
FGD3	ILMN_1781721	-1.22	-0.48	-0.10	0.03	0.20	0.00	0.01	0.70	0.87	0.07
FLJ46309	ILMN_1804396	-1.23	-0.63	-0.18	-0.15	-0.17	0.05	0.01	0.26	0.23	0.24
YPEL1	ILMN_1865764	-1.23	-0.76	-0.13	0.00	-0.01	0.01	0.03	0.64	1.00	0.95
FAM8A1	ILMN_1726306	-1.24	-0.62	-0.25	-0.25	-0.23	0.00	0.03	0.12	0.10	0.13
SNRPN	ILMN_1657857	-1.24	-0.84	-0.34	0.00	0.10	0.00	0.03	0.06	0.98	0.29
SAMD3	ILMN_1651496	-1.24	-0.55	0.07	-0.07	-0.08	0.02	0.01	0.29	0.65	0.17
LOC728661	ILMN_1661439	-1.24	-0.88	-0.07	-0.05	-0.17	0.02	0.04	0.78	0.85	0.56

RAB8B	ILMN_1747303	-1.24	-0.80	-0.15	-0.13	-0.24	0.02	0.01	0.53	0.35	0.18
PRKCA	ILMN_1742569	-1.24	-0.53	-0.22	-0.17	-0.34	0.00	0.03	0.30	0.24	0.05
CEBPD	ILMN_1813938	-1.25	-0.79	0.00	-0.10	-0.23	0.01	0.02	0.99	0.63	0.30
SYTL2	ILMN_1777895	-1.25	-0.85	0.08	0.00	-0.03	0.00	0.01	0.63	0.98	0.88
PRKCB	ILMN_1748124	-1.25	-1.00	-0.20	-0.20	-0.31	0.00	0.01	0.21	0.36	0.10
BTN3A3	ILMN_1778240	-1.25	-0.76	-0.18	-0.05	-0.11	0.01	0.02	0.34	0.81	0.51
HIST1H2BD	ILMN_1755303	-1.25	-0.87	-0.19	-0.04	-0.07	0.00	0.02	0.46	0.86	0.76
SGSM2	ILMN_2336609	-1.25	-0.91	-0.52	-0.13	-0.10	0.01	0.04	0.19	0.58	0.65
ARHGEF3	ILMN_1815719	-1.25	-0.61	-0.01	-0.06	-0.16	0.01	0.04	0.96	0.66	0.36
POLR3GL	ILMN_1742124	-1.26	-0.70	-0.10	-0.10	-0.09	0.00	0.00	0.42	0.37	0.52
VEZF1	ILMN_2347068	-1.26	-0.92	-0.38	-0.16	-0.14	0.01	0.01	0.26	0.37	0.49
FAM190B	ILMN_1727045	-1.26	-0.75	0.00	0.04	-0.17	0.00	0.00	0.99	0.71	0.14
PJA2	ILMN_1737298	-1.26	-0.74	-0.15	-0.16	-0.28	0.01	0.01	0.45	0.35	0.17
KRT81	ILMN_1772686	-1.27	-1.03	-0.42	-0.12	0.04	0.02	0.04	0.24	0.73	0.90
F2R	ILMN_1652825	-1.27	-0.65	0.03	-0.14	-0.17	0.04	0.00	0.86	0.03	0.01
LOC100188949	ILMN_1797425	-1.27	-0.88	-0.34	-0.10	-0.06	0.01	0.02	0.21	0.65	0.78
LRRC37B	ILMN_1698478	-1.27	-0.75	-0.27	-0.24	-0.21	0.01	0.05	0.35	0.39	0.42
PLCG2	ILMN_1756862	-1.28	-0.87	-0.24	-0.16	-0.21	0.00	0.03	0.54	0.54	0.47
RBL2	ILMN_1737394	-1.28	-0.79	0.04	0.27	0.11	0.02	0.03	0.89	0.49	0.72
CECR1	ILMN_1846776	-1.28	-0.79	-0.06	-0.01	-0.05	0.00	0.01	0.85	0.96	0.81
DPY19L1	ILMN_2355033	-1.28	-1.37	-1.23	0.04	0.23	0.01	0.01	0.01	0.91	0.51
DOCK11	ILMN_1656372	-1.28	-0.86	-0.21	-0.26	-0.32	0.01	0.03	0.47	0.37	0.30

ZNF217	ILMN_1801442	-1.29	-0.64	-0.16	-0.02	-0.21	0.01	0.00	0.13	0.88	0.21
STOM	ILMN_1796537	-1.29	-0.74	-0.22	-0.20	-0.12	0.00	0.01	0.30	0.37	0.53
SH2D3C	ILMN_1751708	-1.29	-0.74	-0.33	0.00	-0.02	0.00	0.02	0.13	0.99	0.90
MAST3	ILMN_1749213	-1.30	-0.78	-0.28	-0.32	-0.32	0.00	0.02	0.24	0.18	0.19
PVRIG	ILMN_2375825	-1.30	-0.66	-0.08	0.06	0.12	0.06	0.02	0.77	0.69	0.37
ANKRD57	ILMN_1776788	-1.30	-1.36	-1.09	-0.15	0.03	0.02	0.02	0.03	0.66	0.94
IL10RA	ILMN_1795158	-1.30	-0.75	-0.12	-0.01	-0.03	0.01	0.03	0.25	0.96	0.67
PAQR8	ILMN_3283680	-1.30	-0.94	-0.28	0.01	-0.12	0.00	0.01	0.16	0.97	0.59
LOC730313	ILMN_1772821	-1.31	-0.71	-0.35	-0.24	-0.54	0.03	0.03	0.17	0.30	0.07
ATP9A	ILMN_1659158	-1.31	-1.27	-1.07	-0.07	0.09	0.01	0.02	0.02	0.78	0.77
PYHIN1	ILMN_1655307	-1.31	-0.56	0.06	-0.14	-0.09	0.00	0.02	0.80	0.35	0.61
LOC642362	ILMN_1776678	-1.31	-1.34	-1.02	-0.02	0.32	0.03	0.03	0.03	0.95	0.42
RHOC	ILMN_2379130	-1.31	-0.65	-0.18	0.04	0.13	0.00	0.02	0.49	0.83	0.55
SAMD3	ILMN_1756417	-1.31	-0.62	-0.01	0.02	0.05	0.01	0.00	0.94	0.87	0.71
KIAA1370	ILMN_1682929	-1.32	-0.77	-0.12	-0.12	-0.19	0.00	0.02	0.60	0.62	0.40
MKRN1	ILMN_1665982	-1.32	-0.52	-0.10	-0.17	-0.07	0.19	0.00	0.50	0.18	0.38
STAT4	ILMN_2178226	-1.32	-0.60	-0.07	-0.09	-0.10	0.04	0.01	0.17	0.30	0.13
GIMAP7	ILMN_1719986	-1.33	-0.57	0.06	-0.07	-0.04	0.06	0.00	0.59	0.28	0.33
PDCD4	ILMN_2229922	-1.33	-0.43	-0.02	0.17	0.10	0.04	0.01	0.80	0.14	0.32
BNIP3	ILMN_1775734	-1.33	-1.17	-0.77	-0.22	0.02	0.01	0.03	0.04	0.23	0.79
ARL6IP6	ILMN_1717934	-1.33	-0.78	-0.19	-0.14	-0.02	0.03	0.01	0.19	0.38	0.92
PLCG1	ILMN_1774930	-1.33	-0.84	-0.31	-0.26	-0.23	0.00	0.00	0.07	0.09	0.15
SYT11	ILMN_1798654	-1.34	-0.66	-0.30	0.12	0.04	0.00	0.05	0.42	0.56	0.86
SLC25A23	ILMN_1671583	-1.34	-0.93	-0.48	-0.05	0.13	0.00	0.01	0.07	0.87	0.57

BCL11B	ILMN_1808707	-1.35	-0.58	-0.15	0.05	-0.07	0.01	0.00	0.39	0.80	0.65
MYH9	ILMN_1791847	-1.35	-0.82	-0.08	-0.15	-0.23	0.01	0.00	0.39	0.17	0.21
GLIPR2	ILMN_2345015	-1.35	-0.66	-0.15	0.15	0.23	0.00	0.02	0.34	0.32	0.18
SYTL2	ILMN_2129388	-1.35	-0.83	-0.02	0.01	-0.07	0.01	0.01	0.94	0.96	0.70
TRIM48	ILMN_1780861	-1.36	-1.34	-1.10	-0.13	0.23	0.02	0.02	0.03	0.71	0.51
C14ORF4	ILMN_1678671	-1.36	-1.42	-1.08	-0.19	0.05	0.02	0.00	0.01	0.60	0.81
PDGFD	ILMN_1715603	-1.36	-0.92	-0.14	-0.13	-0.21	0.00	0.01	0.49	0.56	0.35
KLHL24	ILMN_1714108	-1.36	-0.72	-0.10	-0.16	-0.30	0.00	0.05	0.70	0.51	0.38
ADD3	ILMN_1774661	-1.37	-0.88	-0.03	-0.25	-0.23	0.04	0.03	0.90	0.31	0.24
LBA1	ILMN_1797964	-1.37	-0.85	-0.01	0.00	-0.15	0.00	0.01	0.96	0.99	0.53
LPAR5	ILMN_2208413	-1.37	-0.39	-0.09	-0.05	-0.08	0.09	0.02	0.50	0.39	0.40
C12ORF35	ILMN_1658494	-1.37	-0.74	0.03	0.08	-0.01	0.00	0.00	0.81	0.53	0.96
TIAF1	ILMN_3239135	-1.38	-0.74	-0.36	-0.16	-0.20	0.00	0.03	0.23	0.51	0.46
ATP6V1A	ILMN_2368318	-1.38	-0.69	-0.14	-0.08	-0.12	0.01	0.01	0.03	0.11	0.08
TMEM71	ILMN_3247835	-1.38	-0.80	-0.19	0.09	0.18	0.02	0.03	0.52	0.65	0.41
SPN	ILMN_2183510	-1.38	-0.83	-0.30	-0.23	-0.28	0.01	0.04	0.26	0.36	0.28
C5ORF41	ILMN_2228732	-1.38	-0.98	-0.19	-0.22	-0.43	0.00	0.02	0.34	0.31	0.10
SAMD9	ILMN_2115633	-1.39	-0.86	-0.19	-0.22	-0.20	0.00	0.01	0.22	0.15	0.19
VNN2	ILMN_1800898	-1.39	-0.99	-0.27	-0.19	-0.15	0.01	0.02	0.36	0.51	0.58
C5ORF41	ILMN_1748473	-1.40	-0.90	-0.17	-0.19	-0.38	0.00	0.01	0.37	0.32	0.13
RASSF2	ILMN_1713369	-1.40	-0.87	-0.13	-0.17	-0.14	0.02	0.04	0.39	0.40	0.32
OPTN	ILMN_1752582	-1.40	-0.84	-0.20	-0.27	-0.23	0.01	0.00	0.34	0.07	0.08
LIPA	ILMN_1788604	-1.40	-0.94	-0.42	-0.37	-0.20	0.00	0.00	0.03	0.04	0.12
STMN3	ILMN_1696127	-1.40	-0.77	-0.35	0.02	0.12	0.00	0.03	0.16	0.90	0.35

MLLT11	ILMN_1668411	-1.40	-1.00	-0.46	-0.22	-0.24	0.01	0.02	0.04	0.19	0.15
TTC3	ILMN_1763884	-1.40	-1.01	-0.39	-0.35	-0.47	0.00	0.01	0.10	0.13	0.07
FAM113B	ILMN_1787844	-1.40	-0.64	-0.17	0.11	0.12	0.00	0.00	0.51	0.28	0.18
ITM2C	ILMN_2195821	-1.40	-0.99	-0.25	0.09	0.10	0.00	0.01	0.40	0.61	0.50
SLC44A2	ILMN_2222074	-1.41	-0.85	-0.29	0.06	0.05	0.00	0.02	0.50	0.79	0.85
LOC728661	ILMN_1803312	-1.41	-0.87	-0.27	-0.33	-0.33	0.00	0.00	0.08	0.03	0.03
ADD3	ILMN_3237656	-1.41	-0.88	-0.20	-0.15	-0.27	0.01	0.04	0.53	0.66	0.35
MYH10	ILMN_1702787	-1.41	-1.45	-1.21	-0.29	-0.04	0.04	0.04	0.05	0.53	0.93
HS.371609	ILMN_2194852	-1.42	-0.81	-0.19	-0.02	-0.13	0.01	0.04	0.58	0.96	0.69
PLS3	ILMN_2364376	-1.42	-1.41	-1.12	-0.36	-0.20	0.02	0.03	0.04	0.28	0.56
MKNK2	ILMN_1706498	-1.43	-1.03	-0.41	-0.05	-0.06	0.00	0.00	0.13	0.72	0.62
GIMAP8	ILMN_2144426	-1.44	-0.78	-0.10	0.00	0.01	0.02	0.02	0.17	0.99	0.90
E2F3	ILMN_1753112	-1.44	-0.82	-0.13	-0.32	-0.44	0.01	0.01	0.40	0.10	0.04
HS.296031	ILMN_2381899	-1.45	-0.85	-0.18	0.05	-0.19	0.00	0.00	0.25	0.79	0.28
RAB37	ILMN_1756071	-1.46	-0.97	-0.33	-0.01	0.05	0.01	0.02	0.28	0.97	0.87
SH3BGRL	ILMN_1775829	-1.46	-0.98	-0.23	-0.26	-0.38	0.00	0.02	0.44	0.24	0.13
CATSPER2	ILMN_2330861	-1.46	-0.78	-0.39	-0.16	-0.43	0.01	0.02	0.12	0.44	0.12
APOL3	ILMN_1912662	-1.46	-0.69	-0.05	0.18	0.10	0.04	0.00	0.65	0.12	0.36
UBL3	ILMN_1759097	-1.47	-0.94	-0.10	-0.15	-0.04	0.01	0.02	0.13	0.44	0.74
SUSD3	ILMN_2180371	-1.47	-0.81	-0.32	0.16	0.20	0.01	0.05	0.30	0.60	0.53
NDRG3	ILMN_1788931	-1.47	-0.86	-0.23	-0.17	-0.10	0.00	0.00	0.20	0.20	0.49
NIN	ILMN_1728605	-1.48	-0.86	-0.22	-0.22	-0.26	0.02	0.04	0.51	0.51	0.45
ANKDD1A	ILMN_1787762	-1.48	-0.95	-0.34	-0.07	-0.10	0.00	0.00	0.07	0.55	0.45
ERMP1	ILMN_1756920	-1.48	-0.80	-0.16	-0.31	-0.22	0.00	0.03	0.47	0.06	0.25

DOCK8	ILMN_1803819	-1.48	-0.95	0.00	-0.30	-0.48	0.00	0.01	1.00	0.14	0.05
ITM2B	ILMN_1709683	-1.48	-0.79	0.00	-0.30	-0.26	0.02	0.03	0.99	0.19	0.23
TMEM14C	ILMN_1672503	-1.49	-0.90	-0.24	-0.11	-0.06	0.01	0.03	0.34	0.59	0.79
ANXA8	ILMN_2321578	-1.49	-1.46	-1.13	-0.26	-0.01	0.03	0.03	0.05	0.47	0.99
NMT2	ILMN_1668417	-1.49	-0.73	-0.07	-0.04	0.05	0.01	0.05	0.81	0.89	0.85
HS.356079	ILMN_1794875	-1.49	-0.99	-0.25	0.01	-0.16	0.00	0.02	0.41	0.97	0.53
SNURF	ILMN_1771800	-1.49	-1.05	-0.45	-0.03	-0.03	0.00	0.02	0.06	0.82	0.84
ILK	ILMN_1742866	-1.52	-0.68	-0.32	0.03	0.09	0.00	0.00	0.03	0.73	0.40
ZMAT3	ILMN_2160476	-1.52	-1.00	-0.02	-0.01	-0.14	0.01	0.02	0.95	0.97	0.70
GPR68	ILMN_1742001	-1.53	-0.69	-0.02	-0.02	-0.09	0.06	0.00	0.76	0.73	0.18
PHF21A	ILMN_2395451	-1.53	-0.81	-0.12	0.05	-0.02	0.00	0.01	0.44	0.74	0.92
BIN1	ILMN_2044453	-1.53	-1.08	-0.48	0.13	0.06	0.01	0.01	0.05	0.46	0.72
CAT	ILMN_1708778	-1.54	-0.89	-0.20	-0.11	0.01	0.00	0.00	0.05	0.26	0.88
LAPTM5	ILMN_1652525	-1.54	-0.83	-0.04	-0.02	-0.08	0.06	0.01	0.58	0.73	0.37
RGL4	ILMN_2117223	-1.54	-0.97	-0.35	0.13	0.20	0.01	0.02	0.30	0.42	0.37
GIMAP4	ILMN_1813685	-1.54	-0.61	0.00	0.06	0.09	0.09	0.03	0.99	0.60	0.42
NR5A2	ILMN_1651826	-1.55	-0.79	-0.08	0.04	-0.07	0.04	0.05	0.59	0.77	0.52
FGR	ILMN_1807042	-1.55	-0.84	-0.41	0.06	0.04	0.03	0.00	0.21	0.62	0.75
Sep-09	ILMN_1738749	-1.55	-0.72	-0.06	0.03	-0.02	0.03	0.00	0.77	0.81	0.83
FGR	ILMN_1781373	-1.56	-0.93	-0.35	-0.26	-0.13	0.01	0.00	0.03	0.08	0.48
C12ORF35	ILMN_1765860	-1.56	-0.83	-0.11	-0.31	-0.38	0.00	0.02	0.78	0.17	0.12
FLOT2	ILMN_1742026	-1.57	-0.91	-0.39	0.01	0.05	0.00	0.03	0.35	0.95	0.46
NR5A2	ILMN_1729234	-1.57	-0.71	-0.13	-0.04	-0.11	0.02	0.02	0.56	0.79	0.53
LOC100132	ILMN_3242900	-1.58	-0.84	-0.38	-0.26	-0.38	0.01	0.02	0.13	0.24	0.13

391											
GIMAP6	ILMN_2097793	-1.60	-0.71	-0.02	0.11	0.13	0.00	0.01	0.89	0.35	0.31
FAM125B	ILMN_2396272	-1.60	-0.91	-0.23	-0.11	-0.26	0.00	0.01	0.33	0.60	0.17
ERAP2	ILMN_3251629	-1.60	-0.97	-0.10	-0.04	-0.33	0.01	0.01	0.59	0.85	0.18
CADM1	ILMN_1757627	-1.63	-1.43	-0.84	0.00	0.06	0.02	0.01	0.09	0.99	0.89
PAG1	ILMN_2041788	-1.65	-0.98	-0.36	-0.24	-0.35	0.01	0.02	0.12	0.25	0.13
KRT86	ILMN_1671142	-1.65	-1.16	-0.46	0.01	0.07	0.01	0.04	0.30	0.98	0.86
BIN1	ILMN_1682567	-1.65	-1.14	-0.50	-0.14	-0.03	0.00	0.02	0.03	0.24	0.79
ABLIM1	ILMN_1706015	-1.65	-1.11	0.08	0.12	-0.03	0.01	0.01	0.74	0.70	0.92
DPYSL2	ILMN_1759184	-1.66	-1.09	-0.40	-0.17	-0.09	0.01	0.01	0.14	0.43	0.67
FAIM3	ILMN_1782050	-1.68	-1.02	-0.04	0.04	0.08	0.00	0.02	0.82	0.84	0.63
LOC340274	ILMN_1695509	-1.68	-1.73	-1.24	0.08	0.42	0.01	0.01	0.01	0.81	0.17
MXD4	ILMN_3279169	-1.70	-0.91	-0.22	0.21	0.19	0.00	0.01	0.60	0.47	0.31
RASGRP3	ILMN_1669502	-1.70	-0.99	-0.28	-0.04	0.02	0.01	0.03	0.01	0.64	0.80
PPP2R2B	ILMN_2169261	-1.71	-0.84	-0.26	0.05	0.07	0.00	0.00	0.23	0.72	0.63
AKTIP	ILMN_2412927	-1.71	-0.91	-0.19	-0.23	-0.23	0.01	0.00	0.33	0.19	0.22
MT1F	ILMN_1699496	-1.72	-0.89	-0.27	-0.05	-0.02	0.01	0.01	0.10	0.61	0.90
LOC283116	ILMN_1676515	-1.72	-1.70	-1.31	-0.22	0.13	0.03	0.03	0.04	0.60	0.76
MFGE8	ILMN_1753648	-1.72	-1.68	-1.34	-0.14	0.14	0.03	0.03	0.04	0.76	0.78
TSC22D3	ILMN_1791296	-1.73	-1.09	-0.08	0.02	0.03	0.00	0.00	0.77	0.95	0.88
LOC100130516	ILMN_1793371	-1.73	-1.09	-0.63	-0.13	-0.34	0.01	0.02	0.06	0.57	0.28
SORL1	ILMN_3250110	-1.76	-1.21	-0.38	0.13	-0.08	0.01	0.02	0.29	0.67	0.81
LOC653111	ILMN_2160929	-1.77	-1.79	-1.31	-0.13	0.18	0.02	0.02	0.03	0.71	0.61

ARHGAP9	ILMN_2150851	-1.77	-1.04	-0.30	-0.36	-0.37	0.00	0.00	0.28	0.08	0.04
IL23A	ILMN_2351298	-1.78	-1.66	-1.20	0.07	0.35	0.00	0.00	0.01	0.81	0.18
CNN2	ILMN_1793476	-1.80	-1.10	-0.55	-0.05	0.00	0.00	0.00	0.24	0.75	0.99
CDKN2D	ILMN_2302757	-1.80	-1.24	-0.62	-0.19	0.03	0.00	0.01	0.07	0.12	0.88
ZBP1	ILMN_1811303	-1.80	-1.21	-0.22	0.14	0.17	0.00	0.00	0.41	0.56	0.34
STK38	ILMN_1669447	-1.81	-1.22	-0.18	0.03	-0.01	0.00	0.01	0.33	0.91	0.97
PRKCDBP	ILMN_1673936	-1.82	-1.92	-1.50	0.04	0.49	0.03	0.03	0.03	0.94	0.36
FCGBP	ILMN_1803317	-1.82	-1.03	-0.28	0.16	0.11	0.00	0.02	0.48	0.66	0.73
RXRA	ILMN_1729142	-1.84	-1.74	-1.23	-0.03	0.14	0.02	0.02	0.03	0.95	0.76
CD5	ILMN_1740555	-1.85	-1.25	-0.41	-0.12	-0.04	0.00	0.02	0.22	0.72	0.91
FBXO32	ILMN_1680132	-1.85	-1.02	-0.16	-0.12	-0.13	0.00	0.02	0.61	0.66	0.61
ADD3	ILMN_1765686	-1.85	-1.05	-0.27	-0.38	-0.44	0.03	0.04	0.17	0.11	0.01
RHOU	ILMN_1687315	-1.88	-0.83	-0.28	-0.14	-0.02	0.02	0.04	0.14	0.38	0.91
TP53INP1	ILMN_3251714	-1.89	-1.15	-0.25	-0.13	-0.18	0.00	0.01	0.32	0.49	0.35
IGSF3	ILMN_3275388	-1.90	-1.92	-1.47	-0.06	0.05	0.02	0.02	0.02	0.84	0.89
CCM2	ILMN_1688702	-1.93	-1.05	-0.05	-0.08	-0.25	0.02	0.01	0.73	0.75	0.04
GPSM3	ILMN_1670807	-1.96	-0.99	-0.17	-0.18	-0.23	0.00	0.04	0.44	0.42	0.34
HS.579631	ILMN_1798256	-2.00	-2.02	-1.21	0.37	0.85	0.05	0.04	0.11	0.62	0.21
CTDSP2	ILMN_1703123	-2.01	-0.96	-0.35	0.05	0.05	0.00	0.01	0.36	0.74	0.75
YPEL3	ILMN_1722834	-2.01	-0.99	-0.01	0.04	0.08	0.00	0.01	0.96	0.88	0.73
TC2N	ILMN_2214197	-2.01	-1.14	-0.36	-0.24	-0.27	0.01	0.04	0.01	0.06	0.02
ADRB2	ILMN_1815154	-2.03	-0.98	-0.25	-0.12	0.00	0.00	0.00	0.13	0.29	0.97
KIF1A	ILMN_1759330	-2.06	-2.05	-1.53	-0.02	0.17	0.02	0.02	0.01	0.97	0.74
VNN2	ILMN_2173004	-2.07	-1.05	-0.22	-0.11	-0.09	0.02	0.01	0.05	0.19	0.28

TSC22D3	ILMN_1701621	-2.08	-1.32	-0.09	-0.23	-0.16	0.00	0.01	0.74	0.38	0.56
DDIT4L	ILMN_2366654	-2.09	-0.99	-0.40	-0.06	-0.05	0.00	0.02	0.17	0.80	0.87
ASS1	ILMN_1711516	-2.11	-2.07	-1.43	0.00	0.23	0.01	0.01	0.03	0.99	0.57
TP53INP1	ILMN_2055156	-2.16	-1.37	-0.29	0.09	-0.03	0.00	0.00	0.04	0.37	0.62
FYB	ILMN_1762021	-2.16	-1.11	-0.17	-0.28	-0.32	0.01	0.00	0.37	0.18	0.13
CCL22	ILMN_2150856	-2.18	-2.05	-1.47	0.02	0.36	0.00	0.00	0.00	0.95	0.16
ABLIM1	ILMN_1785161	-2.23	-1.29	0.09	0.07	-0.19	0.00	0.04	0.61	0.79	0.38
SORL1	ILMN_1724040	-2.31	-1.56	-0.31	-0.05	-0.38	0.00	0.02	0.39	0.89	0.41
AHNAK	ILMN_1804735	-2.31	-1.54	-0.55	-0.06	-0.22	0.01	0.03	0.24	0.89	0.64
MARCKS	ILMN_1704353	-2.46	-2.48	-1.70	-0.09	0.14	0.01	0.00	0.00	0.80	0.70
SRPK2	ILMN_2363450	-2.47	-1.59	-0.42	-0.17	-0.16	0.00	0.01	0.10	0.29	0.32
PIK3IP1	ILMN_1881909	-2.62	-1.19	-0.19	0.12	0.08	0.00	0.03	0.68	0.77	0.83
SPRYD5	ILMN_2089073	-2.73	-2.74	-1.85	-0.13	0.25	0.01	0.01	0.02	0.79	0.55
SERPINB2	ILMN_1778087	-2.89	-2.87	-1.95	-0.42	-0.10	0.01	0.01	0.00	0.38	0.77
FSCN1	ILMN_1788108	-3.01	-2.95	-1.84	-0.05	0.12	0.01	0.01	0.01	0.91	0.80
ASS1	ILMN_1787127	-3.04	-2.90	-1.77	-0.13	0.18	0.01	0.01	0.02	0.78	0.68
SERPINB2	ILMN_1769634	-3.09	-3.03	-2.05	0.01	0.46	0.01	0.01	0.00	0.99	0.26
BASP1	ILMN_1813763	-3.45	-3.39	-2.05	-0.31	-0.06	0.01	0.01	0.01	0.45	0.90

5. Clone C23 Gene Differential Expressions Table (fold change greater than 2 at 2μM, 75 probes ↑, 25 probes ↓)

(Descending order)		log2 (fold change value, mean)				*p*-value (two-tailed t test)			
Gene ID	**Probe ID**	**2μM**	**0.4μM**	**0.08μM**	**0.016μM**	**2μM**	**0.4μM**	**0.08μM**	**0.016μM**
TNFRSF9	ILMN_1813379	3.40	2.49	1.27	0.21	0.00	0.00	0.00	0.40
TNIP3	ILMN_1707591	2.09	0.95	0.20	0.01	0.01	0.00	0.24	0.49
MAL	ILMN_2320330	2.06	1.74	1.07	0.23	0.00	0.00	0.00	0.30
ZBED2	ILMN_1651365	1.96	1.06	0.33	-0.03	0.01	0.01	0.22	0.66
IL2RA	ILMN_1683774	1.93	1.13	0.50	0.01	0.01	0.01	0.12	0.96
TNS3	ILMN_1667893	1.84	1.48	0.72	0.10	0.03	0.05	0.05	0.44
MAL	ILMN_2327860	1.82	1.49	0.85	0.19	0.00	0.00	0.01	0.39
HS.390407	ILMN_1906423	1.73	0.82	0.15	0.11	0.01	0.10	0.69	0.80
NINJ1	ILMN_1815086	1.63	1.18	0.59	0.11	0.01	0.02	0.11	0.67
CCL3	ILMN_1671509	1.58	1.02	0.50	0.34	0.03	0.06	0.25	0.50
METTL1	ILMN_3306997	1.54	0.86	0.39	-0.07	0.00	0.04	0.18	0.75
LYST	ILMN_1663131	1.53	0.86	0.14	-0.01	0.01	0.02	0.63	0.98
FABP5L2	ILMN_3266606	1.53	0.69	0.15	-0.07	0.00	0.11	0.54	0.81
TNFRSF4	ILMN_2112256	1.50	1.31	0.56	0.20	0.02	0.10	0.23	0.64
HAVCR2	ILMN_1693826	1.50	0.79	0.25	-0.03	0.03	0.13	0.66	0.96
SERPINE2	ILMN_1655595	1.43	0.60	0.12	-0.03	0.06	0.03	0.11	0.76
FABP5L2	ILMN_3178258	1.42	0.46	-0.17	-0.10	0.00	0.04	0.40	0.39
ADO	ILMN_1690352	1.41	0.72	0.38	0.09	0.06	0.03	0.00	0.28
CSF2	ILMN_1661861	1.41	0.99	0.72	0.16	0.00	0.03	0.02	0.02
CTLA4	ILMN_1763487	1.39	0.96	0.44	0.18	0.01	0.01	0.06	0.35

PUS7	ILMN_1779353	1.38	0.78	0.27	0.00	0.01	0.12	0.35	0.99
CTLA4	ILMN_2261627	1.37	0.83	0.39	0.01	0.00	0.02	0.17	0.97
daDA1	ILMN_1687978	1.34	0.85	0.38	0.09	0.01	0.03	0.29	0.75
RRP12	ILMN_1767253	1.33	0.70	0.21	0.05	0.01	0.07	0.38	0.81
LOC642956	ILMN_3210741	1.33	0.78	0.12	0.14	0.01	0.03	0.58	0.53
RRS1	ILMN_1767658	1.31	0.63	0.29	0.17	0.00	0.06	0.16	0.36
FABP5	ILMN_2146761	1.31	0.75	0.25	0.08	0.00	0.03	0.13	0.54
LOC100129066	ILMN_3235051	1.28	1.13	0.44	0.15	0.01	0.01	0.09	0.47
CTXN1	ILMN_1759766	1.28	0.50	0.11	0.03	0.07	0.21	0.54	0.85
IFNG	ILMN_2207291	1.27	0.77	0.27	-0.05	0.01	0.06	0.31	0.84
METTL1	ILMN_1815190	1.27	0.63	0.25	0.06	0.00	0.10	0.28	0.79
BZW2	ILMN_1676548	1.25	0.55	0.18	0.02	0.01	0.07	0.48	0.95
CYP1B1	ILMN_1693338	1.25	0.31	0.06	-0.12	0.13	0.57	0.91	0.79
CCL3L1	ILMN_1747355	1.24	0.86	0.43	0.19	0.05	0.08	0.28	0.69
SLC3A2	ILMN_1726456	1.23	0.66	0.27	0.08	0.02	0.07	0.34	0.78
TRIB1	ILMN_1803811	1.23	0.75	0.16	-0.01	0.03	0.00	0.25	0.82
MTHFD1L	ILMN_1772521	1.22	0.56	0.15	-0.04	0.00	0.03	0.42	0.80
DUSP5	ILMN_1656501	1.21	0.91	0.45	0.10	0.01	0.00	0.05	0.47
PAICS	ILMN_2392546	1.20	0.68	0.30	0.01	0.00	0.02	0.16	0.97
PAICS	ILMN_1773760	1.19	0.62	0.19	-0.12	0.01	0.06	0.40	0.58
SFXN1	ILMN_2205935	1.19	0.78	0.37	0.05	0.02	0.07	0.31	0.90
HS.373429	ILMN_1862684	1.18	0.44	0.06	0.01	0.02	0.02	0.36	0.88

CCL3L3	ILMN_2105573	1.18	0.71	0.28	0.14	0.05	0.11	0.42	0.74
CCL1	ILMN_2086965	1.18	1.43	1.17	0.26	0.06	0.11	0.00	0.09
C12ORF48	ILMN_1654429	1.17	0.37	-0.01	-0.07	0.04	0.29	0.97	0.83
MIR155HG	ILMN_3248910	1.17	0.50	0.20	-0.14	0.17	0.42	0.75	0.82
MAF	ILMN_1719543	1.17	0.44	0.15	0.02	0.01	0.32	0.65	0.96
NME1	ILMN_1741133	1.16	0.65	0.20	-0.03	0.00	0.05	0.33	0.86
TNFRSF18	ILMN_2349633	1.14	0.90	0.24	0.06	0.03	0.09	0.10	0.49
SGK	ILMN_1702487	1.14	0.86	0.47	0.15	0.02	0.01	0.01	0.02
FAM3C	ILMN_2368773	1.14	0.54	0.25	0.13	0.00	0.04	0.24	0.39
DPH2	ILMN_2375418	1.14	0.59	0.15	-0.12	0.02	0.13	0.58	0.66
WARS	ILMN_2337655	1.14	0.88	0.36	0.11	0.02	0.03	0.21	0.65
IL27RA	ILMN_1688152	1.12	0.92	0.45	0.18	0.00	0.03	0.19	0.46
BOP1	ILMN_1715583	1.12	0.53	0.21	0.01	0.02	0.14	0.48	0.98
MGC87042	ILMN_1663575	1.12	0.41	0.08	-0.11	0.04	0.35	0.84	0.78
NR4A2	ILMN_1782305	1.11	0.59	0.26	-0.01	0.12	0.17	0.08	0.92
HSP90AB1	ILMN_1673711	1.10	0.72	0.34	0.20	0.01	0.04	0.22	0.41
MAMLD1	ILMN_1680856	1.10	0.56	0.21	0.04	0.01	0.00	0.03	0.75
NPTX1	ILMN_1814221	1.08	0.56	0.26	0.08	0.13	0.14	0.24	0.63
GPATCH4	ILMN_2383305	1.07	0.49	0.20	0.05	0.02	0.16	0.46	0.85
MAP3K6	ILMN_1694539	1.07	0.87	0.46	0.10	0.00	0.01	0.03	0.49
DDX21	ILMN_1735461	1.06	0.51	0.25	-0.06	0.01	0.11	0.35	0.78
LMCD1	ILMN_1754969	1.06	0.37	0.12	0.00	0.02	0.11	0.57	0.99
SLC3A2	ILMN_1679041	1.05	0.88	0.40	0.30	0.01	0.01	0.23	0.27

WARS	ILMN_1727271	1.04	0.86	0.37	0.14	0.01	0.02	0.10	0.42
TSPAN17	ILMN_2374383	1.03	0.48	0.17	0.16	0.11	0.25	0.42	0.52
IER3	ILMN_1682717	1.02	0.67	0.40	0.10	0.12	0.33	0.36	0.76
TSPAN17	ILMN_1777881	1.02	0.53	0.20	0.13	0.14	0.30	0.55	0.70
GADD45B	ILMN_1718977	1.02	0.58	0.39	0.12	0.08	0.16	0.17	0.57
ZDHHC9	ILMN_1803824	1.02	0.53	0.16	0.01	0.01	0.05	0.30	0.92
SLC27A2	ILMN_1700831	1.02	0.53	0.21	-0.02	0.04	0.13	0.22	0.92
EBNA1BP2	ILMN_1768127	1.01	0.47	0.12	0.07	0.00	0.05	0.39	0.58
C3ORF26	ILMN_2215545	1.00	0.61	0.10	0.05	0.03	0.09	0.73	0.84
GPATCH4	ILMN_2383306	1.00	0.43	0.17	-0.02	0.01	0.12	0.27	0.91
GYPC	ILMN_1682332	-1.00	-0.44	0.00	0.09	0.01	0.02	1.00	0.46
SLC44A1	ILMN_1700695	-1.01	-0.55	-0.07	-0.02	0.02	0.23	0.84	0.95
RSAD2	ILMN_1657871	-1.02	-0.14	0.06	0.03	0.02	0.74	0.89	0.93
IFI44L	ILMN_1723912	-1.03	-0.26	-0.07	-0.10	0.07	0.67	0.91	0.85
PLAC8	ILMN_2093343	-1.04	-0.45	-0.08	-0.11	0.07	0.48	0.88	0.82
RAB37	ILMN_2255579	-1.06	-0.59	-0.08	-0.02	0.06	0.23	0.84	0.97
PLAC8	ILMN_1653026	-1.06	-0.45	-0.09	-0.12	0.12	0.54	0.89	0.84
NMT2	ILMN_1656378	-1.06	-0.52	-0.23	-0.06	0.00	0.06	0.16	0.69
FCRLA	ILMN_1691071	-1.07	-0.48	-0.09	-0.01	0.23	0.64	0.93	1.00
TNFRSF17	ILMN_1768016	-1.07	-0.48	-0.06	-0.06	0.04	0.42	0.89	0.88
CLIC3	ILMN_1796423	-1.10	-0.64	-0.24	0.13	0.02	0.13	0.45	0.71
FSCN1	ILMN_1808707	-1.11	-0.51	-0.03	-0.14	0.31	0.66	0.98	0.87
ADA	ILMN_1803686	-1.12	-0.45	-0.17	0.04	0.03	0.07	0.26	0.77
CDKN2D	ILMN_1748883	-1.19	-0.53	-0.16	0.12	0.01	0.00	0.08	0.11

LIME1	ILMN_2183687	-1.22	-0.65	-0.22	0.04	0.01	0.01	0.09	0.77
CD79A	ILMN_1734878	-1.23	-0.62	-0.03	-0.10	0.14	0.46	0.96	0.88
ADRB2	ILMN_1695590	-1.23	-0.74	-0.25	-0.07	0.02	0.01	0.34	0.75
PDLIM1	ILMN_1788955	-1.23	-0.60	-0.23	-0.05	0.05	0.33	0.68	0.90
RGL4	ILMN_1663422	-1.24	-0.61	-0.22	0.11	0.02	0.02	0.18	0.57
ZNF683	ILMN_1678238	-1.24	-0.65	-0.13	0.03	0.04	0.11	0.67	0.93
ZBP1	ILMN_1765994	-1.31	-0.46	-0.01	0.09	0.02	0.23	0.98	0.79
IFIT1	ILMN_1707695	-1.47	-0.48	-0.06	0.00	0.12	0.62	0.95	1.00
KLF2	ILMN_1735930	-1.64	-0.93	-0.34	-0.08	0.02	0.05	0.19	0.76
IGJ	ILMN_2105441	-1.97	-0.82	-0.21	-0.38	0.06	0.13	0.51	0.23
IGLL1	ILMN_2393765	-2.65	-0.57	0.16	-0.08	0.20	0.46	0.75	0.90

6. Common genes between CTL clones A3 and C23.

Up-regulate [A3-1μM FC>1.5 & C23-2μM FC>1.5] 155 genes
TNFRSF9, EGR2, RRS1, LYST, NME1, GLT25D1, EBNA1BP2, TNIP3, GAR1, LOC642956, NOLC1, FABP5L2, METTL1, FABP5, NDUFAF2, LOC100129066, ECE2, NINJ1, KIAA0020, GPATCH4, WDR12, SLC7A5, CTLA4, VARS, PAICS, CTPS, SEH1L, BOLA2, DCTPP1, TRIB1, RRP12, SLC39A14, BZW2, PRMT3, BATF, C3ORF26, AK3L1, PIP5K1B, CCT7, CCDC86, MTP18, IL2RA, LOC100132139, SLC3A2, MRPS17, IARS, TIMM8A, NXT1, FAM3C, DUSP4, BLVRA, PUS7, C10ORF61, BOP1, UBIAD1, MAMLD1, FAM86A, POLD2, HSP90AB1, IMPDH2, NHP2, PHLDA1, SLC7A1, PFAS, MRTO4, NAMPT, SFXN4, MTHFD1L, HS.10862, SIAH2, PPARG, GART, TFB2M, C1QBP, CDK4, UTP14A, PRDX4, DPH2, FASLG, NCL, AGMAT, PTRH2, HS.390407, SLC27A2, TFRC, EXOSC5, AK2, BCCIP, NOL6, ZBED2, C17ORF79, TCTN3, ZDHHC9, MARS, LOC644214, SLC35F2, NPM3, WDR74, IFRD2, MRPL12, DDX10, TIMM23, WDR4, ATIC, RPF2, POLR3H, C7ORF40, SRM, ENTPD1, CIRH1A, HS.25892, LOC729608, PHB, SRPRB, NR2C2AP, IFNG, C10ORF2, GTPBP4, POLR1C, TTC27, FLJ39827, DDX21, RRP15, TIMD4, EIF3B, CSF2, CCT2, ALDH18A1, MAP1LC3A, C12ORF48, PPRC1, CD83, RPL34, CYCSL1, MAF, UBE2F, TRAP1, SIGMAR1, HAVCR2, PKM2, DKC1, NDFIP2, SFXN1, RANBP1, EIF4G1, CDK6, BATF3, LOC100130919, ABCE1, TNFRSF1B, GPR56, MYB, FASN, CTNNAL1, EIF4A1

Down-regulate [A3-1μM FC>1.5 & C23-2μM FC>1.5] 47 genes
CAMK2G, CDKN2D, SLAMF8, ADRB2, NMT2, MGST3, GLIPR2, STMN3, RGL4, CAT, CD8A, C4ORF34, ZBP1, RASSF1, VNN2, FCRL6, TMEM71, TC2N, BIN1, FAM8A1, SIGIRR, RBL2, HS.356079, SIDT2, C11ORF67, TRPV2, PRKCB, SORL1, STK38, ABLIM1, PRAGMIN, NDRG3, SUSD3, TNFSF12, FLOT2, YPEL1, TIAF1, PDLIM1, LOC100188949, BBS2, YPEL3, ABR, RAB37, LAPTM5, MT1E, AHNAK, SLC25A23

A3[10μM & 1μM & 0.1μM] & C23[2μM & 0.4μM & 0.08μM] 3 genes
TNFRSF9, EGR2, CCL1